Estimation of Brake Force on an Open Wheel Racing Car Using Artificial Neural Networks

By

Garth Campbell Heron, BEng. (Mech) Hons.

Submitted in the fulfilment of the requirements for the Degree of

Master of Engineering Science

At the

Engineering (Civil & Mechanical)

University of Tasmania (April, 2002)

STATEMENT OF ORIGINALITY AND AUTHORITY OF ACCESS

This thesis contains no material that has been accepted for a degree or diploma by the University of Tasmania or any other institution, except by way of background information and has been duly acknowledged in the thesis, and to the best of the author's knowledge and belief no material has been previously published or written by another person except where due acknowledgment is made in the text of the thesis.

This thesis contains confidential information and is not to be disclosed or made available for loan or copy without the express permission of the University of Tasmania (i). Once released the thesis may be made available for loan and limited copying in accordance with the Copyright Act 1968.

(i) Inquires should be directed to the Research and Development Office.

Signed: 

Dated this tenth day of April 2002

The nature of automobile dynamics is complex. While they might not be aware of it, the driver of a vehicle is making many complex decisions producing a complex series of actions that effect the motion of the vehicle. Usually the driver can perform a sequence of actions which move the vehicle in a way in which the driver intends, however, occasionally all drivers find themselves having to correct the vehicle in a way that they did not expect.

The problem here is in the control system and the high performance available in the vehicles that are driven on the roads. With the brake pedal linked directly to the force on the brake disks, the driver of the vehicle simply applies pressure that corresponds to the rate at which they intend to stop. At the limits of tyre adhesion this breaks down as more brake pressure fails the slow the vehicle quicker, and the vehicle actually takes longer to stop.

To produce safer vehicles, car developers and manufacturers have developed anti-lock brakes and stability control systems. These state of the art systems monitor driver commands that inherently reflect their intention and the behaviour of the vehicle. When the vehicle behaves in a way that does not follow the driver's intent the system intervenes and selectively applies braking, limits engine power or changes other relevant parameters to assist the driver in retaining control of the vehicle. Systems such as these use mathematical models based on simplified assumptions of vehicle behaviour. Because of this they are built to be robust, commercially available systems fail to capitalise on the full performance potential of the vehicle. Since systems such as these become active in emergency situations, every small gain in performance can make up the difference between life and death.

Neural networks, as emerging decision making tools offer another approach to the problem of modelling non-linear dynamic, multi variable vehicle physics. Neural networks use artificial intelligence to find relationships between inputs and outputs. These relationships are not assumed or based upon a simplified physical analysis, but are built based on the past experiences of the network.

For automobile dynamic prediction a special vehicle '*Intelligent Car*' was conceived, constructed and tested in real world driving conditions. Structured driving tests were carried out gathering sufficient data to train ant test the potential of neural networks for the application. The results from these tests represent some of the first outcomes from preliminary research in the '*Intelligent Car*' Project.

This study outlines the design and development of the University of Tasmania's *Intelligent Car* together with results from training various neural network models to predict its brake forces and comparison with measured values.

Weapon against road toll

By Greta Harrison

TASMANIA may not immediately spring to mind as a world leader in cutting-edge automotive technology, but a team of researchers from the University of Tasmania is proving otherwise.

A group of academics and undergraduates from the School of Engineering has designed and built an "intelligent car" which they hope will contribute to increased road safety and a lower road toll.

The project has been developed in conjunction with Germany's University of Stralsund, which selected Tasmania ahead of other universities on the mainland and in the United States.

Project co-ordinator Dr Vishy Karri said the prototype SAE formula racing car used artificial intelligence technology to compensate for driver error, in a system which could soon be applied to domestic vehicles.

"The driver still has to do the overall navigation, but the intelligent feedback system helps give the driver a safer driving environment," he said.

"If a driver makes a mistake, the system will compensate and help put the [illegible] track."

Dr Karri sa[illegible] tech features ated included networks' wh workings of t sensor fusion unsafe runnin measuring er and brake for ing conditions, safety criteria

Dr Karri sa the car also

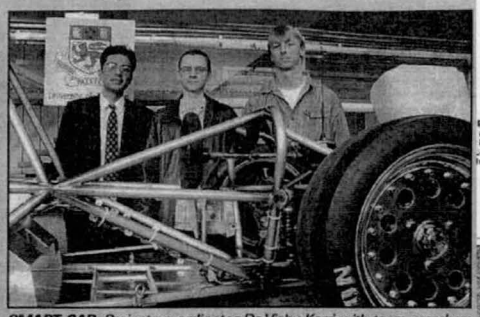

SMART CAR: Project co-ordinator Dr Vishy Karri with team members Garth Heron and Cranston Polson, of the University of Tasmania's School of Engineering

Intelligent car project working to reduce road toll

AFTER some intensive cosmetic surgery, the intelligent car was ready for its debut in Hobart earlier this month.

The car's body has now been fitted, meaning it's as sleek as any other race car.

The car was a joint project between engineering students at the University of Tasmania and some international

"The research that was carried out has been a partnership between Strausland University in Germany, which is a leading technical university and ourselves," School of Engineering Professor Frank Bullen said.

"We have postgraduate students from Germany, Denmark and other European countries working on the program."

The vehicle, which is powered by a 70 kW motorcycle engine, is starting trials at Baskerville Raceway to determine if the technology can be used in a domestic vehicle.

It uses sensors to create artificial intelligence to sense changes in the environment and react accordingly.

Its designers believe it has the potential to drastically reduce the road toll.

"It's both a teaching and research program so most of the car was built by undergraduate, third-year students in the first six months of the year.

"The refinements have been made by a team of postgraduate students," Professor Bullen said.

By Work experience student Erin Aherne.

Uni potential in human-like computers

By KATHY GRUBE
Education Reporter

TASMANIA could become the Artificially Intelligent Island if an initiative by a University of Tasmania academic takes off.

Engineering lecturer Dr Vishy Karri believes there is great potential for the university to unite researchers from psychology, mathematics, computer science and engineering to develop world-first artificial intelligence projects.

Their aim would be to create "virtual human" computers.

"Artificial intelligence research is a multi-disciplinary subject," Dr Karri said.

"However, it has traditionally been researched by each discipline alone without sharing information between them.

"There are some multi-disciplinary groups in New South Wales working on artificial intelligence projects and I would like to see Tasmanian researchers doing something similar."

Dr Karri is an organiser of an international conference

wards his goal and would raise the profile of artificial intelligence research at the University of Tasmania.

There are already projects being researched there.

These include the joint project between the University of Tasmania engineering school and a university in Germany to develop an artificially intelligent car that can avoid accidents and control its safe driving speed.

The engineering school has also been developing artificial intelligent process modelling for Comalco during the past five years and the school of computer science is studying neural networks and how the brain rationalises.

Professor Marimuthu Palaniswami, of the University of Melbourne, was a keynote speaker at the conference yesterday.

He discussed public perception of artificial intelligence and said there was no need for the public to fear the technology just because of its name.

"There are many misconceptions about what artificial

Here comes the car that thinks ahead

By ALISON RIBBON
Education Reporter

THEY are already a lap ahead of world technology and they aren't about to apply the brakes.

Institution of Engineers Australia national president Martin Cole was at the University of Tasmania yesterday to inspect the engineering school's artificially intelligent race car.

"This is going to continue to be a fascinating project for them," Dr Cole said of the car's research team.

"As a racing driver myself, I understand the problems they are trying to deal with and I will be interested to see if they can reduce risks."

The Tasmanian university's engineering school and a team from the University of Stralsund in Germany joined forces in November last year to build a car that can almost drive itself and instantly react to any given situation, such as slowing at corners.

Dr Cole said it was important a culture of innovation be created in Australia.

"We rely so much on the tourist trade here, but do we all want to be people who look after hotels?" he said.

"The first thing we have to do is believe in ourselves. We need to encourage young scientists, and businesses and the community have to stand behind them."

Dr Vishy Karri, project leader for the intelligent race car, said his team's innovative approach had enabled the development of an intelligent race car optimised for both fuel economy and maximum safe speed without overturning.

"All the techniques we have put into this are suitable for Formula One cars," Dr Karri said.

"This car will make decisions for you and save you from accidents. It thinks for itself and reacts to conditions."

He said the car would be "ready and racing" by December, in time for the 2001 Formula SAE — a competition for engineering students to conceive, design, fabricate and compete with small Formula One-style racing cars.

The competition, in Victoria, will this year involve participation by 15 Australian and 25 international universities.

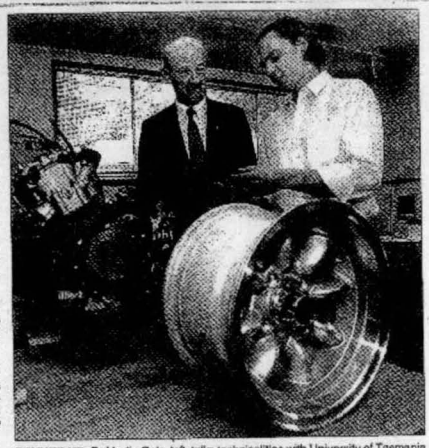

REVVED UP: Dr Martin Cole, left, talks technicalities with University of Tasmania postgraduate student Garth Heron, of Lenah Valley. Picture: JAMES KERR

'Intelligent' car steers toward future of safer roads

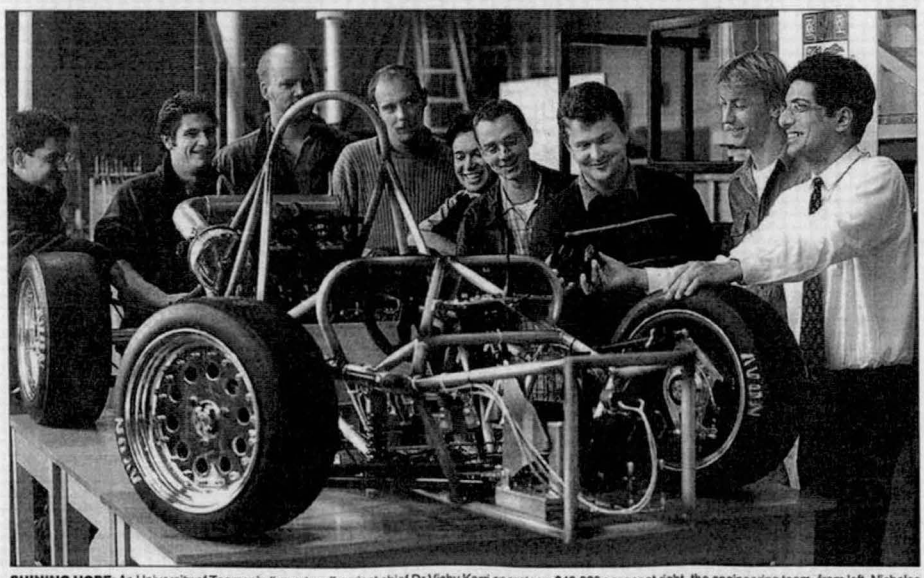

SHINING HOPE: As University of Tasmania "smart car" project chief Dr Vishy Karri operates a $40,000 sensor at right, the engineering team, from left, Nicholas Jones, Nicholas Dwyer, Robert Neben, Bent Rosenkilde, David Butler, Garth Heron, Tim Moore and Cranston Polson looks on. Picture: EDDIE SAFARIK

AN "intelligent" car with the potential to dramatically cut the road toll was yesterday polished and buffed for its Tasmanian launch.

Using sensors, the car is able to alter shock pressure, wheel and engine speed and "react" to road conditions.

It has been developed by the University of Tasmania's engineering school and will be officially launched at Wrest Point Hotel Casino tomorrow.

Engineering academic Vishy Karri said the production team was overjoyed with the results.

"It is fantastic. It is state-of-the-art technology and we are on a par with our German counterparts at the University of Stralsund," Dr Karri said.

He said the technology would eventually be used for commercially available vehicles to increase safety aspects.

"The system would increase safety significantly by automatically slowing the car speed and changing other parameters to suit the conditions," Dr Karri said.

"One day a car may even have vision sensors that will allow it to avoid a collision with another car or obstacle."

Don't tell me how to drive

The Corporate Box

Tony De Bolfo

The head of a team of dedicated engineers within the faculty of the Hobart-based University of Tasmania took the liberty of "calling all corporations" this week.

Dr Vishy Karri of the university's department of engineering initiated a public plea for a prospective sponsor to assist with the funding, design and manufacture of the world's first "artificially intelligent" race car.

The subsidy sought is relatively paltry given the project's potential multimillion-dollar value. As Karri said, "Around $40,000 to $50,000 in sponsorship would certainly accelerate matters enormously. In return, the company gets to align itself with the first project of its kind anywhere."

Karri is working with Professor Peter Rossnamen of Germany's world-renowned University of Stralsund school of mechanical engineering to design and build the intelligent car. It will be designed to "think for itself" and react to any situation with a selection of active parameters, including shock pressure, wheel and engine speed, and tyre and brake pressure, which can be altered to suit driving conditions.

ACKNOWLEDGMENTS

This work was conducted as part of a research team and represents some outcomes from the collaboration of the *'Intelligent Car'* research team here at the University of Tasmania and colleagues from the University of Stralsund.

Great thanks go to my supervisor Dr Vishy Karri for all of his support and guidance. His motivation and support has been absolute throughout the course of this research.

I would like to thank David Butler for the dedication, hard work, design talent and personal sacrifices he has made for this project. From the initial stages of the *'Intelligent Car'* concept David has been there to generate and reflect innovative ideas and designs. The vehicle is a design success because of his co-operation in the design of the chassis, suspension, wheel assembly, drivetrain, driver ergonomics, steering system, cooling system, braking system and many other components too numerous to mention here. Thanks Dave.

I personally thank the workshop staff and Peter Dove for their assistance in construction of the *'Intelligent Car'* Prototype and the Engineering faculty for making this project possible. Thanks to Helen Cunningham for her work, dedication and innovative wiring loom design, Nick Jones and Robert Neben for their great work on the measurement system, Nick Dwyer for leading the construction of the body work and also Cranston Polson for his contribution to the engine.

I would like to thank my partner and best friend Anita George for her support, encouragement and inspiration.

Finally I would like to thank my family for the support throughout my degree and research work.

CONTENTS

1 INTRODUCTION 1

1.1 HOW NEURAL NETWORKS ARE DIFFERENT FORM TRADITIONAL AND EXPERT SYSTEMS: AN ALTERNATIVE APPROACH 3

1.2 FUNDAMENTAL CONCEPTS IN VEHICLE PHYSICS 6

1.2.1 Tyre forces 6

1.2.2 Weight transferral 8

2 LITERATURE SURVEY 11

2.1 TYRE SLIP (LONGITUDINAL SLIP, λ_L) 11

2.2 LATERAL SLIP 14

2.3 LOAD COMBINATIONS 19

2.4 COMMERCIAL STATE OF THE ART AUTOMOTIVE CONTROL SYSTEMS USING ELECTRONIC BRAKE-FORCE DISTRIBUTION (EBD) 24

2.4.1 Further Advancement: The Brake Slip Controller 30

2.4.2 Traction Control Systems (TCS) 35

2.5 ELECTRONIC SUSPENSION MONITORING, REGULATION AND CONTROL 36

2.6 VEHICLE STABILITY CONTROL 37

2.6.1 Vehicle Yaw rate and Slip Angle Controller 42

2.7 NEURAL NETWORK APPLICATIONS AND CONTROL TO PREDICT AUTOMOTIVE PERFORMANCE 46

2.7.1 Advantageous Characteristics of Neural Networks 51

2.7.2 Neural Network Artificial Intelligence 51

2.8 FEED-FORWARD NEURAL NETWORKS 54

2.9 RECURRENT NEURAL NETWORKS 55

2.10 SUPERVISED AND UNSUPERVISED TRAINING 56

2.11 OPTIMISING NEURAL NETWORK PERFORMANCE 56

2.11.1 Network Input and Output Normalisation 56

2.11.2 Design of Neural Network training data 57

2.11.3 Neural Network Testing 58

2.12 NEURAL NETWORK ARCHITECTURE 58

2.13 BACKPROPAGATION NEURAL NETWORKS 60

2.13.1 Algorithm for backpropagation neural network training 65

2.14 GENERAL REGRESSION NEURAL NETWORK 66

3 DESIGN OF TEST RIG 70

3.1 CHASSIS DYNAMICS 72

3.2 FRAME DESIGN 76

3.3 FRAME DEVELOPMENT 77

3.3.1 Finite Element Analysis (FEA) *79*
3.3.2 Computer Aided Design *83*
3.3.3 Frame Construction *84*
3.4 SUSPENSION DESIGN 85
3.5 SUSPENSION DEVELOPMENT 86
3.5.1 Identification of Optimal Vehicle Width *89*
3.5.2 Optimisation of Front Track Width *96*
3.5.3 Dynamic Component Design *98*
3.6 FINAL STATIC SUSPENSION GEOMETRY 101
3.7 WHEEL ASSEMBLY DEVELOPMENT 103
3.7.1 Rims and Tyres *104*
3.7.2 Brake System *105*
3.7.3 Stub Axle and Bearings *107*
3.7.4 Oil Seals *112*
3.7.5 Wheel / Brake Hub *113*
3.7.6 Upright *114*
3.7.7 Assembly *116*
3.8 DRIVETRAIN DESIGN 118
3.8.1 Composite Disks *118*
3.8.2 Drive Shafts *120*
3.8.3 Differential Selection and Application *122*
3.9 ENGINE SYSTEMS DESIGN 124
3.9.1 Fuel Injection System *124*
3.9.2 Exhaust *129*
3.9.3 Engine Management System *130*
3.9.4 Fuel System *130*
3.10 WIRING LOOM DESIGN 132
3.10.1 Physical layout of the wiring loom *133*
3.10.2 Waterproofing *134*
3.10.3 Wire colours *134*
3.10.4 Wire Specification *134*
3.10.5 Wire wrapping *135*
3.10.6 Heat Protection *135*
3.10.7 Easy removal of all components *136*
3.10.8 Kill switches *136*
3.10.9 Brake Light *137*
3.10.10 Engine Cam Sensor Circuit *137*
3.11 FUSE BOX CIRCUIT AND LAYOUT DESIGN 139
3.11.1 Physical considerations *139*

3.11.2 Circuit Design *139*
3.11.3 Physical circuit layout *139*
3.11.4 Fuse specification *140*
3.12 DASHBOARD – LAYOUT AND CIRCUITRY 141
3.12.1 Physical considerations *141*
3.12.2 Circuit design *143*
3.12.3 Physical layout *143*
3.13 ELECTRICAL SYSTEM SPECIFICATIONS 144

4 INSTRUMENTATION DESCRIPTION 145

4.1 INPUT TYPE INSTRUMENTATION 147
4.1.1 Wheel Speed Hall Effect Sensor *148*
4.1.2 Three Axis Acceleration & Pitch/Roll/Yaw Angle Measurement: Crossbow DMU AHRS400CA-200 Sensor *155*
4.1.3 Wheel Travel: Gefran PZ12A Linear Potentiometer – 100mm *161*
4.1.4 Linear Potentiometer Installation and Calibration *164*
4.1.5 Steering Angle: MoTeC 10 Turn, Gear Driven Rotary Potentiometer *167*
4.1.6 Brake Force: Honeywell Eclipse Hydraulic Pressure Sensor – 2000psi *171*
4.2 DATA ACQUISITION TYPE INSTRUMENTATION 175
4.2.1 MoTeC Advance Dash Logger (ADL-4) *175*
4.2.2 Wiring Loom *177*
4.2.3 CAN Communication Cable *179*
4.3 OUTPUT TYPE INSTRUMENTATION 180
4.3.1 Research Computer *180*
4.3.2 Radio Modems: RFI-9256 Data Strike Series 3 Spread Spectrum Radio Modem and Auxiliary Equipment *181*
4.4 THE DEVELOPED MEASURING SYSTEM 183

5 TRAINING AND TESTING OFF-LINE NEURAL NETWORK MODELS 186

5.1 STRATEGY FOR PREDICTION 188
5.2 TYPES OF TRAINING COURSES 189
5.3 BACK PROPAGATION NEURAL NETWORK RESULTS 192
5.3.1 Course 1: Straight Line Acceleration and Braking – Front Brake Force Prediction *194*
5.3.2 Course 1: Straight Line Acceleration and Braking – Rear Brake Force Prediction *196*
5.3.3 Course 2: Figure Eight – Front Brake Force Prediction *198*
5.3.4 Course 2: Figure Eight – Rear Brake Force Prediction *200*
5.4 GENERAL REGRESSION NEURAL NETWORK RESULTS 202
5.5 CONCLUDING REMARKS 202

6 FINAL CONCLUDING REMARKS AND PROPOSED FUTURE WORK 204

7 REFERENCES 207

8 APPENDIX A –GENERAL REGRESSION NEURAL NETWORK RESULTS 216

9 APPENDIX B –FRAME DESIGN AND FEA 221

10 APPENDIX C – SUSPENSION DESIGN 233

11 APPENDIX D – WHEEL ASSEMBLY 241

12 APPENDIX E – BRAKE PEDAL ASSEMBLY 251

13 APPENDIX F – DRIVETRAIN DESIGN 253

14 APPENDIX G – ELECTRICAL SYSTEMS DESIGN 261

15 APPENDIX H – TEST RIG SENSOR AND TELEMETRY DESIGN 265

16 APPENDIX I – ENGINE SPECIFICATIONS 290

17 APPENDIX J – TESTING DATA 294

TABLE OF FIGURES

Figure 1-1 Characteristics of Neural Network and Traditional Computing Systems. 3
Figure 1-2 Neural Network and Expert Systems Comparison. 5
Figure 1-3 Tyre pressure distribution. [5] 7
Figure 1-4 Moment acting on a braked wheel 7
Figure 1-5 Vehicle in equilibrium [6] 8
Figure 1-6 Weight transferral: (a)under acceleration (b)while turning [6] 8
Figure 1-7 Optimal brake force distribution due to weight transferral under braking [7] 9
Figure 2-1 Friction factor vs slip [1] 13
Figure 2-2 Lateral forces during cornering 15
Figure 2-3 Lateral force as a function of normal force and slip angle. [9] 16
Figure 2-4 Lateral forces generated by the front wheels during vehicle cornering. [9] 17
Figure 2-5 The friction circle [1] 19
Figure 2-6 Total tyre force capability map [9] 21
Figure 2-7 Friction circle plot from measured data for a typical sports car [9] 22
Figure 2-8 Longitudinal, F_L and lateral forces, F_S as a function of slip ratio, λ_L and Slip angle, α.[8] 23
Figure 2-9 Hydraulic circuit of two channel ABS [11]. 25
Figure 2-10 Three channel ABS Hydraulic circuit 26
Figure 2-11 Four Channel ABS Hydraulic circuit. 26
Figure 2-12 4 channel ABS Electronic Control Unit (ECU) [12] 27
Figure 2-13 Modern ABS control unit logic [13] 28
Figure 2-14 Operational region of ABS allowing for steering input while braking at best efficiency. 29
Figure 2-15 Controller structure for the Bosch Brake Slip Controller.[14] 32
Figure 2-16 ABS in star topology 33
Figure 2-17 The merging of automotive systems. [7] 34
Figure 2-18 Simplistic view demonstrating active control systems during a cornering manoeuvre. 37
Figure 2-19 Bosch/Mercedes-Benz ESP Vehicle Dynamics Control (VDC) system. [14] 38
Figure 2-20 Bosch-Mercedes Electronic Stability Program (ESP) yaw control using differential electronic brake force distribution: (a)without ESP, (b) with ESP, (c) Graphical results showing handling response. [5] 40
Figure 2-21 Dynamic vehicle model used in predicting yaw moment changes.[14] 41
Figure 2-22 Bosch vehicle yaw rate and slip angle controller structure. [14] 44
Figure 2-23 "Automobile Autopilot" model freeway used to develop vehicle control Neural Networks 48
Figure 2-24 Neural network use in the Automobile Autopilot [18] 49
Figure 2-25 The structure of an artificial neuron 51
Figure 2-26 Threshold and sigmoidal activation functions 53
Figure 2-27 Feed forward neural network structure 55
Figure 2-28 Graphical example of overfitting on a polynomial approximation.[18] 59

Figure 2-29 Backpropagation (multi layered feed forward) neural network architecture with exploded output layer processing neuron [22] 60
Figure 2-30 Exploded hidden layer processing neuron [Fred Frost 34][R-ROJAS] 62
Figure 2-31 Basic General Regression Neural Network (GRNN) architecture. 67
Figure 3-1 Vehicle dynamics were found to be influenced by an astoundingly large number of factors. These pictures were taken during early stages of testing at Baskerville Raceway – Hobart, Tasmania. 72
Figure 3-2 Mid-mounted engine layout of the test vehicle 73
Figure 3-3 Reclined driver position of the test car. Note the far forward driving position 74
Figure 3-4: PVC mock frame 79
Figure 3-5: FEA frame model [Strand 1] 81
Figure 3-6: FEA results for cornering under brakes 82
Figure 3-7: FEA torsional results under 1 Nm 82
Figure 3-8: CAD drawing of the frame 83
Figure 3-9: Mild steel frame 84
Figure 3-10 Formula SAE vehicles are designed to operate on tight autocross style tracks resulting in compact design. Photo courtesy of SAE (USA). 86
Figure 3-11 Minimum practical clearances were specified between the seat and engine 87
Figure 3-12 The lateral distance between wheels, termed track width, is one of the first critical decisions faced by a vehicle designer 88
Figure 3-13 Test vehicle during autocross trials. 89
Figure 3-14 An experimental slalom course. 91
Figure 3-15 Identification of experimental slalom course variables 92
Figure 3-16 Geometry of turning vehicle 96
Figure 3-17 Pullrod suspension system with inboard coil over shock absorber used on the test vehicle. 98
Figure 3-18 Keeping the outside wheels vertical during cornering 99
Figure 3-19 The pull-rod suspension. 102
Figure 3-20 Front and rear uprights and bearing arrangements 102
Figure 3-21: Tyre and rim 104
Figure 3-22 13-inch rims permit the use of larger disk brakes. 105
Figure 3-23: Brake rotor and caliper 106
Figure 3-24: (a) On centre (b) off centre bearings 107
Figure 3-25: FEA wheel model cross sections (a) with centred bearings (b) with off centre bearings 109
Figure 3-26: Stub axle 112
Figure 3-27: Oil seal 113
Figure 3-28: Wheel / brake hub 114
Figure 3-29: Upright 115
Figure 3-30: Wheel assembly 117
Figure 3-31. Kevlar composite disks supplied by GKN motorsport used in the test vehicle transmission. 118

Figure 3-32 Unidirectional Kevlar fibre construction of the composite disks *118*
Figure 3-33 Perfect static alignment of the rear axel is required to keep composite disks from failure. *119*
Figure 3-34 Large diameter hollow aluminium drive shafts dominate the rear of the car *120*
Figure 3-35 Aluminium alloy drive shafts bolted directly to the GKN composite disks. *121*
Figure 3-36 Quaife ATB differential with pressed on ball bearings. *122*
Figure 3-37 Differential mounting arrangement; a) photo taken during frame construction, b) rear frame design dominated by differential mounting considerations *123*
Figure 3-38 Differential mounts *123*
Figure 3-39 Inlet manifold *127*
Figure 3-40 Exhaust manifold and muffler *129*
Figure 3-41 Fuse box location. Note the black wrapped wiring loom located directly above the box. *133*
Figure 3-42 Conduit, triple insulated wiring loom under nose cone. *135*
Figure 3-43 Kill switches *136*
Figure 3-44 Location of the engine cam sensor circuit case *138*
Figure 3-45 The yellow colour of the automotive fuses *140*
Figure 3-46 ADL location on dashboard. *141*
Figure 3-47 Com ports are located on the dashboard for high levels of access during testing and data transference with the remote PCs *142*
Figure 3-48 Rear connection from wiring loom to Com ports. *142*
Figure 4-1 Research measurand as identified in through the collaboration of Professor Rossmanek and Dr Karri. *145*
Figure 4-2 The research measurand depicted on the test rig. *146*
Figure 4-3 The Input Type Instrumentation Sensors *147*
Figure 4-4 The Honeywell GT1 Series Hall Effect Gear Tooth Sensor *148*
Figure 4-5 Gear tooth sensor construction and wiring diagram *149*
Figure 4-6 Hall effect sensor in relation to gear tooth wheel. *150*
Figure 4-7 Induced voltage changes. *150*
Figure 4-8 a) Three piece rim, b) outside view of rim bolts, c) inside view of rim bolts. *152*
Figure 4-9 Simulation setup used in testing the Hall effect sensor. *153*
Figure 4-10 Hall effect sensor mount *154*
Figure 4-11 Dash manager calibration of hall effect sensor *155*
Figure 4-12 The DMU AHRS400CA-200 Sensor *156*
Figure 4-13 Block diagram of the DMU-AHRS sensor *157*
Figure 4-14 Block diagram depicting the signal conditioning operations. *159*
Figure 4-15 The DMU-AHRS400CA-200 coordinate system *159*
Figure 4-16 Error specification of the DMU sensor. *160*
Figure 4-17 Wheel travel linear potentiometer mounted to the test rig. *161*
Figure 4-18 Electrical configuration of the linear potentiometer sensor *162*
Figure 4-19 A representation of a Linear Potentiometer *163*

Figure 4-20 Installation of rear linear potentiometer. *164*
Figure 4-21 calibration curve for front right linear potentiometer. *166*
Figure 4-22 The dial height gauge placed underneath the stub axel nut. *167*
Figure 4-23 Steering Angle Sensor. *168*
Figure 4-24 Steering Angle Sensor installed on the test rig. *168*
Figure 4-25 a) The protractor clamped to the steering wheel at its zero position, b) the reference pointer at zero degrees and, c) thirty degrees clockwise. *170*
Figure 4-26 The calibration curve for the steering angle sensor. *171*
Figure 4-27 The Eclipse Pressure Transducer. *172*
Figure 4-28 Cross-section of a typical quartz pressure sensor. *173*
Figure 4-29 The calibration curve loaded from the existing index available in the Dash Manager software. *174*
Figure 4-30 The MoTeC Advance Dash Logger. *176*
Figure 4-31 Real Time Clock *178*
Figure 4-32 Research Computer *180*
Figure 4-33 RFI-9256 Data Strike Series 3 Spread Spectrum Radio Modem *181*
Figure 4-34 Block diagram of the complete measuring system *184*
Figure 4-35 A diagram illustrating the inputs and outputs of the measuring system *185*
Figure 5-1 Test Vehicle gathering data during dynamic vehicle trials *186*
Figure 5-2 Test courses for neural network training: a) Straight-line acceleration and braking: course 1. b) Figure eight with hairpin and sweeper: course 2. ..... *189*
Figure 5-3 Course 1: Straight-line acceleration and braking test photographed during early stages of testing. *190*
Figure 5-4 Course 2: Figure eight test course data generation. *191*
Figure 5-5 Braking and cornering at different levels of attack producing data sets at different levels of tyre slip. *191*
Figure 5-6 Selected backpropagation neural network featuring double layer architecture with seven hidden layer nodes in each. *193*
Figure 5-7 Front Brake Hydraulic Pressure estimation for test course 1 and calculated absolute error. Errors for peaks 1, 2 and 4 are not due to the neural network (see text for explanation). *195*
Figure 5-8 Rear Brake Hydraulic Pressure estimation for test course 1. ..... *197*
Figure 5-9 Figure eight front brake hydraulic pressure estimation by double layer backpropagation neural network *199*
Figure 5-10 Figure eight rear brake hydraulic pressure estimation by double layer backpropagation neural network *201*

Chapter One

INTRODUCTION

Accurate dynamic brake pressure information is critical for any sophisticated electronic driving assistance system. This represents one of the inputs by the driver of the vehicle along with accelerator and steering wheel position and is used to control and guide a vehicle in motion.

Driving assistance systems using electronic control and intervention technology are already standard equipment on many commercially available vehicles, in the medium to upper market sectors. Advances in vehicle technology ensure that these systems filter down into lower market sectors as new technology and increased production lowers the cost.

Consequently there is a need to develop systems that are of higher performance, safer and cheaper. Development of such systems is recognised as one of the automotive industry's most important challenges. One method of achieving this is by understanding the degree of influence of various system parameters on vehicle braking performance and eliminating those that are non-contributing. This will make the system robust and efficient for computational purposes.

Further is a need to predict brake force values in advance for use in the intervention decision making process of driving assistance systems. By predicting brake force values on line, a brake force controller algorithm coupled with active control systems could keep these within desired optimum performance limits during braking. This study is aimed at contributing toward the development of neural network based dynamic vehicle control systems for predicting braking performance.

Established pressure control methods used in Anti-lock Braking Systems (ABS) have evolved into sophisticated, well proven designs and are also now commonly

incorporated into more complete control systems. Driving assistance systems such as Mercedes-Benz's *Electronic Stability Program* [1] and BMW's *Dynamic Stability Control* [2] assist the driver in avoiding accidents and maintaining control of the vehicle under normal driving conditions. As these systems are refined, the safe driving envelope of an average driver is stretched.

Such state of the art designs use a multitude of sensors and control by *Expert Systems*, as discussed in the next section, to make decisions on what course of action is required. However, every control system has strengths, weaknesses and limitations. By their own admission, the manufacturers of these systems try to find "the best compromise".

In relation to applicability and robustness of the Bosch vehicle dynamic control (VDC) system, Van Zanten et. al. [3] stated: "Due to the design properties of the controller which is based on physical models a basic application of the controller can be achieved by a set of parameters for the models which describe the dynamics of the vehicle and the actuators" . It is these physical models which have been developed to predict, as close as possible, the physical behaviour of any particular vehicle

Limitations of these systems arise wherever conditions dictate that the physical models used by the electronic controller do not sufficiently describe the actual behaviour of the vehicle. Therefore, developers of these brake control systems are using increasingly complicated Traditional and Expert Systems based models in an attempt to increase driver control under circumstances where the assumptions made in defining the simpler physical models are inapplicable.

While many manufacturers are constantly addressing their conventional control systems, emerging technologies such as neural networks and fuzzy logic are replacing conventional systems in increasingly complex non-linear dynamic applications. The following section briefly highlights the major differences between these methods.

1.1 How Neural Networks are Different form Traditional and Expert Systems: An Alternative Approach

Neural networks offer an alternative way to analyse and develop data into functional predictive models. Neural Networks are a powerful engineering tool, as they can be used to recognise patterns in data and later make generalised decisions based on those patterns.

Traditional computing methods have been proven for well defined and categorised problems such as keeping an inventory, managing finances and statistical analysis. Neural networks, on the other hand, with their intrinsic ability to learn are used as intelligent tools for decision making processes. [Figure 1-1] highlights the major characteristics and applications of traditional and Neural Network based systems.

Characteristics	Neural Network	Traditional Computing (including Expert Systems)
Processing style	Parallel	Sequential
	Gestalt (Right Brained)	Logically (Left Brained)
Functions	Images	Rules
	Pictures	Concepts
	Controls	Calculations
Learning Method	Example Based	Rule Based
Applications	Sensor Processing, Image, Speech and Pattern Recognition	Accounting, Statistical Analysis, Word Processing, Mathematics, Inventory

Figure 1-1 Characteristics of Neural Network and Traditional Computing Systems.

Computing system development is often categorised into generational steps. The first generation of computer systems used switches and wires with the second generation born from the development of transistors. Third generation involved integrated circuits

and solid state technology with the use of higher level languages such as FORTRAN, C, and COBOL. The fourth generation involves end user tools such as "code generators".

The fifth generation of computing, often called Expert Systems use Artificial Intelligence, commonly in the form of an interference engine, together with a knowledge base. The generic interference engine handles the user interface, external files, program access and scheduling. The knowledge base contains all information specific to the given application allowing a user to define the rules that govern the given process. Note that the user does not need to know traditional programming techniques in order fulfil this function.

The user does however need to know both what they want the computer to do and also how the larger mechanism of the expert system shell works. This shell is part of the interference engine and directs the computer through the implementation of the user needs. In this manner, the expert system generates the decision-making programming for the individual process. The macro program that the expert system uses to create these *process programs* develops rules in a complex way.

Efforts to develop a general expert system for the use with various processes have encountered problems. Increases in system complexity results in the requirement for greater computing power and the system becomes too slow. The current success and feasibility of expert systems is somewhat limited to specific, narrowly confined, applications.

Sometimes referred to as the sixth generation of computing, artificial neural networks represent a completely different approach to problem solving. Artificial neural networks do not require assumptions to be made by a programmer in order to model a system. Instead artificial neural networks can be trained using measured data, as a result a neural network can be used to find and identify patterns within data that are previously unidentified.

[Figure 1-2] highlights the different features of neural network and expert systems characteristics. It can be seen in this Figure that the neural network systems are

modeled, in part, on the biological brain where the expert systems are not. This biological based architecture of the neural network gives the network many of it's other characteristics such as the high fault tolerance, the adaptable learning capabilities and the self programming connections.

Characteristics	Neural Network	Expert Systems
Memory	Integrated	separate
Processing Approach	Multiple Simultaneous Data Processing: Data Set Processing	Sequential: Single Problem Rule Processing
Connections	Dynamic, Self Programming	Externally Programmable Program: Mechanism Must be Supplied
Self Learning	Continuously Adaptable	Only Algorithmic Parameters are Modified
Fault Tolerance	Significant, Gradual Introduction of Error with Sequential Neuron Failure	Special Processors Required for Fault Tolerance
Use of Neuro-biology in design	Moderate	None
Hardware Requirements for Speed	Requires Multiple Custom-Built Microchips or large Processors	Requires Large Processors

Figure 1-2 Neural Network and Expert Systems Comparison.

Although Artificial Neural Networks are self-programming, the network architecture must be designed appropriately in order to be useful as problem solving tools [4]. In order to do this, a good understanding of the physical problem is required. In this work the physical problem involves measuring and predicting brake forces in order to

incorporate these functions into a neural network electronic brake control based driver assistance system.

In order to identify ways in which an electronic brake control based driver assistance system could operate, it is imperative to understand the nature in which a vehicle interacts with its surroundings. The following sections discuss the details of vehicle/driving environment interaction with particular attention to the most important dynamic connection between the road/track surface and the tyres.

1.2 FUNDAMENTAL CONCEPTS IN VEHICLE PHYSICS

Vehicles in motion are effected by many different kinds of forces. During normal operation, a vehicle will be subjected to forces along the longitudinal axis such as propulsive force, aerodynamic drag, rolling resistance, and braking forces. At the same time some forces are applied laterally such as cornering forces (centripetal forces) and cross wind loading. The road or track surface provides a normal force allowing transference of all net force acting on the vehicle through the tyre contact patches.

The tyre contact patch, depicted in [Figure 1-3], is the proportion of the tyre in contact with the road or track surface. It is the transitional element where vehicle dynamics, performance and stability are ultimately defined.

1.2.1 Tyre forces

The road or track supporting the weight of the vehicle exerts normal tyre forces. These normal tyre forces reshape the tyre against the road's surface. In this way, normal tyre forces are distributed over the tyre contact patch in a pressure distribution.

The construction of tyres prevents this pressure distribution from being uniform [5]. The sidewall s of the tyre that are developed and constructed taking cornering forces into account are also affected by reshaping under the weight of the vehicle, resulting commonly in a trapezoidal type of pressure distribution with slightly raised pressure

points (local maxima) along transitions between sidewalls and tyre tread. The complex shape of a typical tyre pressure distribution over the contact patch is shown in [Figure 1-3].

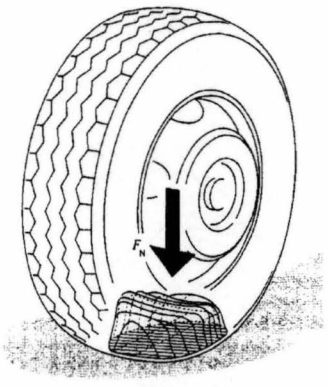

Figure 1-3 Tyre pressure distribution. [5]

Longitudinal forces act on the tyre as it is rolling along the road or track surface. The net result of these forces is acceleration of the vehicle under power or during braking. These forces can be seen in [Figure 1-4] where a braking torque is applied to a rolling wheel.

The magnitude of such a braking force is the product of the torque applied to the wheel through the brake disk (M_B) and the radius of the tyre (r). There is, however, a limiting condition reached when the tyre begins to slip against the road surface. In this case the accelerating or braking force is equal to the product of the normal tyre force (F_N) and the coefficient of friction of the tyre/surface combination (μ).

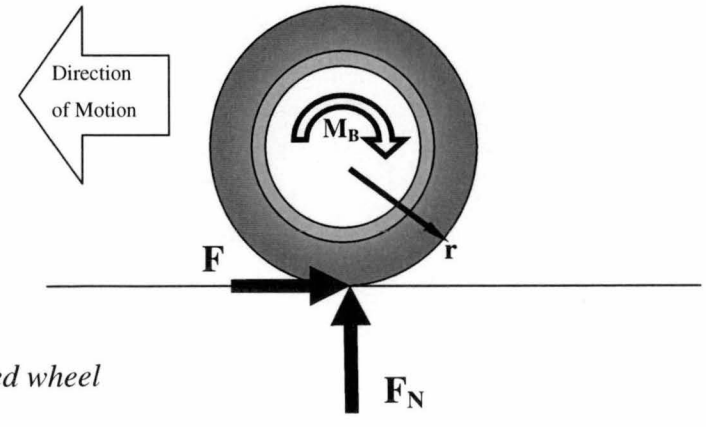

Figure 1-4 Moment acting on a braked wheel

1.2.2 Weight transferral

The value of the normal force on the tyre is dependent on the weight, and is also subject to acceleration, of the vehicle. [Figure 1-5] shows a vehicle in a steady state with neutral weight distribution (all four wheels loaded to the same level). In this depiction the vehicle with neutral weight distribution can either be standing still (static equilibrium) or at a constant velocity (dynamic equilibrium).

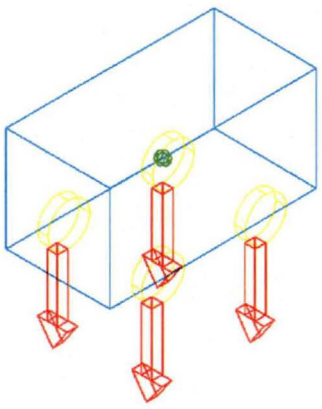

Figure 1-5 Vehicle in equilibrium [6]

In [Figure 1-6 (a)] the same vehicle is depicted under straight-line acceleration. The acceleration of the car causes transferral of weight from the tyres at the front of the vehicle to the tyres at the rear. This weight transference can be seen visually as cars 'squat' under power or as drag cars 'wheelie' (extreme case where all weight is transferred to the rear tyres).

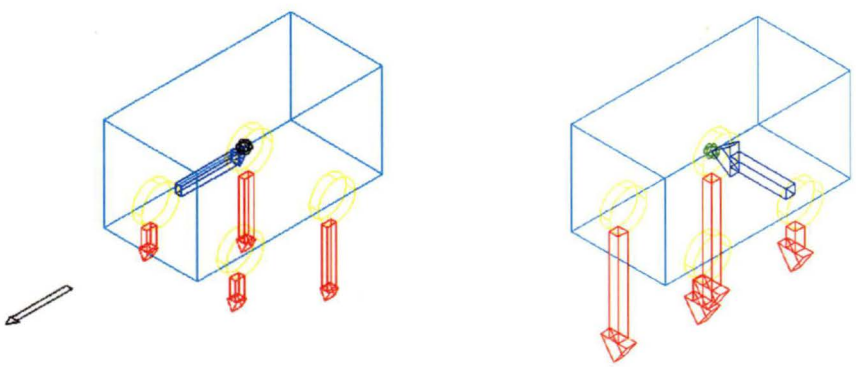

(a) (b)

Figure 1-6 Weight transferral: (a)under acceleration (b)while turning [6]

In a similar way weight is transferred under cornering and braking. This transference of weight (changes in normal force) can be seen in [Figure 1-6 (b)].

Weight transferral has the effect of altering the ultimate brake force that can be transmitted through the tyre contact patch since the limiting condition is reached where the braking force is equal to the product of the normal tyre force (F_N) and the coefficient of friction of the tyre/surface combination (μ).

Since brake force is dynamic and the introduces weight transference as braking proceeds, the ultimate brake force which can be sustained by the front and rear tyres is also dynamic and changes with increases in braking pressures. These changes shown graphically in [Figure 1-7].

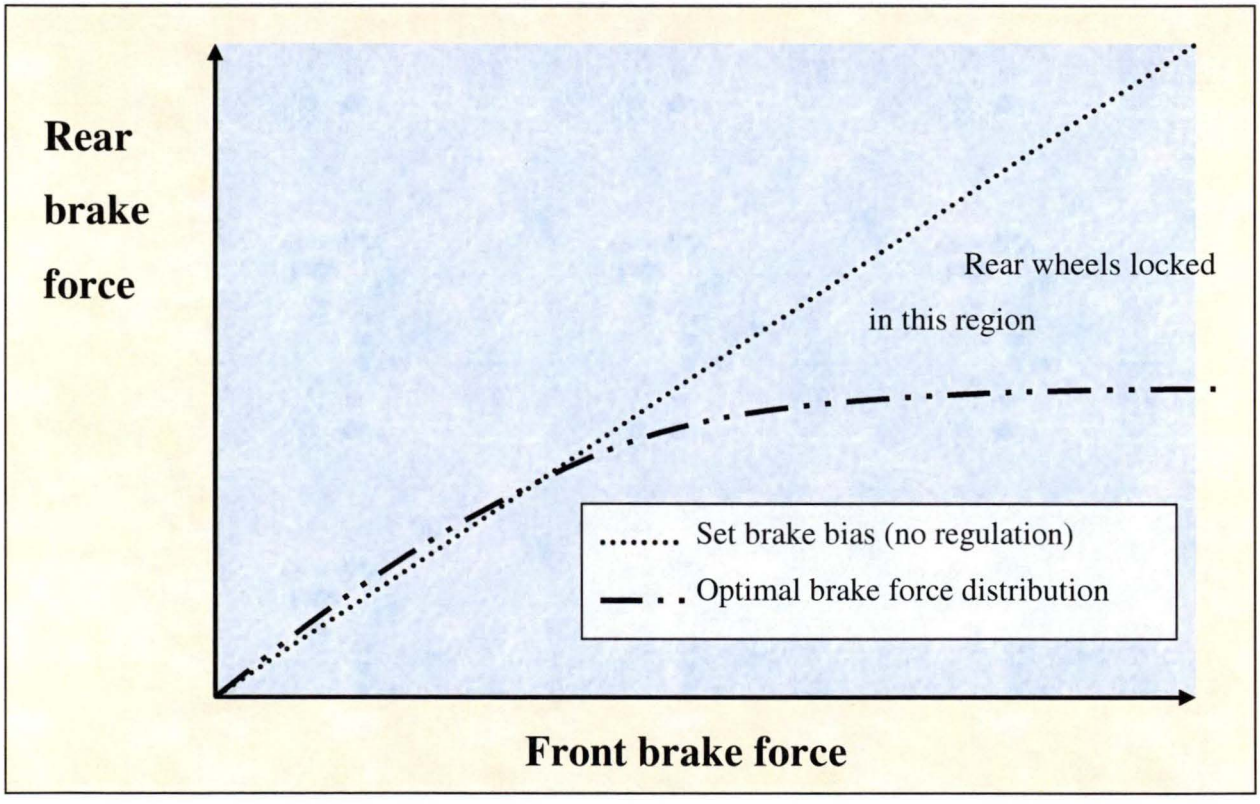

Figure 1-7 Optimal brake force distribution due to weight transferral under braking [7].

[Figure 1-7] shows how the optimum front:rear brake force distribution changes as overall brake force is increased. Weight transferral is responsible for the shape of the

optimum curve where the brake force distribution is the same as the corresponding normal tyre force distribution.

While braking, weight transfers from the rear wheels to the front. Applying equal (or even properly adjusted fixed proportional) brake force to front and rear wheels will eventually cause the rear wheels to lock under hard braking. If the optimal distribution curve is followed, all four wheels will slip at the same level until locked.

The conventional models used in brake force control systems, with the aid of mechanic and dynamic testing, get increasingly complex as the number of control parameters are increased. As discussed earlier neural networks are alternative modeling techniques and the next section will deal with both conventional and emerging NN attempts in automotive control. Within the next chapter is a review of state of the art in brake pressure studies and commercial control systems. There is a need however, in the first instance to understand and define the terms of vehicle dynamic control and most importantly the nature of tyre slip that ultimately defines the limit of all automobile dynamics.

Chapter Two

LITERATURE SURVEY

Friction between a vehicle tyre and the road/track surface is used to drive, brake and steer a vehicle in motion. In order to estimate braking pressures under all conditions it is necessary to understand the forces transmitted through the contact patch between the tyres and the road/track.

The problem of estimating and predicting brake forces originates from the complex nature of tyre slip in both longitudinal and lateral directions simultaneously. The following parameters are defined:

- Longitudinal Tyre Slip, λ_L
- Lateral tyre slip

It is also important to understand how these parameters limit and effect the forces transmitted through the tyre contact patch for all loading (accelerating steering and braking) combinations. These parameters and their consequences are discussed in this section.

2.1 TYRE SLIP (LONGITUDINAL SLIP, λ_L)

Rather than attempting to actually measure the road coefficient of friction of the tyre/surface combination (μ) which varies with the conditions, it is convenient to use longitudinal tyre slip, λ_L, where $\mu = f(\lambda_L)$ to describe wheel slip dynamics.

Tyre slip is an expression of the difference between the distance actually covered by the tyre tread and the distance covered by the vehicle. Whether or not the vehicle in question is visually spinning the wheels, the inherent flexibility of the tyres on any driven wheels will give some degree of slip.

Therefore there is a need to define a measurement scale for slip, traditionally this is in the form of a slip ratio. This provides a reference for further analysis since the forces generated at the tyre contact patches are a function of the slip ratio [Equation 2-1].

$$\lambda_L = \frac{x_2 - x_1}{\max(x_1, x_2)}$$

Equation 2-1 Slip ratio definition [8]

Where: x_1 = vehicle speed

x_2 = wheel speed

While rolling along any surface of a road or track, a driven or braked wheel is subjected to deformation while continuously flexing, accepting roughness and irregularities. The dampening properties of rubber dictate that only part of this deformation energy is recovered as each portion of the tyre is cycled through the contact patch. Some of this energy can be observed as the tyres begin to heat up.

Physically the extent of force transfer through to the road or track surface, and hence acceleration, is dependent on tyre slip rates. The relationship between tyre slip and tyre coefficient of friction is the same [1] whether the vehicle is braking or accelerating. This relationship is described in [Figure 2-1].

Friction factor $\mu_{A/B}$ as function of slip λ during braking

1 Radial tire on dry concrete,
2 Cross-ply winter tire on wet asphalt,
3 Radial tire on loose snow,
4 Radial tire on wet black ice.
Cross-hatched surfaces:
Transition from stable to instable range.

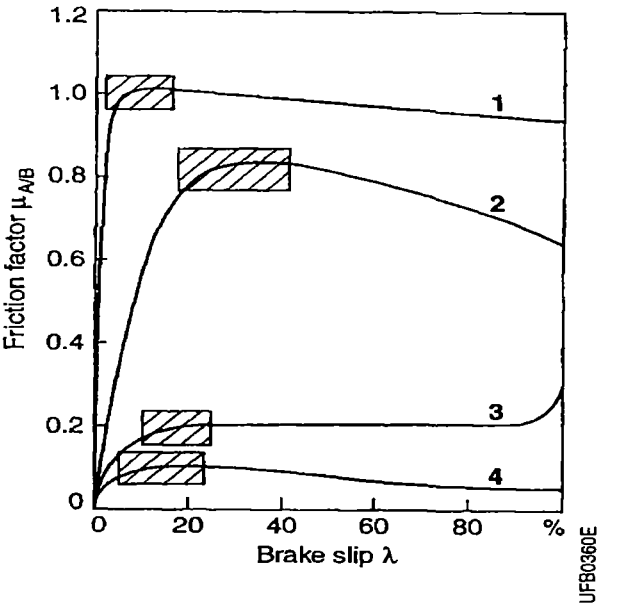

Figure 2-1 Friction factor vs slip [1]

[Figure 2-1] shows brake slip and friction factor plots for various tyre and surface combinations. The general trend shows a rapid increase in friction factor in the first 5 - 20% of brake slip. This is the area where the majority of normal driving and to a smaller extent motor racing takes place - at minimal slip rates within a stable part of the curve.

The next important feature of the plots are the peaks, highlighted by the hatched rectangles, where the tyre is achieving the maximum levels of friction (friction factor) on the road or track surface. This corresponds to maximum acceleration of the vehicle under braking and is the ultimate point where anti-lock braking systems (discussed later) aim to operate the vehicle. It also corresponds to the transition from stable to unstable braking.

The remainder of the plots shows a decline in friction factor as the wheels tend toward fully locked at 100% brake slip. This is the unstable portion of the curve since any increases in slip generated will lead to full wheel lock typically within tenths of a second.

An interesting phenomenon is observed in [Figure 2-1, curve **3**] where there is a sharp increase in friction factor in the last 10% as the radial tyre is locked on loose snow. This is related to geometric changes in tyre/surface interaction. On loose surfaces such as gravel or snow a locked wheel will gather a pyramid of the surface material from the leading edge of the contact patch and around the front of the tyre. This pyramid effectively increases the size of the contact patch and provides additional drag on the wheel. This phenomena is worth noting as it represents an exception to the general trend that can not be ignored when applying brake controller systems to off road vehicles.

Perhaps the most relevant observation that can be made from the *Radial tyre on dry concrete* plot [Figure 2-1, curve **1**] that locking the wheels only reduces the friction factor and hence braking distance by less than10% of maximum possible values. While this alone may prevent an accident, it does not seem like enough to warrant such attention to anti lock systems. The answer to this is due to the lack of directional control (steering) available while the wheels are locked.

The level of longitudinal slip effects the forces that can be generated laterally by the tyres. In the case of full wheel lock the lateral (steering) forces obtainable from the tyres is reduced significantly from free rolling wheels. The following section highlights the dynamics of lateral tyre force generation and how changing normal forces and longitudinal slip effects it. Firstly however, lateral slip must be defined.

2.2 LATERAL SLIP

Lateral tyre force experienced by a vehicle during cornering or in a heavy side wind loading situation causes lateral slip of the tyre. The result of this is that the tyre slips in a direction other than longitudinal.

Consider a wheel viewed from above with a side ways loading F_S:

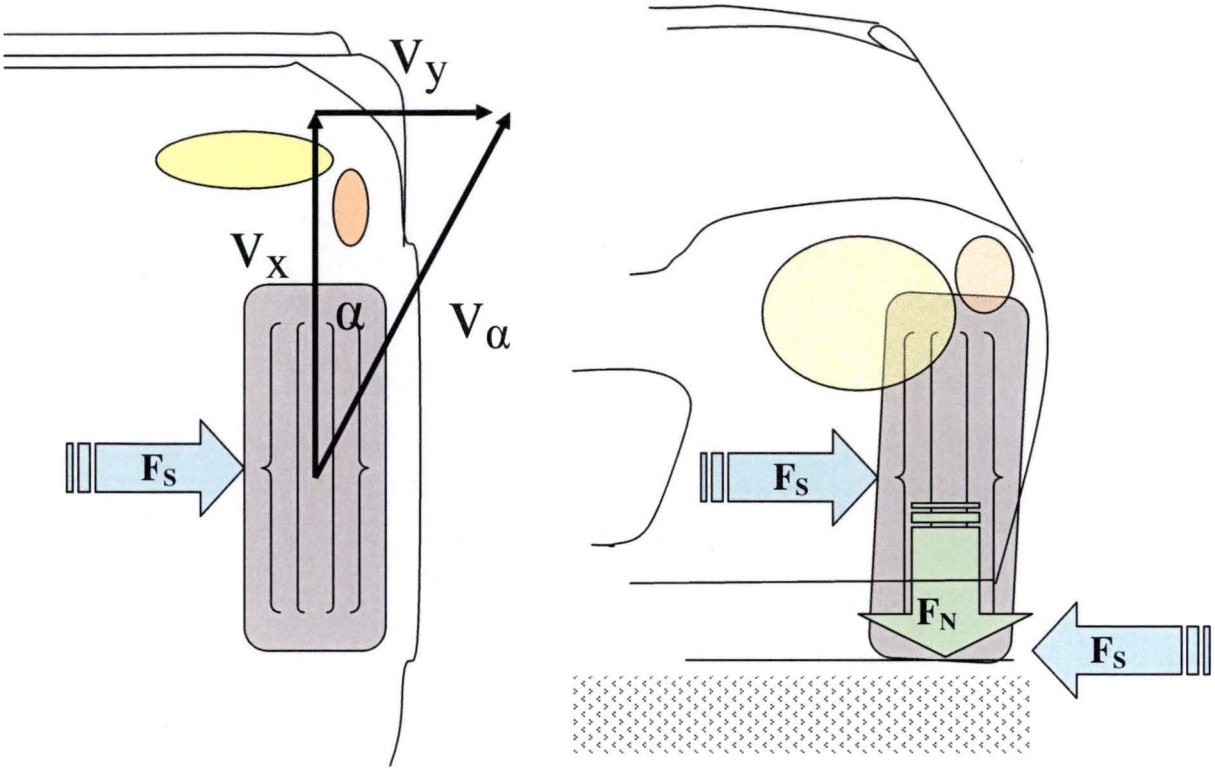

Figure 2-2 Lateral forces during cornering

In [Figure 2-2], the wheel is loaded at the hub in the direction shown. The result of this is that the wheel travels with velocity, V_α. The angle between the longitudinal velocity, V_x, and V_α is defined as the slip angle, α, shown on the left-hand side of [Figure 2-2].

The ratio of lateral velocity, V_y, and V_x is defined as lateral slip (ratio). The ratio of the lateral force to the wheel normal force through the tyre is defined as the coefficient of lateral force μ_S. Note the geometric relationship:

$$\alpha = \tan^{-1}\frac{Vy}{Vx}$$

Equation 2-2

Where: V_y/V_x = lateral slip (ratio).

Equation 2-3

The relationship between lateral force and the wheel normal force is complex. This is further complicated as slip angle in introduced as a variable. [Figure 2-3] shows the general trend of the relationship between lateral force and the wheel normal force with the higher curves on the chart representing greater slip angles.

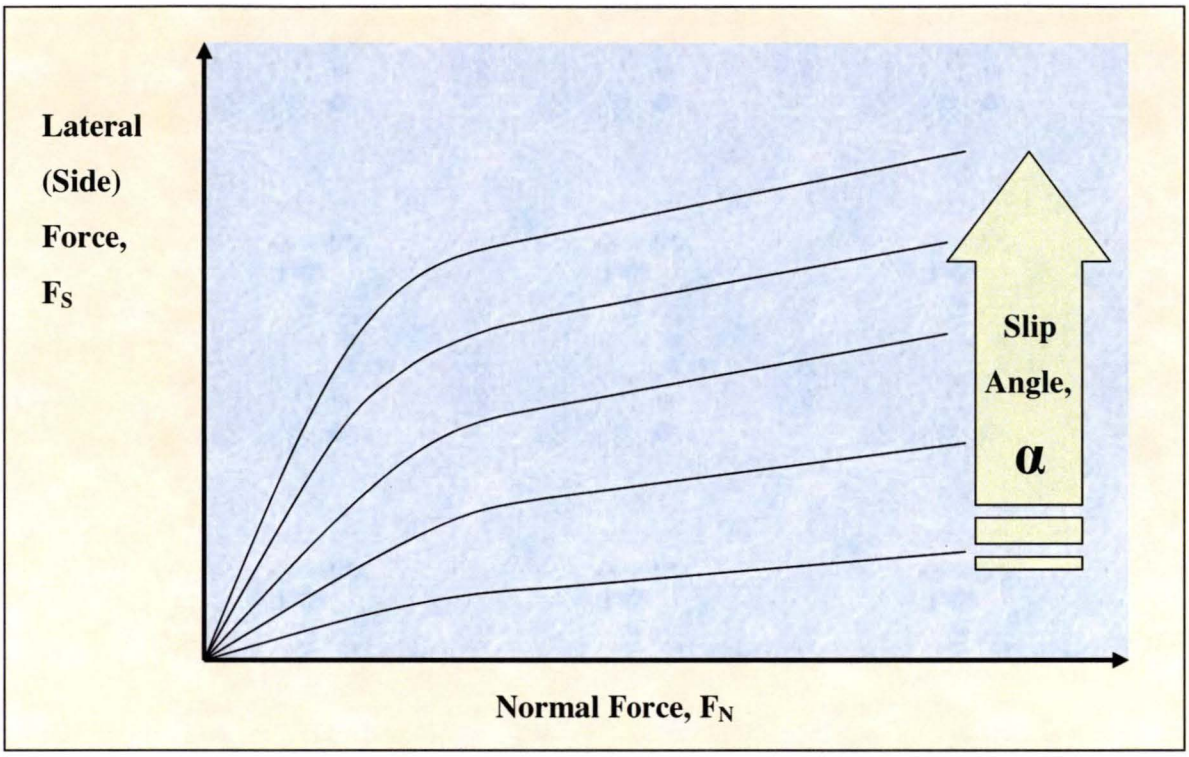

Figure 2-3 Lateral force as a function of normal force and slip angle. [9]

[Figure 2-4] shows the same graphical information as [Figure 2-3] with an example of a rear wheel drive vehicle's front wheels during a cornering manoeuvre Imposed on the Figure. This example is cited in a effort to describe the nature of the Figure and how it applies to vehicle dynamics.

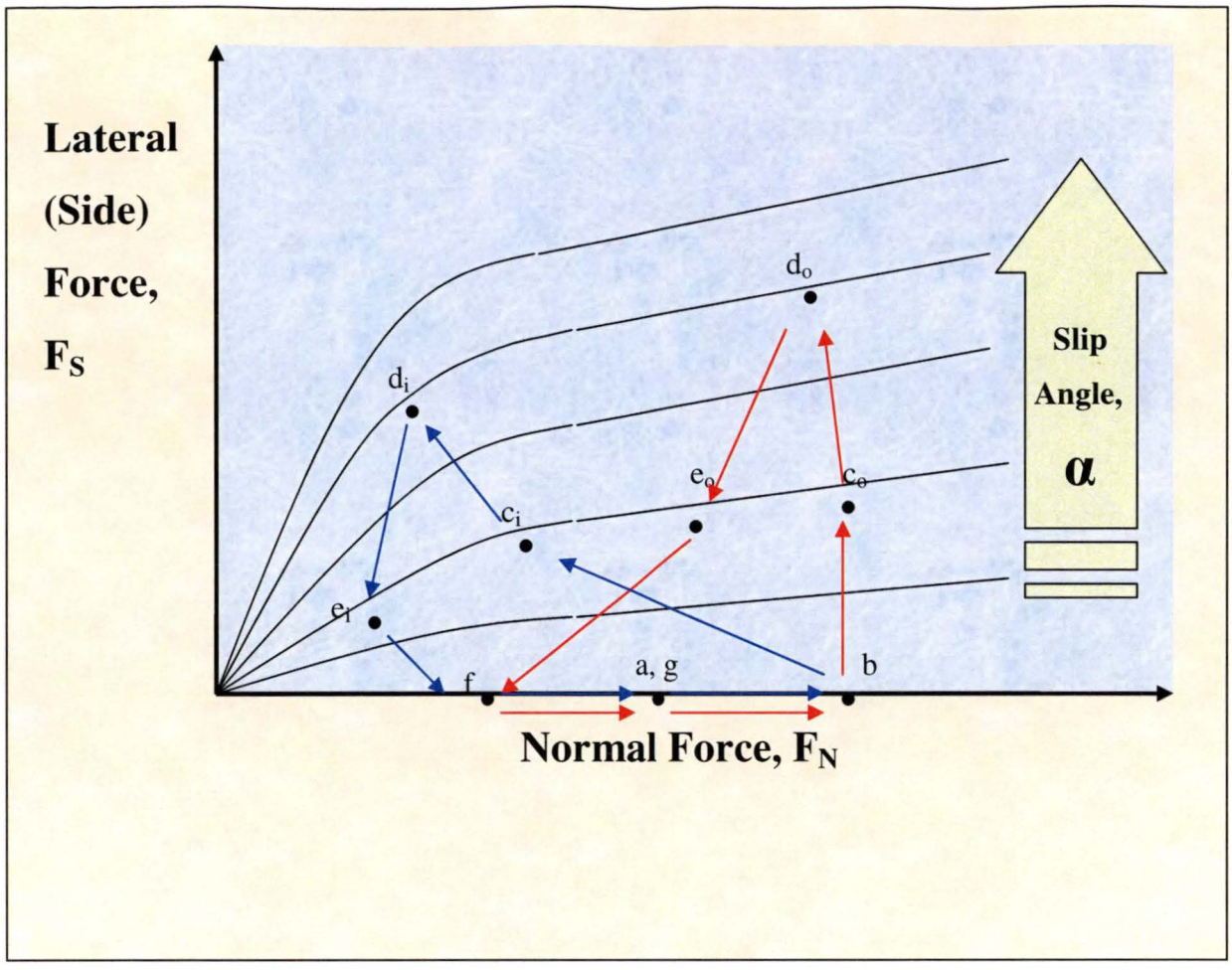

Figure 2-4 Lateral forces generated by the front wheels during vehicle cornering. [9]

Now it is also important at this stage to consider that the normal force on an individual wheel will vary as the vehicle is accelerated, steered and braked due to weight transferral effects as discussed in the introduction.

With reference to Figure 2-4, an analysis will be carried out on a rear wheel drive vehicle while completing a cornering manoeuvre on a typical test course. This is a simplified analysis where the front wheels will be followed and the vehicle is driving within the stable portion of the slip curve [Figure 2-1]. Further geometric complications related to the level of Ackerman steering [10] and smaller geometric effects are omitted.

Before the corner at point **a** in [Figure 2-4], the vehicle is in dynamic equilibrium (not accelerating with a constant velocity). Approaching the corner, the vehicle is braked

until point **b**, transferring much of the weight of the vehicle onto the front wheels. At point **b** the front wheels are steered. The steering angle is slowly increased through points $\mathbf{c_I}$ and $\mathbf{c_o}$ until maximum lateral forces and slip angles are reached at points $\mathbf{d_I}$ and $\mathbf{d_o}$ corresponding to the apex of the corner. Here it is clear the normal force on the inside tyre denoted by $\mathbf{d_i}$ is significantly less than that of the outside tire denoted by $\mathbf{d_o}$ due to the weight transference associated with the high lateral acceleration of the vehicle.

After the apex the steering angle is slowly decreased. Acceleration out of the corner begins to relieve the front wheels of load through points $\mathbf{e_I}$ and $\mathbf{e_o}$. At point **f**, the vehicle is exiting the corner and is under pure longitudinal acceleration. The vehicle eventually reaches terminal speed (dynamic equilibrium) at point **g**, corresponding to the condition before the corner, **a**.

From this example it can be seen that a tyre under normal driving conditions is subject to both lateral and longitudinal forces simultaneously. The next section looks at this in detail, as combinations of lateral and longitudinal loads impose limits on the driving envelope of an automobile.

2.3 LOAD COMBINATIONS

Loading on a vehicle tyre is very rarely purely longitudinal or lateral. The majority of the time vehicles are simultaneously steered and braked or accelerated. Since there is only a finite amount of traction available from the tyres, any vehicle is only able to brake or accelerate at maximum rates when it is in a straight line. Similarly, to maintain maximum sideways loading and hence corner speed, a vehicle must not be accelerated longitudinally.

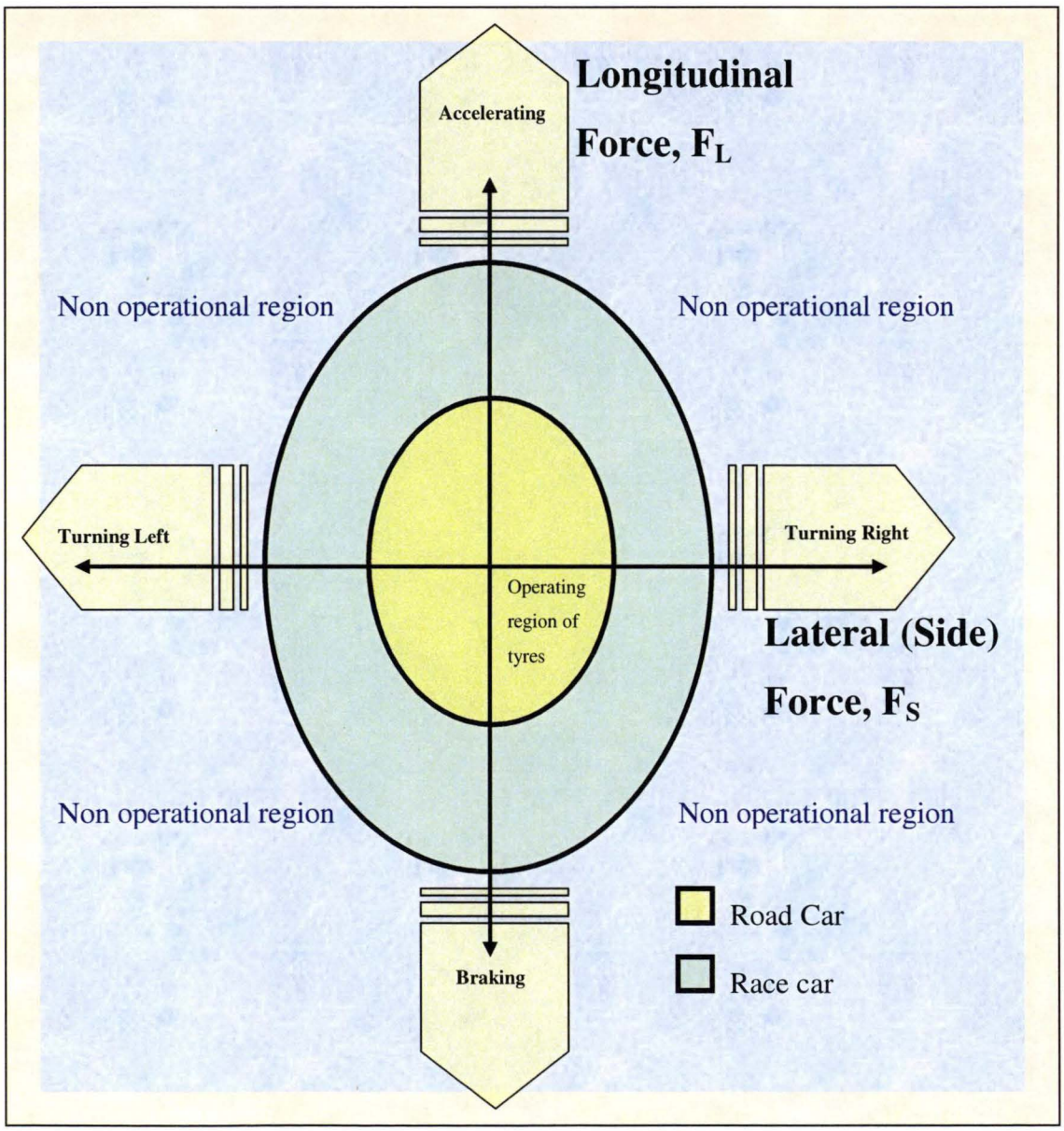

Figure 2-5 The friction circle [1]

Plotting load combinations of all possible lateral and longitudinal force results in a diagram known as the friction circle that defines the limits of combined acceleration, braking and cornering.

The friction circle [Figure 2-5] is an expression of the total driving envelope of a vehicle. On the friction circle plot, a circular or oval shape represents the driving envelope of any particular vehicle. The operational region inside the circle represents values of combined loading that are possible for a given vehicle/tyre/surface combination. The non-operational region represented by the area outside the circle is a region where the maximum physical forces that can be produced by the tyres as shown in [Figure 2-1] are exceeded. A vehicle therefore can never operate outside its own friction circle.

On the friction circle plot [Figure 2-5] is a generalised friction circle plot for a road car and a generalised plot for a racecar. Racecars typically offer higher performance in the areas of grip on the road/track surface since they are purpose built or modified to achieve fast lap or stage times. Thus the friction circle of a racecar is much larger than that of a typical road car since the racecar can generate greater forces while accelerating, braking and cornering. Though the driving envelope is larger, a racecar has a friction circle plot that is similar in shape to the road vehicle since the same limits apply. Both race tyres and road tyres can only produce their greatest lateral forces while free wheeling (not accelerating or braking) and their greatest longitudinal forces in a straight line.

Combining the information in [Figure 2-3 (2-4)] and [Figure 2-5] allows gives an appreciation of individual tyre force capability for each tyre as it is effected by weight transferral while accelerating, braking and cornering. Thus a map can be created to express the total tyre force capability of the tyres.

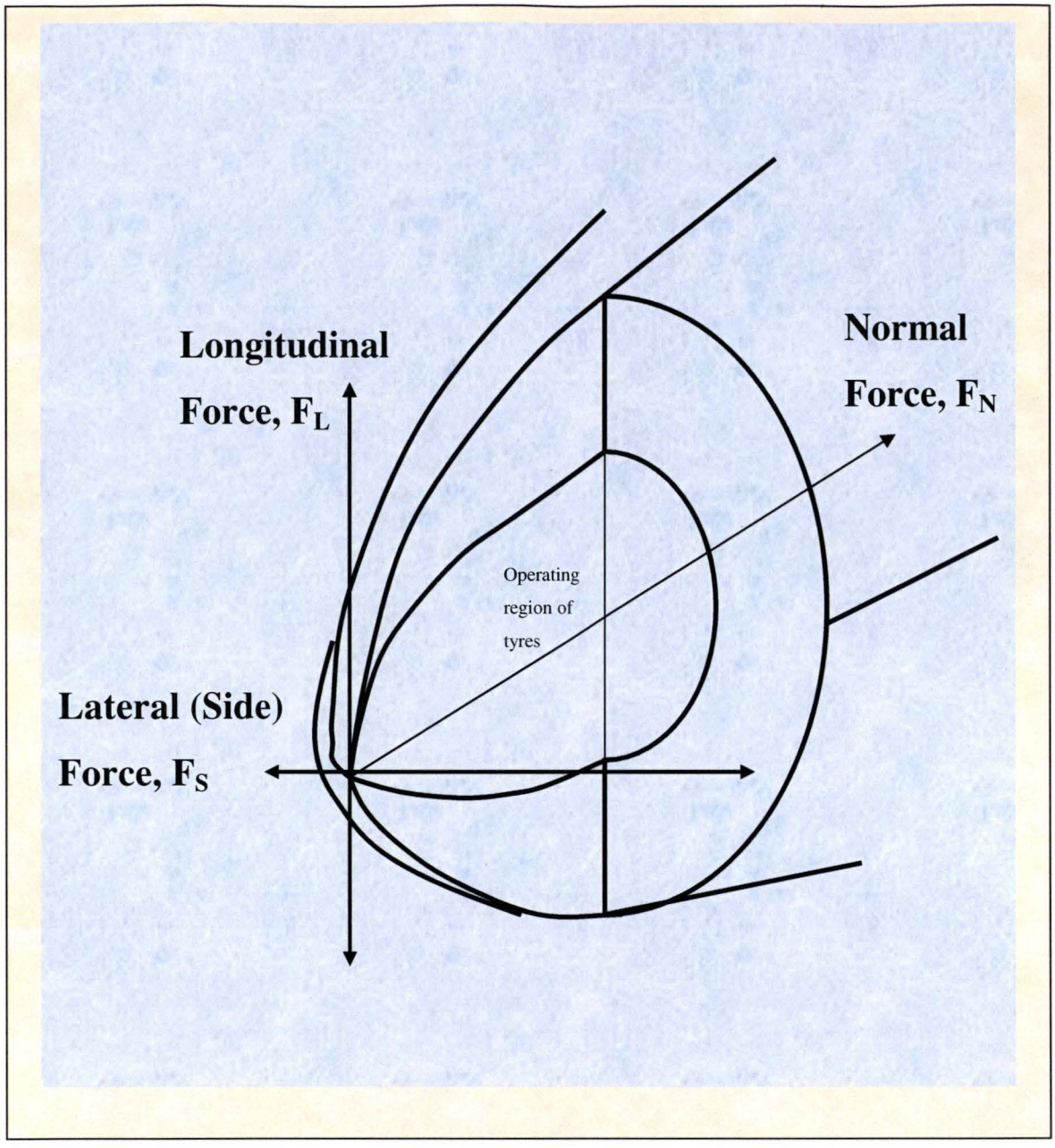

Figure 2-6 Total tyre force capability map [9]

As plotted in [Figure 2-5] the friction circle axes indicate forces in the lateral and longitudinal directions, however this does not allow for direct comparison of vehicle performance from one vehicle to another. The problem with direct comparison can be seen in [Figure 2-6] where it is evident that a heavier vehicle (larger normal forces) will produce larger lateral and longitudinal tyre forces. For direct comparison, friction circles are plotted for vehicles using accelerations in the longitudinal and lateral

directions, usually expressed in g . [Figure 2-7] [8] is a plot from measured data showing typical values achieved by a sports car.

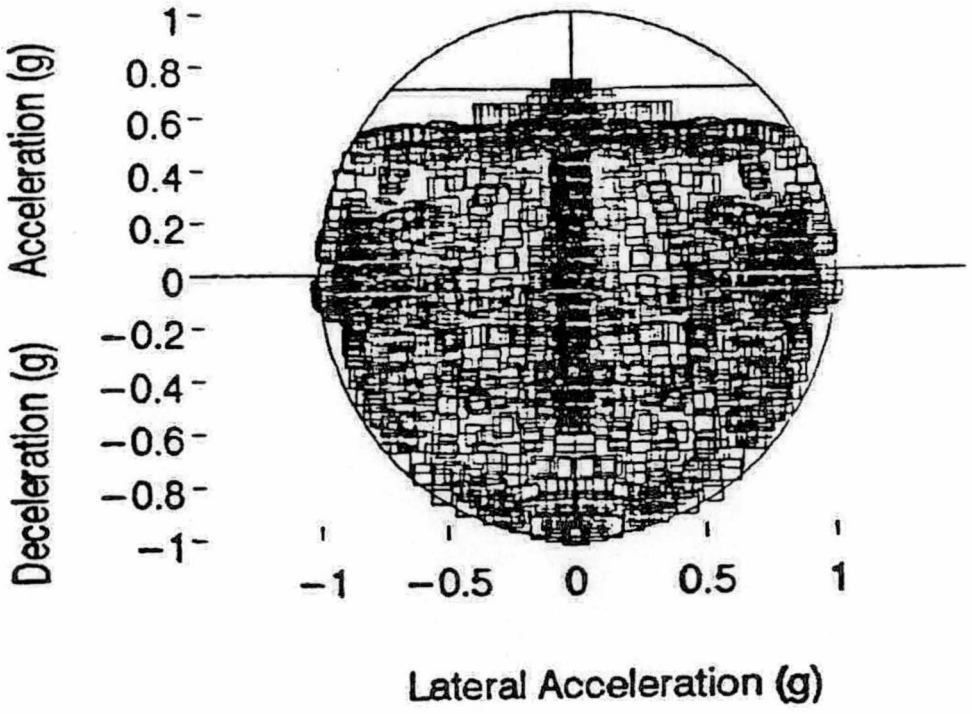

Figure 2-7 Friction circle plot from measured data for a typical sports car [9]

[Figure 2-6] represents the physical limits of forces transmitted through a vehicle tyre under while subject to changing normal forces due to weight transferral. What the diagram does not do however, is describe how these physical limits are affected by tyre slip (λ_L) and slip angle (α) defined earlier in this chapter.

When tyres are operated under conditions where both longitudinal and lateral slip is present any increases in longitudinal slip reduces the lateral force experienced by the tyre.

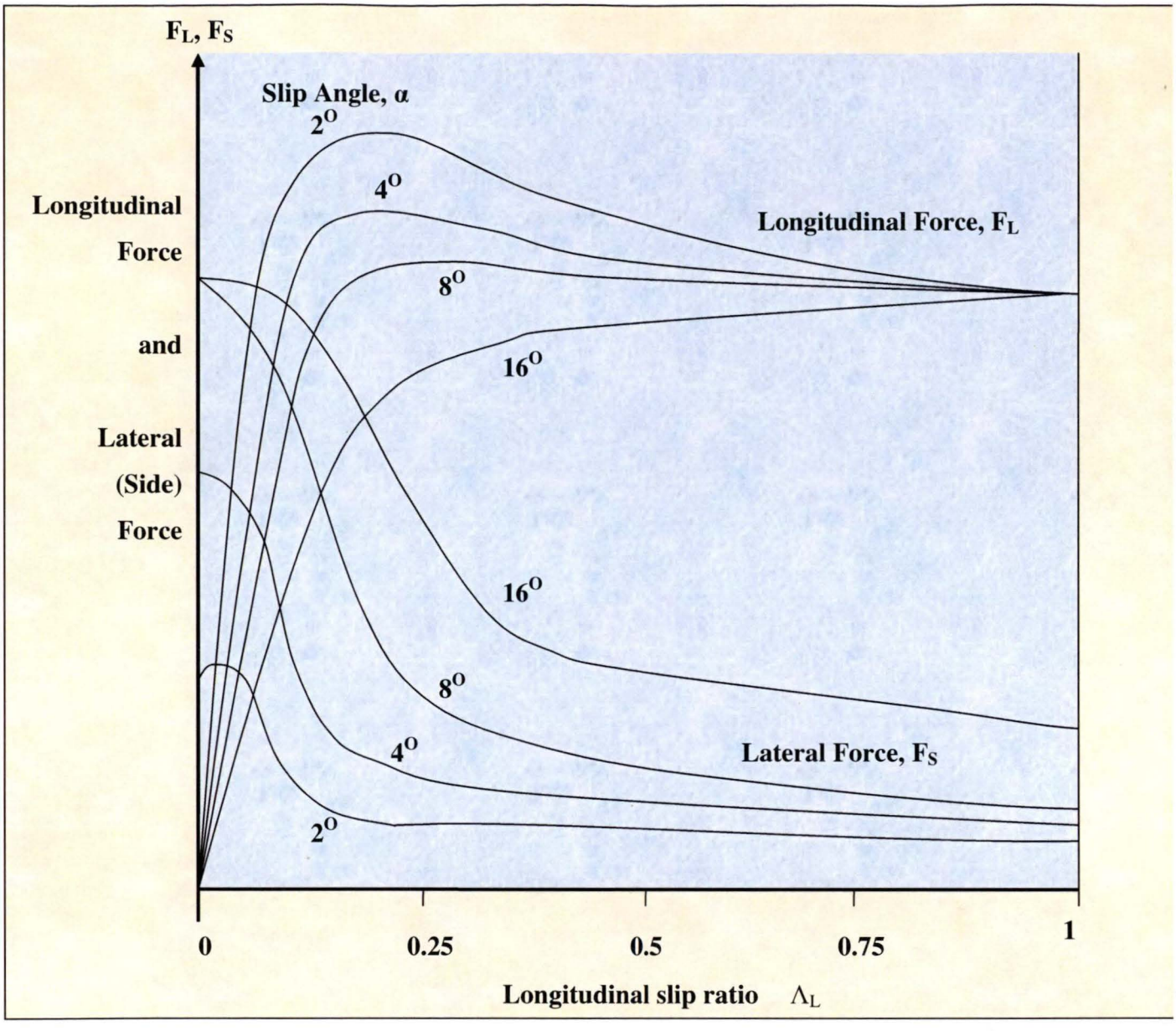

Figure 2-8 Longitudinal, F_L and lateral forces, F_S as a function of slip ratio, λ_L and Slip angle, α.[8]

[Figure 2-8] shows that small slip angles allow for high longitudinal forces and result in small lateral forces. Conversely, larger slip angles correspond to lower longitudinal and higher lateral forces.

In [Figure 2-8] lateral forces are at their maximum where there is no longitudinal slip. This phenomenon is observed in the friction circle diagram [Figure2-5] where the circle intercepts the horizontal axis and corresponds to the all possible force generated through the tyre contact patch being used to steer the vehicle.

[Figure 2-8] also shows another trend which can also be seen on the friction circle [Figure 2-5] where the slip angle approaches zero as the longitudinal forces increase to maximum limiting values. On the friction circle diagram this is the point where the circle intersects the vertical axis. These maximum limiting values correspond to maximum longitudinal acceleration (or braking) of the vehicle.

This description of the forces that can be generated through the tyre contact patches to control a vehicle leads to the next section where there is discussion on the commercially available state of the art control systems that use electronic brake-force distribution or EBD. Controllers for these systems are predominantly based on fundamental tyre/surface interaction.

2.4 Commercial State of the Art Automotive Control Systems Using Electronic Brake-force Distribution (EBD)

Electronic brake-force distribution (EBD) is one of the most useful tools available today for maintaining control of vehicles during emergency situations. There are many different systems which use EBD, these include things like Traction Control Systems (TCS), Electronic Stability Programs (ESP, also known as DSC [Dynamic Stability Control], VSC [Vehicle Stability Controller], VDC [Vehicle Dynamics Controller], UCC (TRAXXAR) [Unified Chassis Control] and many others) and Anti-lock Brake Systems (ABS).

As an example of EBD, the principles and development of Anti-lock Braking Systems, ABS, will be discussed in detail. Early ABS were only two channel [Figure 2-9] where

each of the front wheels were controlled individually while each rear wheel is controlled simultaneously with the diagonal front wheel outlined by Demel et al [11].

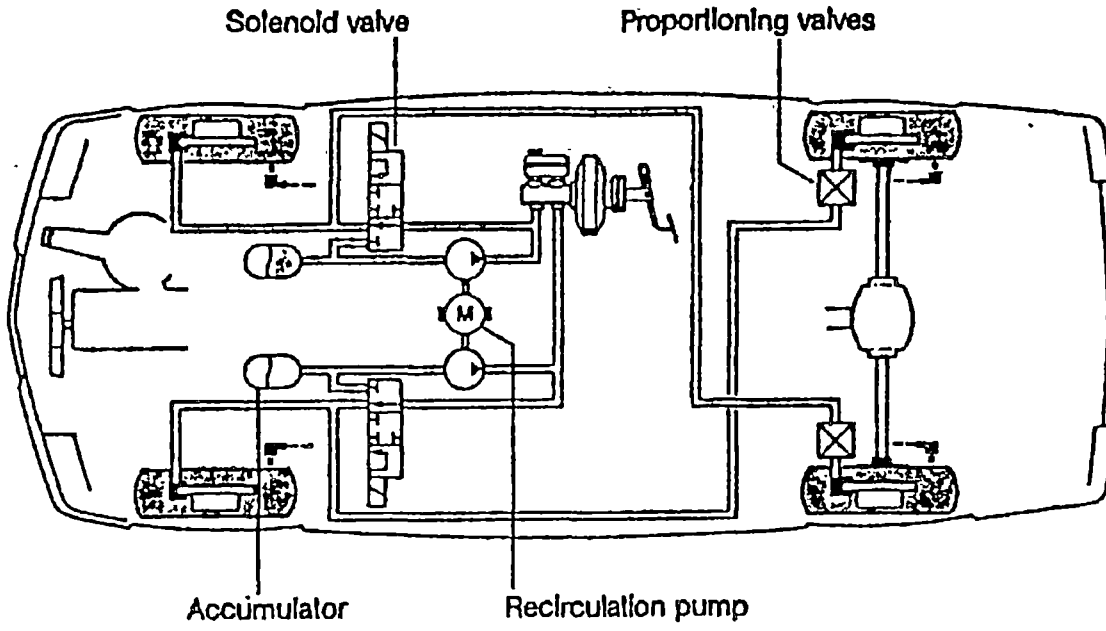

Figure 2-9 Hydraulic circuit of two channel ABS [11].

As depicted in [Figure 2-9] the hydraulic circuit of simple ABS contains:

- 1solenoid valve per channel
- Accumulator(s)
- At least 1 recirculation pump

[Figure 2-9] also includes proportioning valves to limit pressure to the rear calipers and delay rear wheel lock up during hard braking. This is only necessary on two channel systems where the rear wheels have no pressure limiting solenoid of their own.

Three channel systems [Figure 2-10] soon followed which measured the wheel speed of each individual front wheel as well as the speed of the differential or transmission [7] and control pressure. Alternatively three channel systems have been installed with four wheel speed sensors using the "select low principle" [11] where the controller selects the lowest rear rotational wheel speed to determine how best to limit brake force to both rear wheels.

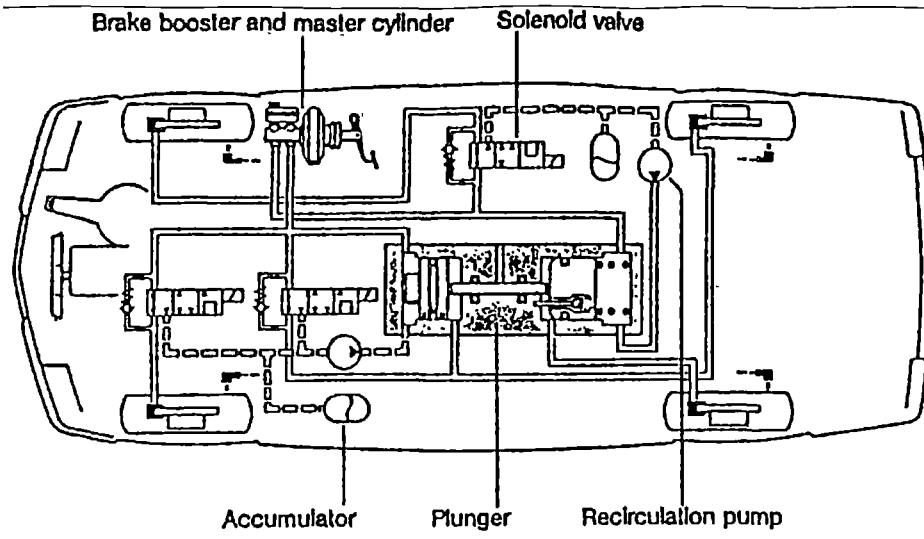

Figure 2-10 Three channel ABS Hydraulic circuit

In the differential speed measuring type of three channel ABS the probability of locking a rear wheel during emergency braking is actually quite high. With all three channel ABS maximum braking effectiveness is unlikely to be achieved by the rear wheels in anything other than ideal conditions. Despite these limitations three channel systems are still widely used on vehicles with modest price tags.

To achieve optimum braking performance the individual pressures of each wheel brake needs to be controlled. This is a requirement since each corner of the vehicle in a dynamic driving environment experiences slightly different conditions. Thus Four channel ABS [Figure 2-11] (one solenoid valve per wheel) has become an industry standard for safety and performance in the sport and luxury car sectors.

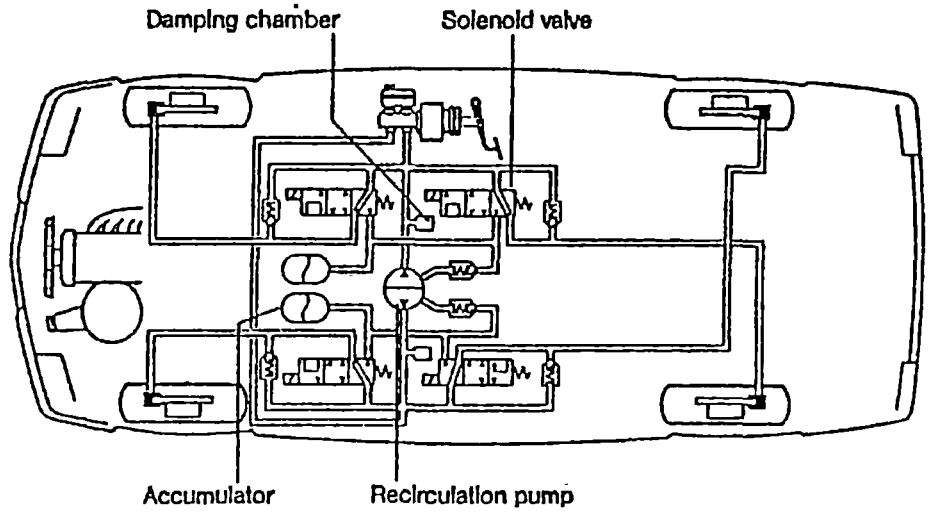

Figure 2-11 Four Channel ABS Hydraulic circuit.

Solenoid valves or actuators in ABS are controlled by an Electronic Control Unit or ECU [Figure 2-12]. In the least instance, this unit monitors all wheel speed sensors, estimates the level of "lock" based upon calculated accelerations of each wheel and is capable of decreasing and increasing the pressures in the brake lines.

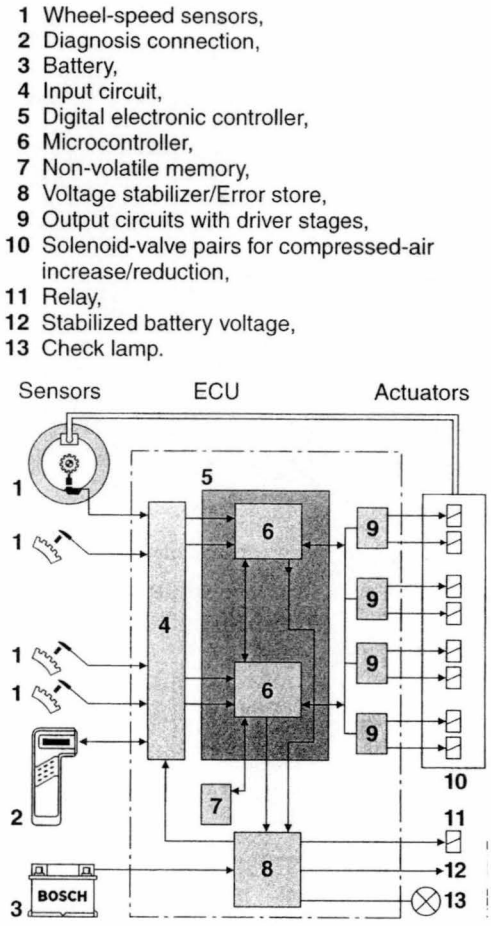

Figure 2-12 4 channel ABS Electronic Control Unit (ECU) [12]

In more sophisticated ABS [65], the ABS ECU [Figure 2-12] receives the request of the driver through their application of the brake pedal. The ECU is constantly measuring the rotational velocity of the wheels and from this can determine the rotational acceleration of all wheels at any given time. The ECU can then proceed to calculate the error between the driver request and the actual vehicle dynamics.

Using a pre-programmed model, the ECU knows that the maximum rate of acceleration under braking is, say, 9.8m/s or 1g for the particular vehicle (see friction circle plot for a typical sports car [Figure 2-7]). By constantly monitoring the wheel speeds, the ECU

can calculates the corresponding acceleration of each wheel. If the acceleration of any given wheel is more than the maximum 1g possible for the vehicle, then the ECU determines that the wheel is slipping and decreases the pressure in the brake line by opening the actuator or solenoid valve for a discreet period of time. As the wheel spins back up to the speed of the vehicle, the controller begins to pulse open the actuator or solenoid valve to maintain threshold braking at the maximum 1g.

The logic for a modern, sophisticated ABS ECU is shown diagrammatically in [Figure 2-13]:

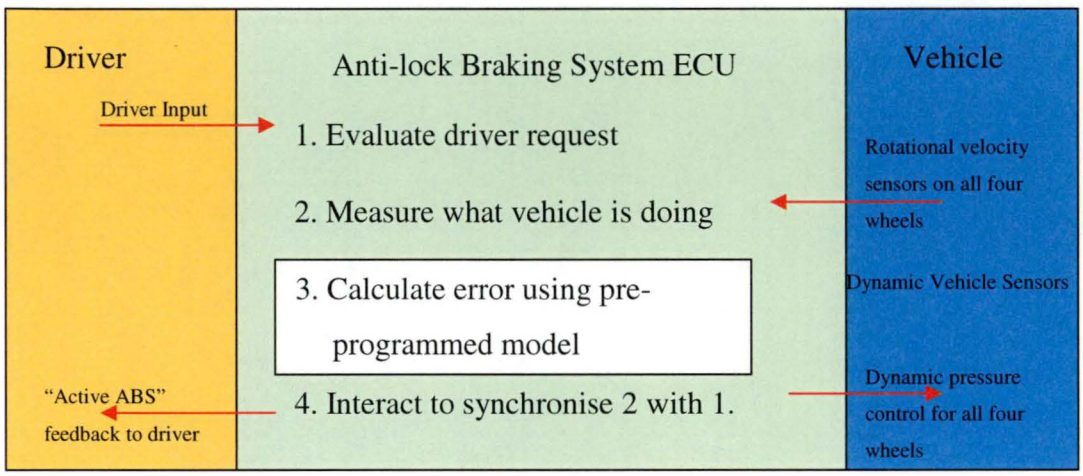

Figure 2-13 Modern ABS control unit logic [13]

Sophisticated current ABS ECU [Figure 2-12] use pre-programmed models, which contain assumptions, made by the ECU programmer. Thus the controllers need to be made robust in order to avoid catastrophic results. For instance, a sports vehicle capable of threshold braking on a dry track may not be able threshold brake on a wet road with the same ABS since the peak of the friction factor vs. slip plot [Figure 2-1] is not in the same region of slip. As a consequence, the ABS controlled vehicle will only be capable of achieving optimum braking under set conditions corresponding to whatever assumptions are made in the pre- programmed model.

From a graphical perspective, the operational region of ABS is depicted in [Figure 2-14] where the vehicle has some steering input, possibly to avoid an obstacle. The ABS has been programmed to operate in this region of wheel slip to ensure that the lateral force available from the tyre contact patch is sufficient to steer the vehicle.

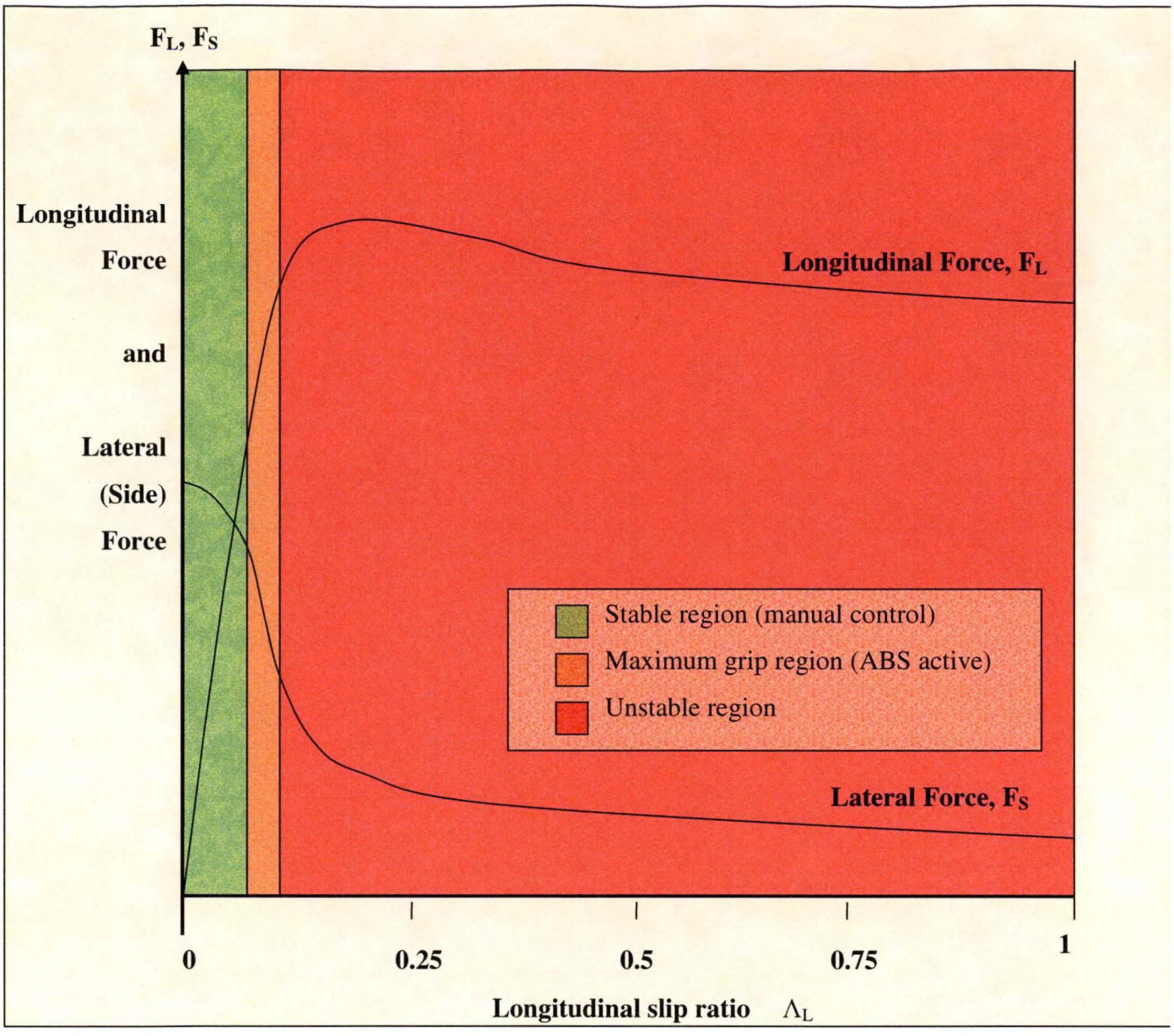

Figure 2-14 Operational region of ABS allowing for steering input while braking at best efficiency. Note that the unstable region is never reached while the ABS is switched on under normal driving conditions. [8, 12]

An ABS maintains the slip ratio within the region defined in [Figure 2-14] as dictated by the pre-programmed model during threshold or emergency braking. For optimum braking, which is braking in the shortest possible distance, this region needs to be moved further to the right hand side of the figure toward the longitudinal force peak and

into the unstable part of the plot. However, in the interests of robustness and maintenance of sufficient lateral force braking distance is often sacrificed and the active ABS region is conservatively kept well within the stable zone

To enhance the accuracy and achieve better braking performance it is possible to gain a better approximation of individual wheel slip than by simply using acceleration based algorithms. This has been achieved through the inclusion of a brake slip controller discussed in the next section.

2.4.1 Further Advancement: The Brake Slip Controller

Acceleration based electronic brake control has one major limitation: The controller assumes that the vehicle can brake at a given maximum rate regardless of conditions. This can lead to the controller allowing values of wheel slip to extend beyond the 5%-10% (dry road conditions) that is required for maximum braking effectiveness. In order to ensure maximum braking effectiveness under all conditions brake slip controllers have been developed which can "test" the individual tyre slip values. The problem of measuring tyre slip is, however, extremely complex [13,1,9].

If tire compliance is ignored a linear differential equation can be used as a first approximation to the actual rotational wheel dynamics. However, the tyre slip is the basic quantity used in the control process and the equation of motion becomes non-linear after transformation from wheel rotation to tyre slip as a variable [14]. Furthermore the brake force depends non-linearly on the tyre slip.

To make matters even more complicated the brake torque can not be controlled directly using the current braking systems (disk and drum hydraulic brakes). The system of activating the brakes once the controller makes a decision involves an intricate series of events that would be difficult to accurately model and involves many external factors like brake wear and temperature. For the reasons outlined here, a simple and robust Proportional-Integral-Differential (PID) [15] controller [Figure 2-15] is often employed.

It is difficult to directly measure tyre slip under typical road or track conditions since we require a true measurement of ground speed or free-rolling wheel velocity. An estimate of this value can be made using a technique where the brake pressure in the corresponding wheel is relieved to a lesser constant value for sufficient time to test a stable brake slip value. By using the known tyre stiffness (C_λ) as well as estimated values of tyre normal force (F_N) and tyre brake force (F_B) a nominal free-rolling wheel velocity is given by:

$$v_{WhlFree} = v_{Whl} \cdot \frac{C_\lambda}{C_\lambda - \frac{F_B}{F_N}}$$

Equation 2-4 [14], [15]

Where: $v_{WhlFree}$ = Nominal free-rolling wheel velocity.

v_{Whl} = Measured wheel velocity.

C_λ =Tyre stiffness (known for a given tyre).

F_B = Estimated tyre brake force.

F_N = Estimated values of tyre normal force.

To apply this, the control of wheel slip must be interrupted in order to start the procedure for the corresponding wheel. This will of course have an effect on the way in which the vehicle behaves. To minimise the influence of the test procedure:

- Under braking, the relative speed of the wheels is constantly monitored and the fastest rotating wheel is said to approximate the vehicle velocity.
- The free rolling velocities of the other three wheels are computed from the approximate vehicle velocity.
- The procedure for determining the free rolling wheel velocity is then initiated for the wheel in which a reduction of brake pressure would **least** effect the vehicles dynamic behaviour.

The Bosch brake slip controller [13] uses many other parameters in order to achieve its' aim to test the degree of individual tire slip and decide upon the control action as can be seen in the controller structure [Figure 2-15].

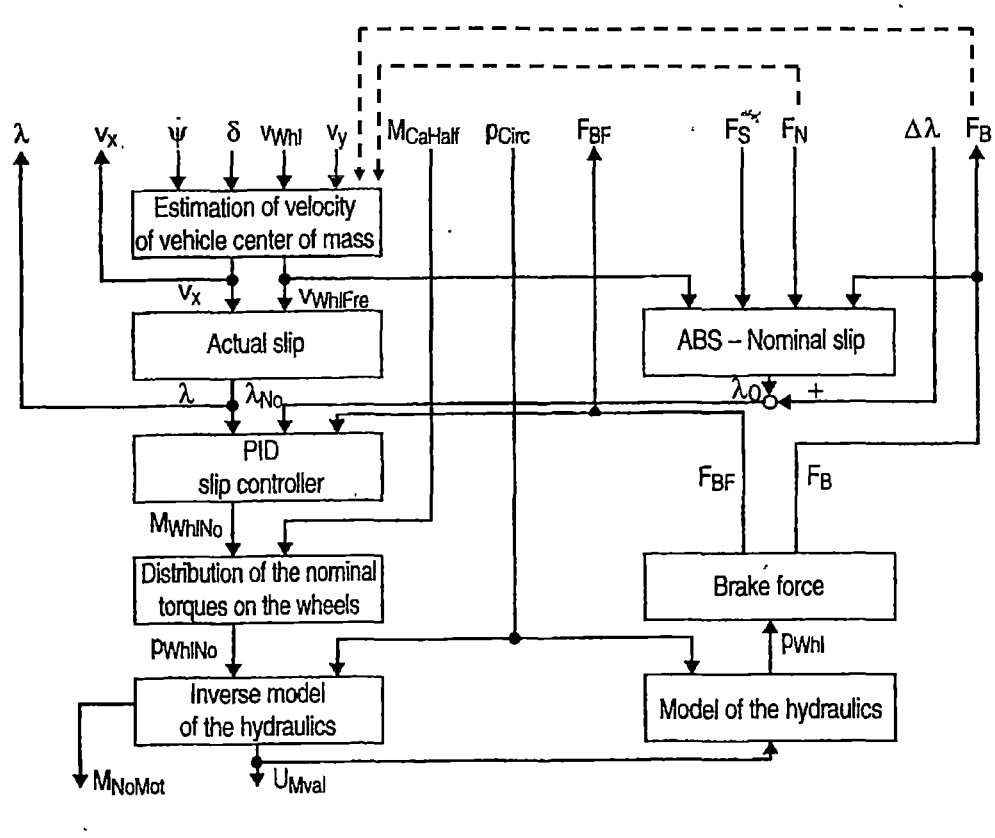

Figure 2-15 Controller structure for the Bosch Brake Slip Controller.[14]

Note in [Figure 2-15] that the free rolling wheel velocity, $v_{WhlFree,,}$ in this controller structure is calculated in the '*Estimation of velocity of vehicle centre of mass*' block. The longitudinal velocity, v_x is estimated in the same block using the free rolling wheel velocity, $v_{WhlFree,,}$ the estimated lateral velocity, v_y, the measured steering wheel angle, δ, and the measured yaw velocity, ψ.

Controllers such as the Bosch brake slip controller [Figure 2-15] are finely tuned in their operation but still use approximation formulae such as the estimation for free rolling wheel velocity [Equation 2-4]. Thus even the sophisticated controllers carry with them assumptions made in these approximations as discussed previously.

To conclude this section on ABS it is important to discuss typical control configuration and how ABS is incorporated into the overall vehicle control system.

In typical ABS, the sensors are conFigured in "star" topology with the ABS electronic control unit, ECU. On the more advanced current systems the ABS ECU will be connected to share information over a serial communication network (typically CAN) as can be seen in [Figure 2-16] with other ECU like navigation ECU, automatic gear box ECU and engine management systems. There may also be the requirement to connect with a lower speed bus and the non real time ECU within the vehicle, in which case a gateway ECU may be employed.

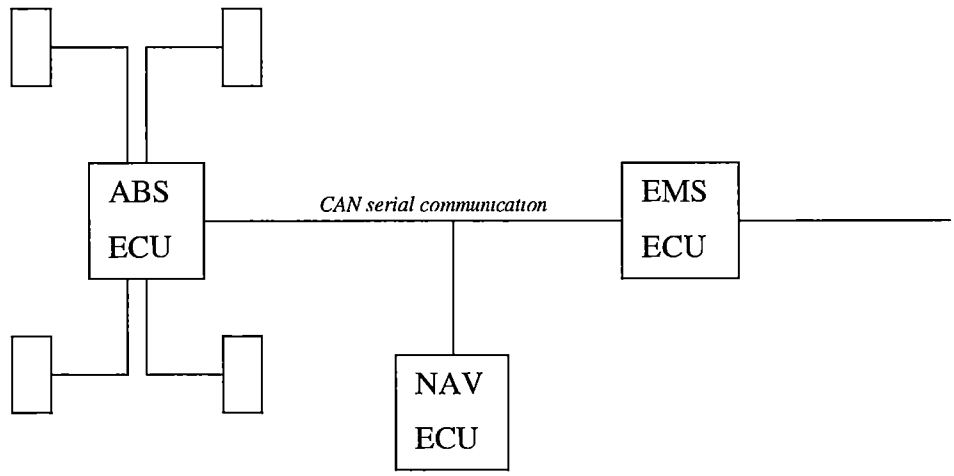

Figure 2-16 ABS in star topology.

If you were to take a close look at the state of the art of any luxury car you would find in the vicinity of 80 – 90 electronic control units or ECU which are used to control everything from electric windows and sunroofs to active suspension systems and electronically biased differentials. As the complexity of the systems increases so does the requirement for an ever-increasing number of sensors.

Vehicles are becoming heavily networked environments as outlined by Ross Bannatyre, Motorola Inc.[16]. "By establishing communications between different automotive control systems, information can be shared efficiently in order to enhance vehicle performance and safety. The availability and sharing of information from sources such as braking, steering, suspension and powertrain will very soon result in vehicles that are very advanced in safety, handling and convenience."

The future is in not just sharing information between systems but in combining these dynamic control systems into fully integrated systems [7]. [Figure 2-17] below indicates the way in which five different automotive sub systems are being merged. Note that the central feature in this development is the braking system, which will play a key role in the highly automated advanced chassis control system.

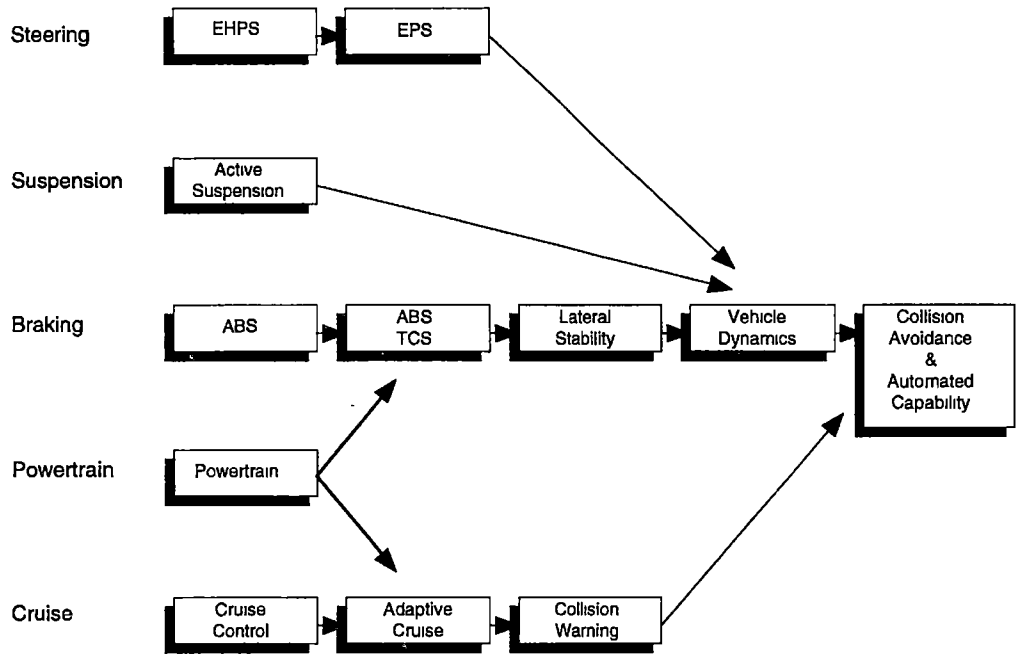

Figure 2-17 The merging of automotive systems. [7]

2.4.2 Traction Control Systems (TCS)

Current traction control systems typically use either Electronic Brake-force Distribution (EBD), engine power retardation, or a combination of the two. Here we will only briefly discuss the EBD type since power retardation (engine power limiting) is not part of the scope of this thesis. EBD traction control works almost exactly the same as ABS except that the system is in play under acceleration rather than braking. Systems typically use wheel speed sensors and may or may not utilise the sensors on the non-driven wheels. This is dependant on the application since a Traction Control System (TCS) designed for a 4x4 all terrain vehicle is likely to be very different from a system designed for a open wheel racecar in both system design and the sensors used.

Electronic brake-force distribution (EBD) traction control can also, in one sense, remove the requirement for a limited slip differential. With an open differential the slipping wheel can be braked transmitting drive through to the wheel(s) with grip. However there are both advantages and disadvantages to using EBD over mechanical forms of traction control like limited slip differentials.

In common with ABS the most advanced EBD TCS available today on luxury cars [13]:

1. Evaluates the driver's request as expressed through the accelerator pedal.
2. Measures what the vehicle is doing by through wheel speed sensors.
3. Calculates the "error" using a pre-programmed model of vehicle behaviour.
4. Uses EBD to synchronise 2 with 1.

Quite simply, EBD TCS is ABS under acceleration where, like ABS, the aim is to keep the driven wheels within the 5%-10% range of slip in order to retain maximum controllability and acceleration [3].

2.5 ELECTRONIC SUSPENSION MONITORING, REGULATION AND CONTROL

While EBD ABS and TCS can make the most of the grip available, they are not direct methods of increasing the grip or altering the forces developed between the tyre and the road surface. To achieve this, it is possible to alter the dynamic load on individual wheels through the means of suspension control. In other words the normal force between the tyres and the road/track can be distributed actively between the four wheels or can be instantaneously altered within physical limits.

The suspension on a vehicle can be controlled either directly via means of pneumatic or hydraulic systems or indirectly through the use of electronically controlled adjustable dampeners etc. Simple systems do not actually measure the position of the suspension, thus the system has no means for gathering feedback. The most effective systems do measure the position of the suspension through the use of linear potentiometers or similar devices

The use of measuring devices on passive suspension is also becoming popular on luxury vehicles as part of their dynamic control systems. This provides dynamic information for wheel loading, which in turn can be used to approximate instantaneous levels of grip available from each tyre.

2.6 VEHICLE STABILITY CONTROL

Vehicle stability control systems known as ESP (Electronic Stability Control – Mercedes) or DSC (Dynamic Stability Control – BMW) and many others has only recently become available on production luxury vehicles and has already proven to significantly improve the safety and controllability of passenger vehicles. Since first released on the Mercedes-Benz S 600 coupe in mid 1995, other automotive companies like BMW and Volkswagen have been quick to develop and market their own systems.

Stability Programs can incorporate ABS and/or TCS, since the aim is to prevent tyre slip on the road surface and maintain maximum levels of acceleration (forwards, backwards and sideways). Perhaps the simplest way to think of the three systems is to consider a car approaching a corner, cornering and accelerating away as can be seen in [Figure 2-18].

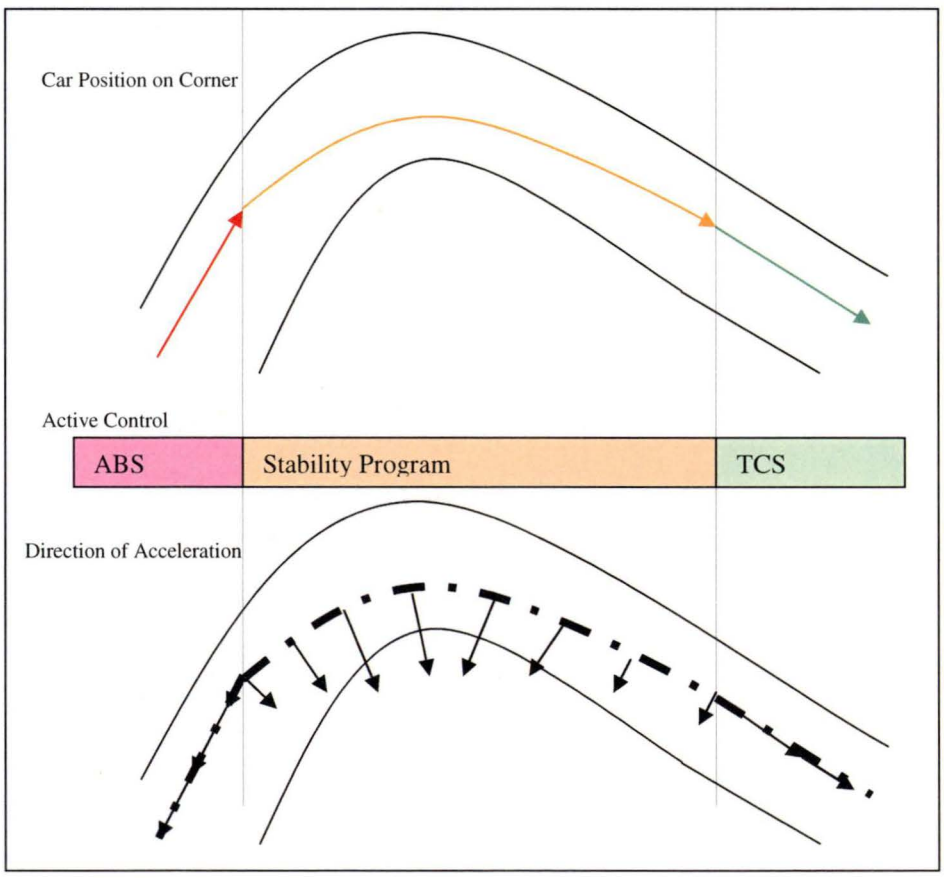

Figure 2-18 Simplistic view demonstrating active control systems during a cornering manoeuvre.

[Figure 2-18] shows a vehicle cornering on its limits of adhesion. The bar indicates that the ABS is active on the approach to the corner, the ESP is active through the corner and the TCS is active while accelerating away from the corner. However this is a simplistic look at when each system is active, since the exact moment when ABS becomes ESP and ESP becomes TCS is hard to define, hence the move towards one integrated system.

The more sophisticated stability programs require more sensors in order to function properly than simple ABS and TCS systems. Essentially this stems from the requirement to "know" whether the vehicle is in a state of understeer, oversteer, sideways drift, or a normal driving attitude.

The Bosch/Mercedes-Benz ESP uses [3]:

1. A steering angle sensor
2. Wheel speed sensors on all four wheels
3. A lateral acceleration sensor
4. A yaw sensor
5. A brake pressure sensor

The Relative positions of these sensors can be seen in [Figure 2-19] where a vehicle slip controller, as discussed previously, is integrated into the overall Electronic Stability Program (ESP).

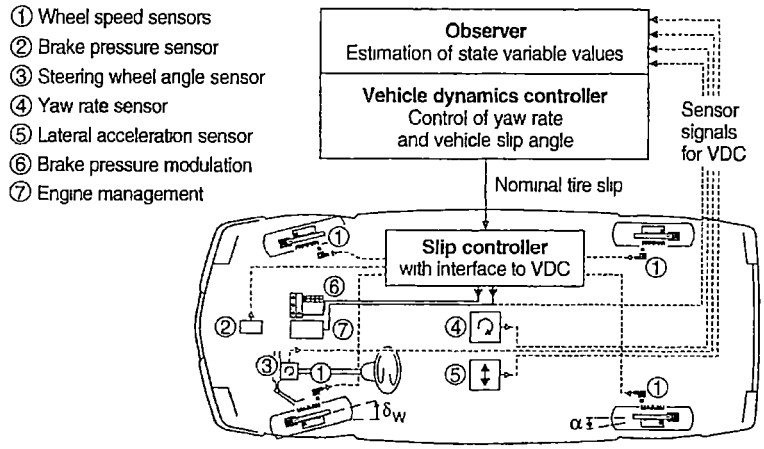

Figure 2-19 Bosch/Mercedes-Benz ESP Vehicle Dynamics Control (VDC) system. [14]

Typically, the information from these sensors [Figure 2-19] is then fed into the ECU that determines, among other things [5]:

1. Where the driver is intending the car to go.
2. At what speed does the driver intend to get there, i.e. are they braking, accelerating or coasting.
3. The cars status; level of oversteer or understeer, and level of drift/grip

The ESP ECU will then compare this with a stored mathematical reference model and will apply selective breaking (EBD) in an attempt to match the vehicle's behaviour with the intended actions of the driver.

The working concept of the most basic function of ESP is actually quite simple. The sensors determine whether the vehicle is yawing more or less than the driver intends and applies a corrective moment using different braking forces on either side of the vehicle.

It has been outlined that longitudinal and lateral forces on a tire (F_L, F_s) depend on the tyre slip (λ), the slip angle (α) and the normal tire force (F_N) [5]. For a given slip angle the lateral force generated by a tyre decreases with increasing magnitude of tyre slip. In other words for a given α, F_L decreases as λ increases. Stability control systems, including the Bosch ESP, typically use this fundamental tyre property in order to specifically control lateral tyre forces and hence the yaw moment on the vehicle. The effects of stability control systems such as ESP can be seen in [Figure 2-20] where two vehicles, one with ESP and one without, are steered around a right-left-right-left slalom type corner combination with the same steering input. Note in this diagram that the vehicle without ESP becomes increasingly unstable from the first corner.

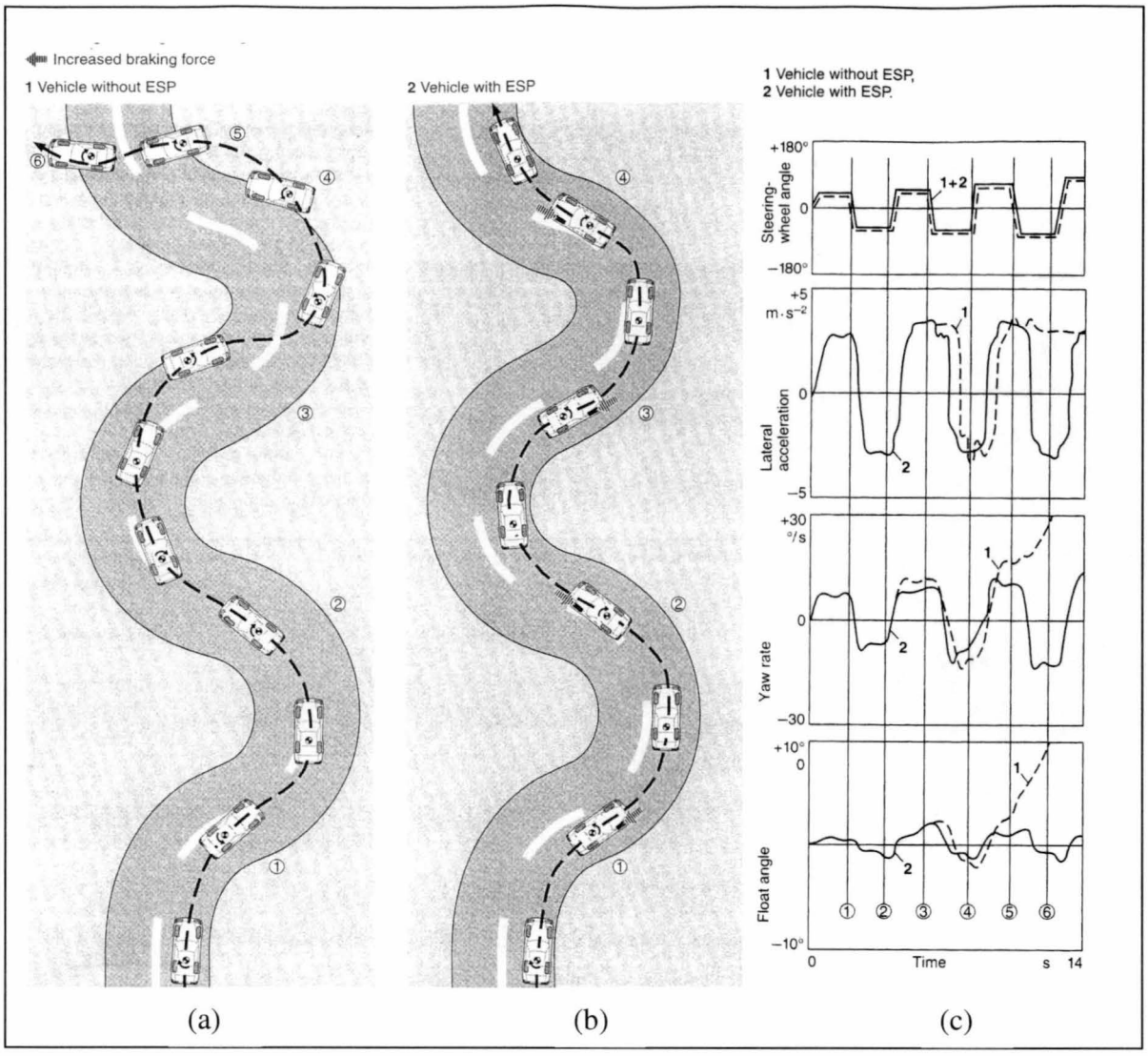

Figure 2-20 Bosch-Mercedes Electronic Stability Program (ESP) yaw control using differential electronic brake force distribution: (a)without ESP, (b) with ESP, (c) Graphical results showing handling response. [5]

A typical vehicle stability control system uses approximations to predict changes in parameters that can not be measured easily.

As an example, the following simple algorithm [13] can be used in order to give a first approximation of the changes in yaw moment due to small changes in slip magnitude, $\Delta\lambda$, of the front left tyre.

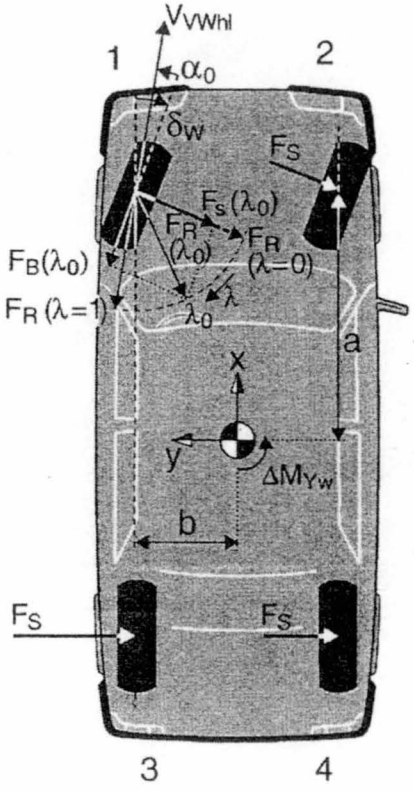

Figure 2-21 Dynamic vehicle model used in predicting yaw moment changes.[14]

$$\Delta M_{Yw} = -\frac{\partial F_S}{\partial \lambda} \cdot \Delta\lambda\left(a \cdot \cos\delta_W - b \cdot \sin\delta_W\right) + \frac{\delta F_B}{\partial \lambda} \cdot \Delta\lambda\left(a \cdot \sin\delta_W + b \cdot \cos\delta_W\right)$$

Equation 2-5 [14]

Where: $\Delta\lambda$ = the known (previously estimated) small change in slip magnitude of the front left tyre.

$\partial F_S/\partial\lambda$ = the rate of change of lateral force of the tyre with respect to the rate of change of tyre slip.

δ_W = (steering) wheel angle, see [Figure 2-21]

a = longitudinal distance from the front wheels to the centre of gravity, see [Figure 2-21]

b = lateral distance from the front wheels to the centre of gravity.

And similarly, the changes in the lateral and longitudinal forces:

$$\Delta F_x = -\frac{\partial F_S}{\partial \lambda} \cdot \Delta\lambda \cdot \sin\delta_W - \frac{\delta F_B}{\partial \lambda} \cdot \Delta\lambda \cdot \cos\delta_W$$

Equation 2-6 [14]

$$\Delta F_y = -\frac{\partial F_S}{\partial \lambda} \cdot \Delta\lambda \cdot \cos\delta_W + \frac{\delta F_B}{\partial \lambda} \cdot \Delta\lambda \cdot \sin\delta_W$$

Equation 2-7 [14]

Of note is that these relationships are extremely non-linear. This is due to the force derivatives being highly dependant on the operating point of the tyre which in this analysis are denoted by λ_0 (Initial tyre slip magnitude) and α_0 (initial tyre slip angle).

From these equations [5] it is clear that increasing the tyre slip, your control variable, rotates the resultant tyre force about the yawing plane of the vehicle changing not only the yaw moment, but also the lateral force and the longitudinal force on the vehicle.

This rotation is used by the vehicle yaw and slip controller, deciding which tyre slip should change and by how much. The unfortunate side is that the changes in lateral forces can lead to an undesirable increase in lateral deviation of the vehicle (sliding off the road) and the longitudinal forces on the tyres can produce involuntary deceleration of the vehicle (undesired braking). Current development of ESP centres on minimising these undesirable characteristics.

2.6.1 Vehicle Yaw rate and Slip Angle Controller

With the principles behind controlling yaw using electronic brake force distribution techniques, we can now describe the manor in which the vehicle yaw and slip controller physically accomplishes the goal of increasing vehicle stability.

For a vehicle during stationary turns there is a relationship between steering wheel angle, vehicle velocity and yaw velocity or yaw rate, Ψ. This becomes the first nominal value for yaw velocity, and can be expressed as [14]:

$$\psi_{No} = \frac{v_x \cdot \delta_W}{(a+c)(1+\frac{v_x^2}{v_{CH}^2})}$$

Equation 2-8 [15]

Where: v_x = vehicle velocity in the x (longitudinal) direction

v_{CH} = Characteristic vehicle velocity

δ_W = (steering) wheel angle, see [Figure 2-21]

a = longitudinal distance from the front wheels to the centre of gravity, see [Figure 2-21]

c = longitudinal distance from the rear wheels to the centre of gravity.

This relationship, however, is not valid if the coefficient of friction of the track surface is low. Thus, it is necessary to limit this nominal yaw rate:

$$\psi_{No.} \leq \mu \cdot \frac{g}{v_x}$$

Equation 2-9 [14]

Where: μ = Road/tyre combination coefficient of friction.

The problem is not yet complete since the vehicle can still slide excessively sideways due to the lateral acceleration, which during turns with no wheel slippage is equal to the product of yaw velocity and vehicle velocity. In a state of excessive sliding the lateral forces can not be increased any further, so the controller needs to decrease the vehicle slip angle. By making appropriate decreases in the nominal yaw velocity, creating a third ψ_{No}, the controller is able to further optimise the Electronic Brake-force Distribution.

The Bosch Electronic Stability Program, ESP [14][15][1], uses many other parameters in order to achieve its' aim to maintain higher levels of vehicle control and to decide upon the control action, as can be seen in the controller structure [Figure 2-22].

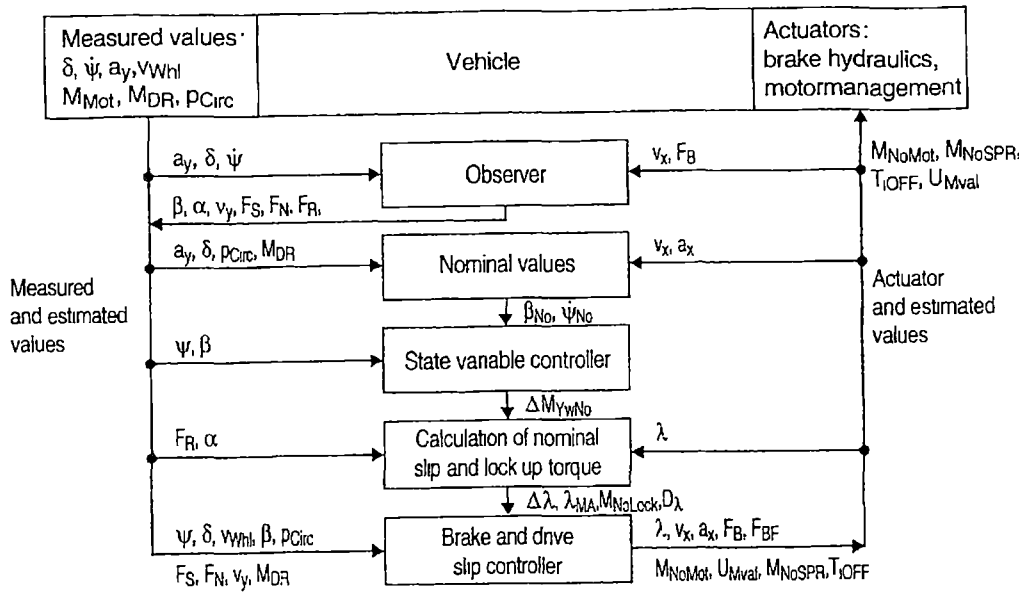

Figure 2-22 Bosch vehicle yaw rate and slip angle controller structure. [14]

Inputs into the ESP controller [Figure 2-22] include:

- The wheel velocity for each wheel, v_{Whl}.
- The measured yaw velocity, Ψ.
- The Lateral acceleration of the vehicle, a_y.
- The actual engine torque, M_{Mot}
- The engine torque requested by the driver, M_{DR}
- The brake circuit pressure induced by the driver, P_{Circ}

Note the correspondence to the sensor layout on the vehicle [Figure 2-19]

The *Observer* component of the controller [Figure 2-22] develops values for:

- Slip angle of each wheel, α.
- Slip angle of the vehicle, β.
- Lateral vehicle velocity, v_y.
- Lateral force on each tyre, F_S.
- Normal force on each tyre, F_N.
- Resultant force on each tyre, F_R.

This si done using basic geometrical and physical relationships as can be seen in models such as [Figure 2-21].

Using these inputs the controller [Figure 2-22] is now able to make comparisons between the state of the vehicle and the requests by the driver. It achieves this through comparison with nominal values:

- The nominal yaw velocity, $\psi_{No.}$, determined as discussed.
- The nominal slip angle, $\beta_{No.}$, determined in a similar way.

Through the *State variable controller* in [Figure 2-22], a determination of the current state of the vehicle is made, that is whether the car is sliding, oversteering or understeering and a nominal corrective change in moment, ΔM_{YwNo}, is calculated to correct the condition.

The *Calculation of Nominal slip and lock up torque* component uses the nominal corrective change in moment, ΔM_{YwNo}, the resultant forces F_R and the slip angles, α, on each tyre to calculate:

- The required small changes in tyre slip of each tyre, $\Delta\lambda$.
- The nominal average drive slip of the driven wheels, λ_{MA}.
- Nominal brake torque difference between the driven wheels, M_{NoLock}.
- Tolerance band of drive slip difference between wheels, D_λ.

Finally the information from the *Calculation of nominal slip and lock up torque* component is input along with the other calculated and measured parameters to the *Brake slip controller,* as discussed previously, and the *Drive slip controller* which processes the information In a similar way. These controllers [Figure 2-15] contain algorithms that are necessary for the calculation of slip and nominal slip of each tyre and control of the brake pressures using the actuators in the hydraulic lines.

Note that there are several feedback loops in the Bosch/ESP vehicle yaw and slip angle controller [Figure 2-22] where the components use previously estimated values in order to estimate the next set of values more accurately.

The Bosch/ESP vehicle yaw and slip angle controller [Figure 2-22] is a sophisticated, well proven system for dynamic Electronic Brake-force Distribution (EBD) vehicle control. The controller is, however, built on a series of empirically and geometrically

derived approximations as discussed. The system is therefore vulnerable when conditions arise that are not well described by those approximations.

To prevent the occurrence of catastrophic results under adverse conditions, the controller is robustly designed. The adverse side to this robustness is that some performance is sacrifices in the interests of safety. On the subject of applicability and robustness of the Bosch Vehicle Dynamics Controller, Van Zanten et al (Bosch) [15]: "To find the best compromise according to the customer demands the system can be tuned in either direction. For example stopping distances on homogeneous roads for full braking can be reduced while keeping the vehicle usually stable however, the manoeuvrability will be reduced." These compromises fail to take full advantage of Electronic Brake-force Distribution (EBD) under all conditions.

Neural networks offer an alternative approach to empirical/geometrical approximation based systems and are not subject to the same limitations. Emerging neural network technology is slowly replacing these types of systems in other fields but is only now becoming useful for complex automotive control as computing power becomes cheaper and more compact.

2.7 NEURAL NETWORK APPLICATIONS AND CONTROL TO PREDICT AUTOMOTIVE PERFORMANCE

Neural networks have been used in a wide range of areas in order to predict the performance of a given system. In automotive areas of research their use has been predominantly in engine management systems. A typical example of this is Chris M. Atkinson's SAE technical paper "Virtual Sensing: a Neural Network-based Intelligent Performance and Emissions Prediction System for On-Board Diagnostics and Engine Control" [17].

Atkinson was primarily concerned with the emissions side of things since that is where legislation (in countries where the biggest automotive markets are) is constantly applying pressure to the automotive industry. Important as it is, the focus on the

emission control has put engine control systems in front of dynamic chassis behaviour control systems in terms of technology, research and development. There is little doubt that neural network systems have been developed for dynamic chassis behaviour control by many of the worlds leading automobile producers. The development of such systems is both expensive and time consuming so it is easy to see why these systems remain closely guarded secrets.

Many neural network models have been developed for engine control, as it is only a matter of using the sensors which modern engines already have to control electronic regulators like fuel injectors, spark plug coils, fly by wire throttles etc. Hence it can be done for little outlay and is the focus of many academic papers and thesis, which are freely available and demonstrate the potential for artificially intelligent systems in engine control. It is only recently that the "sensor explosion" has begun to make its way into the commercial luxury vehicle chassis.

Following on in this progression, it would seem that the use of neural networks in vehicle dynamic control systems is the next step. The only questions remaining are how should these systems be integrated and what types of neural networks are suitable for dynamic automotive applications.

In the past, development of dynamic automotive neural networks has primarily been conducted on a theoretical basis by independent and academic researchers since physical testing for full size self controlled vehicles is costly and can be dangerous. Despite these and other limitations, some researchers have realised the potential of Neural Networks in automobile control.

In 1987 J Shepanski and S.Macy as illustrated in R. Hecht-Nielsen, "Neurocomputing", [18] developed what they called an "automobile autopilot" through simulation of "almost real" driving conditions with some restrictions in an effort to make the problem tractable. Not the least of these restrictions were major assumptions of the road environment including that the vehicle would only be travelling on a two lane freeway with wide shoulders (which the vehicle could be driven along) upon which all traffic was moving in the same direction.

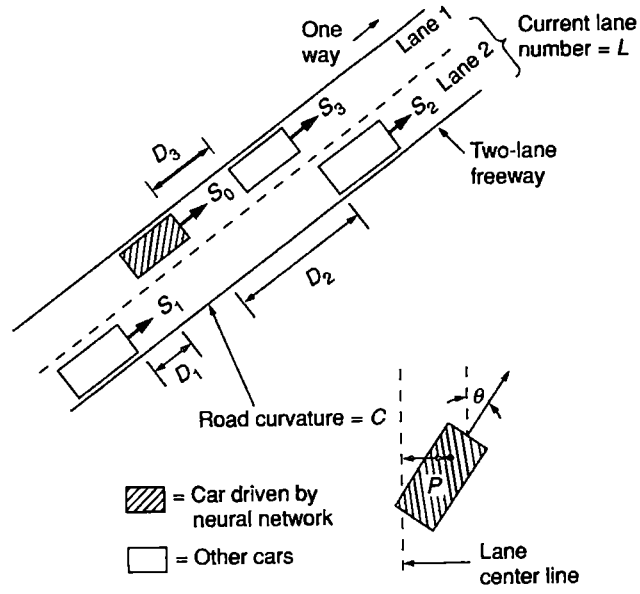

Figure 2-23 "Automobile Autopilot" model freeway used to develop vehicle control Neural Networks in under simplified conditions [18]

The Neural Network driven vehicle can travel in either lane of the freeway where other simulated cars drive at various speeds and perform certain manoeuvres. In this simulation, the other cars are pre-programmed and do not deviate if threatened by the NN controlled vehicle. The researchers justified this by the claim that successful collision avoidance manoeuvres are uncommon in real world driving situations since usually the driver does not recognise the threat of a collision until it is too late. This lack of response by other cars does, however, simplify the problem to what was deemed a manageable level.

Furthermore, while unable to manoeuvre to avoid accidents the other cars will not rear-end the NN driven car and hence the vehicle is relieved of the task of dealing with cars behind.

The "automobile autopilot" [18] consisted of two independent neural networks:

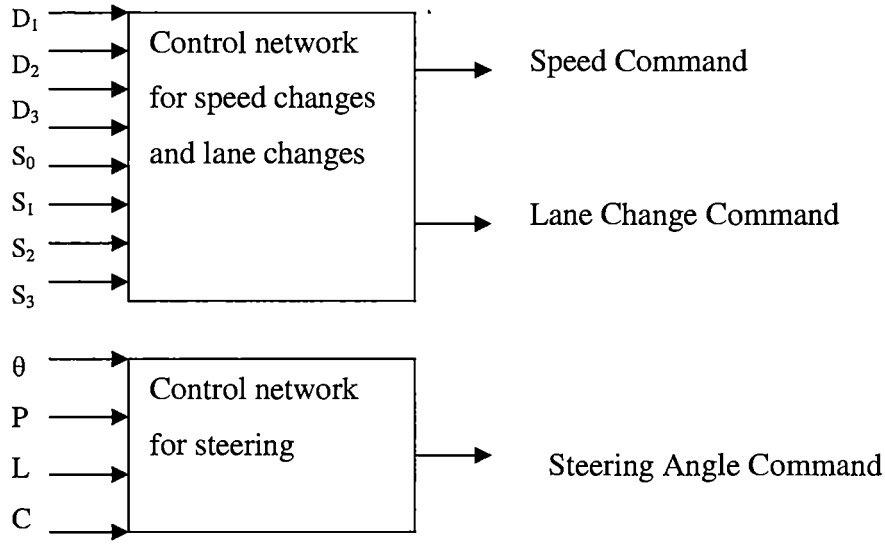

Figure 2-24 Neural network use in the Automobile Autopilot [18]

Where they identified the following input variables:

D_1 =The distance from the rear bumper of the NN driven vehicle to the front bumper of the nearest car in the other lane that is next to or behind the NN driven vehicle

D_2 =The distance from the front bumper of the NN driven vehicle to the rear bumper of the nearest car in the other lane that lies ahead of the NN driven vehicle.

D_3 =The distance from the front bumper of the NN driven vehicle to the rear bumper of the nearest car ahead in same lane.

S_0 =The forward speed of the NN driven vehicle.

S_1 =The speed of the nearest car in the other lane next to or behind the NN driven vehicle

S_2 = The speed of the nearest car in the other lane ahead of the NN driven vehicle

S_3 = The speed of the nearest car in the same lane ahead of the NN driven vehicle

Θ = The angle between the longitudinal axis of the NN driven vehicle and the lane in which it is driving in.

P =The lateral displacement of the NN driven vehicle centre line from the centre-line of the lane it is driving in

L =The number lane in which the NN car is driving in (i.e. 1 or 2)

C =The road curvature at the point where the NN driven vehicle is currently located.

Both the *speed and lane change* and the *steering* control networks are back propagation types. The steering network is responsible purely for keeping the vehicle within the lane it is travelling in, adjusting steering angle in an attempt to keep the car in the centre of its lane. The control network for speed and lane changes adjusts the speed of the vehicle and decides when to change lanes. Progress of the vehicle model is monitored through the use of simple graphics on a screen.

A human driver using traditional steering, accelerating and braking inputs and a special lane change command performed training of the "automobile autopilot". This lane change command does not correspond to traditional driving inputs and has been justified for the sake of the model to be a manoeuvre that can be pre-programmed as a chain of commands. The lane change command does not centre the car in the other lane, this is a function of the steering network.

The networks have demonstrated competency in "intelligently" negotiating the simulated driving conditions. The model also demonstrated close adherence to the driving style of the training driver. For example, a relaxed conservative driver will train the networks to drive the vehicle in a relaxed manor. A fast driver may train the networks to drive quickly and overtake where possible.

2.7.1 Advantageous Characteristics of Neural Networks

- Neural Networks are trained or taught rather than programmed. Automated learning is possible from examples - the need for programmers to make assumptions about the form of the relationship between input and output is removed.
- Rather than having separate memory, controller and stored external program linking them (operating system), the operation of neural networks is implicitly controlled.
- The form of a Neural Network gives the system an associative memory. Inherently the network associates items taught to it, grouping similar items together within the structure.
- Neural Networks are capable of generalising. This gives the network the ability to group categories of objects based on a series of examples.
- Neural Networks are robust. Networks will continue to operate after significant quantities of its neurons and interconnections fail. Performance of the neural network under these conditions will degrade smoothly with the loss of these neurons.
- Neural Networks can be structured to be self organising. These networks generalise from data patterns without requiring specific instructions on what to look for or what to learn.

2.7.2 Neural Network Artificial Intelligence

In an engineering sense, artificial neural networks are systems that replicate the principles and functions of a human brain.

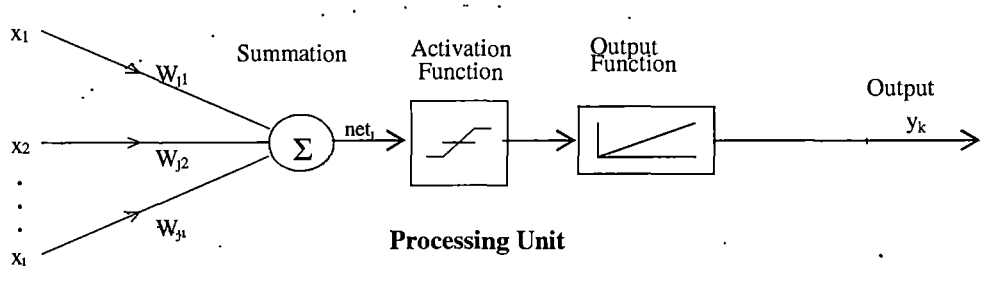

Figure 2-25 The structure of an artificial neuron

Similar to a biological neuron, an artificial neuron receives inputs from other neurones within the network, processes those inputs and sends a single output. In this manner, neurones relate to each other via weighted connections.

In the sketch above, the inputs to the neuron are x_1, x_2, ...x_i, the origin of these defined by the network architecture. The weighted connections are denoted as W_{j1},W_{j2}...W_{ji} corresponding to these inputs.

The processing capability of an artificial neuron is the combination of three functions:

1. The input function
2. The activation function
3. The output function

The input function multiplies each input by the corresponding weight and sums the weighted inputs for *i* number of input neurones. Thus the net input to the j^{th} neuron activation function, net_j, can be described as [19]:

$$net_j = \sum_i x_i W_{ji} \qquad \textit{Equation 2-10}$$

The activation function can be any function that is differentiable and monotonically increasing [20]. The output of the activation function is conventionally limited to between 0 and 1 or alternatively –1 and +1. The type of activation function used governs this range. Simple neural network models use step or threshold functions, popular in early systems. This particular activation function outputs a 1 if the weighted sum of the inputs is greater than a programmed threshold, if not the output is a zero.

More general non-linear sigmoid (logistic) functions have seen widespread use in more recent times. Sigmoid functions follow a curve with a continuous positive slope (derivative is always +ve), contain only real-values and are bound by limits.

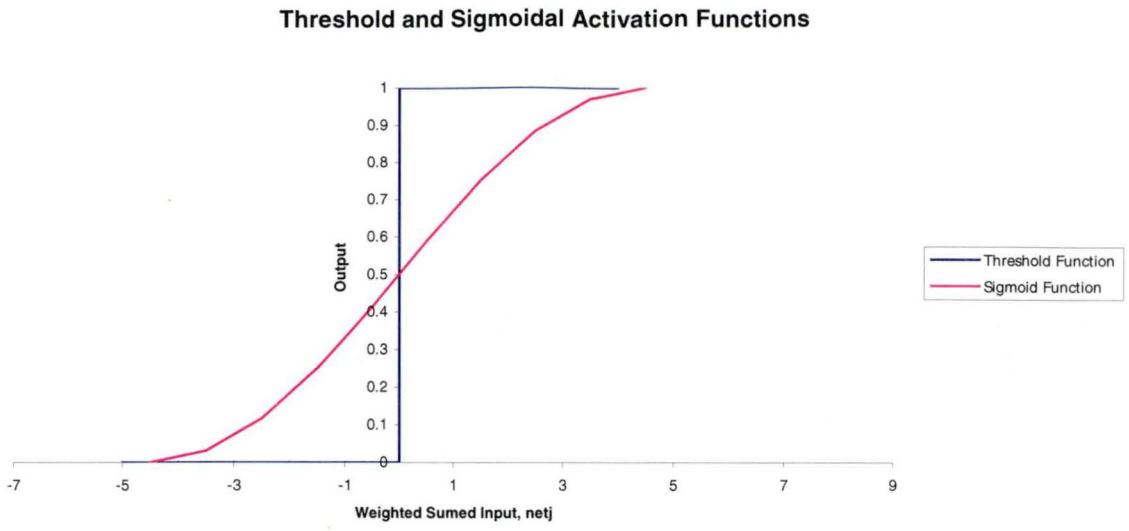

Figure 2-26 Threshold and sigmoidal activation functions

The equation governing the sigmoid activation function is given by [21]:

$$f(net) = \frac{1}{1 + \exp(-net)} \qquad \textit{Equation 2-11}$$

Hence the derivative can be found simply:

$$f'(net) = f(net) * (1 - f(net)) \qquad \textit{Equation 2-12}$$

In popular, contemporary neural networks the output from the activation function is commonly chosen as the output from the neuron. Thus in current practices, the output function does nothing to alter the value produced by the activation function. It is important to remember, however, that this is not always the case and under certain circumstances an effective output function can be very valuable.

Each neuron in a neural network can be thought of as a primitive function, taking a specific input and producing a defined output. When these are combined in a network, however, they possess the capability of mapping an n-dimensional real input to an m-dimensional real output. Hence a neural network is often treated by engineers as a "black box" where the results rather than the process are important.

A neural network is not programmed to estimate results for specific applications, instead the network "learns" to solve the problem through a process called 'neural network training'. This process involves refining the values of the weighted connections, $W_{j1}, W_{j2} \ldots W_{ji}$ in our example neuron. These weights are specific to, and need to be computed for, the application.

There is no direct way to calculate the ultimate weighting. The weighted connections are continuously adjusted during neural network training using algorithms or 'learning rules' [18]. The specific learning rule used will depend on what type of neural network model is being applied.

Neural networks are categorised under two major model classes:

1. Feed-forward Neural Networks
2. Recurrent Neural Networks

Furthermore, methods for neural network training are often broadly categorised into:

1. Supervised training
2. Un-supervised training.

For example, The *Perceptron* neural network developed by Frank Rosenblatt, in 1962 [22] can be described as a *Feed-forward* network with *supervised* training.

2.8 FEED-FORWARD NEURAL NETWORKS

Feed-forward neural networks operate under the principle that the information or input activity signals propagate in one direction only. Basic or fundamental feed-forward neural networks consist of a single input layer, numerous hidden layers, and a single output layer.

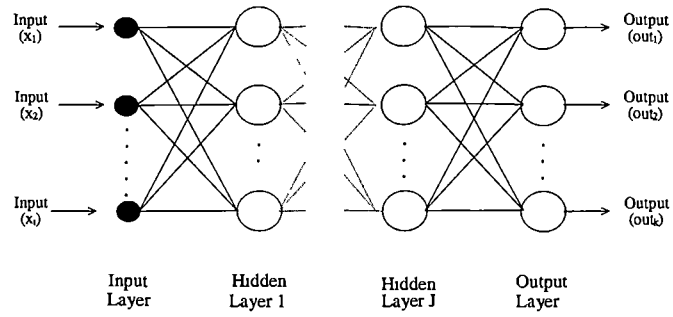

Figure 2-27 Feed forward neural network structure

After the input layer, the neurons in each consecutive layer receive an array of data through network interconnects. This array is then processed within the neuron to produce a single output, which is fed into every neuron in the next layer. This process is repeated through the neural network to the output layer.

2.9 RECURRENT NEURAL NETWORKS

All recurrent neural networks posses at least one feedback loop. This means that at least some activity signals do not follow a straight path through the network, rather the output from one layer or set of neurones are sent back through some or all of the layers previously seen. Thus a recurrent neural network is dynamic since the network will evolve as time elapses for a given initial state.

It is important then that the architecture for a recurrent network is chosen carefully for a particular application such that the network converges toward a state of equilibrium. If the recurrent neural network is stable, this can eventually be reached.

Recurrent neural networks are useful for applications involving intensive computational problems and also the in the storage of information (memory applications).

2.10 SUPERVISED AND UNSUPERVISED TRAINING

Neural networks can be trained using either supervised or unsupervised techniques.

Supervised training is the name given to any neural network training were a teacher provides input patterns and corresponding output patterns similar to those expected to be encountered by the network during operation. Using an iterative process the network dynamically adjusts its weights until the error between the output from the neural network and the target output reaches a minimum.

Unsupervised training is employed often when only input vectors are available. This type of training is suited to raw collections of data where the network is used to create categories by finding similar features and correlations in training input sets. In creating these categories the network must discover for itself the existence of patterns, regularities and separating properties.

2.11 OPTIMISING NEURAL NETWORK PERFORMANCE

To achieve optimum performance from a neural network careful consideration is required in relation to:

- The 'condition' of the network input and target output vectors
- Design of the training data
- Methods for testing and evaluating the network performance

2.11.1 Network Input and Output Normalisation

A Neural Network sees improvements in performance when insignificant characteristics and information is removed form the input data set. Usually values of standard deviations and offsets are independent of the important aspects of individual input vector components. The effect of this type of insignificant data complicates the task of the Neural Network and decreases the network performance. For this reason the input vectors to the network are often normalised.

Normalising involves scaling of the input parameters such that the network sees each individual component of the input vector as being of equal magnitude. As a consequence, the network is presented with information that has no implicit bias toward any given input parameter(s). A side effect of normalisation is increased numerical stability of the network data process.

In most cases training algorithms minimise the total error of all outputs. Thus if target output vector components are unequal in magnitude, individual outputs with larger deviations will be favoured, as they will dominate the error sum. Hence normalisation of the target output data is critical to achieving true minimisation of total error. This, however, is often designed into the network through the use of bound activation functions such as both the threshold and sigmoid types that are usually given and are therefore limited to a range of between zero and 1, ie. ($0 \leq f(x) \leq 1$).

2.11.2 Design of Neural Network training data

The development of the training set for a Neural Network will dictate its performance. The size of the training set required to provide the network with adequate training is one of the most important considerations first encountered by the trainer. However, it has been proved that the general learning problem for neural networks is *intractable* [22], which means that it can not be solved efficiently for every possible input vector. From an engineering perspective where Neural Networks are used as tools for solving specific and real problems qualitative decisions need to be made about the size of the training set.

In order for a trained network to be effective the training set must be large and complete enough to satisfy at least the following two goals:

- Adequate representation must be given to every variable in the training set. Often the data used in training will consist of several sub groups having a tendency toward

a particular trend or pattern. It is important that each of these patterns or classes is given sufficient representation.

- For each class there must be enough examples to ensure balanced, statistical variation. In many cases Neural Networks are employed where the data is noisy, that is they consist of random patterns superimposed on to the actual input values. Training sets must be large enough to provide sufficient examples in the full range of likely noise effects.

2.11.3 Neural Network Testing

Once the training of a network has been completed a test set is employed to evaluate the performance of the network [23]. This is a set of data previously unseen and acts to test whether or not the network is able to generalise successfully through multi-dimensional interpolation. The results of thorough network testing are a good indication of how useful the network is as a tool for the application.

2.12 NEURAL NETWORK ARCHITECTURE

Network architecture refers to the structure of the network used. In feed forward neural networks this refers to the number of neurons in each layer and the number of hidden layers. Generally the number of neurons in the input layer directly corresponds to the input vector. Similarly, the set of neurons in the output layer usually corresponds to the number of outputs required.

That said, the only questions remaining are how many hidden layers are required and how many neurons are required in each of the hidden layers.
A typical feed forward neural network contains at least one hidden layer but there is no theoretical upper limit. It has been shown mathematically that at
Least four layers (three hidden layers plus an output layer) are required to solve highly complex problems. For the vast majority of practical problems it is rarely necessary to use more than 1 hidden layer [24]. The use of two hidden layers is usually only necessary when the function learned by the network is discontinuous.

Increases in the number of hidden layers results in rapid increases in the creation of localised false minima. This may lead to the network becoming stuck in one of these minima after many time consuming iterations - resulting in the need to start re-training.

Furthermore the additional layers, through which errors must be back propagated, makes the gradient of the modelled network unstable. Successful optimisation using gradient-directed optimisation algorithms is dependent on the reasonable stability of the network gradient. For these reasons it is desirable to use as few hidden layers as is practical.

Selecting an appropriate number of neurons in the hidden layer is a balancing act between to few - starving the network of the necessary resources, and to many which will result in overfitting of data.

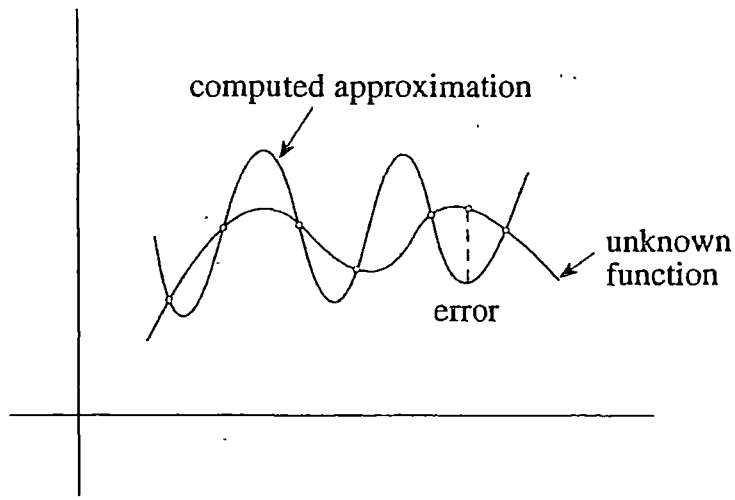

Figure 2-28 Graphical example of overfitting on a polynomial approximation.[18]

As with the number of hidden layers, it is often better to use as few neurons in each layer as possible to obtain a satisfactory solution.

2.13 BACKPROPAGATION NEURAL NETWORKS

Backpropagation networks constitute one of the most widely used paradigms. They are a powerful mapping tool that has been successfully applied to a wide range of physical and computational problems from credit application scoring to image compression [18] to mechanics of prediction of aluminium production [25].

Backpropagation networks are multi layered feed-forward neural networks that have been trained using an error backpropagation procedure. This is a supervised mode of learning where a systematic method is used to adjust the weighted connections within the network.

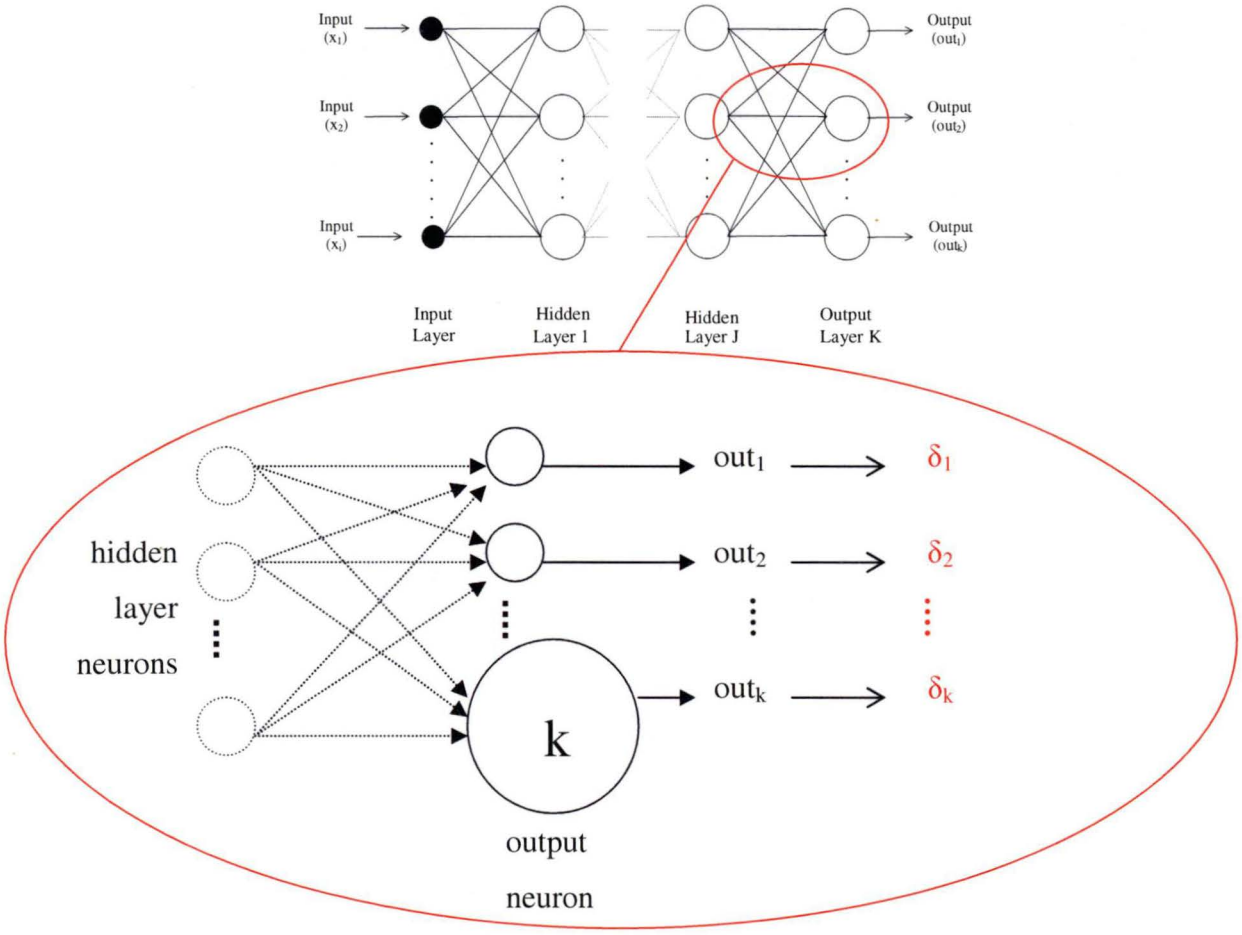

Figure 2-29 Backpropagation (multi layered feed forward) neural network architecture with exploded output layer processing neuron [22]

The backpropagation procedure begins with the calculation of error at the output layer. From each neuron in the output layer a single, real number is output. During training the output vector provides target outputs for each of these outputs from all neurons in the layer.

The error, δ_k, can then be calculated for neuron k in the output layer:

$$\delta_k = (t_k - a_k) f'(net_k)$$

Equation 2-13

Where: f'(x) = first derivative of the activation function

net_k = the weighted sum of inputs to neuron k

t_k = target value for output from neuron k

a_k= output value from neuron k

Commonly the activation function used in the backpropagation neural network is the logistic or sigmoidal function. Recall:

$$f(net) = \frac{1}{1 + \exp(-net)}$$

Thus the error is scaled to make a large correction when the weighted sum of the inputs is small, and a larger correction when the weighted sum of the inputs is large.

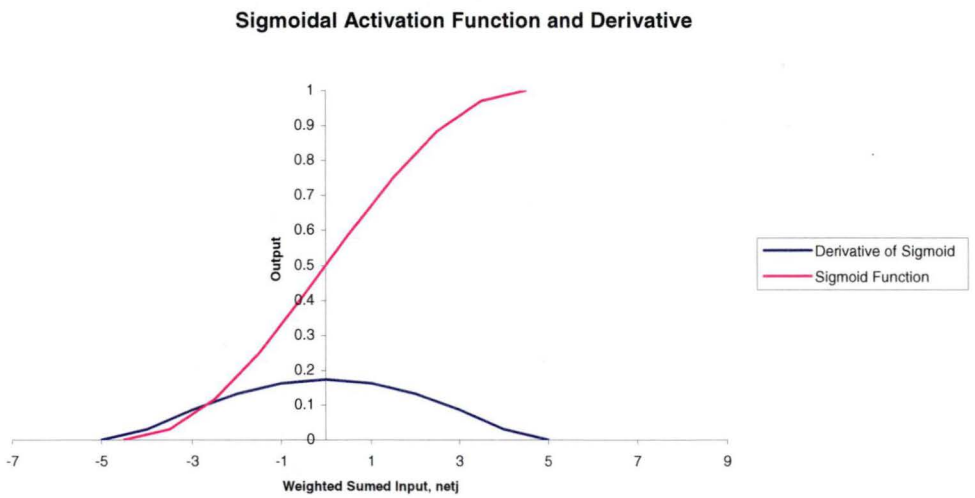

The backpropagation procedure continues with the calculation of the error at the hidden layer, J:

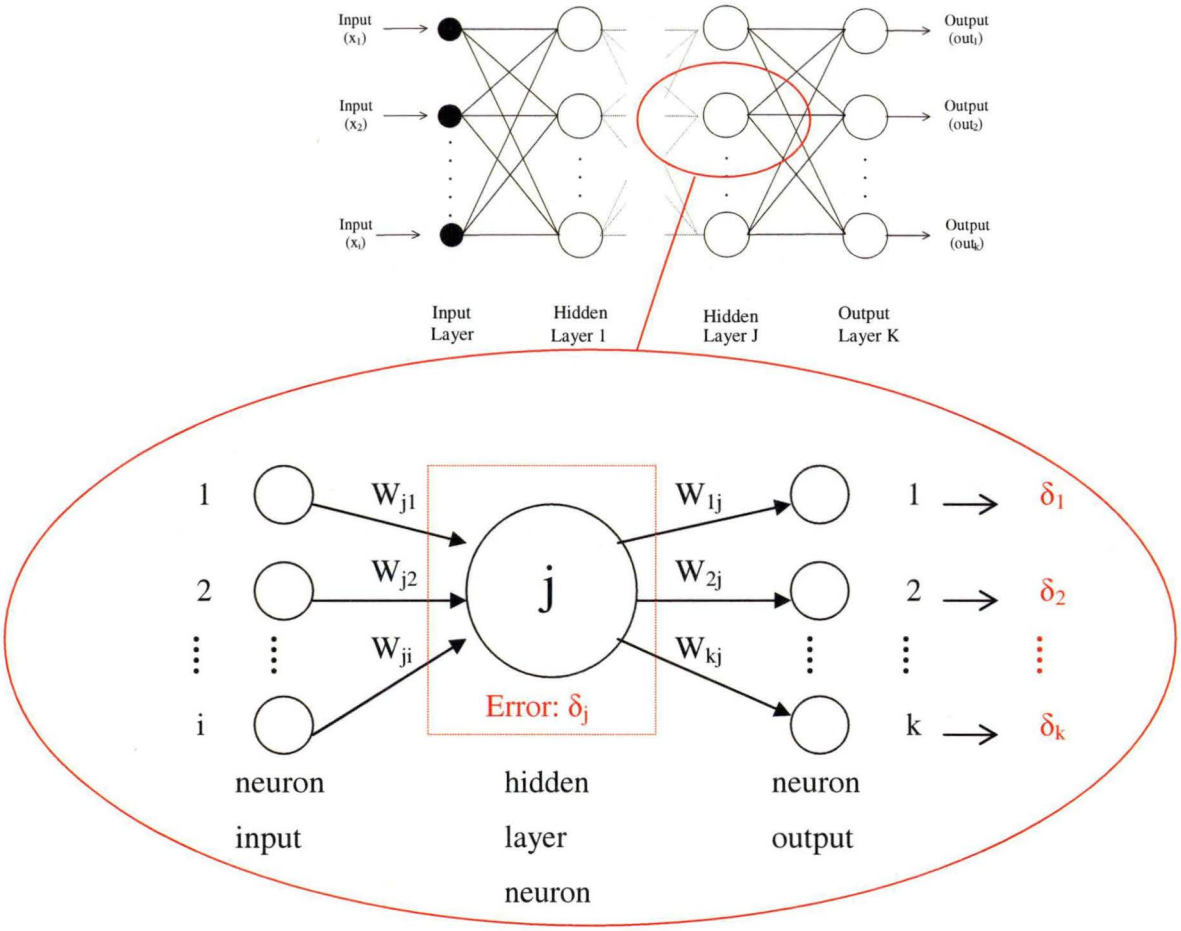

Figure 2-30 Exploded hidden layer processing neuron [Fred Frost 34][R-ROJAS]

For the hidden layer neuron j above the calculation of error involves the weighted sum of δ values from all neurons connected to its output. Thus an equation for the calculation of δ_j [26]:

$$\delta_j = \left[\sum_k \delta_k W_{kj}\right] f'(net_j)$$

Equation 2-14

Where: f'(x) = first derivative of the activation function

net_j = the weighted sum of inputs to neuron j

δ_k = error value calculated for neuron k

W_{ki} = weighted connection from hidden layer neuron j to output layer neuron k

Each interconnection weight can now be adjusted using the error calculated for the corresponding neuron input. That is, the error calculated for a given neuron is used to adjust the weighted connections on the input side [26]. The 'delta rule':

$$\Delta W_{ji} = \eta \, \delta_j \, a_i \qquad \textit{Equation 2-15: Delta Rule}$$

Where: W_{ji} = weighted connection to neuron j from neuron i

η = learning rate constant, $0<\eta<1$

δ_j = error value calculated for neuron j

a_i = output value from neuron i

Thus the adjustment of the interconnection weight W_{ji} is entirely dependent on the parameters η, δ_j and a_i. Of note is that the rate of change of the weighted connection, W_{ji}, is proportional to the magnitude of the error for neuron j. This means that a large error value in neuron j will cause a rapid change in the weighted connection between neuron i and j.

The learning rate, η, determines the convergence speed of the neural network and is important to achieve the correct balance. If set too high, this will lead to instability of the network. If set too low the network learning rate will be excessively slow. This learning rate can also be altered dynamically during the convergence process, beginning at a high value and decreasing during the learning phase.

To Improve the rate of convergence a momentum term can be added to the delta rule for adjusting interconnection weights. This momentum term effectively dampens oscillations during the convergence process. The term is only applied to update the weight changes in the following iteration. With the addition of this momentum term, the resulting rule is referred to as the 'generalised delta rule'.

$\Delta W_{ji}^{k} = \eta\, \delta_j\, a_i + \alpha \Delta W_{ji}^{k-1}$ *Equation 2-16: Generalised Delta Rule*

Where: ΔW_{ji}^{k} = weighted connection adjustment to neuron j from neuron i on iteration k

ΔW_{ji}^{k-1} = weighted connection adjustment to neuron j from neuron I on iteration (k-1)

α = momentum term constant, $0 < \alpha < 1$

η = learning rate constant, $0 < \eta < 1$

δ_j = error value calculated for neuron j

a_i = output value from neuron i

Weights in the neural network are usually initialised to random small values. Commonly these are values between –0.5 and 0.5, alternatively –1 and 1, or another suitable interval. This weight initialisation procedure has a substantial influence on the rate of convergence of the neural network. The random weights disturb the network and allow correct weights to develop as the convergence process advances.

To achieve an assessment of how close a trained or partially trained network is predicting the desired outputs the Root Mean Square or RMS error is often calculated for the network:

$$RMS_{error} = \sqrt{\frac{\sum_{p}\sum_{k}\left(t_{kp} - a_{kp}\right)^2}{n_p n_k}}$$

Equation 2-17

Where: t_{kp} = target for output neuron k after presentation of pattern p

a_{kp} = actual output generated by NN output neuron k after presentation of pattern p.

n_p = number of training patterns

n_k = number of neurons in the output layer

As a general rule, an RMS value of less than 0.1 means that the network has adequately learned its training set [27].

2.13.1 Algorithm for backpropagation neural network training

- 1. Initialise all interconnecting weights by assigning small random values.
- 2. Expose the neural network input layer to the first input vector from the training set and acquire the output vector from the output layer.
- 3. Compare this output vector from the network with the corresponding training set output vector. Here the error associated with each neuron is calculated using [Equation 3-4]and [Equation 3-5].
- 4. Using [Equation 3-6], or alternatively [Equation 3-7], the weight adjustment can be calculated for interconnections between neurons.
- 5. Repeat steps 2,3 and 4 for all input and corresponding output vectors from the training set
- 6. Test the overall RMS error of the network using [Equation 3-7] for every input and corresponding output vector within the testing set. This will provide an indication of the overall predictive capability of the neural network

2.14 GENERAL REGRESSION NEURAL NETWORK

A GRNN is a memory based feedforward neural network, it responds to an input pattern by processing the input data from one layer to the next with no feedback paths. GRNNs feature fast training times, can model nonlinear functions, and have been shown to perform well in noisy environments given enough data [28].

The primary advantage of the GRNN is the speed at which the network can be trained. Training a GRNN is performed in one pass of the training data through the network, the training data values are copied to become the weight vectors between layers. While the advantages of the GRNN include fast training times, ability to handle both linear and nonlinear data and the fact that the smoothing parameter is the only adjustable parameter, thereby making overtraining less likely, the GRNN also has some associated disadvantages. For example, the GRNN requires many training samples to adequately span the variation in the data, and it requires that all training samples be stored for future use. In addition, the GRNN has trouble with irrelevant inputs and there is no intuitive method for selecting the optimal smoothing parameter.

The architecture of a basic GRNN, shown in [Figure 2-31], has four layers; input, pattern, summation and output, with weighted connections w_{ji} between the input and pattern layer and A_i and B_i between the pattern and summation layer. There are i input neurons, j pattern neurons, $k+1$ summation neurons and k output neurons.

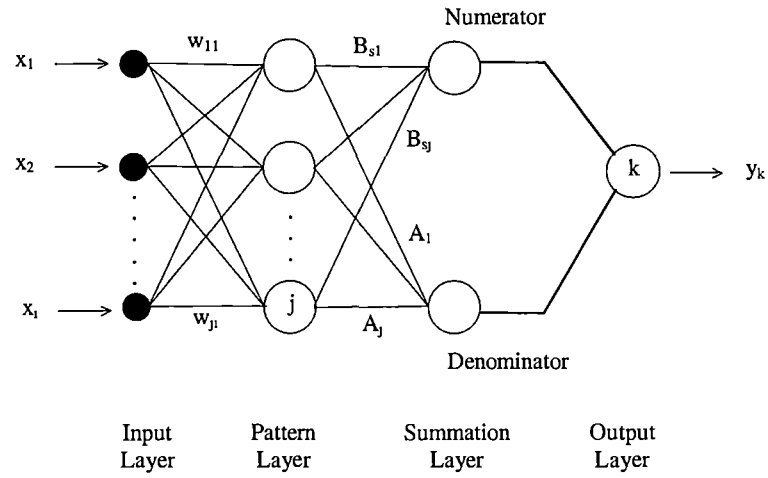

Figure 2-31 Basic General Regression Neural Network (GRNN) architecture.

The function of the input layer is to pass forward the activity patterns presented to the network to all neurons in the pattern layer. The number of input layer neurons is equal to the dimension of the input vector. The neurons in the pattern layer perform a nonlinear transformation of the input patterns. When a new vector X is entered into the network, it is subtracted from the stored weight vector representing each activity pattern. Either the squares or the absolute values of the differences are summed and fed into a nonlinear activation function. The activation function normally used is the exponential function shown in the following equation:

$$f(net_i) = \exp[\frac{-net_i}{\sigma}] \qquad \textit{Equation 2-18}$$

where, $f(net_i)$ = output from pattern layer neuron i,

net_i = sum of differences between input and weight vector for pattern layer neuron i.

σ = smoothing factor

The output from all neurons in the pattern layer then becomes input for all neurons in the summation layer. For a single output network the summation layer consists of a denominator neuron and a numerator neuron. For each additional output unit a single

numerator is added. Hence, the summation layer consists of a single denominator unit and *n* numerator units, where *n* equals the number of output neurons. The summation layer neurons perform a dot product between a weight vector and a vector composed of the signals from the pattern units. For the denominator summation neuron, the weight vector is unity, so a simple sum is performed, represented by the following equation:

$$den_{out} = \sum_{J} f(net_J) * A_J \qquad \textit{Equation 2-19}$$

where, den_{out} = output from denominator summation neuron,

$f(net_j)$ = output from pattern layer neuron *j*, and

A_j = weight connecting denominator summation neuron to all pattern layer neurons, equal to one for all A_j

For the numerator summation neuron, the weight connecting it to each pattern layer neuron is equal to the value of the dependent variable for the training case of that pattern layer neuron [28]. Hence, the numerator summation neuron performs a computation represented by the following equation:

$$num_{outs} = \sum_{J} f(net_J) * B_{sJ} \qquad \textit{Equation 2-20}$$

where, num_{outs} = output from numerator summation neuron *s*,

$f(net_j)$ = output from pattern layer neuron *j*, and

B_{sj} = weight connecting numerator summation neuron *s* to all pattern layer neurons

The output from the denominator and numerator summation neurons are sent to the output layer neurons, the function of which is to divide the output of the associated numerator summation neuron by the output of the denominator summation neuron.

As a pre-processing step, it is usually necessary to scale all input variables such that they have approximately the same ranges of variances. The need for this stems from the fact that the underlying probability density function is to be estimated with a kernel that has the same width in each dimension

A training algorithm for the general regression neural network:

Step 1. Determine a suitable value for the smoothing parameter, σ.
Step 2. Set input to pattern layer weights, w_{ji}, equal to the values of the independent variables in the training data set.
Step 3. Set pattern to summation layer denominator weights, A_j, equal to a value of one.
Step 4. Set pattern to summation layer numerator weights, B_{sj}, equal to the values of the dependent variables in the training data set.
Step 5. Pass the entire training data set through the network and calculate the network output in each instance using [Equation 2-18] for the pattern layer neurons, and [Equation 2-19] and [Equation 2-20] for the summation layer denominator and numerator neurons, respectively.
Step 6. Calculate network output by dividing the numerator output by the denominator output for k output neurons.
Step 7. Compute and observe the prediction error of the network by comparing the predicted output with the target output.
Step 8. If the prediction error is unacceptable, change the value of the smoothing parameter and repeat Steps 5 to 7.
Step 9. Repeat Step 8 until the prediction error is minimum.

Chapter Three

DESIGN OF TEST RIG

The requirement for a vehicle providing on-line brake-force and dynamic chassis parameter measurement resulted in the test rig development described within this chapter.

By developing a vehicle specifically for the purpose of data collection and automotive Neural Network development inherent problems associated with modifying vehicles built for other purposes were avoided. Commercial vehicles are designed for specific markets and not for installations of complex telemetry and dynamic chassis measurement systems. Further, testing and analysis of a commercial vehicle to gather data about the design, for instance information about the rigidity of the chassis, is expensive and time consuming.

From a purely scientific point of view, the development of a specific test vehicle allowed the removal of as many unknowns as possible. To achieve this, ground-up design of this vehicle was undertaken. This presented some problems associated with the complex nature of vehicle design and concerns for driver safety.

In much the same way, driver and general safety concerns in prototype and one off racing vehicles has lead to the development of rules for racing classes where the vehicles can be constructed and designed quickly and safely within the guidelines. Formula SAE is one such class.

The Formula SAE competition was formed in the USA in 1981 and is now also running in Europe and Australia. The competition is for engineering students to conceive, design, fabricate, and compete with small formula-style racing cars. The restrictions on the cars frame and engine are limited so that the knowledge, creativity, and imagination of the student are challenged. The cars are built with a team effort over a period of

about one year and are taken to a host institution (Ford, Toyota, Holden or Mitsubishi) for judging and comparison with other competitors. The end result is a great experience for young engineers in a meaningful engineering project as well as the opportunity of working in a dedicated team effort.

For the purpose of this competition, the students are to assume that a manufacturing firm has engaged them to produce a prototype car for evaluation as a production team. The intended sales market is the non-professional weekend autocross racer. Therefore, the car must have very high performance in terms of its acceleration, braking, and handling qualities.

The car must be low in cost, easy to maintain, and reliable. In addition, the cars marketability is enhanced by other factors such as aesthetics, comfort and use of common parts. The challenge to the design team is to design and fabricate a prototype car that best meets these goals and intents. Each design will be compared and judged with other competing designs to determine the best overall car.

The cars are designed entirely by the students and compete for overall supremacy in:

- Presentation
- Engineering Design
- Cost Analysis
- Acceleration
- Skid-pad performance
- Autocross event
- Fuel economy event
- Endurance event

Incidentally, the prototype race car / test rig which is the subject of this chapter won the Australasian Acceleration event, won the prize for the best use of innovative electrical systems, ranked 3rd in Australia overall out of 16 entrants and sixth worldwide in the 2001 International-Australasian Formulae SAE competition. At the Holden proving grounds in Melbourne, Australia.

3.1 CHASSIS DYNAMICS

The handling of a prototype test/racing car is influenced by an astoundingly large number of factors. Initially, major factors identified were:

Weight distribution
Position of the centre of gravity
Polar moments of inertia of the vehicle about the three axes
Frame design
Suspension design, wheelbase and track widths
Wheel assembly, brake design and tyre selection
The amount of power driving the rear wheels

The weight distribution of a racecar refers predominantly to the wheel loading. This is of greatest significance since the tyre contact patches are arguably the biggest factor in defining the way a racecar will handle. Of course, the weight distribution of a car is dynamic, acceleration in any direction as well as any down force experienced by the moving vehicle will have an effect on the wheel loading.

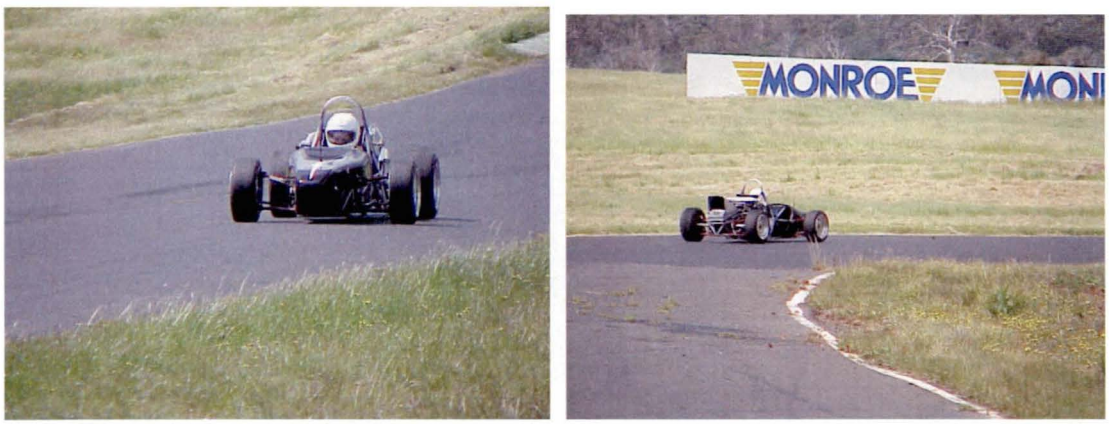

Figure 3-1 Vehicle dynamics were found to be influenced by an astoundingly large number of factors. These pictures were taken during early stages of testing at Baskerville Raceway – Hobart, Tasmania.

To further complicate matters, the overall weight of the vehicle will change as the fuel load is burned and, if the fuel tank is not positioned at the centre of gravity, even the relative wheel loadings will change.

The static weight distribution defines the position of the centre of gravity in the horizontal plane. However the position of the centre of gravity vertically will have a large influence on the overall vehicle handling as well as the weight transfer characteristics of the car while accelerating. Note that the changing fuel load will again have an effect on the position of the centre of gravity.

It is worth noting here that for any given class of racecar, as with Formula SAE, the weight distribution is to a large extent predetermined to quite tight limits. For instance, if we are adopting a conventional layout (admittedly, there are other options) with a 600cc motorcycle engine and gearbox it means that the engine will be mid mounted with the driver in front and the drive axel behind. Then the wheelbase will be somewhere in the vicinity of 1600mm-2000mm and the static weight distribution of the vehicle will be somewhere between 40/60 and 55/45 (Front/Rear).

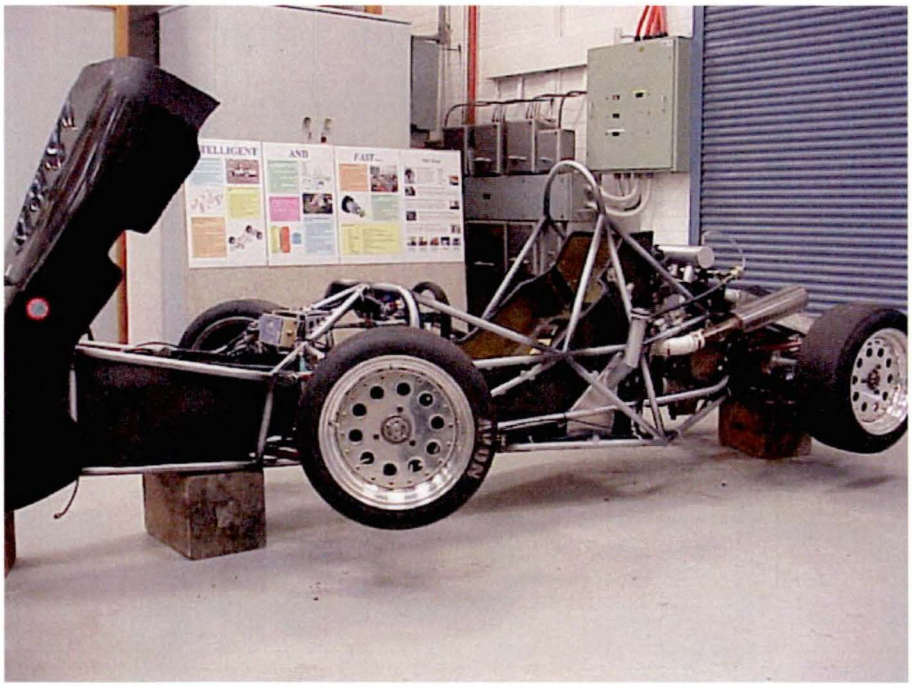

Figure 3-2 Mid-mounted engine layout of the test vehicle

Similarly, the vertical position of the centre of gravity will be largely predetermined. The lowest part of the engine, chassis and driver should not be allowed to make contact with the track under normal driving conditions. On the other hand, the lower the centre of gravity, the smaller the weight transfer characteristics during acceleration, braking and cornering. This all points toward the racecar designers attitude of "how low can you go". Again if we use the formulae SAE example this will put the centre of gravity at about 0.4m this is provided that placement of the other heavy equipment has been carefully considered and is as low as possible.

A very reclined driver position was decided upon early as it had the effect of minimising the total height of the car, the frontal area and lowering the centre of gravity. As well as this the driver was moved as far forward as possible in an attempt to gain a desirable weight distribution.

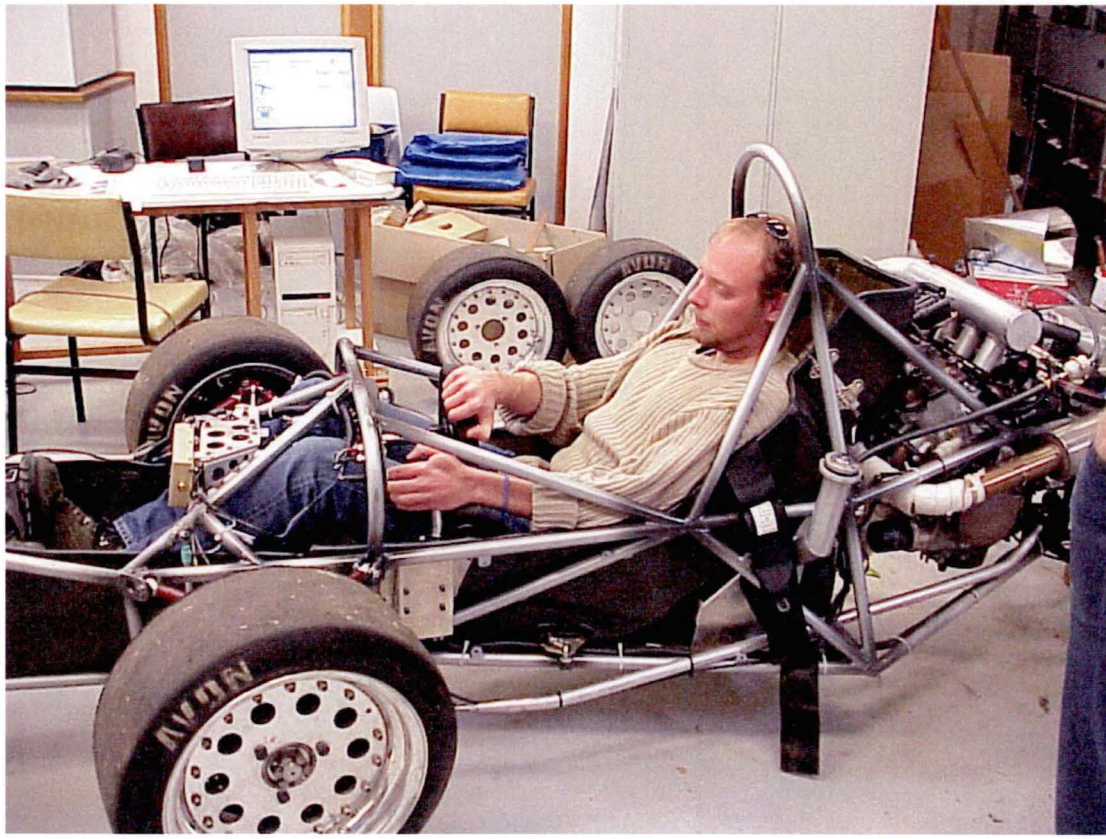

Figure 3-3 Reclined driver position of the test car. Note the far forward driving position.

Polar moments of inertia quantify the "readiness" with which the vehicle can be deflected from its path. There are three axes with which we need to consider that

represent the yawing, pitching and rolling actions. Traditionally racecar designers and drivers are mostly concerned with the yawing polar moment of inertia.

Conceptually a vehicle with the main masses situated towards the ends is considered to have a high polar moment of inertia in yaw, this means that from a drivers point of view that the car will respond reluctantly to steering input. Conversely, a vehicle with the main masses situated very near to the centre of gravity will have a low moment of inertia in yaw, and will respond quickly to steering input. The high moment of inertia vehicle will be more reluctant to spin, however once spinning it will take more stopping than a low moment of inertia vehicle. A low moment of inertia vehicle will exhibit "twitchy" handling characteristics that require "lightening" quick reflexes on the part of the drivers.

Very little can be done to affect the polar moments of inertia other that to get the radiator, fuel tank and other heavy components as close to the centre of gravity as possible. In practice, other aspects of the car design in effect dictate the polar moments of inertia and in practice the difference between a high moment of inertia and a low polar moment of inertia formulae SAE car is very small. However throughout the history of racing many credible drivers have reported that they can "feel" small modifications to their cars which race engineers would say are immeasurable.

Because of the windy and slow nature of the Formula SAE race track, the decision was to make the polar moment of inertia in yaw as small as possible and that meant keeping as many of the components as close to the centre of the car as possible. This approach was also consistent with the desire to keep the car as compact and also as light as possible since wiring, plumbing other connection lengths would be minimised.

The effect this has on the car as a test rig is that the range of acceptable yaw angles before spin out will be increased. This is a very desirable quality as it increases the effective/useful resolution of the yaw sensor.

3.2 FRAME DESIGN

The design of the frame presented many challenges since the high performance vehicle was required to fulfil its specific purpose as a test rig for Neural Network development.

The frame was designed and constructed:

1. To provide stable mounting points for all measurement equipment including the suspension linear potentiometers, steering wheel position sensor, pitch, roll, yaw and 3d acceleration sensor.

2. To provide both rigid and stable mounting points for all necessary running gear including the engine, seat, suspension wishbones, steering, drivetrain, radiator, fuel tank and pump and filters, harnesses and body work.

3. To conform to the international rules of Formula SAE Competition for driver and general safety [31].

4. To minimise the forces experienced by the frame, its overall size (especially the frontal area) and weight and to maximise rigidity particularly torsional to optimise performance.

The reclined driver position facilitated the placement of the main pitch, roll, yaw and 3d acceleration sensor at very close to the centre of mass. Ideally this is where it needs to be located however this is usually within the driver.

3.3 FRAME DEVELOPMENT

A Formula SAE-A racecar must meet an array of design and safety requirements set out in the competition rules [31]. The design of the frame, being the single largest component within the car, must consider every specification layed out within the rules, anticipate the requirements for the installation of each component and allow space for the addition of various sensors as they are called for. The overall design of the vehicle revolves around the shape of the frame, and so its construction must consider all aspects of the intended design. In the interests of high performance it is important to design to close tolerances, which entails strict identification of the various component positions and overall design requirements. These requirements include:

Rule Based Requirements:

- Open wheel and open cockpit type vehicle
- Wheel base of at least 1500mm
- Inclusion of front and rear suspension
- Engine size limit of 610cc
- Single seat design (no passengers)
- Front and rear roll over hoop positioning, dimensions and supports
- Side impact protection bar inclusions
- Bulkhead dimensions
- Crush zone dimensions
- Manufacturing materials (or demonstrated equivalence)

Construction Based Requirements:

- Must be as light as possible, while maintaining a long lifetime
- Must be reasonably simple and cheap to construct
- Must strive to make the car as compact as possible
- Must be reasonably ergonomic
- Must encourage component positioning to provide a low centre of gravity, and approximately 50 / 50 weight distribution between the front and rear wheels
- Must provided ample stiffness to encourage superior handling

- Must house the following major components in their respective optimum positions:
  - Pedals
  - Seat and harness
  - Suspension wishbones, springs and pull rod pivots
  - Steering components
  - Gear changer mechanism
  - Fuel Tank
  - Engine and associated equipment
  - Differential
  - Radiator
  - Bodywork
  - Electrical equipment (engine management computer, data logger, radio modem, etc)
  - Assorted sensors

These rule and construction based requirements form the basis of the design criteria for the frame. To this end, the frame of choice was decided to be a tubular steel space frame of varying member diameters and wall thicknesses.

Upon the initial stages of the frame design it was evident that in order for the frame design to proceed, a general idea of what components were going to be used, and where they were going to be positioned was required. This mainly included the driver, suspension, drivetrain and engine positions, and initial designs centred on the respective positions of each of these. As the frame started to conceptually take shape, other components where included into the design to provide the close tolerances required and efficient load paths for minimum weight. This required the component selection process to proceed concurrently with the frame design, with the identification of appropriate parts often significantly altering the shape and form of the frame.

As such, many frame designs were made, and altered, to suit different component choices and positions, while also maintaining perceived structural integrity using the least members possible. As an aid to this process, an easily modifiable PVC piping

mock frame was constructed, as shown in [Figure 3-4]. This enabled an iterative process that led to a stage where the correct parts could be ordered for later addition to the frame and a frame design that met the spatial requirements of the overall vehicle design and component positioning.

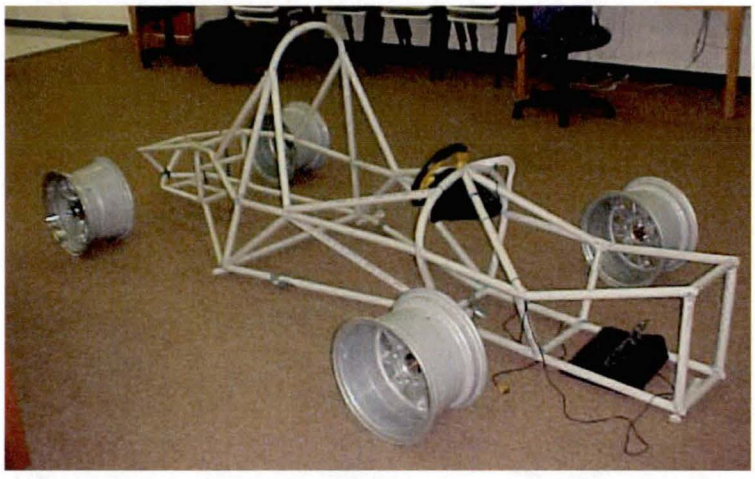

Figure 3-4: PVC mock frame

3.3.1 Finite Element Analysis (FEA)

Once the frame was designed to meet the component positioning requirements, its structural integrity and load paths had to be tested in the interests of assessing its strength, rigidity and overall weight. Being a very complex system it was decided the easiest and most time effective way to do this was through FEA. However, at this stage only a very vague idea of expected driving conditions was known. Vehicle mass and mass distribution where not known, either were the maximum accelerations from throttle, braking and cornering. Excessive values were assumed for these, that where not expected to be reached in even extreme driving conditions. This effectively introduced a safety factor into the modelling process, avoiding the need to apply it elsewhere. These values were:

Acceleration due to Throttle	$= 15ms^{-2}$	$= 1.5g$
Acceleration due to Braking	$= 3ms^{-2}$	$= 3g$
Acceleration due to Cornering	$= 2.5ms^{-2}$	$= 2.5g$

Acceleration due to Gravity	= $10ms^{-2}$	= 1g
Vehicle Mass (wet, with driver)	= 360 kg	
Front / Rear Mass Distribution	= 47 / 53	

The model was then created in Strand7 [23], using only beam elements. This simplified the model construction and also made the results simple to understand. Material restrictions and availability were also taken into account and, as a result, only 25mm OD mild steel tubing of wall thicknesses 2.6mm and 1.6mm were chosen for the construction of the frame.

In an attempt to make the loading on the frame as accurate as possible a number of measures were taken, and are depicted in [Figure 3-5]. Firstly, a suspension system was included in the model, the dimensions of which had been under development concurrently with the frame. This included wishbones that were allowed to freely pivot on the frame (simulating rod ends) and a pull rod type suspension spring arrangement. The wishbone ends were then fixed in space to simulate the reactive forces of the wheels. Secondly, masses were applied to the frame to simulate component masses, such as the engine and driver. The masses where applied as 10kg 'blocks', each attached to member intersections distributed throughout the frame, in an attempt to gain the car's estimated weight distribution and centre of gravity. Thirdly, the frame was artificially stiffened around the engine mounts with additional members. This was done because the frame design around that area relies on the engine to act as a sub-member, increasing stiffness but receiving minimal loads.

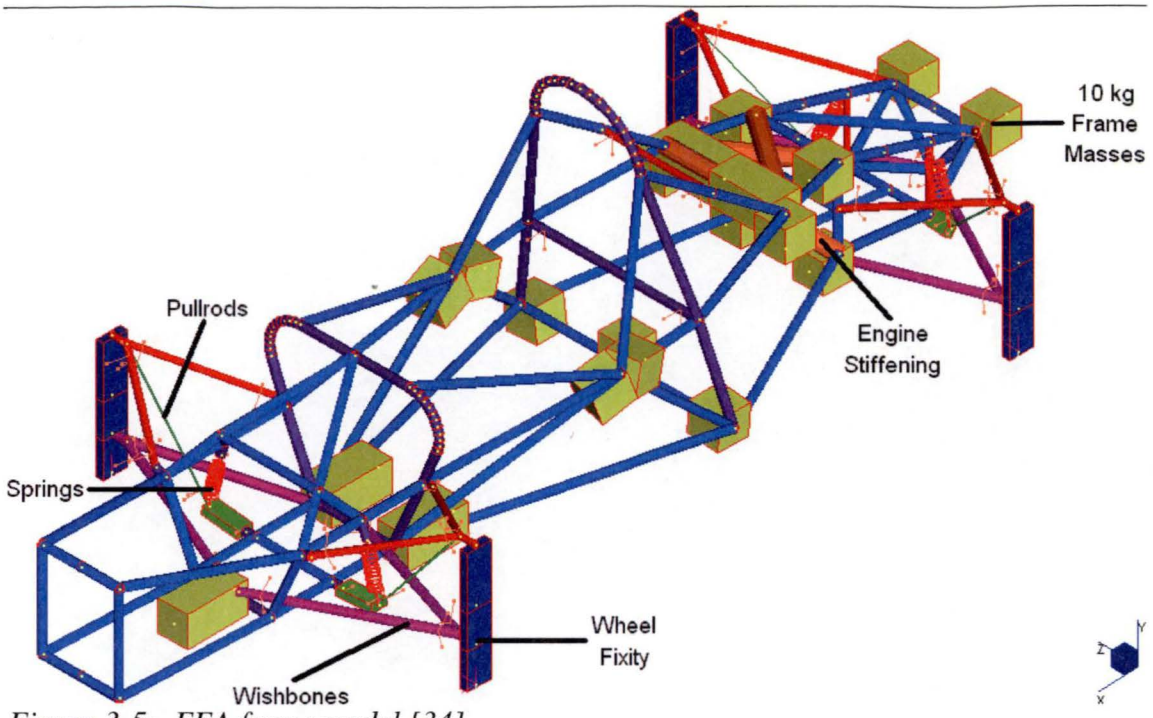

Figure 3-5: FEA frame model [34]

By altering wheel fixity conditions a number of loading cases were created, each case using the applicable acceleration values above and are shown in "Appendix B". The cases were:

- Normal driving
- Hard throttle
- Hard braking
- Hard cornering
- Cornering under throttle
- Cornering under brakes [Figure 3-6]
- Torsional stiffness [Figure 3-7]

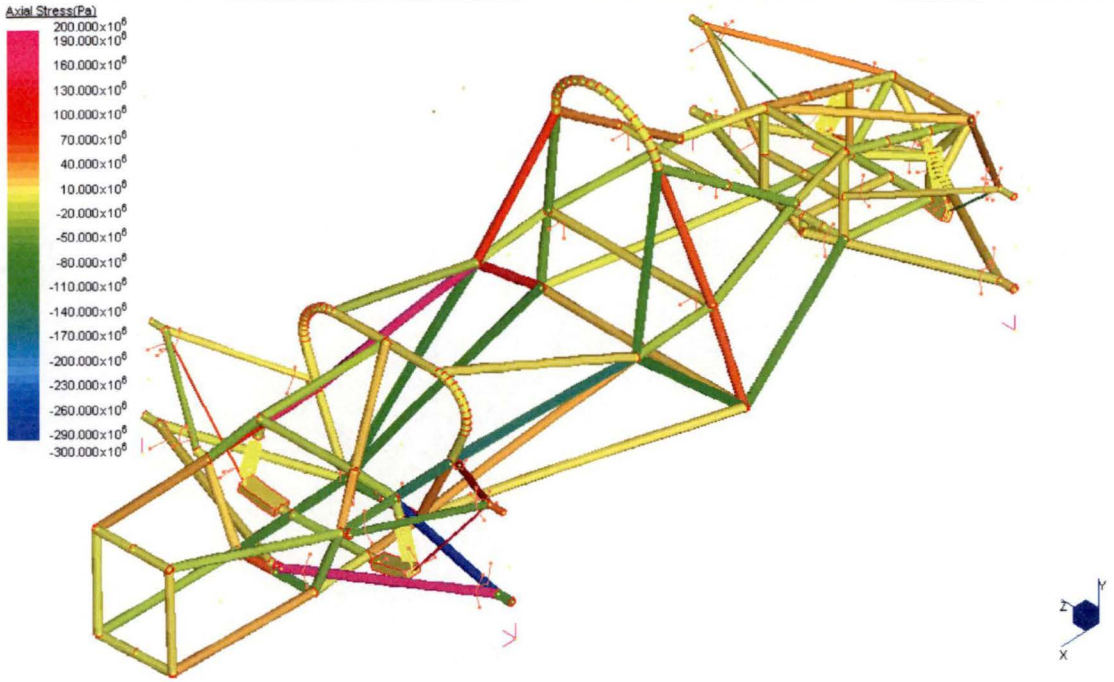

Figure 3-6: FEA results for cornering under brakes

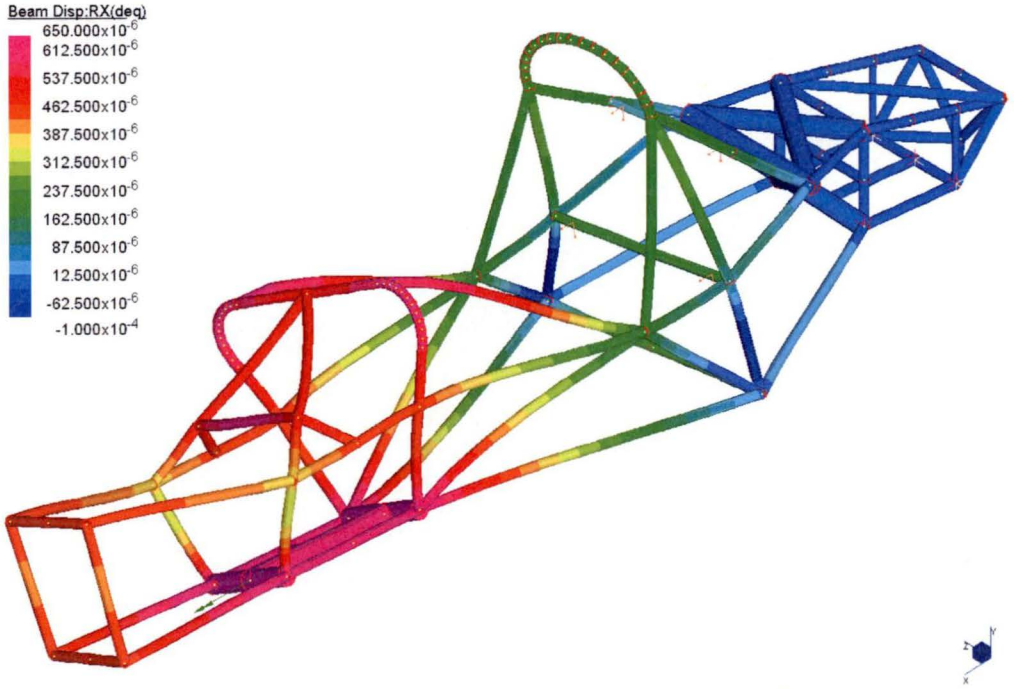

Figure 3-7: FEA torsional results under 1 Nm

These loading cases gave FEA results for member loadings and member deflections, allowing the easy identification of severely loaded or deflected members or the detection of superfluous ones. As such, the frame again went through a number of design iterations, as efforts were made to decrease its weight while maintaining stiffness and strength. The end result being a frame model that was well below its strength limit and had a torsional stiffness of 0.6° per 1kNm load between front and rear suspension points.

3.3.2 Computer Aided Design

Once frame dimensions and member sizes where defined using FEA the last requirement before construction could take place was to have CAD drawings ready. This was primarily to enable full dimensioning of the frame so member lengths and positions could be found for its construction, a feature that Strand7 lacked. To this end, a wire frame model of member centre lines was exported from the FEA package into the three-dimensional drawing package, CADKey [35]. It was then converted into a 'solid' model with complete member diameters and wall thicknesses ([Figure 3-8]), and later dimensioned for use in the frame construction. The complete set of dimensions are given in "Appendix B'.

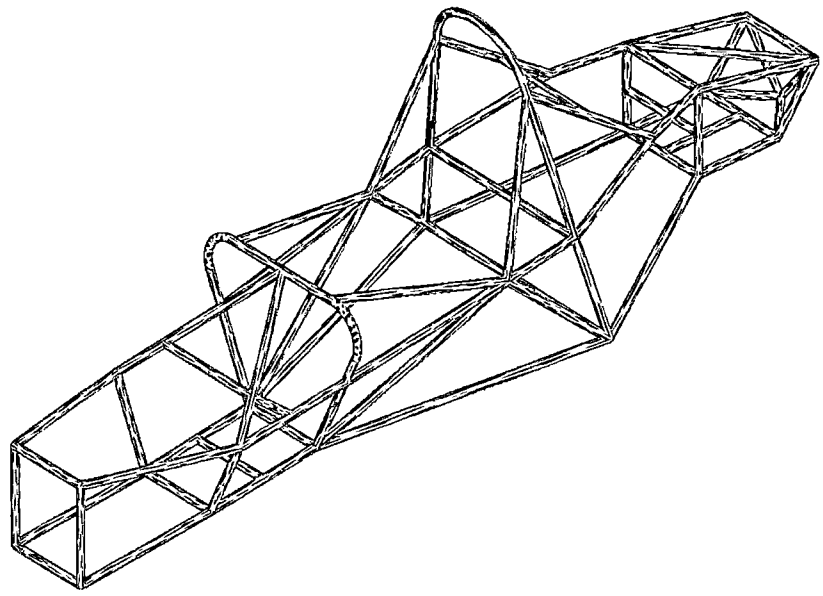

Figure 3-8: CAD drawing of the frame

3.3.3 Frame Construction

Frame construction proceeded in a number of steps. It was decided from the outset that the frame was going to be MIG welded due to workshop limitations and that it was going to be welded using a jig. The form that the jig took was as a steel table from which many of the members where lightly welded (tacked) into place in their correct positions. This provided an excellent baseline to work from as well as reducing the amount that the frame distorted due to residual welding stresses once it was removed from the jig.

Construction followed a logical sequence. The front and rear roll over hoops where first bent into shape and construction between them began. Members where cut to the correct lengths and their ends tapered to ensure a good fit to at the joints, which were subsequently welded. The front bulkhead was constructed next, followed by the engine bay and finally the rear most section, ensuring that a sequence of welding was maintained to minimise buckling due to welding stresses. The frame was then removed from the jig and all of the final welding was completed with minimal frame distortion. The complete frame is shown in [Figure Mild steel frame].

The 140 or so mountings for the various components such as the suspension system, the engine, the differential and the seat and seat belt were then designed, constructed and welded to the frame as required. With all of the mountings completed, the frame was painted using automotive acrylic paint, and assembly began.

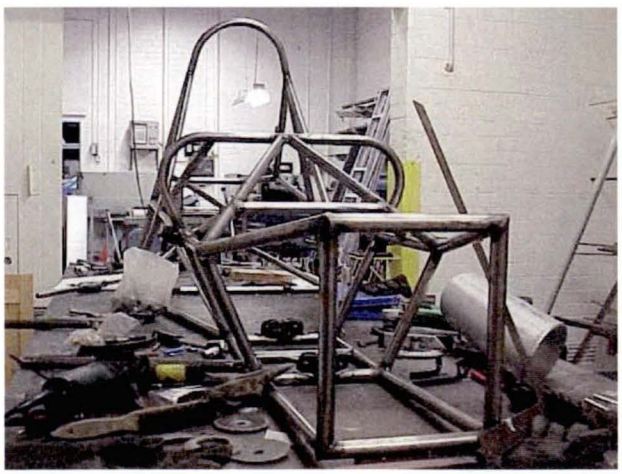

Figure 3-9: Mild steel frame

3.4 SUSPENSION DESIGN

As with the frame design, the design of the suspension paid careful consideration to the vehicle as a test rig for Neural Network Development.

The suspension was designed and constructed:

1. To provide stable mounting points for all measurement equipment.
2. To conform to the international rules of Formula SAE Competition for driver and general safety.
3. To minimise the forces experienced by the frame.

   The major forces on the frame are transmitted through the suspension. The type, geometry and mounting of the suspension perform a key role in both the kind of forces experienced by the frame and also the magnitude of those forces.
4. To conform to the chosen optimal suspension geometry and an appropriate level of strength and serviceability.
5. To minimise the overall size (especially the frontal area) and weight of the suspension system.
6. To facilitate easy geometric changes, part replacement and "tuning".
7. To use as few parts as possible.
8. To share as many common parts between corners as possible.

3.5 SUSPENSION DEVELOPMENT

The rules and nature of Formula SAE directly specify many of the constraints on the vehicle's suspension design. On top of this the competition course -type of corners, general layout and specified surface dictate how the suspension will be required to operate if the vehicle is to take full advantage of the level of grip available from the tires. Simply put, the purpose of a suspension system is to maximise the amount of contact between the racecar's tyres and the road surface. However this is not quite the full story as the dynamic nature of suspension has the effect of changing the distribution weight and inertial forces of the vehicle between the four wheels.

One of the first decisions made was to estimate a suitable wheelbase. The chosen wheelbase of a racecar has a major effect on the weight transfer characteristics of the chassis and will also influence the polar moment of inertia about yaw, high-speed stability and the turning radius. Since one of the key design motif of the vehicle was to keep it as compact as practical, the wheelbase estimation stemmed from our decided driver and engine positions. This worked for the design of this car because it happened to coincide with it's intended use on tight, windy circuits.

Figure 3-10 Formula SAE vehicles are designed to operate on tight autocross style tracks resulting in compact design. Photo courtesy of SAE (USA).

With the driver reclined and the engine located midship, minimum practical clearances were given between the back of the gearbox and the differential spur gear. Since the

drive axles were to be aligned with the differential, the position of the rear axel relative to the driver could be estimated. Now the
fuel tank, radiator, battery, exhaust, pedal box and ancillaries could be juggled about in the spaces between and around the engine and driver until reasonable 'tentative' places for them could be found.

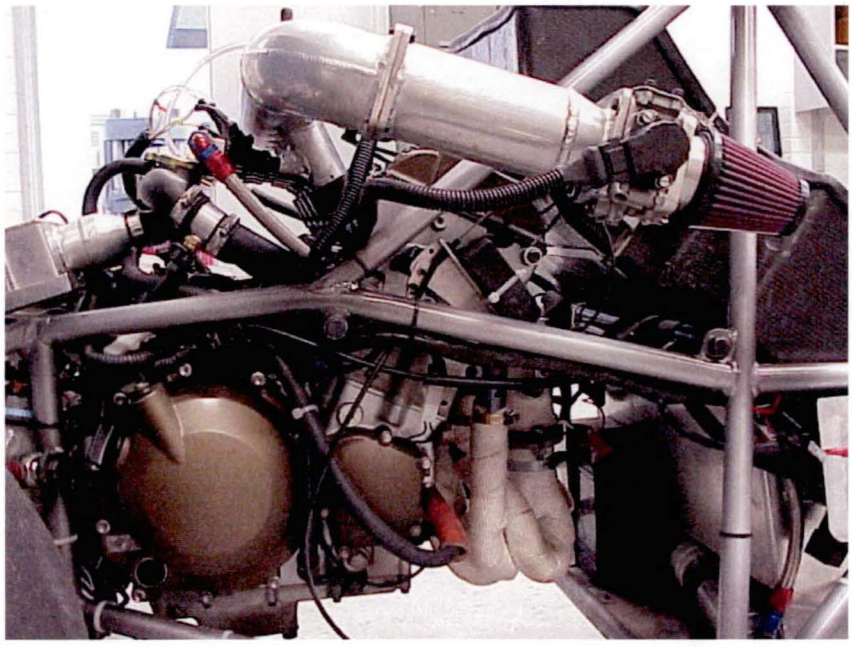

Figure 3-11 Minimum practical clearances were specified between the seat and engine and also the gearbox and final transmission.

The ideal weight distribution of a racecar for neutral cornering characteristics is 50/50, that is, half the static weight on the front wheels and half on the rear. With estimates for the relative weights of the components in their tentative locations, the approximate ideal position of the front wheels could then be calculated. This process is iterative as positions of various components are juggled to find the most practical solution. However, after a day or two of juggling it was decided that a wheelbase of 1800mm would constitute a good target. These initial estimates proved to be reasonable as the final Figure ended up at 1835mm.

The next critical suspension design decision faced was determination of front and rear track widths. Track width is defined as the distance between the front wheel centerlines (front track width) or the distance between the rear wheel centrelines (rear track width).

Note that front and rear track widths may or may not be the same, however the track widths must be decided upon before kinematic analysis of the suspension system can begin.

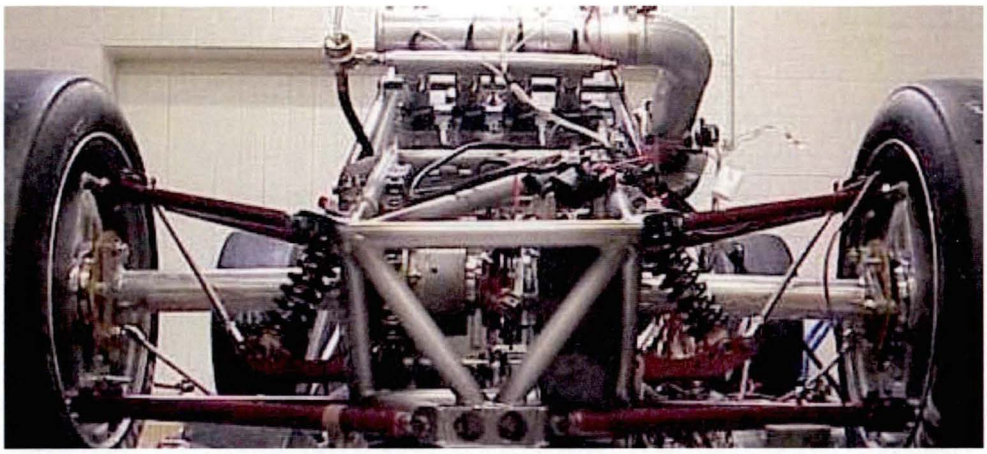

Figure 3-12 The lateral distance between wheels, termed track width, is one of the first critical decisions faced by a vehicle designer.

The decision regarding track widths is critical. During cornering the lateral acceleration causes an overturning moment corresponding to product of the height of the centre of gravity from the road surface, the magnitude of the lateral acceleration and the mass of the vehicle. The track width then directly determines the magnitude of the resisting force through the tires required to overcome this moment. In other words, the track width is one way in which a vehicle designer can directly control the extent of lateral weight transfer.

For this reason the track widths were not as simply arrived at as the wheelbase, since locating the wheels as close as possible to the chassis would result in such a narrow vehicle that overturning would almost certainly be assured. On the other hand a wide vehicle carries not just the disadvantages of increased weight and increased frontal area (drag) over a narrower competitor.

3.5.1 Identification of Optimal Vehicle Width

Figure 3-13 Test vehicle during autocross trials.

Now if we consider an infinitesimal increment of time, dt, during which the vehicle moves through a forward distance dx, and a sideways distance ds.

The forward component of the velocity of the car is then approximately:

$$v = \frac{dx}{dt}$$

Equation 3-1

If we say that at the beginning of the time interval dt the vehicle has no sideways velocity and at the end of the period it has the sideways velocity ds/dt, then the rate of change of velocity (lateral acceleration) for the time period dt is:

$$a = \frac{ds}{dt}\frac{1}{dt}$$

Equation 3-2

Now the lateral distance ds is dependant on the forward speed and the radius of the corner, but instantaneously the ratio of lateral motion to forward motion can be approximated by dx/r, thus :

$$ds = dx\frac{dx}{r}$$

Equation 3-3

And finally:

$$a = \frac{ds}{dt}\frac{1}{dt} = \frac{dx}{dt}\frac{dx}{dt}\frac{1}{r}$$

$$a = \frac{v^2}{r}$$

Equation 3-4

Where: a = lateral acceleration (m/s^2)

v = forward velocity of vehicle (m/s)

r = radius of corner (m)

Thus we have the relationship between lateral acceleration, vehicle velocity and corner radius. So in order to improve out lap times (directly dependant on velocity) we need to corner at the maximum possible lateral acceleration and choose the straightest racing lines around the course. This is obvious, but poor choice of vehicle track widths can prevent the vehicle from physically reaching these limits. Note that down force from aerodynamic aids will not be considered in this simple analysis since they are not to be included in the initial stages of development of the research vehicle.

There are two possible physical limits to lateral acceleration:

1. Overturning.
2. The amount of lateral grip which can be provided by the tyres.

During cornering there is an overturning moment caused by the vertical distance between the centre of gravity (C of G) of the vehicle and the ground, and the cornering force acting at the friction surface at the tyres. The horizontal distance between the C of G and the tyre contact patch, and the weight of the vehicle counteracts this moment.

At the limit of cornering the inside wheels have zero load. Thus:

$$a \cdot g \cdot m \cdot h = m \cdot g \cdot \frac{1}{2} trackwidth$$

$$a \cdot h = \frac{1}{2} trackwidth$$

Equation 3-5

Where: a = lateral acceleration (g)

g = acceleration due to gravity

h = height of C of G (m)

The amount of lateral grip provided by the tyres provides the other limiting factor for lateral acceleration. Given that there is no downforce, the maximum lateral acceleration obtainable from currently available racing slicks is around 1.3g. This is based on skidpan results from some of the top autocross teams.

Wide vehicles have to travel a greater distance around the same circuit than narrow competitors. This is best illustrated on a slalom or chicane but is true for any corner at all.

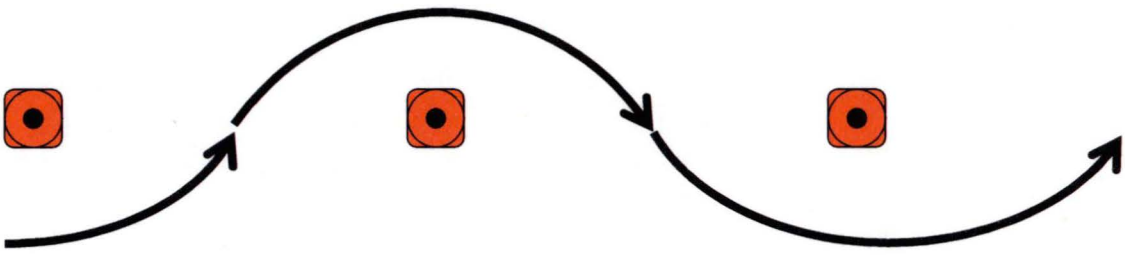

Figure 3-14 An experimental slalom course.

In the slalom course above the car is following the ideal line that are perfect arcs where the maximum lateral acceleration is held for the duration of the slalom changing signs as each cone is rounded.

The following diagram is used determine the radius and length of the vehicle path:

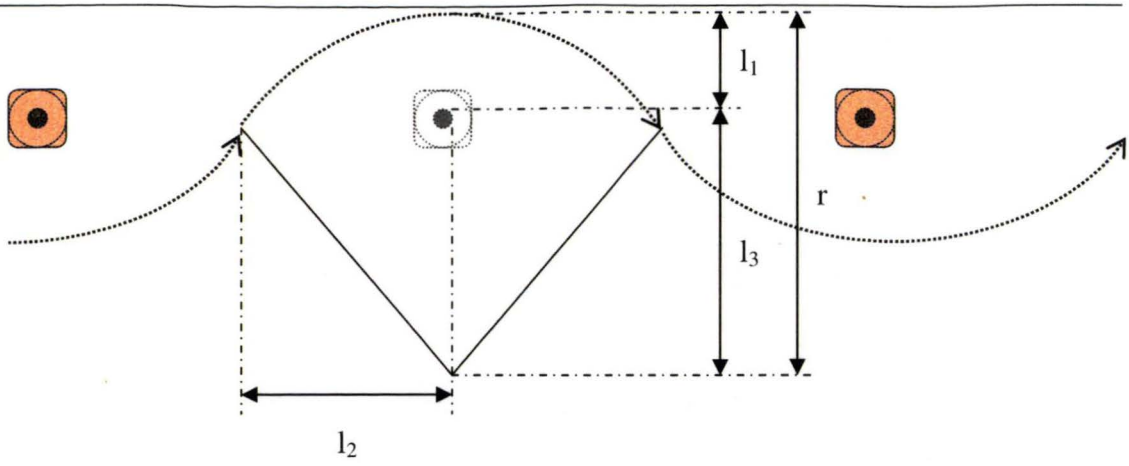

Figure 3-15 Identification of experimental slalom course variables.

From the diagram: $l_1 + l_3 = r$ (a)

$l_3^2 + l_2^2 = r^2$ (b)

Substitute (a) into (b)

$$(r - l_1)^2 + l_2^2 = r^2$$

$$r^2 - 2rl_1 + l_1^2 + l_2^2 = r^2$$

$$l_1^2 + l_2^2 = 2rl_1$$

$$r = (l_1^2 + l_2^2) / 2l_1$$

Equation 3-6

And

$$\text{arc length} = \theta r$$

Equation 3-7

Where $\theta = 2 \sin^{-1} (l_2/r)$

Now a perfect time for the slalom course can be established for a given track width and C of G height.

Numerical Confirmation

For a course of: 10 cones at 10 m apart for a testing field

Track width = 2m is chosen

C of G height = 0.4m for the test vehicle

The roll over threshold from [Equation 3-5] is:

$$a \cdot h = \frac{1}{2} trackwidth$$

$$a \cdot 0.4 = \frac{1}{2} \cdot 2$$

$$a = 3.5g$$

Since the maximum lateral acceleration obtainable from the tyres is about 1.3g ($12.8 m/s^2$), this vehicle will spin out rather than roll over when the cornering limit is exceeded.

To determine the radius of the arc [Equation 3-6]:

$$r = (l_1^2 + l_2^2) / 2l_1$$

Where l_1= 1/2 wheelbase + cone clearance (say 0.1m)

l_2= ½ cone spacing

Thus: $r = (l_1^2 + l_2^2) / 2l_1$

$r = (1.1^2 + 5^2) / 2(1.1)$

$r = 11.9m$

And the distance travelled [Equation 3-7]:

arc length $= \theta r$

Where $\theta = 2 \sin^{-1} (l_2/r)$

arc length $= 2 \sin^{-1} (5/11.9) \times 11.9$

arc length = 10.32m

distance traveled = arc length x no. of cones = 103.2m

Thus the maximum speed at which the vehicle can travel [Equation 3-4]:

$$a = \frac{v^2}{r}$$

$$v^2 = 12.753 \cdot 11.91$$

$$v = 12.326 m/s (44.37 km/h)$$

And the minimum time required to complete the course:

t = distance travelled / velocity

t = 103.2/12.735

t = 8.37 seconds

This analysis was used to create a spreadsheet where varying track widths were tested and the ideal times for the course can be compared. Of note is that a narrow car (1.1m track) can complete the course over 2 seconds (over 25%) quicker than a wide car (2m track).

Table 1 Spreadsheet Analysis of vehicle width and slalom times.

Slalom vehicle analysis

Cof G height = 0.4m

	Maximum Lateral Acceleration (g)					
Track width	From tyres	Roll over threshold	Maximum	Velocity (km/h)	Distance travelled	Time(s)
2.00	1.30	2.50	1.30	44.37	103.20	8.37
1.90	1.30	2.38	1.30	45.33	102.91	8.17
1.80	1.30	2.25	1.30	46.35	102.65	7.97
1.70	1.30	2.13	1.30	47.47	102.39	7.77
1.60	1.30	2.00	1.30	48.68	102.15	7.55
1.50	1.30	1.88	1.30	50.01	101.92	7.34
1.40	1.30	1.75	1.30	51.46	101.70	7.11
1.30	1.30	1.63	1.30	53.07	101.49	6.88
1.25	1.30	1.56	1.30	53.94	101.40	6.77
1.20	1.30	1.50	1.30	54.86	101.30	6.65
1.15	1.30	1.44	1.30	55.83	101.21	6.53
1.10	1.30	1.38	1.30	56.85	101.12	6.40
1.05	1.30	1.31	1.30	57.94	101.04	6.28
1.00	1.30	1.25	1.25	57.95	100.96	6.27
0.90	1.30	1.13	1.13	57.36	100.80	6.33
0.80	1.30	1.00	1.00	56.66	100.67	6.40

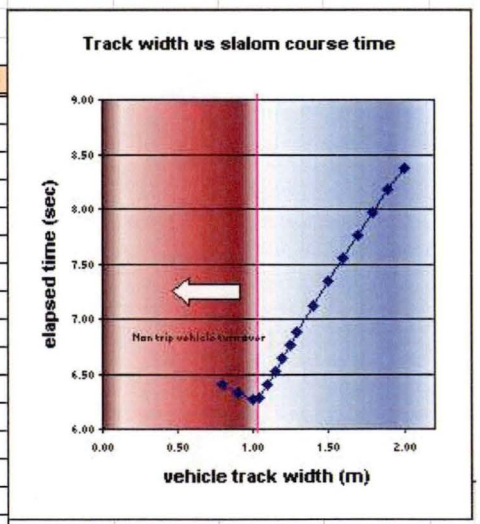

For the test vehicle geometry corresponding to a track width of 1.1m was chosen. Note that this is slightly wider than the optimal 1.05m wide car, in the interests of a roll over safety margin.

According to this simplified analysis, a car with a 1.0m track width can overturn without being tripped, while at 1.05 m the car will slide. But these Figures are based around a maximum 1.3g lateral acceleration that may be significantly less than instantaneous values, which could be attained. This is of importance since the use of very soft, sticky tyre compounds introduces very complex track surface/tyre contact patch relationships.

On the other hand, the estimation of the C of G height is on the conservative side since it is most likely slightly lower in our finished design than the estimated 0.4m.

In the design of the Neural Network development test vehicle, the 1.1m track width represented the upper limit of acceptable risk for vehicle roll over.

3.5.2 Optimisation of Front Track Width

Closer analysis during normal cornering of a vehicle with equal front and rear track widths reveals that the inside rear wheel limits the approach to the inside of the corner, for a car experiencing minimal lateral tyre slip.

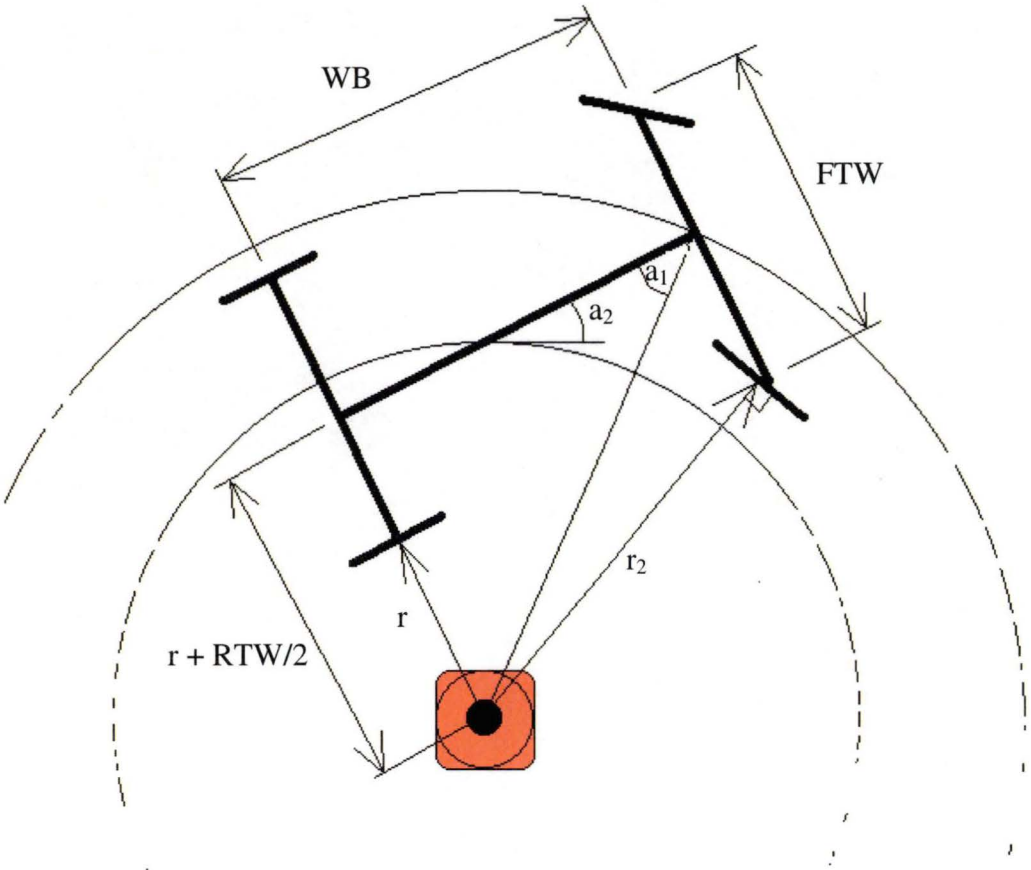

Figure 3-16 Geometry of turning vehicle

From the diagram above the following formula can be derived.

$$r_2^{\,2} = \left(\tfrac{FTW}{2}\right)^2 + \left[\sqrt{\left(r + \tfrac{RTW}{2}\right)^2 + WB^2}\right]^2 - 2 \cdot \tfrac{FTW}{2} \cdot \left[\sqrt{\left(r + \tfrac{RTW}{2}\right)^2 + WB^2}\right] \cdot \cos\left[\tfrac{\pi}{2} - \tan^{-1}\left(\frac{r + \frac{RTW}{2}}{WB}\right)\right]$$

Equation 3-8

Where: r_2 = Arc followed by the inner front wheel

r = Arc followed by inner rear wheel

FTW = Front track width

RTW = Rear track width

WB = Wheel Base

Thus from the dimensions of the car (FTW, RTW and WB) and a given corner radius, (r), we can determine the radius scribed by the front wheels.

Our purpose for this equation however is to determine the maximum amount that we can increase the front track width (and hence increase stability) before the front inner wheel begins to limit our approach to corners. To do this, we need to solve this equation iteratively:

1. Select an appropriate minimum radius for which the vehicle will be turning (remember racing lines and corner apexing). This becomes your value for r.
2. Decide on your wheelbase (WB) using packaging or other constraints.
3. Select a rear track width (RTW) as outlined previously.
4. Estimate an initial value for the front track width (FTW), say 10 % larger than the rear track width.
5. Calculate r_2 using [Equation 3-8].
6. If r_2 is larger than r, increase the value of FTW. If r_2 is smaller than r, decrease the value of FTW.
7. Repeat steps 4-6 until r_2 converges to your chosen r.

Note that this process is easily handled by a spreadsheet where experiments with vehicle dimensions can be analysed very quickly and easily.

There is one other notable reason, on a rear wheel drive car, to design to a wider front - narrower rear chassis. By having a narrower rear track the proportion of roll resisted by the rear tyres is decreased, allowing for increased rear traction while exiting corners. Effectively this allows using more of the rear tyres (particularly the inside tyre) and as a side effect causes more even tyre wear, tyre heat and traction on tracks with a corner bias, i.e. predominantly left-handers or predominantly right-handers. This can be quite significant as weight transferral ensures rear tyres are working hardest while exiting corners.

After performing this analysis, it was decided to increase the front track width to 1.2m, which is perhaps not taking full advantage of the possible gains in stability. This was partly to avoid too radical geometry and also partly due to the break down of this simple analysis once the vehicle begins sliding. We also felt that the chosen track widths offered enough conservative stability, and compactness was one of our key design motifs.

3.5.3 Dynamic Component Design

Suspension design is always a compromise. Different suspension systems offer advantages and disadvantages over others.

Since the vehicle was to be built as part of current investigations without any testing data and was designed by recent graduates (David Butler and Myself) it was decided that whatever type of suspension was used would require maximum adjustability for tuning out any inadequacies which may surface. This was coupled with the general desire to create a system that could be accurately
modelled before manufacturing and was easy to produce. These desired properties directed the decision to use a "conceptually conventional" double wishbone suspension.

To minimise the unsprung weight of the suspension system, pullrod systems were decided upon front and rear with an inboard coil over shock absorber.

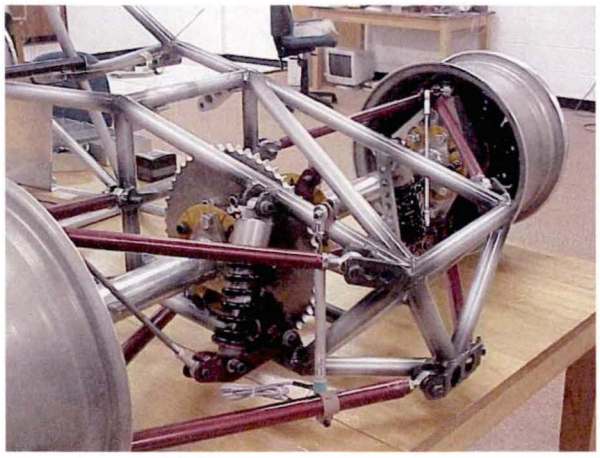

Figure 3-17 Pullrod suspension system with inboard coil over shock absorber used on the test vehicle.

The biggest initial geometric argument faced was between designing a system that maintained ideal bump characteristics and poor roll characteristics, one that maintained good roll characteristics but poor bump, or something in between.

In the design of FSAE courses careful use of chicanes, tight corners and hairpins means that the vehicles rarely (if ever) reach speeds of over 120kph and a good vehicle may average around 60kph for the 1km course. This means a great lap of 1 minute flat is achievable. This is only put into perspective by the very fact that our vehicle has a dry weight of around 235kg and a power output of about 80bhp. This gives us a power to weight ratio of about 340bhp/ton. Comparing this to a Lamborghini Diablo with a mere 220bhp/ton gives an appreciation the tightness of the course.

Furthermore, the course is constructed on either smooth asphalt or concrete. For these reasons it was decided that whatever suspension geometry was adopted, it was required to keep the outside wheels as close to vertical as possible while cornering throughout the range of movement of the suspension - keeping the loaded wheels with the whole width of the tyre on the road is absolutely vital for maintaining corner speed.

Figure 3-18 Keeping the outside wheels vertical during cornering is considered to be the most important characteristic of any racecar suspension system. Here the test vehicle can be seen exiting a tight left-hander during a wet track testing session.

To achieve vertical outside wheels under maximum expected roll the camber change properties under centripetal induced deflection need to be carefully considered. Of note is that when using a double wishbone suspension system the wheels can never remain vertical through their whole range of motion, but for small levels of roll (<5°) this can be controlled by using longer bottom and shorter top suspension arms. A traditional rule of thumb is that the top suspension arm should be about 2/3 the length of the lower arm. This is a Figure arrived at as it gives a good compromise between these desired roll characteristics and also maintaining acceptable geometry in squat/dive under acceleration.

Empirical Figures such as this, arrived at through years of racing successes, offered valuable starting points for the suspension design, however finding an optimum geometry took place through the use of CAD modelling. To minimise the overall width of the frame (hence frontal area) and still have the necessary length difference between upper and lower wishbones, the lower wishbones were chosen to meet in the centre of the vehicle.

This design decision produced many significant packaging problems but was decided as core to the vehicle design and was not compromised. The upper wishbones could then be conventionally mounted to the side of the frame which are spaced to suit with special consideration to driver ergonomics and engine/drivetrain mounting. This arrangement allowed the achievement of the camber change properties of approximately half of one degree on the outside wheels under full roll.

Heights of the front and rear roll centres, the point in the transverse plane of the front (or rear) wheel contact patches about which the sprung mass of the car will rotate under any disturbing force, were chosen to correspond to the expected mass distribution of the vehicle. Through FEA modelling, weights were attached to the frame in locations of major components, and the weight in the plane of the rear contact patch was estimated to be 49mm above the front.

Positioning of the roll centres is not an exact science, but a matter of opinion since it effects the extent of vehicle roll. The front roll centre was chosen at ground level based

upon roll centre positions of successful U.S. formula SAE cars and suggestions offered in racecar design literature [10] and by local racing engineers. Thus the rear roll centre was initially placed 50mm above ground level.

Similarly, appropriate values for the effective swing arm length were decided at between 100% and 150% of the track width. Actual values for these parameters evolved through the iterative process of finding appropriate major component mounting arrangements and driver ergonomics.

Table 2 Final static suspension geometry

3.6 FINAL STATIC SUSPENSION GEOMETRY	
Front track width	1200mm
Rear track width	1100mm
Front roll centre height	8mm
Rear roll centre height	49mm
Front effective swing arm length	1564mm
Rear effective swing arm length	1114mm
Front upper/lower wishbone length ratio	0.534
Rear upper/lower wishbone length ratio	0.688
Front caster angle (rear caster = 0°)	6°
Scrub radius (front and rear)	57mm
King Pin inclination angle (front and rear)	4.2°

The suspension system was designed with the concepts of low parts count, simplicity, compactness, ease of access and widespread use of common parts. All suspension components are specified for minimum weight and maximum adjustability.

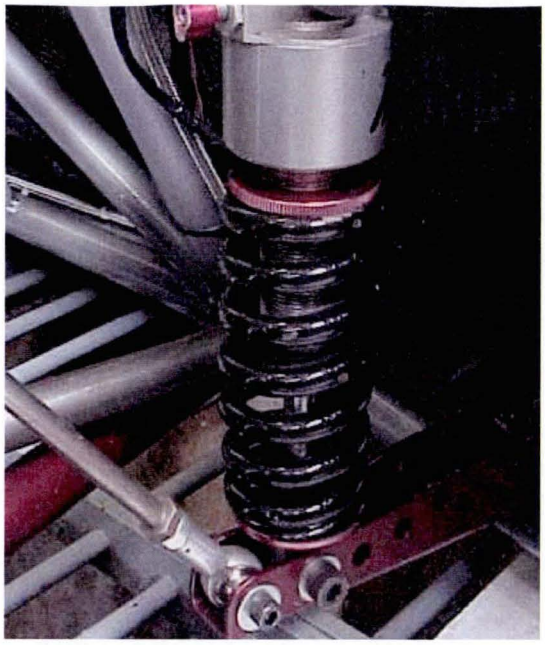

Figure 3-19 The pull-rod suspension provides a progressive spring rate which itself can be changed through positioning on the rocking supports.

Figure 3-20 Front and rear uprights and bearing arrangements are identical, as is the whole hub and stub axel assembly, allowing for ultra low parts count.

3.7 WHEEL ASSEMBLY DEVELOPMENT

The wheel assembly is defined here as the set of components that link the suspension wishbones to the road. This includes the wheel rims and tyres, as well as the brake system, hubs, stub axles, uprights and bearings. The design and integration of these components had to address the following criteria:

- Be simple and relatively cheap to fabricate
- Be as light as possible without compromising strength or lifetime
- Must house the largest brakes possible
- Must not interfere with rim rotation
- Must mount to the wishbones while ensuring adequate suspension and steering movement
- Must have a mount for steering linkages
- Must house a wheel speed sensor
- Must allow attachment to the drive axle for the rear wheels
- Should allow significant adjustment in parameters such as camber and caster to enhance drivability and performance

The same design for the front and rear wheels was also used. The argument for this addressed a number of points, firstly a common design would enable cheaper and easier fabrication. Also, the design requirements between the front and rear wheels where similar. The required mountings for the wishbones were the same front and rear, identical brakes where going to be used on all four wheels, all of the rims were matching and wheel loadings were similar. Conversely however, the front wheels needed to be steered while the rear ones did not, and the rear wheels needed to be driven while the front ones did not. It was decided that a design that allowed the wheels to be driven and steered would be best in this situation because, while it increased the assembly mass, it allowed reduced design and fabrication labour and allowed greater interchangeability of parts.

3.7.1 Rims and Tyres

The selection of rim size severely determines the overall design of the wheel assembly. Formula SAE racecar teams typically select either 10" or 13" rims depending on what their specific requirements are. The selection of 10" rims makes the wheel assembly very light. The size of the tyre is reduced to a great extent and some of the bending moments within the assembly are diminished, resulting in a reduced need for strength. However, the size of the rim also determines the size of the brake discs (rotors). Cars running on 10" rims often have problems with ineffective braking and rotors, which frequently over-heat. 13" rims on the other hand typically add up to 15kg of weight to the car but allow significant room for brakes, allowing for rotor selection which will provide significant stopping performance without overheating problems. These points, coupled with a very limited selection of 10" tyres, resulted in the selection of aluminium 13" rims, as illustrated in [Figure Tyre and rim]. The rims were custom made to suit our required dimensions of 7" width, 144mm backspace offset and 152mm internal diameter needed to fit the wheel assembly components in "Appendix D".

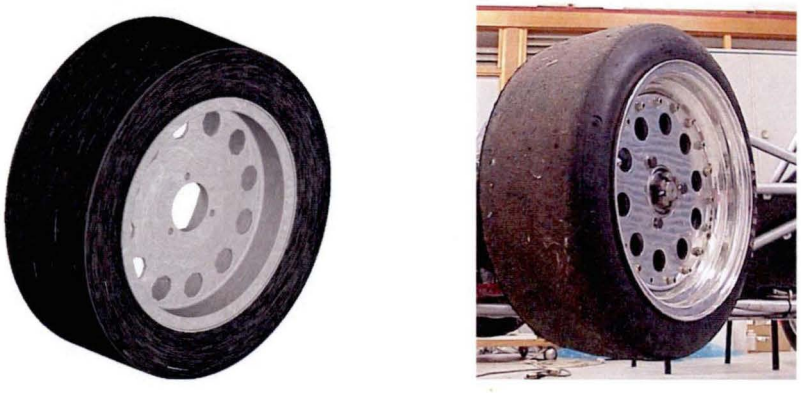

Figure 3-21: Tyre and rim

Rim size selection revolved around availability of tyres in terms of appropriate compounds profiles and widths. Furthermore, research into commonalties between past successful racing cars highlighted the equal importance of braking power and engine power in an autocross style of event. For these reasons 13" wheels were selected.

13" wheels are used in many race applications making race tyres in this size relatively cheap and common. The "hill climbing" compounds ideal for formula SAE competition were available in Australia in this rim size, eliminating the need to privately import

these from the UK as would have been the case with 10" or 12" rims.

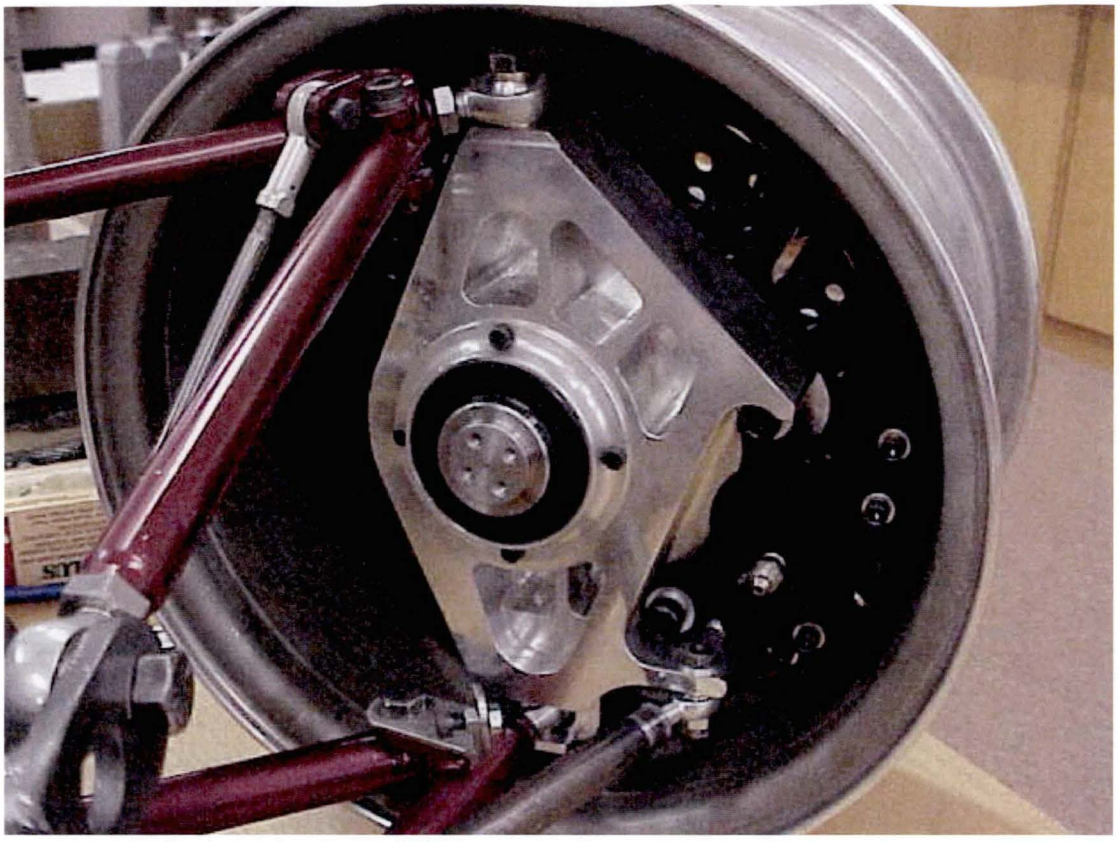

Figure 3-22 13-inch rims permit the use of larger disk brakes.

Larger rims also permit the use of larger brakes if an outboard style of braking system is fitted. Furthermore, for rim sizes smaller than 13" the availability of race braking systems (disks and calipers) is practically non existent. This means that for a 10" wheel "in-house" manufacturing of at least the brake disk was assured.

Aluminium-alloy brake disks that weigh 700g each despite having a diameter of 260mm, were sourced and it was decided that these could be fitted inside a 13" rim with the matching large bore twin piston calipers if a custom 3 piece rim was to be used. All of this went some way toward minimising the additional wheel weight carried by using 13" over 10" wheels and tyres

3.7.2 Brake System

The choice of the disc brake system not only had a large impact on the racecar's braking performance, but also on the design of the wheel assembly. Rotor diameter and type, caliper profile and caliper width all define the dimensions of various components within

the wheel. Because the brakes were going to be purchased, rather than manufactured, it was important to choose the correct system before further work on the wheel assembly design could proceed. Research showed that the possibility of using components from passenger cars, assorted racing cars, motorcycles and go-karts all existed, however finding a design that worked well proved difficult. Car brakes were very heavy but would simplify the design, motorcycle brakes were light and had excellent calipers but finding some to fit in a 13" rim proved fruitless, go-kart brakes were extremely light but their strength was in question and racing car brakes looked perfect but where expensive. The choice came down to if it was more important that the brakes were cheap or light. The decision was made in favour of light in this case, and racing components were used.

Research into racing brake systems to fit 13" rims showed that there was limited choice. Many manufactures made components that were too large, while others made components that were still too heavy. The selection of rotors and calipers supplied from Wilwood High Performance Disc Brakes proved to be the best choice in this case. 10.2" diameter 3 pin mounted aluminium rotors were purchased in conjunction with aluminium billet dynalite single calipers, the specifications of which are shown in "Appendix D" and depicted in [Figure 3-23]. This provided a brake system that fits within the rims with only 4mm of clearance, maximising brake size, and weighing only 1.3kg at each wheel. The decision was also made to use the same brake components for the front and rear wheels. This was done to aid in brake force comparisons during testing and also because smaller brakes for the rear wheels would have reduced the front/rear interchangeability while only saving a small amount of weight and money.

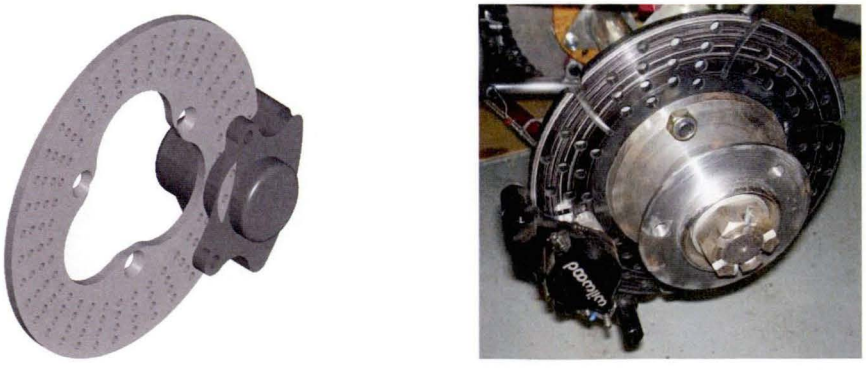

Figure 3-23: Brake rotor and caliper

3.7.3 Stub Axle and Bearings

Passenger vehicles traditionally place the bearings for driven wheels about the vertical centre-line of the rims. While this practice has many benefits such as reduced bearing and stub axle loading it can also increase the complexity of design. This complication comes about because rim construction and brake caliper clearance generally require the brake rotor to also be positioned close to the rim centre-line. This gives two components that require positioning about the same point within the wheel. The most common solution to this problem is to move the brake rotor mounting to the hub of the wheel, thereby creating the traditional 'hat' design. The rotor therefore remains in its optimum position and a significant clearance is left for the bearings to be placed about the rim centre-line. This design however requires extra material to construct the hat, which increases the wheel's mass and rotating inertia. It also complicates the design of the bearing housing within the upright, which must protrude into the hat.

Conversely, the bearings can be placed off-centre. This avoids the need for a brake hat because the rotor can then be attached directly to the stub axle. It also avoids the need for the bearing housings within the upright to protrude. This solution generally reduces the cost for one-off construction as well as reducing the rotating inertia of the wheel but with the drawback of magnified bearing loading, which increases the stub axle and bearing sizes.

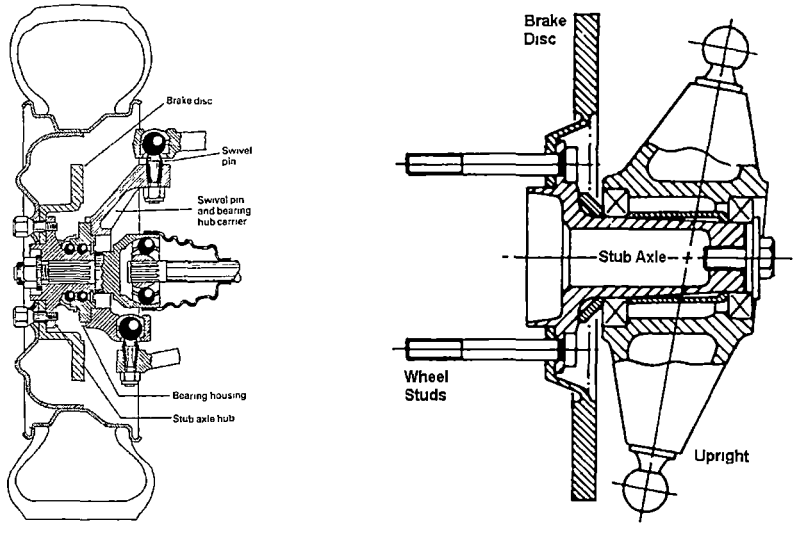

(a) *(b)*

Figure 3-24: (a) On centre (b) off centre bearings

The choice of which design (depicted in [Figure 3-24]) was best came down to which choice best suited the design criteria of the F-SAE racecar. The hat design is almost universally used in the production of passenger vehicles for a number of reasons. It is economical to manufacture for large scale production, is easy to construct (using cast materials), is long lived and is less likely to fail under unexpected driving conditions. However, the car being built is a racecar. It must be light, must have high acceleration and deceleration, must have good handling characteristics and be economical to manufacture in short production runs, in accordance with F-SAE rules. The centred and the off-centred bearing designs must be appraised against these criteria and not on those of commercially available vehicles.

Finite Element Analysis (FEA) [36] was introduced in order to facilitate this design choice. FEA was chosen because it has the advantage of being able to accommodate quite complex loading and design characteristics, while also being able to display the results in a clear and useful manner. Also, since the models were created suitably, they could easily be altered to account for small design changes as the results demanded.

Models of the centred and off centre bearing cases were created to allow comparison. Each model initially used 30mm diameter stub axles, used a set of identical single row tapered roller bearings spaced at the same interval and used matching common parts (such as the brakes and rims). This ensured that the two models are operating from the same initial baseline and allowed simple comparisons. The models were created using 'plate' elements for the wheel components and 'brick' elements for the axle and bearings. This was done to make the models easier to both structure and modify, while preserving accuracy at the axle, where it was required. The plate element properties and thicknesses were chosen as per our own initial design and a pressure of 20psi was applied to the tyre walls and rim to gain a more accurate simulation. The two models are shown in [Figure 3.25].

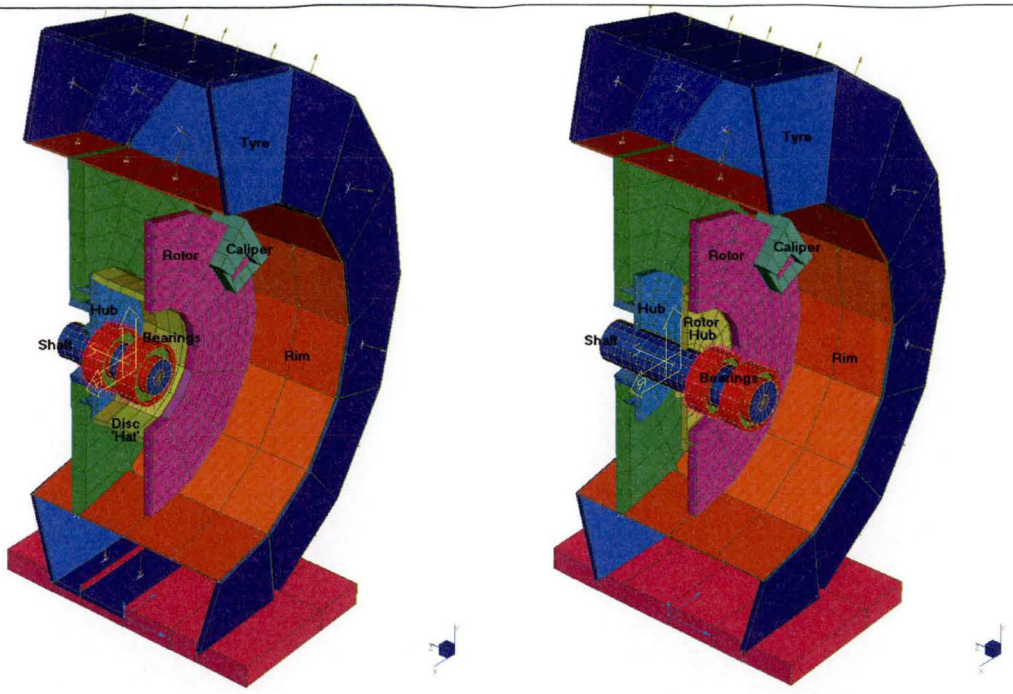

(a) *(b)*

Figure 3-25: FEA wheel model cross sections (a) with centred bearings (b) with off centre bearings [36]

The models were assumed to be stationary (non-rotating), with the bearings fixed in an X arrangement in space but free to rotate. The brake caliper was represented by a fixity condition at a node restricting rotation only and a point load was applied at the bottom of the tyre through a plate representing the ground. The magnitude of the point load was chosen to represent the worst case scenario for this F-SAE racecar, deceleration of $10m/s^2$ (1g) in braking and centrifugal acceleration of $20m/s^2$ (2g) in cornering. Under these accelerations the FEA completed within the "Frame Development" section gave loading conditions of 1.6kN vertically, 4.6kN in the direction of braking (along the length if the car) and 4.9kN from cornering (along the width of the car).

The results ("Appendix D") showed that a 35mm diameter stub axle in the off centre bearing case gave the same internal stresses as the 30mm diameter axle in the centred case. It was these two cases of similar load to yield that was the basis of further comparison, the results as follows:

Table 3:Wheel bearing selection [36]

For Centred Bearings:		**For Off-Centre Bearings:**	
Bearing Loads		Bearing Loads	
F_{radial}	= 23.1kN	F_{radial}	= 33.1kN
F_{axial}	= 4.9kN	F_{axial}	= 4.9kN
Bearing Parameters		Bearing Parameters	
C_{req} (10^8 rev)	= 43.9kN	C_{req} (10^8 rev)	= 62.9kN
Internal Dia.	= 30mm	Internal Dia.	= 35mm
Bearing Choice	= FAG 32206A	Bearing Choice	= FAG 32207A
External Dia.	= 62mm	External Dia.	= 72mm
Axle, Bearing & Brake Hat Weight		Axle, Bearing & Brake Hub Weight	
$W_{assembly}$	= 2.0kg	$W_{assembly}$	= 2.2kg
Moment of Inertia of Axle & Brake Hat		Moment of Inertia of Axle & Brake Hub	
$I_{assembly}$	= $0.31x10^{-3}$ kgm^2	$I_{assembly}$	= $0.19x10^{-3}$ kgm^2
Stub Axle Deflection		Stub Axle Deflection	
Δd_{axle}	= 0.1mm	Δd_{axle}	= 0.5mm

In comparison of the two models it was important to note that the bearing position would significantly effect the design of surrounding components. The design of the upright particularly was subject to change since it must house the bearings in their different respective positions. In the case of the F-SAE racecar, it was found through a short investigation that the upright weights for both cases would be similar, but remained very design dependent. A deviation in the above assembly masses of 200g, while not negligible, can seem less important when considering the design of the upright as well. A simple calculation considering a 330kg racecar accelerating at 10m/s^2 showed that this increase in weight reduces acceleration by 0.02m/s^2 while the increase in moments of inertia account for a completely negligible reduction of 0.0002m/s^2.

The last comparison that could significantly affect the wheel assembly performance was the stub axle deflection. The axle in the off-centre case obviously deflected more than in the centred case because much more of it was subjected to the maximum stress, and therefore strain. This small amount of deflection was not a significant problem in the case of this racecar. It can be shown that the resulting wheel misalignment (0.4° from

vertical) is small when compared to wheel misalignment resulting from car roll and pitch when cornering and braking. Also, the wheel hub mounting, which was not considered in this model, further decreases this deflection.

Budgetary constrains had also to be considered. The difference in the cost of production of the wheel assembly essentially fell to the cost of the upright. This was because all the other components within each of the assemblies could be made using very similar methods. The most cost-effective method of producing a lightweight upright for the very limited number of units required was to machine it out of an aluminium block. In the case of centred-bearings this would require a very thick and expensive plate to machine, while the off-centred bearings will require a plate only about half as thick and much cheaper. Machining the uprights for the off-centred bearings in this case also requires far less material removal resulting in cheaper production costs.

In this summary, the centred bearing design proved slightly lighter, showed marginal increases in handling characteristics and also probably has a longer lifetime due to its added ability to cope with unexpected driving conditions. Conversely, the off-centre design revealed itself to be cheaper to construct in 'one off' production, but at a cost of slightly lower performance and life. The decision was made in favour of the off centre case, using a 35mm stub axle and 35mm ID and 72mm OD single row tapered roller bearings.

The stub axles (show below in [Figure 3-26] and dimensioned in "Appendix D") were made on a CNC lathe using free machining 709M steel. A thread was also placed on one end of each, to allow the addition of a castellated nut that would hold the entire assembly together as well as provide bearing pre-loads. The stub axles were then moved to a mill where a hole for the castle nut cotter pin was drilled and a grove for the keyway was cut.

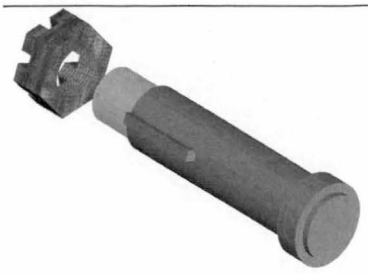

Figure 3-26: Stub axle

Finally a modification was made to the stub axles of the driven wheels to allow the installation of the 'composite disc' CV joint replacements detailed in the "Drivetrain Development" section. These discs transmitted the drive torque and had to be mounted onto the stub axle via a triangular plate with a bolt hole at each corner. The mild steel plates were stick welded, using a special heat treatment process, to the stub axles which also had journals included in their common design to facilitate centering and alignment of the plates.

3.7.4 Oil Seals

One of the disadvantages of using single row tapered roller bearings is that they cannot be purchased in a sealed condition. As such, the design required that a pair of oil seals be used to hold the lubricating grease within the bearing pairs, which were housed within the upright. Oils seals of 40mm ID and 72mm OD were purchased to run on the bearing journal of the stub axle on the suspension side of the upright and on the wheel / brake hub on the other. These seals, however, had to be mounted onto the upright in some fashion, since its design did not enable direct mounting. This was due to increased machining complexity and material cost incurred by including the oil seal mounts into the upright construction.

Oil seal mounts were designed to be interchangeable on either side of the upright. This required them to be as compact as possible since to distance between the upright and the wheel / brake hub was already small. Furthermore, positioning the seals near to the bearings results in the requirement of less grease, reducing weight. This resulted in the CNC construction of 8 aluminium oils seals of a 'bolt on' design shown in [Figure 3-27]

below, with the bolt holes drilled at even intervals, using the mill dividing head, to ensure interchangeability and correct alignment.

Figure 3-27: Oil seal

3.7.5 Wheel / Brake Hub

The wheel / brake hub must serve a number of functions. First and foremost it must provide an attachment for the wheel and the brake rotor to each other, and to the stub axle. It must also provide a means to allow driven wheel torque to be transferred from the stub axle to the wheel as well as provide a system to facilitate bearing pre-loading. Furthermore, a general design had already been established above of a wheel hub plate and a brake hub plate attached to a shaft. There were also the requirements of the inclusion of the oil seal running surface and a keyway to the stub axle.

In addition to these requirement, the dimensions where also defined through the overall assembly design. The position and diameters of wheel mounting was known, as was the details for the brake mounting. The oil seal journal need to be a specific size and the diameter of the sleeve to fix the stub axle was defined. The design of this component was simply focused at producing a component to these very specific requirements that was both cheap and easy to manufacture, while being as light as possible. The result being a 2kg mild steel hub manufactured on the a CNC lathe with the keyway cut with a broach and the bolt holes drilled with a mill with a dividing head, as shown in [Figure 3-28].

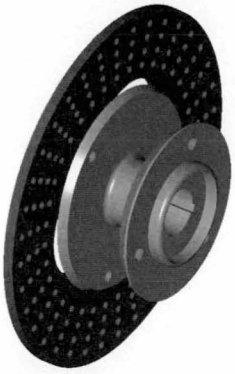

Figure 3-28: Wheel / brake hub

3.7.6 Upright

The design of the upright had many conflicting requirements, and as such was difficult to gain an optimum solution. The decision to use common steered and driven wheel designs also made the design more complex.

The first consideration was the bearings and bearing spacing. The selection of a small bearing spacing allowed for the choice of a relatively thin upright (50mm), but the increased loading resulted in large bearings that forced the upright to be quite wide about its centre.

Suspension mounts where another big consideration. The suspension design called for the placement of the bottom wishbone to be a low as possible, and the placement of the top to be spaced at the same distance from the stub axle centre line. When considering the placement of the wishbones at varying suspension travel positions, the different suspension geometry front and rear and the clearances during turning, the problem becomes very complex. Factors such as kingpin angle (chosen as 4.2°), and caster and camber adjustments also had to be taken into account. In addition it was also decided that, since the forces on the bottom mount where much higher than at the top, the bottom mount would be designed for double shear while the top for single shear only.

The placement of the brake caliper and steering mount where also integral to the design. The brake caliper radial positioning was defined exclusively by the brake rotor

diameter, however it could be placed anywhere on that radius, within reason. The best design, though favours the placement of the caliper as low as possible. This lowers the centre of gravity, reduces the 'back flow' of hydraulic fluid that results from caliper positioning higher than the master cylinder and provides extra strength within the upright in its lower portion, which is subject to large loads. Further investigation into the design of the caliper mounting also showed a small alteration would also allow the integration of the steering mounting into the design with little effort.

Once all of the individual design requirements had been identified a final design for the upright was produced. Factors such as milling limitations, weight reduction and appearance where taken as priorities in the design, which also met all other requirements suitably.

The aluminium uprights were manufactured in a number of steps. The bearing journals were first lathed out to a J6 clearance, with the upright subsequently CNC machined to shape. The suspension joint, steering tie rod joint and brake caliper mounting bolt holes were then manually drilled and taped followed but the drilling of the bolt holes for the oil sealed in the mill dividing head. The resulting product is illustrated in [Figure 3-29] and dimensioned in "Appendix D".

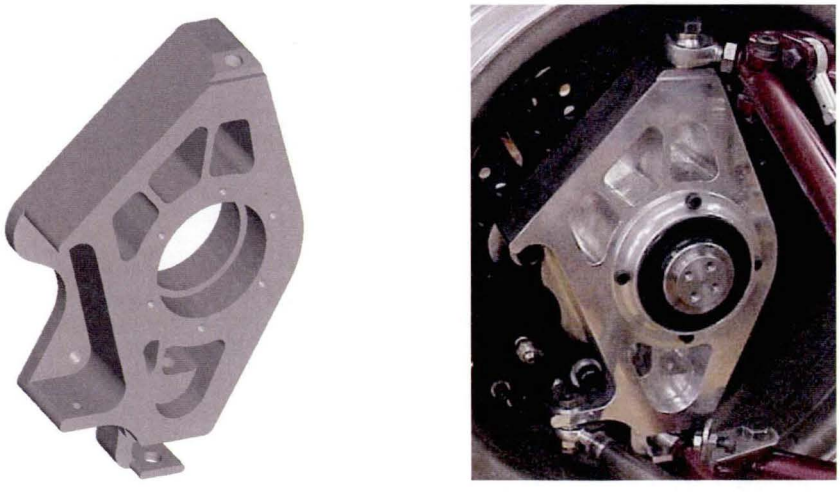

Figure 3-29: Upright

3.7.7 Assembly

Due to the small clearances within each wheel assembly, they must be assembled in a specific manner. [Figure 3-30] shows the exploded and cut-away views of the wheel assemblies, which are put together in the following manner:

1) Press the oil seals into their mountings,
2) Grease the tapered roller bearings,
3) Press and Loctite® the bearing outers into the upright,
4) Slide one of the oil seals along the stub axle to the non threaded end,
5) Press the first bearing inner onto the stub axle and slide it to the journal,
6) Slide the upright over the bearing and bolt and Loctite® the oil seal in place,
7) Press the remaining bearing inner onto the stub axle and bolt and Loctite® the other oil seal in place,
8) Bolt and lock nut the brake rotor to the hub and slide both onto the shaft with the keyway key installed,
9) Place the washer and castellated nut onto the tread end of the stub axle,
10) Bolt and Loctite® the bake caliper into place on the upright,
11) Bolt the rim and tyre to the hub,
12) Tighten the castellated nut to pretension the bearings so that the wheel freely rotates no more than one turn when spun by hand,
13) Insert the cotter pin to stop the castellated nut from loosening,
14) Bolt and Loctite® the suspension and steering rod ends to the upright utilising the brass spacers to ensure full movement,
15) Bolt the rim to the wheel / brake hub.

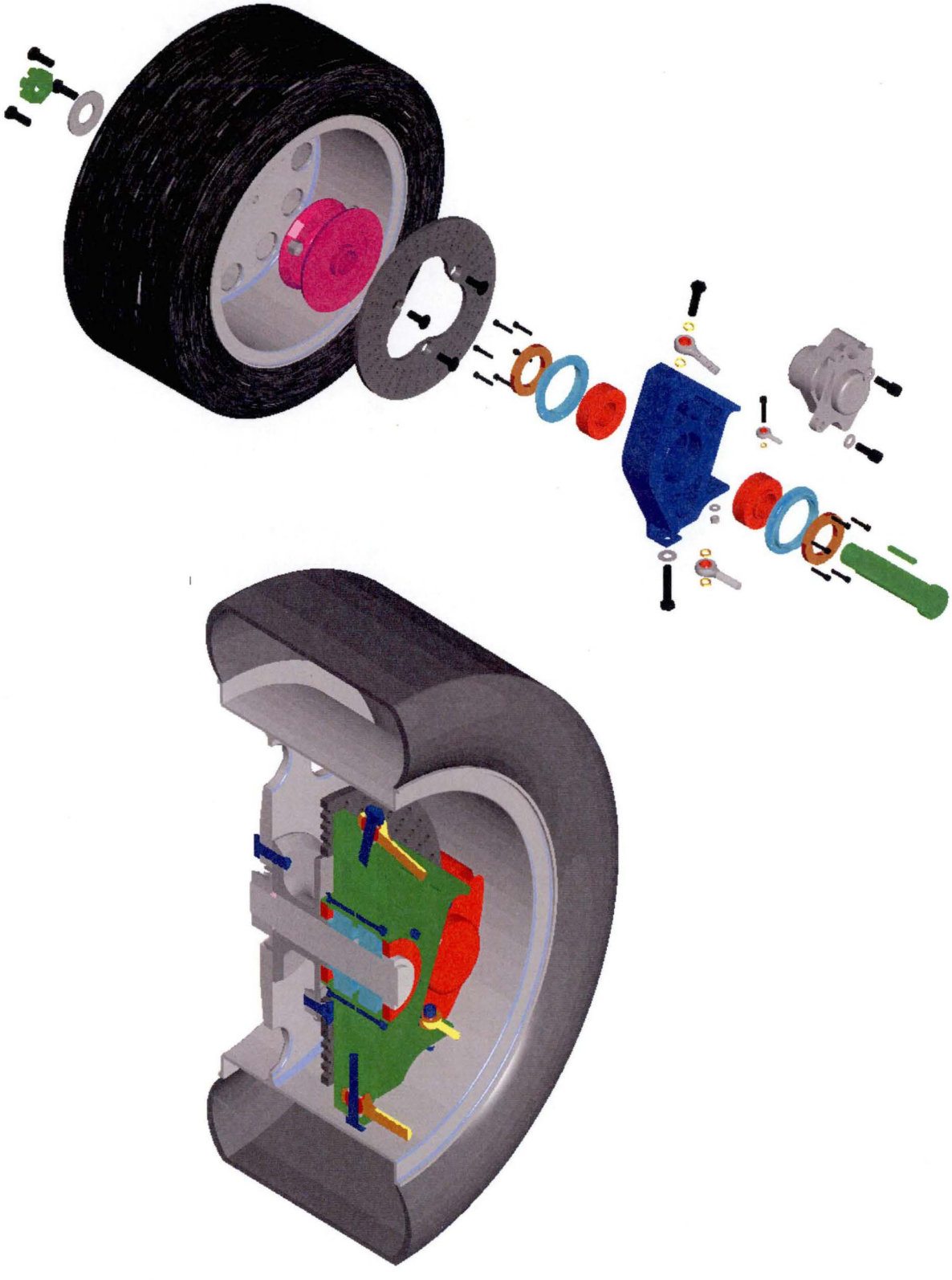

Figure 3-30: Wheel assembly

3.8 DRIVETRAIN DESIGN

Fundamental design principles applied to the drivetrain are low rotating mass and efficient power transmission.

3.8.1 Composite Disks

The drivetrain features extensive use of non-conventional materials. Kevlar composite disks have been used in place of traditional CV or tripod joints saving a total rotating mass of around 6kg.

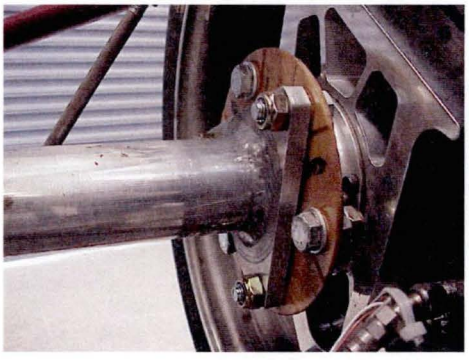

Figure 3-31. Kevlar composite disks supplied by GKN Motorsport used in the test vehicle transmission.

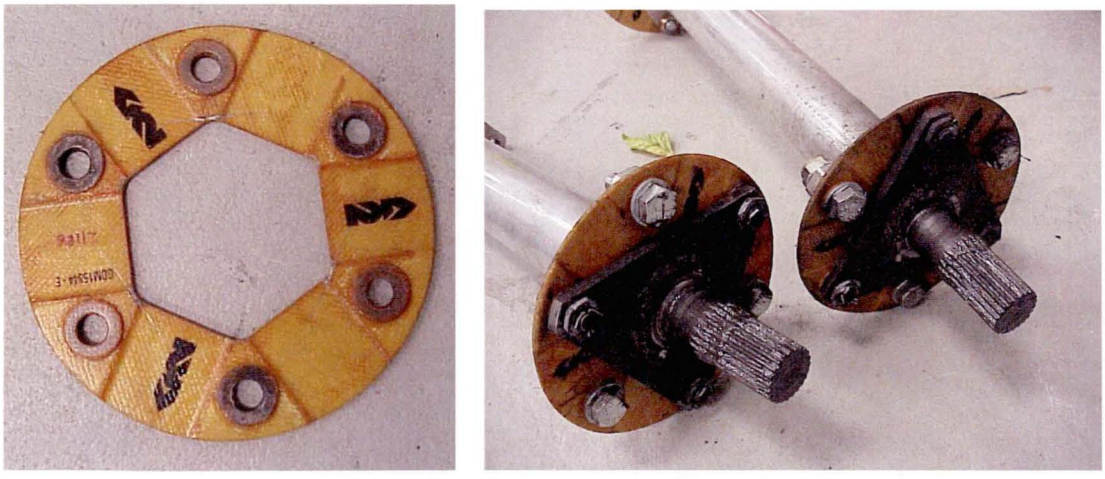

Figure 3-32 Unidirectional Kevlar fibre construction of the composite disks

The composite disks themselves are made form laminated unidirectional kevlar fibre and weigh only 55g each despite having a transmission of torque rating of over

1000Nm. Power transmission efficiency is close to that of a solid shaft since these disks require near perfect operating alignment.

During normal operation, shafts either side of the composite disk(s) must be within 1° of straight. To this end, the height of the entire rear axel and transmission assembly was pre determined by the tyre and rim selection. In order to achieve this 'near perfect' geometry of the transmission assembly many iterations were performed in frame and suspension design at the rear of the vehicle.

To accommodate suspension movement the disks can withstand instantaneous deflections of up to 6°. After over 1000km of track testing no failures of composite disks have occurred.

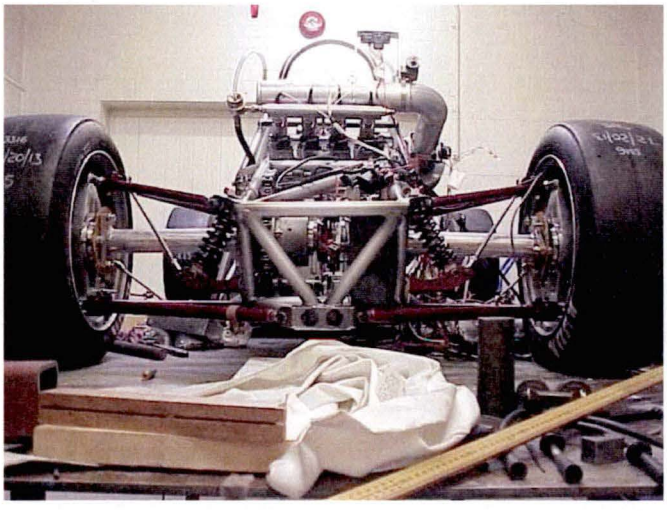

Figure 3-33 Perfect static alignment of the rear axel is required to keep composite disks from failure.

3.8.2 Drive Shafts

The drive shafts are large diameter aluminium-alloy tubes that are both stiffer and lighter than the traditional solid steel. This was achievable since the drive shafts do not use splines for torque transmission but are flanged and bolted directly to the composite disks.

The aluminium drive shafts were designed to exceed the strength and stiffness offered by a traditional 22mm steel drive shaft which are commonly used in racing applications of this nature. The safety factor applied here is upwards of 20 times, owing to the catastrophic nature of drive shaft failure.

Figure 3-34 Large diameter hollow aluminium drive shafts dominate the rear of the car. Note the tight clearances with the pull rods and springs.

Various aluminium sections thought suitable were analysed using FEA techniques. Torque ratings (yeild torque) and torsional deflections were two criteria tested against the 22mm solid steel racing drive shafts using FEA models. The 6mm thick, 50mm OD section aluminium alloy selected exceeds the expected yeild torque rating of the steel shaft, is much lighter and many times stiffer.

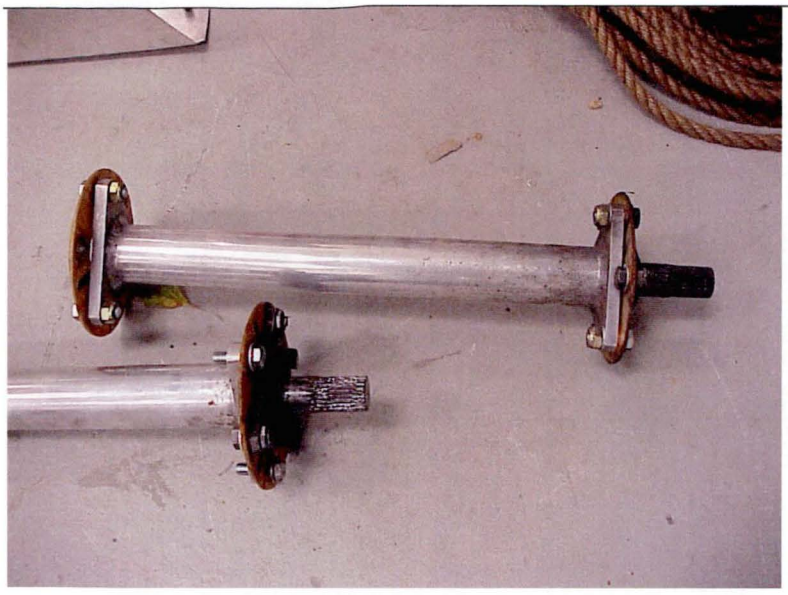

Figure 3-35 Aluminium alloy drive shafts bolted directly to the GKN composite disks.

The alloy drive shaft tubes were tig welded to triangular shaped 8mm thick aluminium alloy end plates using a clamping arrangement for correct alignment. The plates were tacked on before final welding and the run out of the face was checked and adjusted as the welding procedure took place. Finally, the drive shafts were faced in a lathe to ensure the alloy end plates were true.

3.8.3 Differential Selection and Application

A fully sealed Quaife Automatic Torque Biasing (ATB) differential assists in maintaining maximum traction during acceleration and cornering. This unit has proved effective in testing and is the smallest and lightest automatic torque biasing differential available.

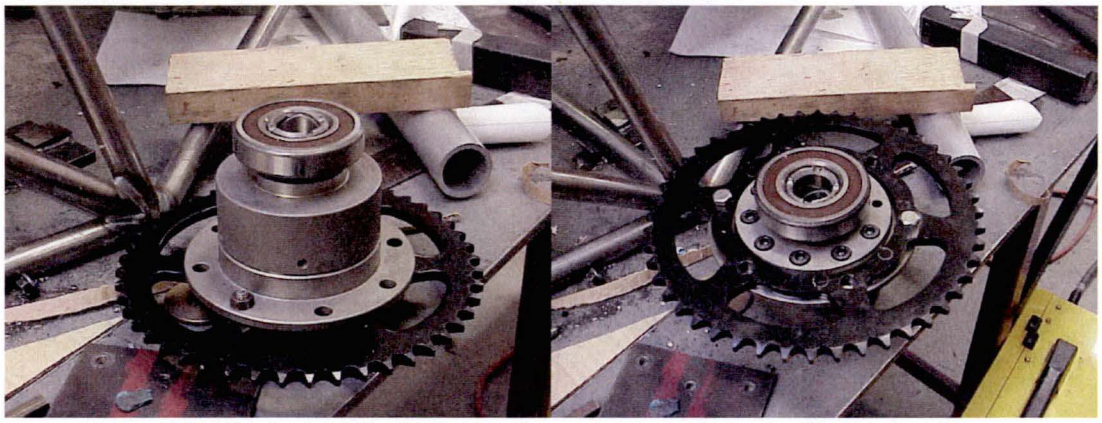

Figure 3-36 Quaife ATB differential with pressed on ball bearings.

The differential unit arrived fully sealed, no modifications were necessary. Blank sprockets were machined to match the bolt pattern on the existing differential flange. Ball bearings were selected and pressed on to the differential casing.

The differential mounting arrangement dominates the rear of the frame structure with an asymmetrical diagonal member supporting the top of the right hand side differential mount (see [Figure 3-37]) also providing triangulation of the drivetrain frame structure

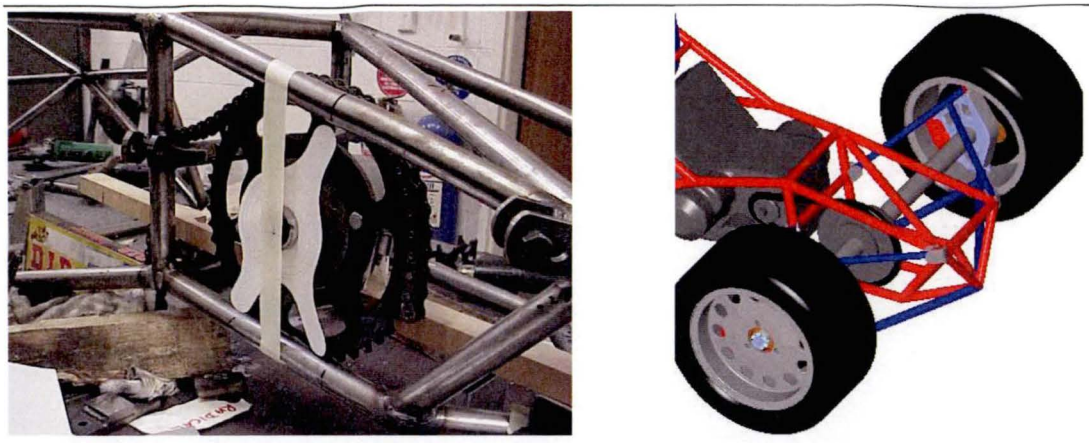

(a) *(b)*

Figure 3-37 Differential mounting arrangement; a) photo taken during frame construction, b) rear frame design dominated by differential mounting considerations

The differential mounts were designed and fabricated out of plain carbon steel and are a sliding fit over the outside of the differential ball bearings. The two mounts are tripods in design and mounting is through the use of three bolts each into tabs welded to the frame

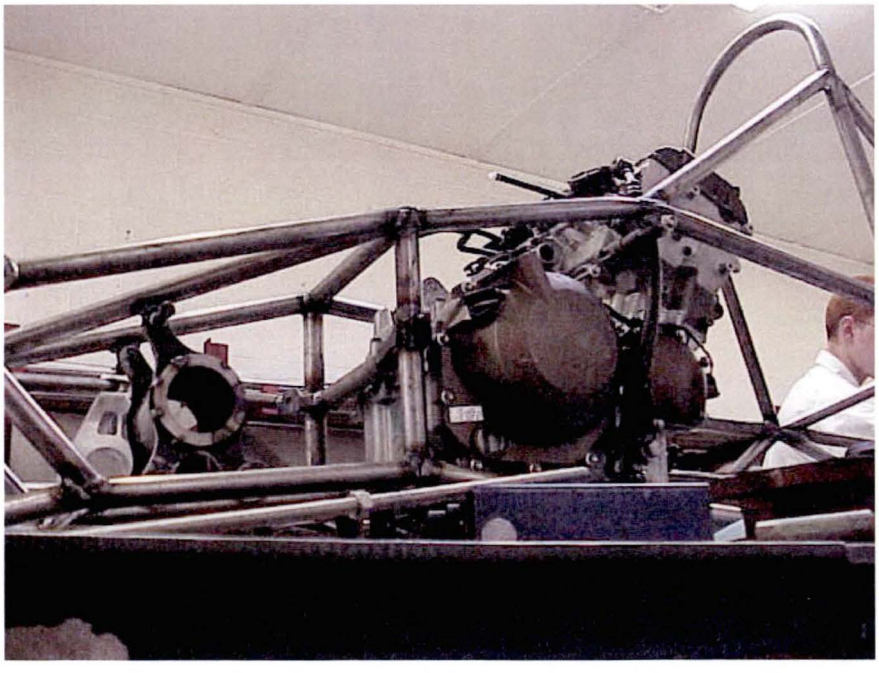

Figure 3-38 Differential mounts shortly after welding mounting tabs to the bare frame of the test vehicle

3.9 ENGINE SYSTEMS DESIGN

The use of a motorcycle engine as the power plant for a F-SAE racecar is a standard choice. The 600cc displacement limit imposed by the rules [31] significantly reduces the possible sources from which an engine can be obtained, and motorcycle engines offer exceptional performance. They are generally highly tuned and lightweight, and, coupled with almost universal inclusion of a sequential gearbox, provide significant power within a compact unit. Most manufactures make a number of such 600cc engines of varying levels of performance and reliability depending on their application, in this case it was decided to focus on the high performance end of the market, and a 2000 model Kawasaki Ninja ZX6 engine was chosen.

The Kawasaki ZX6 plant is a high revving in-line 4 cylinder, 4-stroke, water cooled super-bike engine with double overhead cam. It offered a compression ratio of 11.8:1 with large low RPM torque and high power within a 55kg (dry) unit with 6 forward gears. The engine also has, as standard, a deep oil sump (which is needed to ensure oil flow during high lateral accelerations) and a water jacket style oil cooler integral to the water cooling system providing a reduction in the overall weight.

3.9.1 Fuel Injection System

The Kawasaki Ninja engine typically runs a carburetted air intake system, with separate CV carburettors for each cylinder running from a single air box that receives ram air. This system offers efficient and lightweight fuel control under normal operation, but F-SAE specifications enforce two major limitations. Firstly, all intake air must pass through a 20mm diameter air restrictor, and secondly, the throttle body must be located upstream of the restriction. This, coupled with the fact that the carburettors operate with degraded performance under high lateral accelerations, and their inherent difficulties to tune, lead to the choice of a fuel injection system.

A well design inlet manifold is of great importance in optimising the airflow to the engine. Separation and extended boundary layers along with excessive turbulent eddies are to be avoided where possible. A single plane induction manifold with all intake

runners extending from a common plenum was the design of choice due to the fact that the open plenum smoothes out the induction pulses better than a dual plane manifold and can give better top end power.

3.9.1.1 Intake Runner Length

With the engine running both high and low pressure waves move along the intake plenum due to the opening and closing of the valves (along with air inertia). The idea of engine tuning is to have the high-pressure wave approach the intake valve just before it opens hence forcing in a little more air.

For the reasons described above the intake runner length can be optimised for a specific RPM range making use of the first (or second) set of pressure waves to increase air induction. The formula for this is:

ECD = 720 – Advance Duration – 30 *Equation 3-9*

Hence, with advance duration of 305 degrees our ECD becomes 385 degrees:

Intake ram pipe length

ECD = 385°

Advance duration = 305°

Length = 41.66833mm

V = 1300 ft / sec

RV = 2

D = 0.08m

RPM = 12000

The optimum length is given by

$L = (ECD*0.25*V*2)/(rpm*RV)-(1/2D)$ *Equation 3-10*

Where:

ECD = Effective Cam Duration

RV = Reflective Value

D = Runner Length

Hence for our engine the effective runner length for the second set of pressure waves is 41.66 mm. This theoretical calculation is an estimate and the only way to fully tune to a specific rpm is to vary the intake runner lengths whilst observing the torque and power on a dynamometer or, better still, by track testing with an experienced driver. Peak power may increase but average power may drop. A balance needs to be found. The longer the runner, the better torque at lower rpm is a rule of thumb. There obviously exists a trade off here with specific torque rpm ranges and also average and peak power. Here in lies the reason for trial and error testing with variable length intake runners.

3.9.1.2 Intake Runner Diameter

This is the easiest to work out due to the fact that the intake air velocity should not reach over 60 m/s at maximum rpm. The formula for the intake runner diameter is

*D = Square root of (Litres*VE*RPM)/(V*18.5)* *Equation 3-11*

Inlet ram diameter

D = 0.0402227m

Litres = 0.6

VE = 0.85

RPM = 12000

V = 105.12

Where:

D = Pipe Diameter

Litres = Litres displacement

VE = Volumetric Efficiency

V = Velocity in ft/sec

Hence resulting in a 40.22mm intake diameter. The inlet ports in the engine actually already set this but it is always advisable to fully check intake design calculations.

3.9.1.3 Plenum Volume

There never exist a simple answer for a given application and rpm range but a good rule of thumb is to have the volume at least 50% of the total engine displacement hence $3.6*10^{-3}$ m^3 is sufficient.

Plenum Volume (50-60% of total cylinder displacement)

Cylinder displacement = 0.6 L = $0.0006m^3$

Required volume = $0.00036m^3$

Plenum volume $0.001705m^3$

Plenum radius = $0.03755m^3$

Length = $0.385m^3$

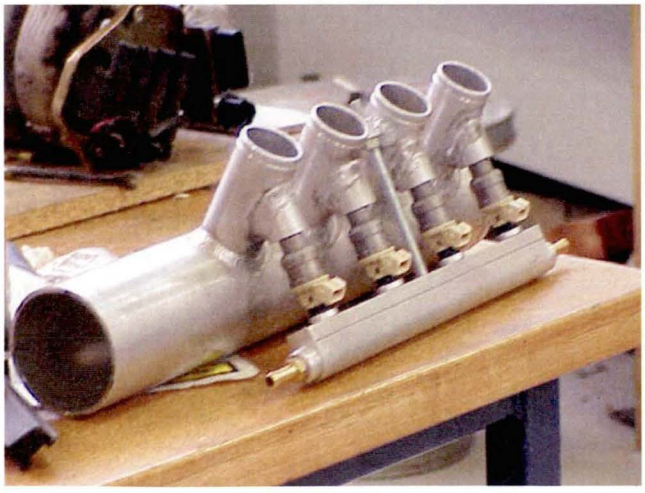

Figure 3-39 Inlet manifold

3.9.1.4 Restrictor

From basic computational flow theory the best application here to maximise airflow is the use of a converging diverging nozzle. Once the contraction ratio is chosen [1] the design criterion becomes the exit flow uniformity, separation, exit boundary layer thickness and space/cost. The actual design parameters become length, wall shape and Reynolds number. Manufacturing is obviously also a large consideration.

The maximum mass flow rate at which the nozzle will choke is given by:

$$m = \left(\frac{2}{\gamma+1}\right)^{\frac{(\gamma+1)}{2(\gamma-1)}} \left(\frac{\gamma}{RT_0}\right) P_o A^* \qquad \textit{Equation 3-12}$$

= 0.0745 kg/s which equates to a volumetric flow rate of 0.06535 m^3/s. The maximum airflow velocity is 159.23m/s.

The actual maximum engine air requirement is 3600000 cc per minute that equates to 0.06 m^3/s of air hence the restrictor will not choke at maximum rpm. The air at maximum rpm has a velocity of 84.88 m/s as it passes through the restrictor.

A matching cubic curve converging section of the nozzle is ideal to minimise separation and flow non-uniformity's but for ease of manufacture a simple radius was chosen for the converging section with an optimum 7 degree diverging section. Due to the plenum diameter the diffuser length is not excessively long to produce undesirably long boundary layers.

3.9.1.5 Throttle Body and Air Cleaner

The throttle body chosen has an inside diameter of 57 mm which is not excessively large to decrease throttle response and not too small to restrict flow. The butterfly placed directly in front of the restrictor intuitively disturbs flow but testing with the

---

[1] Set in our instance from the throttle body diameter and the size of the restriction. = 57/20.

supposedly optimum 0.7* throttle body diameter section in front of the restrictor surprisingly showed no decrease in average horsepower or torque.

The K&N filter was chosen from the maximum inlet airflow Figures and a cone shape was chosen for marginal gains due to the ram air effect.

3.9.2 Exhaust

The outlet ports of the engines are 25.4mm hence the diameter of the extractors was pre-set. Effective length of the outlet pipes [2] was measured from an identical system and fabricated from stainless steel mandrel bends.

The exhaust was fabricated from stainless steel with a perforated 'straight through' pipe surrounded by fibreglass packing to severely lower back pressure that a standard baffle exhaust would otherwise exert on the system. Back-pressure is obviously undesirable, as it would lower the horsepower of the engine at all rpm's due to the extra energy required extracting the used gasses. The outlet pipe is a tuned length producing a standing wave at 9000 rpm. This results in 109 dB of noise 0.5 meters from the exhaust outlet.

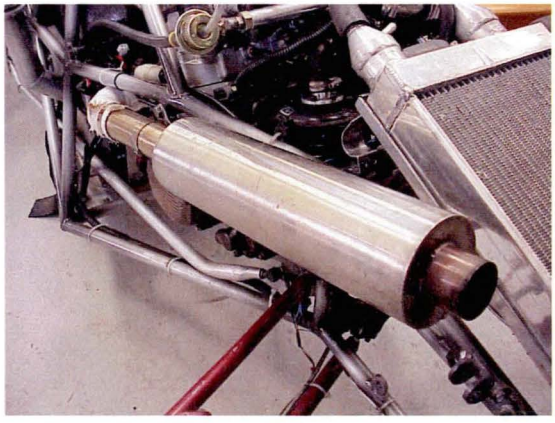

Figure 3-40 Exhaust manifold and muffler

[2] To induce the scavenging from the cylinders as the valves are in overlap.

3.9.3 Engine Management System

Extensive research and management system comparisons were conducted and the MoTeC M4-Pro system was the ideal system for our purpose as it utilises sequential injection along with 3D-map programming. It also has the option of closed and open loop operation allowing feedback from the exhaust oxygen sensor.

The system was installed to use either the throttle position sensor (located on the throttle body) or the manifold air pressure sensor located on the plenum. After extensive tuning with both sensors it was found that the throttle position sensor provided better throttle response hence fine-tuning on the dynamometer was conducted using the throttle position sensor. The MAP sensor is now used to conduct regular manifold pressure checks.

Sequential injection was desired for fuel efficiency and optimum fuel injection timing when the inlet valve opens hence a hall effect sensor was installed on the camshaft. Standard ignition timing is achieved via the factory crank angle sensor.

Other inputs to the ECU are water and air temperature. The water temperature is used for cold start enrichment and the air temperature for adjusting fuel mixtures depending on air density.

The engine was tuned for a Lambda reading of 0.89 that equates to an air/fuel ratio of 13.8:1. This provides a balance between the stoichiometric 14.7:1 for fuel economy and around 13:1 for maximum power. The engine has been tuned both with and without the restrictor. A very interesting comparison can be shown here as the restrictor provided very little enrichment of the mixture as expected.

3.9.4 Fuel System

The fuel system was calculated for flow rates and consequently injector sizes. The duty cycle of an injector is the linear region between 10-90% of the full injector pulse width[3].

[3] Or opening time.

Injectors that are too large will not allow the engine to idle as their minimum pulse width will not allow small enough opening times whereas if the injectors are too small the maximum pulse width will not provide enough fuel at maximum rpm. Low impedance injectors also provide better idle control.

Due to the fact that we were searching for maximum horsepower at maximum rpm each cylinder requires 900000 cc per min of air hence the engine consumes 2211 gms/min. For the required air/fuel ratio an injector that provides between 181 and 221 cc/min of fuel is sufficient[4].

The fuel pump flow rate was calculated to be between 544 cc/min and 665.7 cc/min to provide enough fuel for the injectors at full rpm when they are virtually always open but due to rule specifications[5] the pump selected is good for 400 horsepower. This simply means that an excessive amount of fuel is circulated in the system and returned through the return line. The fuel system runs at 2.5 Bar and the regulator is mounted as close to the end of the fuel line as possible to minimise transient responses to pressure spikes and best maintain constant pressure at the injectors.

The injectors are located on the inlet runners at a location so that the spray fires directly onto the back of the inlet valve when it is closed. This optimises the mixing of the fuel and air due to the heat of the valve assisting in the atomisation of the fuel even though it is open at the time of injection.

[4] The volumetric efficiency was not known hence maximum and minimum Figures were used. The density of unleaded fuel is 0.750g/m^3.

[5] Threaded or OEM type connections required.

3.10 WIRING LOOM DESIGN

In developing a working electrical system for use in the experimental test vehicle the following objectives were identified as essential:

1. Open architecture and expansion capability – for further development of on board electrical systems during automotive Neural Network development.

2. Simplicity - this includes things like minimising the number of wires, using common parts where feasible and designing straight runs between common points.

3. Ease of fault finding – creating fault finding access locations, common locations of like components and using fully colour coded looms.

4. Minimal maintenance requirements – the system developed must be robust and require little maintenance.

5. Neat and aesthetically neutral/appealing.

3.10.1 Physical layout of the wiring loom

The wiring loom was designed to fit neatly away from the major moving parts of the car most likely to cause damage. For this reason the ECU (engine Control Unit) is located well away from the engine under the seat with the ignition module bolted to the floor. As the ECU casing was waterproof further protection was not deemed necessary. The wiring loom runs down the right side of the driver, away from the gear changer on the left, to the fuse box.

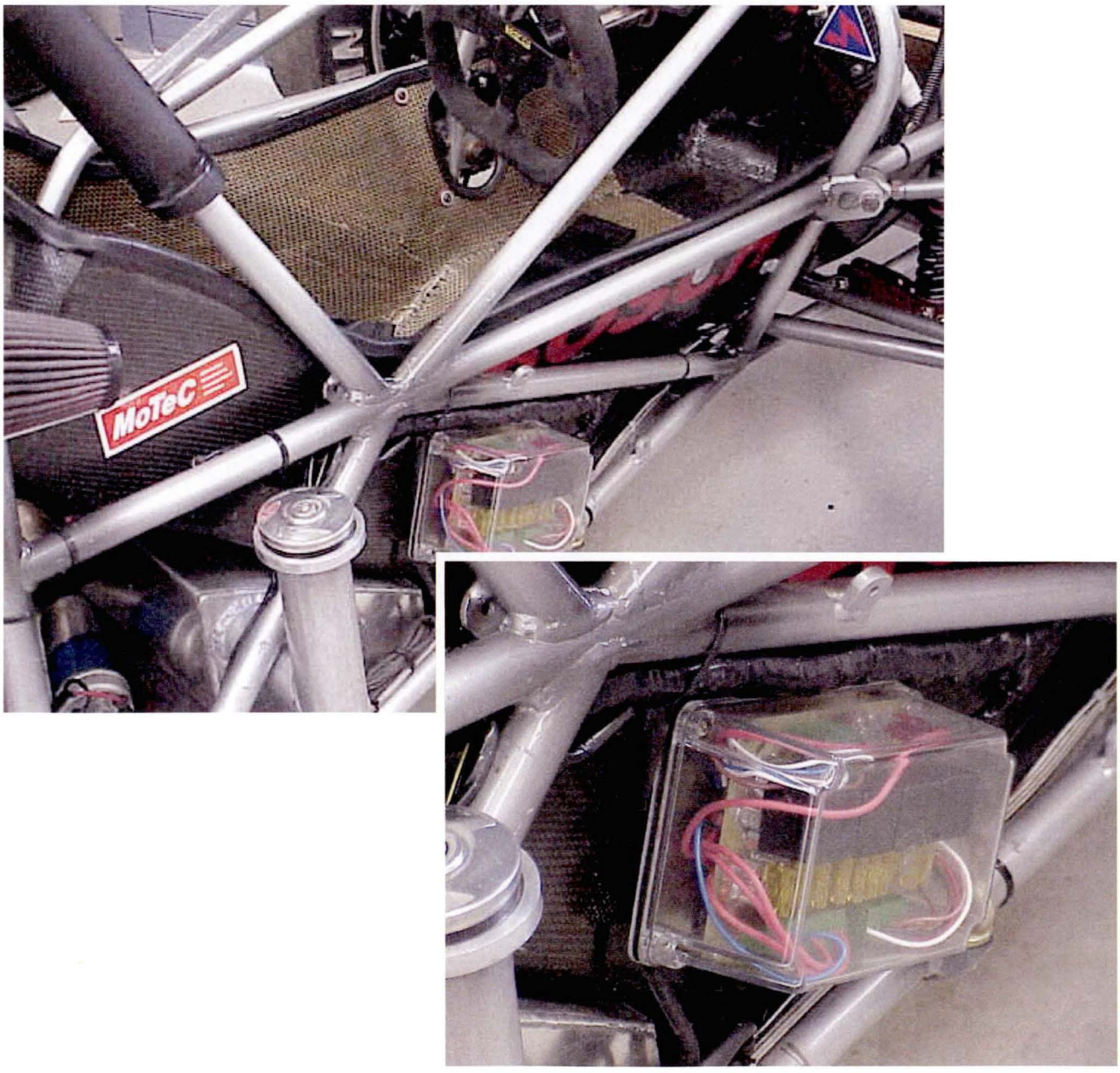

Figure 3-41 Fuse box location. Note the black wrapped wiring loom located directly above the box.

The fuse box is located in a central position to minimise the length of wiring to and from it from all locations on the vehicle and for maintenance purposes. The bulk of the remaining loom continues along this line at a junction with the wiring from the battery located near the starter motor and alternator on the left hand side of the vehicle. The original starter motor, alternator and regulator wires have been retained from the original motorcycle engine loom.

3.10.2 Waterproofing

For reliability during testing it is imperative that the complete wiring loom be dependable in all weather conditions. The major concern in this case is rain and contact with water and mud under wet track conditions.

The insulated cables within the wiring loom are further insulated by comprehensive wrapping in electrical tape in all areas exposed to the elements. The most vulnerable components of the wiring system are the system of relays and fuses that allow the MoTeC system to control the higher currents of the engine control system. Hence the fuse box containing these sensitive components also some and exposed connections required special attention. The fuse box is carefully sealed to avoid difficulty in this area.

3.10.3 Wire colours

The design of the wiring loom assigned a unique wire colour to each component for simplictity of fault finding. Basic electrical conventions were observed as far as practical (black for earth, white or red for power.) Striped automotive wiring would be used for production runs of the loom.

3.10.4 Wire Specification

Wire utilised in this design was chosen to withstand the harsh environment of the automobile. Standard automotive wire has been specifically developed to withstand bombardment with dirt, oil, heat water and low temperatures and hence was specified for all wiring connections. Wiring sizes were taken from the largest likely current rating

of each individual component they served. For instance, the fan wiring could expect a continuous operational current of between 2 and 3 Amp with a stall or start up current in the vicinity of 7 Amp. In this case the wire chosen was rated at 10 Amp. The trade off in weight for this type of decision was deemed necessary for the absolute reliability required of the electrical system.

3.10.5 Wire wrapping

The wiring was wrapped tightly and neatly by hand and covered where possible with conduit for reasons of aesthetics and extra durability.

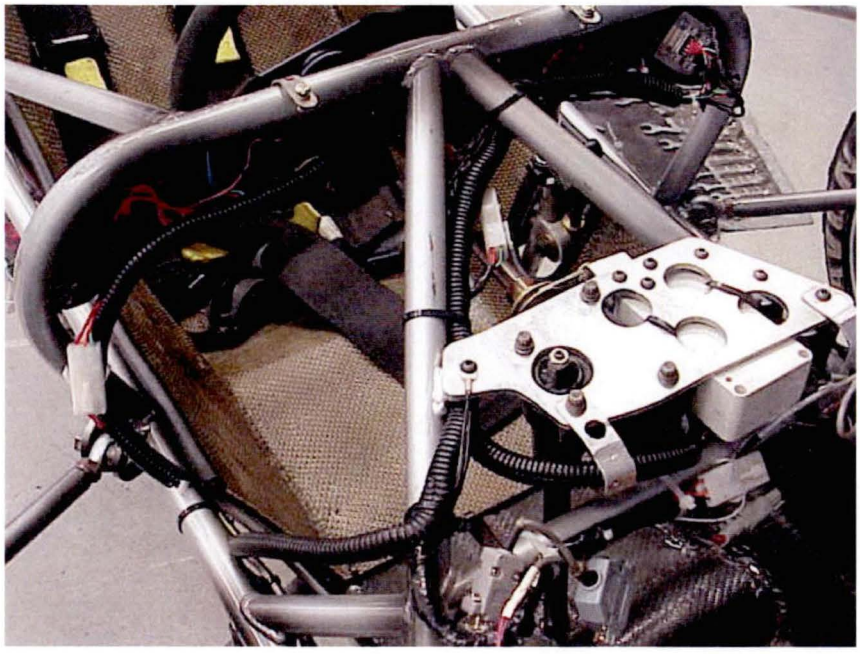

Figure 3-42 Conduit, triple insulated wiring loom under nose cone.

3.10.6 Heat Protection

Care was taken to ensure that the wiring resides as far from hot objects as possible. In most cases the heat was enough of a problem to other components of the car that heat shielding on the exhaust was deemed a more appropriate solution.

3.10.7 Easy removal of all components

To ensure easy removal of all components, wires were crimped and not soldered. Where possible large multiple connectors have been used to eliminate the possibility of mis-connection upon re-installation.

3.10.8 Kill switches

Power for the entire car may be instantly cut using any one of three kill switches. The brake over-run switch is located behind the brake pedal and will activate if the brake is depressed while there is simultaneous failure of both independent braking systems.

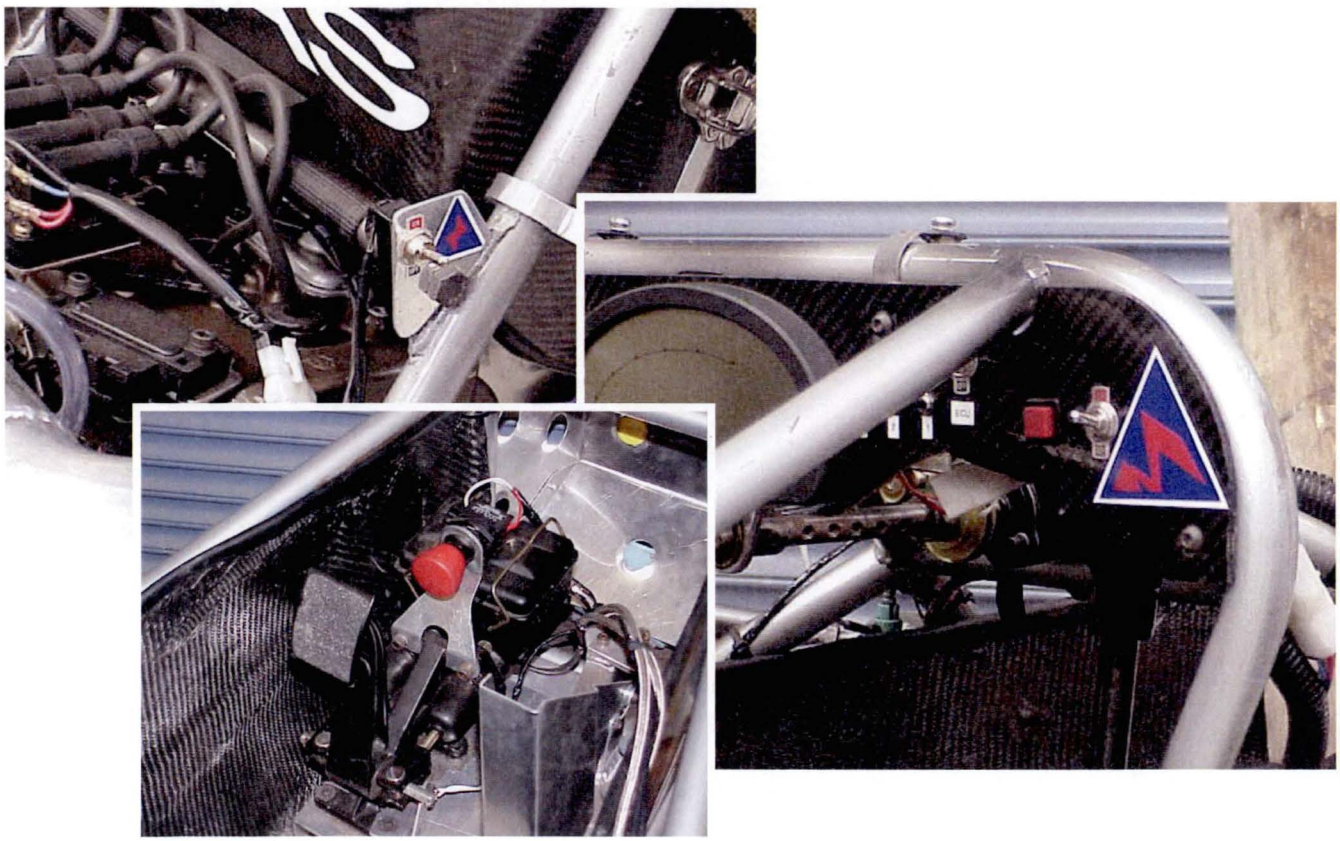

Figure 3-43 Kill switches

The other two kill switches are located on the dashboard to the driver's right and externally next to the head support on the roll bar to the driver's right, in accordance with best practice international FIA safety standards.

Cutting any one of these switches will deactivate the switch line to the main relay. All power to components on the vehicle are sourced from this relay or from the switch line after the kill switches. Both human operated kill switches are clearly labelled with the international electrical symbol of a red spark on a white-edged blue triangle.

3.10.9 Brake Light

A brake light of 15 watt or equivalent is required by SAE international standards. This is to be mounted centrally between the wheel centres and the drivers shoulder height at the rear of the vehicle. For aesthetic reasons a high intensity LED arrangement was selected. The LEDs are mounted in parallel to prevent failure of the complete brake light in the event of one LED failing.

3.10.10 Engine Cam Sensor Circuit

The engine cam angle sensor is used by the ECU to determine the location of the pistons for fuel injection timing. This sensor is a small hall effect type similar in appearance to a transistor, and is activated by a small permanent magnet mounted in the cam sprocket. The pulse from the sensor must be amplified to be read by the ECU input. A simple MOSFET amplification circuit is used for the job. The circuit is built on printed track circuit board and mounted in a box on the outside of the engine.

The sensor wiring is temperature resistant, Kevlar insulated wire designed for harsh conditions. The sensor is mounted into the cam sprocket cavity in an aluminium bracket held by the nearest cam cover bolt. Directions for the setup and calibration of this sensor are included in the ECU help menus.

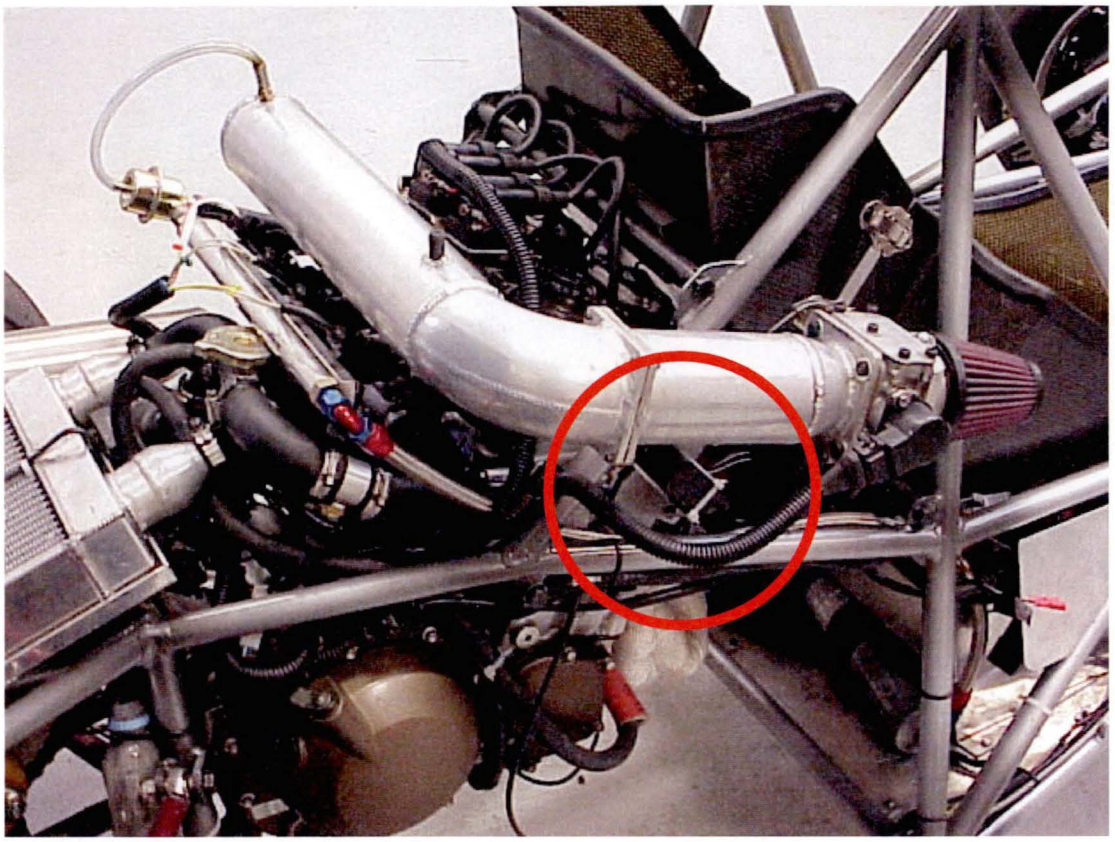

Figure 3-44 Location of the engine cam sensor circuit case.

3.11 FUSE BOX CIRCUIT AND LAYOUT DESIGN

3.11.1 Physical considerations

In fitting with the major objectives of the electrical system, the original loom design with in line fuses and multiple bulky relay mountings was re-designed to incorporate a single fuse and relay box. This box is located in a highly visible, easily accessible location on the outside of the right hand side of the driver cockpit.

The box itself is made of clear material for reasons of fast identification of loose connections or burnt out fuses and relays as well as aesthetics. The wires are fed in groups through the back of the box that allows removal of the box without the loom and vice versa. Rubber grommets have been used along with a rubber gasket so seal the box cover in place. The cover is screwed onto the aluminium backing plate that is then bolted to the frame.

3.11.2 Circuit Design

The circuit for the fuse box was taken almost directly from the MoTeC ECU wiring diagrams. Major alterations involved the removal of a relay that was redundant in this particular application and the unification of relay type used throughout the vehicle. The required diode activated relay was replaced with an in line diode on the circuit to allow fitment of a standard relay in its place. Extra fuses were included for each of the major components, allowing for very simple component fault finding.

3.11.3 Physical circuit layout

One of the major objectives of the fuse box was to find a neat and effective way to mount all the required relays and fuses in one place where they could be easily accessible to check and change. The ideal situation was chosen to be a set of closely located relay and fuse sockets joined to plugs as appropriate by a printed circuit board. The printed circuit board was layered with solder tracks to increase the current rated capacity in excess of 12 Amp.

3.11.4 Fuse specification

Load ratings of fuses were selected according to the component they serve. In general fuses will withstand up to their rated current plus 200% for 2 minutes. The majority of components have around 7-8 Amp start up current with a continuous 2-3 Amp while running. 10 amp fuses are most common in this system. Automotive fuses were specified for their compactness, physical durability (plastic cases) and ease of mounting.

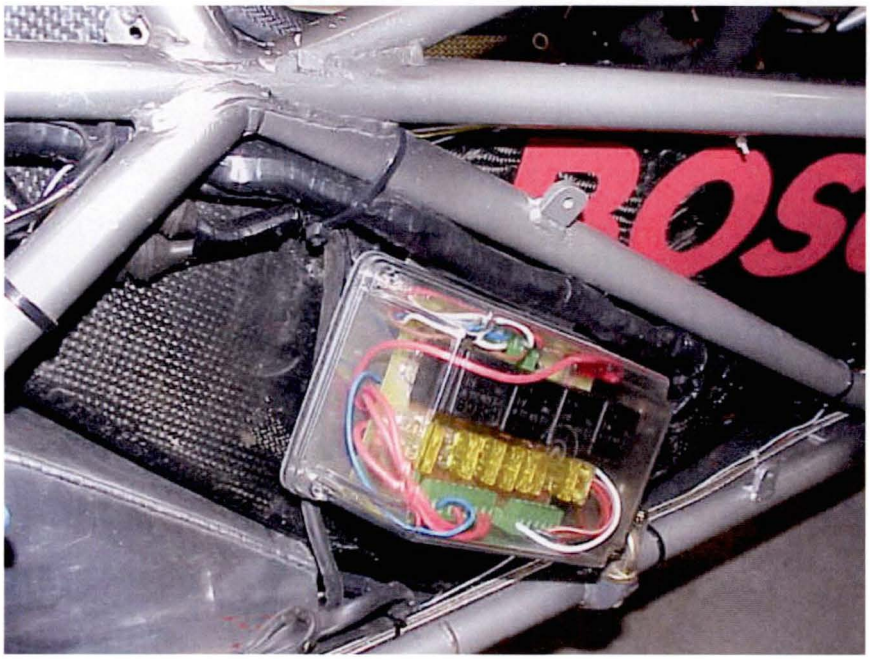

Figure 3-45 The yellow colour of the automotive fuses within the fuse box indicates a rating of 10 amp.

3.12 DASHBOARD – LAYOUT AND CIRCUITRY

3.12.1 Physical considerations

The dashboard is the driver control panel. All the information about the engine and other aspects of the running car is fed to the driver through the Advanced Dash Logger or ADL. Information about the ADL is contained within the telemetry section of this document with reference wiring and programming.

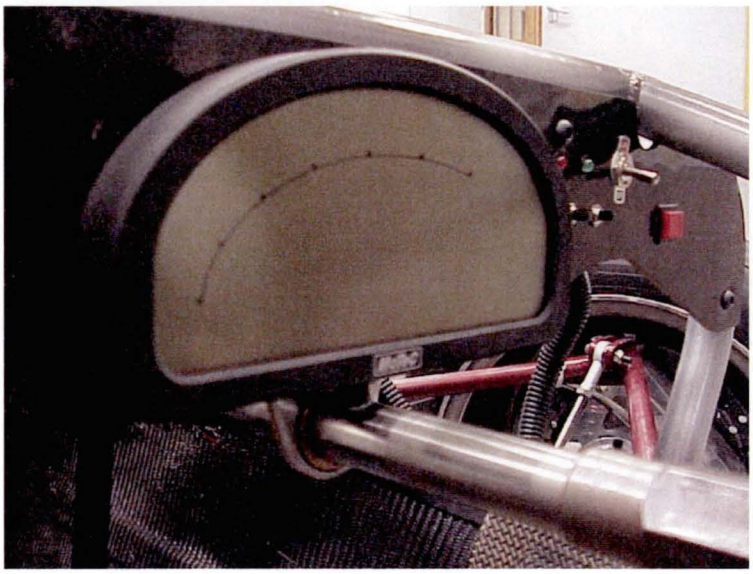

Figure 3-46 ADL location on dashboard.

The dash itself is constructed from a composite sandwich of carbon fibre and foam constructed using vacuum bagging techniques, the fibre was said up on sheets of window glass to ensure a good finish. Profile cutting, drilling and finishing all performed after the bonding process. The dashboard attaches to the frame through bolts and welded tabs.

COM ports featured in the dash are used to facilitate fast and easy connection of the on-board computer systems to an external computing and storage PCs for data logging sessions. The COM ports connect to plugs behind the dash where the ECU and ADL are connected facilitating easy removal of individual units. The trackside computer is simply plugged into the front of the dashboard to down load data or change on-board programmed settings.

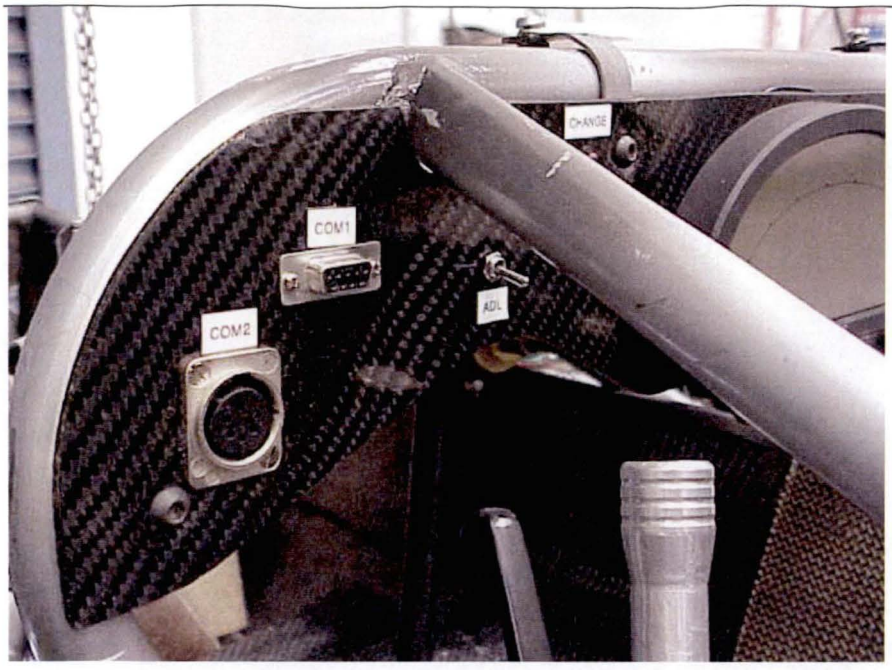

Figure 3-47 Com ports are located on the dashboard for high levels of access during testing and data transference with the remote PCs.

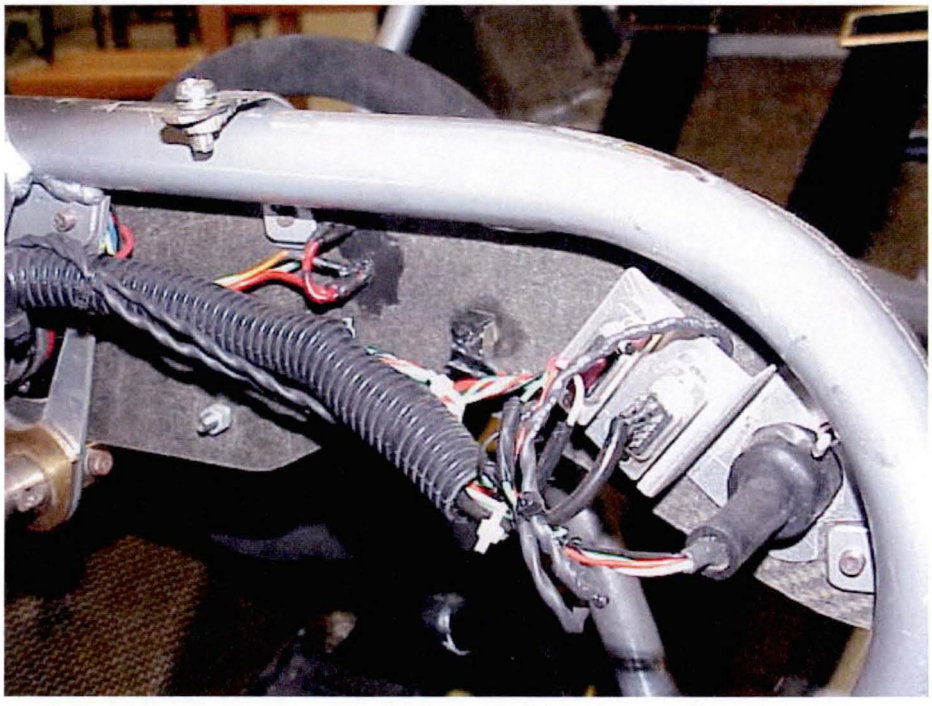

As vibration is significant on the racecar, stress relief for the wiring and solid mountings are a feature of this design. Ease of removal of the dash was a major consideration and was achieved using two main connectors behind either side of the dash.

Figure 3-48 Rear connection from wiring loom to Com ports.

3.12.2 Circuit design

Once the physical layout of the dashboard was determined, the circuit design was largely a matter of connecting the components with the main vehicle circuit. Shrink fit wire covering was used to prevent shorting, and the back of the dash is painted with liquid electrical tape to ensure water resistance.

3.12.3 Physical layout

Physical layout of the dashboard switches and lights follows a logical progression. The most important switches are to the right, away from the gear changer. The neutral and oil warning lights are located close to the ignition switch.

3.13 ELECTRICAL SYSTEM SPECIFICATIONS

Specifications for components of the electrical system are as follows:

Table 4 Electrical system specifications

Item	
Battery	
Type	Gel cell
Capacity	15 Ah
Voltage	12.6 V
Charging System	
Type	Three Phase AC
Alternator output voltage	45 V
Stator coil resistance	0.2-0.6 Ohm
Charging Voltage (regulator / rectifier voltage)	14 – 15 V
Electric Starter System	
Starter motor	12 V
Brush length	12mm
Commutator diameter	28mm

Chapter Four

INSTRUMENTATION DESCRIPTION

This chapter describes the individual components that constitute the instrumentation used on the test rig. The sensor and measurement system provides data for neural network development. To build reliable neural networks to predict and ultimately control a dynamic vehicle, accurate parameter measurement and data recording are essential for network training.

An automobile modelling process undertaken in conjunction with Professor Rossmanek at the University of Stralsund, Germany and Dr Vishy Karri from the University of Tasmania, Australia has been used to identify the subject of measurement or the research measurand. This modelling process concluded that the automobile parameters, tabulated in [Figure 4.1], govern the dynamic behaviour of an automobile and are those automobile parameters that the test rig measuring system is required to measure and record on line.

Research Measurand		
Parameter	Symbol	Units
Wheel speed	ω_w	1/s
Distance	d	m
Speed	v	m/s
Acceleration	a	m/s^2
Yaw angle	ψ	°
Pitch angle	ϑ	°
Roll angle	φ	°
Steer angle	δ	°
Wheel Travel	z_{St}	m
Brake force	F_B	Pa

Figure 4-1 Research measurand as identified in through the collaboration of Professor Rossmanek and Dr Karri.

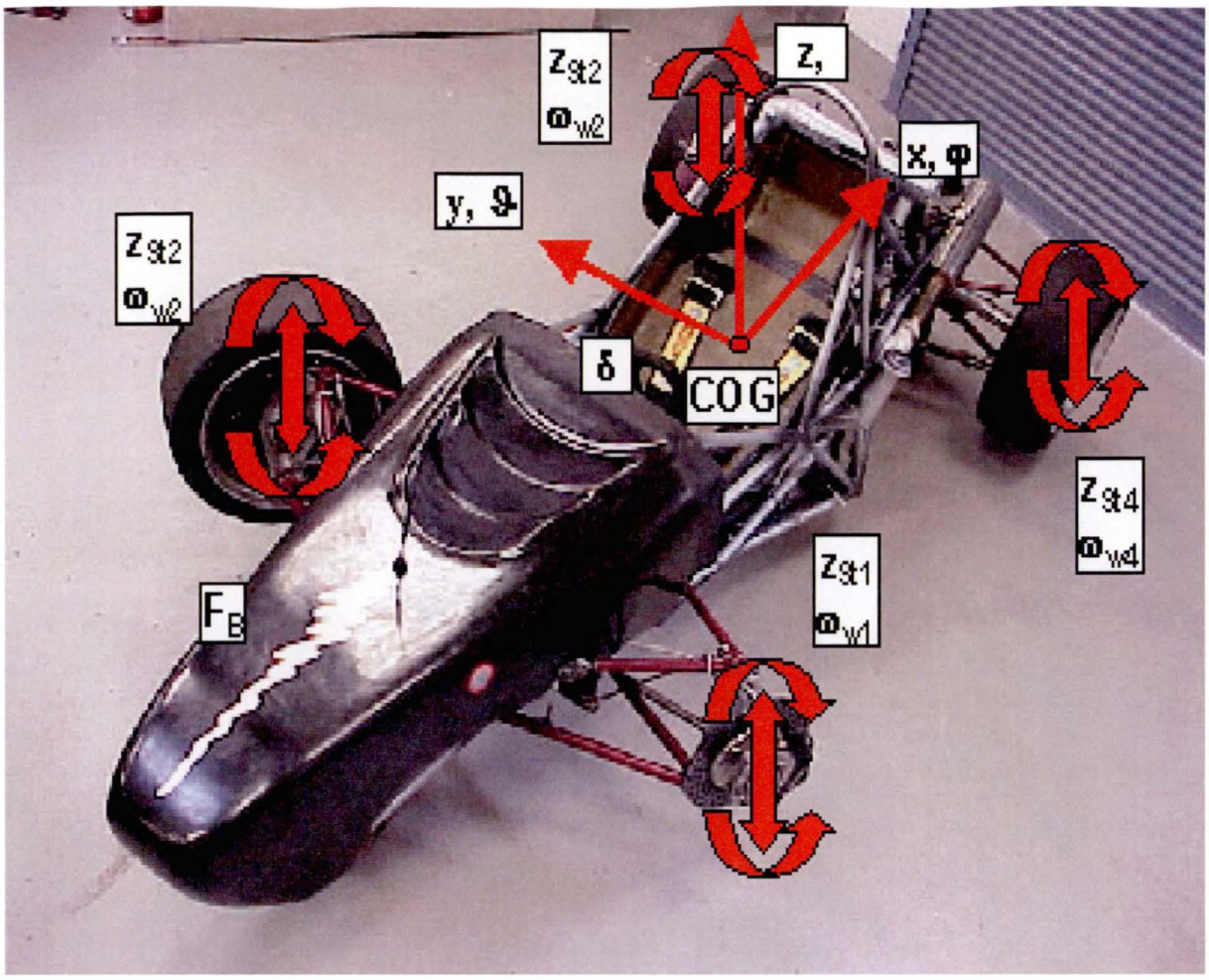

Figure 4-2 The research measurand depicted on the test rig.

[Figure 4-2] illustrates where these parameters as outlined are measured on the test rig. Note:

- The suspension position, z_{St}, and wheel speeds, ω_w, are measured at each wheel.
- Brake forces, F_B, are measured in both front and rear independent braking circuits.
- Accelerations are measured in three directions (three dimensional accelerations)

The instrumentation system on the test rig has three major components. Firstly the test rig instrumentation system is required to measure the dynamic parameters during testing; this is referred to as *Input* (measuring) type instrumentation. Secondly the instrumentation system is required to collect and store the information; this is referred to as *Data Acquisition* type instrumentation. Finally, the instrumentation system is

required to transfer information to trackside and research computers for further analysis; this is referred to as *Output* type instrumentation.

This chapter is divided into three main sections: Section 4.1, describes the Input Type Instrumentation, Section 4.2, describes the Data Acquisition Type Instrumentation and Section 4.3 describes Output Type Instrumentation.

4.1 INPUT TYPE INSTRUMENTATION

Input Type Instrumentation refers to the selected automobile sensors required to detect the changes in the research measurand. Five different types of sensors were required to monitor the identified research automobile parameters. [Figure 4-3] below shows the sensor type, supplier, quantity and the actual parameter measured by the specific sensor.

Measurand	***Sensor Type***	***Supplier***	***Quantity***
Wheel Speed	*Honeywell Gear Tooth GT1 Series Hall Effect Sensor*	*MoTeC*	*4*
Three Axis Acceleration	*Crossbow DMU AHRS400-200 Sensor*	*Davidson Industrial Measurement*	*1*
Pitch Angle			
Roll Angle			
Yaw Angle			
Steering Angle	*MoTeC (Spectrol) 10 turn, gear driven rotary potentiometer*	*MoTeC*	*1*
Spring Travel	*Gefran Linear Potentiometer – 100mm*	*MoTeC*	*4*
Brake Force	*Honeywell Eclipse Pressure Sensor – 2000psi*	*MoTeC*	*2*

Figure 4-3 The Input Type Instrumentation Sensors

The sections to follow describe each of the above sensors with reference to the sensor operational principals and associated sensor measuring range, accuracy and resolution.

4.1.1 Wheel Speed Hall Effect Sensor

A digital output Gear Tooth Hall Effect Sensor is used to measure the four-wheel speeds of the Racecar. The Hall effect sensor used in this application is a magnetically biased integrated circuit, designed to accurately sense movement of metal materials. Gear Tooth Hall Effect Sensors are so called as a ferrous metal gear tooth wheel is conventionally used in their operation. The Hall effect gear tooth sensor is shown in [Figure 4-4].

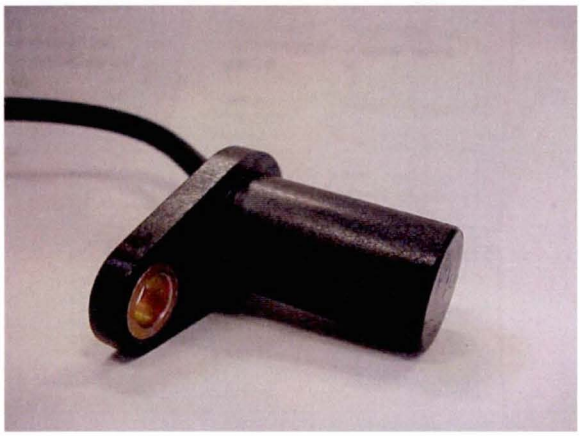

Figure 4-4 The Honeywell GT1 Series Hall Effect Gear Tooth Sensor

Hall effect sensors are based on an electrical phenomenon, discovered by Dr Edwin Hall in 1879, that occurs when a current flows through a conducting material in a magnetic field. If a current is flowing perpendicular to a magnetic field, the Hall effect is observed as a potential difference or voltage developed across the material. The produced Hall voltage is perpendicular to both the direction of the current and the direction of the magnetic field. The value of the Hall voltage is proportional to the current and the magnetic field intensity. If there no magnetic field present in the system no Hall effect voltage is induced. It took the advent of semi-conducting materials in the 1950's before the Hall effect principal was used as a sensor. Currently Hall effect

sensors are used to measure rotational speeds of different automotive processes. They are used in automobile applications such as camshaft and crankshaft speed sensors, transmission speed sensors, tachometers and are the wheel speed sensors used in ABS and Traction Control driver supporting facilities.

The Hall effect sensor is composed of an integrated circuit, made up of discrete capacitors and a bias magnet, that is sealed in a probe type, non-magnetic plastic package for physical protection and cost effective installation. The Hall effect sensor consists of three wires. One wire is the power source or voltage, the second wire supplies the sensor ground and the third wire is the signal wire that provides the output or measurement sensor reading value. The configuration and wiring diagram is depicted in [Figure 4-5].

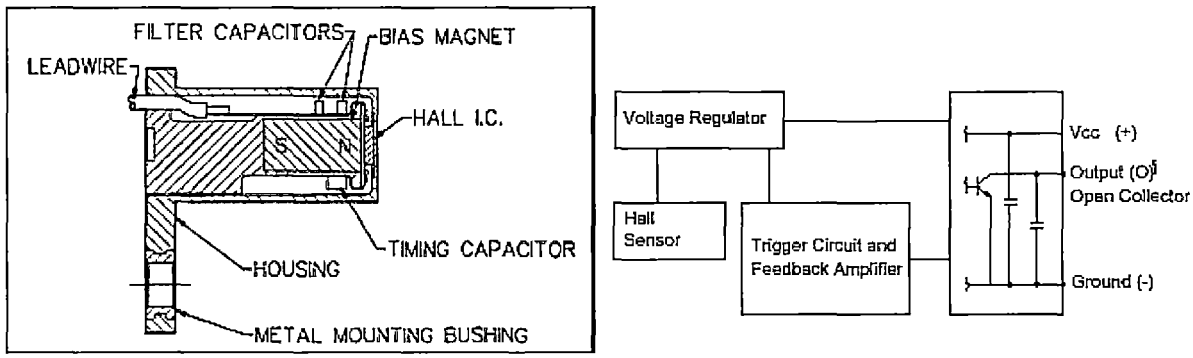

Figure 4-5 Gear tooth sensor construction and wiring diagram

As a gear tooth wheel passes the Hall effect sensor face, as depicted in [Figure 4-6], it concentrates the magnetic flux away from the sensor's in built bias magnet. The sensor detects the change in magnetic flux level and hence as explained above there is a drop in the induced voltage across the sensor, which translates into a change in the sensor voltage output. The digital output switches between the supply voltage when it passes a gap in the tooth wheel and the saturation voltage (0.4 V) when it passes a tooth. [Figure 4-7] illustrates the drop in induced voltage across the sensor as the gear tooth wheels teeth move past the face of the Hall Effect sensor.

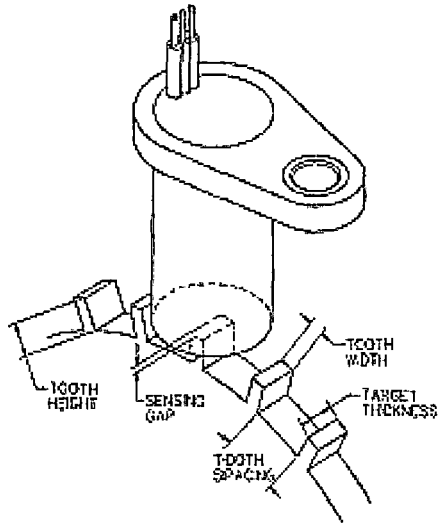

Figure 4-6 Hall effect sensor in relation to gear tooth wheel.

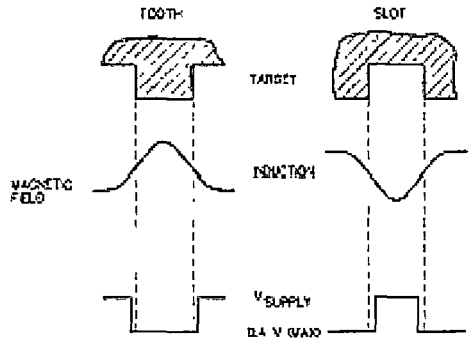

Figure 4-7 Induced voltage changes. Note V_{Supply} when the sensor passes a gap and V = 0.4 V_{max} when the sensor passes a tooth.

The sensor uses a discrete capacitor to store a reference voltage that is directly proportional to the maximum magnetic field strength, (the no tooth magnetic field strength), the operating position at which the face of the Hall effect sensor passes a slot in the wheel. A digital output signal is triggered when the magnet field sensed by the hall element changes by a predefined amount. A feedback circuit is integrated into the silicon integrated circuit and is used to reduce the effects of temperature and other error affecting variables.

The Honeywell Gear Tooth (GT1 Series) technical specification brochure and the MoTeC Hall effect sensor CAD drawing are provided in "Appendix H". As the output from this Hall effect sensor is digital, the accuracy in the sensed measurement is dependant primarily on how the sensor is positioned with respect to the ferrous metal gear tooth wheel.

The performance and accuracy of the Hall effect sensors is dependent mainly on the way the sensors are positioned in relation to the target material[6] and also on the magnetic characteristics of the target. The following variables have been identified to effect the operation of Hall effect sensors and were considered in combination during the sensor installation process.

Target material, geometry, and speed
Sensor/target air gap: that is the distance between the sensor and the target material
Operating temperature:
The proximity of magnetic materials to the sensor and target

Initially the installation process required the development of a suitable gear tooth wheel for sensor operation. However, suitable points of attachment of such a wheel on the test rig could not be found at all four wheels. It was possible to attach such a device on the stub axels[7] of the front wheels. However, this could not be achieved on the two back wheels of the automobile, as the drive shaft of the test rig obstructed any available site of installation. An alternative solution had to be found that involved the use of a magnetic (metallic) material in a regular repetitive formation, that would provide a similar output from the Hall effect sensor, as that produced when in use with a gear tooth wheel.

A solution to this problem was found using the heads of the bolts that hold the aluminium face plate of the wheels to the rim of the wheels. The bolts, which are

[6] Target material refers to the metallic material that concentrates the magnetic flux away from the Hall effect sensor

[7] There are four holes present on the front two stub axels where initially a gear tooth wheel was to be attached

positioned in a uniform circular formation around the face plate, act as the sensor target. The sensor target is the metallic element necessary to draw the magnetic flux away from the sensor thus producing a signal output. The wheel rims made from aluminium, a non-magnetic material behave as the non-target material. [Figure4-8] shows the bolt arrangement on the inside of the rims of the wheels. This arrangement with a repetitive series of targets and non target areas in a circular formation facilitates the same function in operation as the gear tooth wheel in terms of producing a change in the magnetic flux of the sensor. In theory this solution is feasible as long as the sensor can be positioned close enough and in a direct line with the rotating bolt heads on the inside of the wheel.

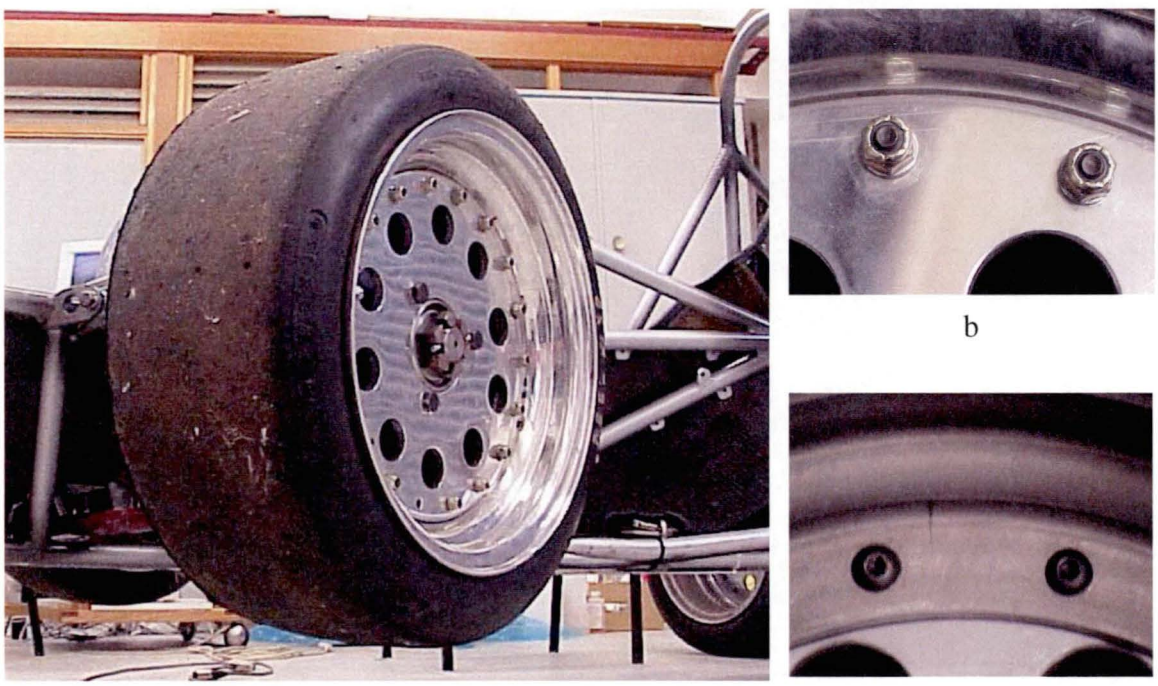

a b c

Figure 4-8 a) Three piece rim, b) outside view of rim bolts, c) inside view of rim bolts.

Testing was required to determine if this unconventional Hall effect sensing arrangement would work in practice to confirm if the materials in use as the magnetic and non-magnetic targets possessed the desirable qualities to produce a reliable signal from the Hall effect sensor.

Each hall effect sensor required a suitable mounting position to be found close enough to the inside of the wheel rims to ensure a 1- 2 mm gap between the sensor and the bolt

head. The Hall effect sensor was mounted from the Wilwood brake calipers from a ¼ inch bolt. A special mount [Figure 4-8] was fabricated to position the Hall effect sensor to the target site area. With the sensor installed, the wheel was spun manually to simulate the rotation of the wheel in operation. The signal output from the Hall effect sensor was observed [Figure 4-9]. It was necessary to adjust the position of the Hall effect sensor and its mount a number of times in order to align it directly above the rim bolt head, before square pulses were continuously observed whilst rotating the wheel.

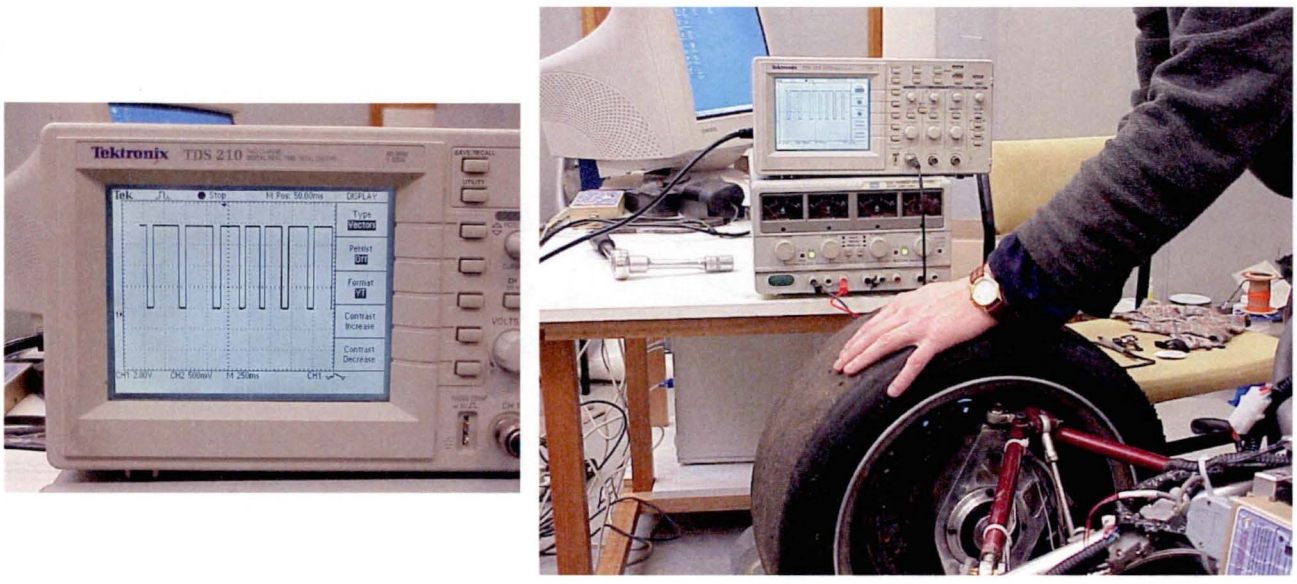

Figure 4-9 Simulation setup used in testing the Hall effect sensor.

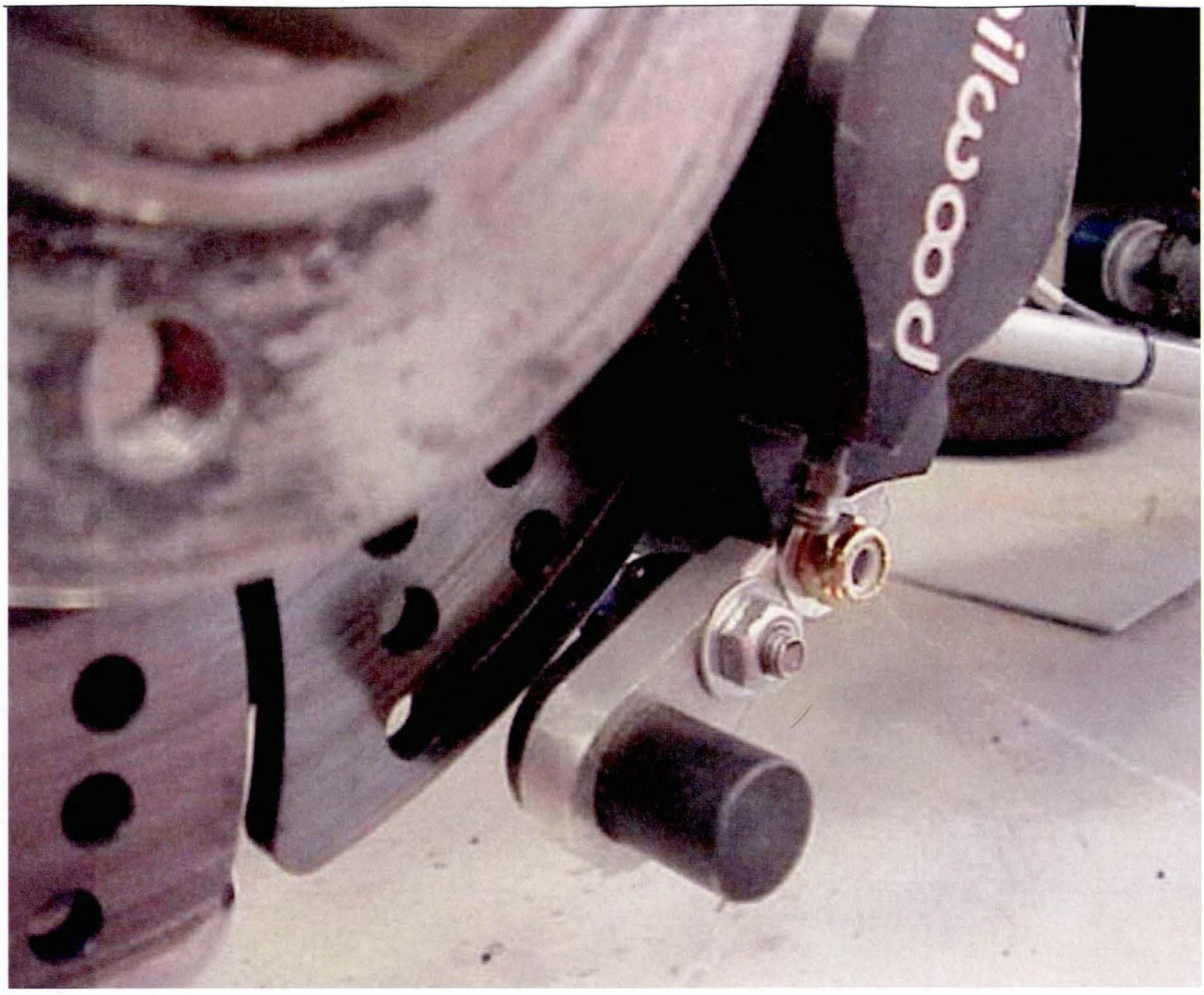

Figure 4-10 Hall effect sensor mount.

The calibration function of the Dash Manager [Figure 4-11] software was used to convert the digital output signal of the Hall effect sensor into a wheel velocity. Sensor calibration required the wheel speed calculation for one complete revolution of the wheel, in a single second. One revolution of the wheel is equivalent to eighteen sensor signal pulses being generated per second, as there are eighteen bolts around each wheel. To determine the speed of the wheel for one cycle per second the diameter of the wheels had to be measured and the circumference of each calculated[8]. This was then entered in the calibration function in the Dash Manager software, as shown in [Figure 4-11], which shows the calibration curve of the rear right wheel. A similar calibration curve was

[8] The font tyre on the Race Car are slightly smaller in size than the back tyres thus the back and front tyre diameters had to be individually measured.

found for the two front wheels. However one revolution of the front wheels results in a smaller velocity as the front wheels are smaller in diameter than the back wheels.

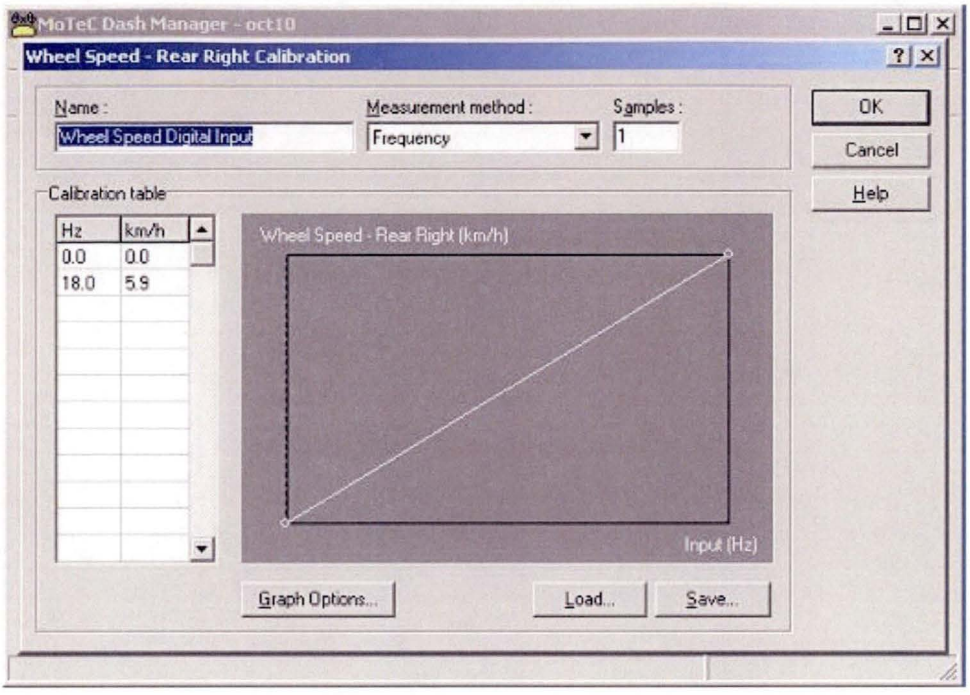

Figure 4-11 Dash manager calibration of hall effect sensor

4.1.2 Three Axis Acceleration & Pitch/Roll/Yaw Angle Measurement: Crossbow DMU AHRS400CA-200 Sensor

The measurement of the automobiles acceleration and operational dynamic angles is to be measured at the centre of gravity of the vehicle. This requirement results in one location on the test rig being needed for more than one automobile parameter measurement. To overcome this problem a sensor cluster needs to be formed at the vehicle's centre gravity. This could be achieved in one of two ways, (1) by the use of a number of sensors to measure the individual automobile parameters of acceleration and dynamic automobile angles separately, or (2) to source a sensor that had the capacity to measure all the parameters in a single unit. The perceived problem involved in developing the sensor cluster from a number of individual sensors, was sensor positioning problems at the test rig's centre of gravity. Calibration of the individual sensors, to eliminate the inaccuracy in sensor measurements was also seen to be a future

difficulty with this approach. The error in sensor measurement if this approach was used would arise from the sensors being installed at a location near the centre gravity of the test rig and not at the exact centre of gravity of the vehicle.

Therefore a single sensor was sought that had the capacity to measure all the measurand parameters needed to be monitored at the test rig's centre of gravity. The main advantage of selecting a single sensor for the measurement of the centre of gravity parameters was identified in the ease of sensor installation and calibration, with the knowledge of minimising the risk involved in potential installation errors in the sensor output, compared with installing individual sensors. The Crossbow DMU AHRS400-CA sensor was identified as being the most appropriate sensor for this application. A picture of the sensor can be seen below in [Figure 4-12].

Figure 4-12 The DMU AHRS400CA-200 Sensor

The DMU-AHRS is a sensor clustering measurement system, designed to measure nine parameters including stabilised pitch, roll and yaw angular rates and angles and three-axis acceleration in a dynamic environment. The DMU-AHRS measures these variables by using a combination of micro-machined three-axis accelerometers, three-axis rotational rate sensors, and three-axis magnetometers. The addition of a three-axis magnetometer also allows the DMU-AHRS to make a true measurement of magnetic

heading. The sensor can output the measured data in two forms, either in analog form or as a serial data package in the form of a RS232 digital output. [Figure 4-13] depicts a block diagram of the DMU-AHRS sensor cluster measuring system.

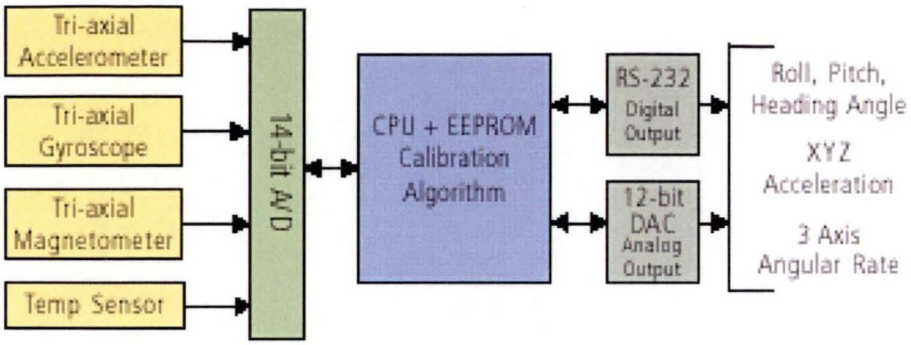

Figure 4-13 Block diagram of the DMU-AHRS sensor

The Crossbow DMU contains three accelerometers and three angular rate gyros and magnetic sensors. The magnetic sensors are miniature fluxgate sensors. The presence of magnetic sensors inside the DMU-AHRS means that the sensor should not be exposed to large magnetic fields, as this has the potential to permanently magnetise the internal components of the DMU-AHRS and degrade its magnetic heading accuracy. The basic principal of operation of the accelerometers and the angular rate gyro sensing components will be discussed below.

The three MEMS[9] accelerometers are made from surface micro-machined silicon devices that use differential capacitance to sense acceleration. All accelerometers can be thought of as measuring the relative displacement of a spring mass system. Capacitive accelerometers operate by sensing a change in electrical capacitance, with respect to an applied acceleration. When subject to a fixed or constant acceleration, the capacitance value is constant, resulting in a measurement signal proportional to uniform acceleration.

Typical capacitive accelerometers are structured with a diaphragm that undergoes distortion in the presence of acceleration. Two fixed plates, sandwich the diaphragm,

[9] Micro Electrical Mechanical System

creating the capacitor unit. Changes in acceleration are detected by measuring the capacitance changes resulting from the separation of the two plates due to a movement of the diaphragm. The capacitance is inversely proportional to gap distance between the two plates and therefore the displacement of the diaphragm is a non-linear hyperbolic function.

The sensor is designed so that the acceleration of the measured medium causes the diaphragm of the sensor to distort which results in a change in the capacitance of the sensor, due to a distance change between the two parallel plates that support the diaphragm. The change in capacitance is used in a bridge circuit that performs signal conditioning on the sensors' output signal to achieve linearisation and hence an output signal that is proportional to the input acceleration of the system under investigation.

The three angular rate gyroscopic sensors consist of vibrating ceramic plates that use a silicon MEMS structure to measure the Coriolis force in order to measure the angular rotation rate around a given axis. The advantage of this approach is that the output of the angular rate is independent of the acceleration output. In the 1830's G. Coriolis discovered that an object moving perpendicular to a rotating frame will cause an observer on the rotating frame to see an apparent acceleration of the object. The DMU's angular rate gyros experience a Coriolis acceleration by the angular rotation of a vibrating silicon MEMS structure induced by the dynamic movement of the testing apparatus. A change in the direction around one axis of a driving transducer induces a vibration in a detection transducer on another axis. An oscillator circuit is used to control the vibration and signal-conditioning converts measurements to an angular rate output. In general, the apparent Coriolis acceleration A and Force F is given by:

$$A = 2\omega V\sin(\phi) \qquad \text{and} \qquad F = 2m\omega V\sin(\phi)$$

where ω is the angular velocity of the rotating axes relative to a fixed set of axes, V is the velocity of the bar, and ϕ is the angle between the vectors ω and V.
From observing the above equations it is apparent that the Coriolis force is proportional to w or angular velocity. The Coriolis force is converted to a voltage by the detector element and signal conditioning circuitry. As the mass of the structure and the vibration

velocity of the sensor components are both known quantities, the angular velocity ω is easily derived and provided to the DMU. The sensor integrates the angular velocity signals with respect to time to convert angular rates, measured in °/s into angular ° outputs. [Figure 4-6] depicts a block diagram illustrating this operation.

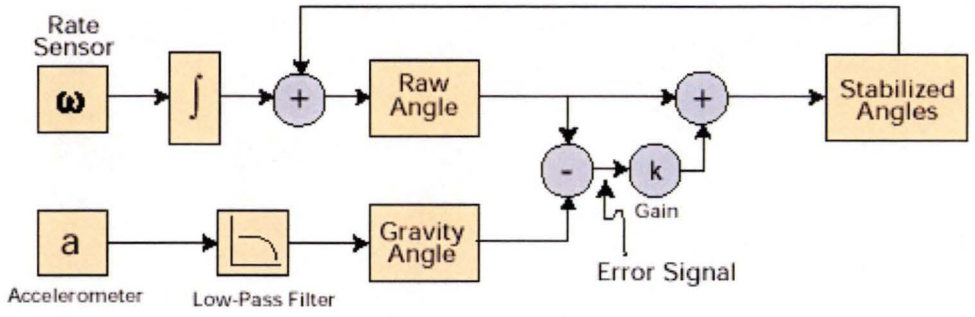

Figure 4-14 Block diagram depicting the signal conditioning operations.

The DMU-AHRS sensor has a predefined coordinate system to which the accelerometers, angular rate sensors and magnetic sensors are aligned. The coordinate system is shown on a label attached to the connector side of the sensor. The sensor axis orientation forms an orthogonal right-hand coordinate system with the z-axis defined as positive in the downward direction. The system is depicted in Figure 4-7.

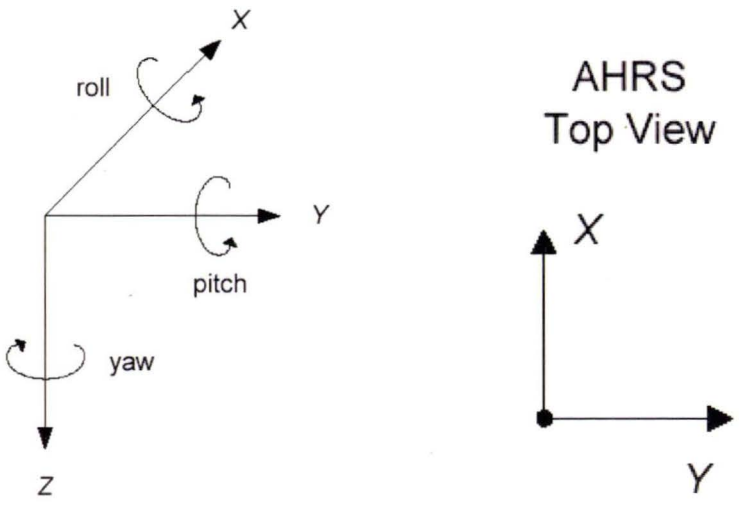

Figure 4-15 The DMU-AHRS400CA-200 coordinate system.

The sensors' coordinate system defines a positive acceleration when it is oriented towards the positive side of the coordinate axis. Therefore if the sensor was only measuring the effects of gravity it would produce an output in the z axis direction of +g and would read 0 g for both the acceleration in the x and y directions. The direction of positive angular rotational rates is defined by the right hand rule. This means a clockwise motion of the accelerometer when positioned on a horizontal surface would produce a positive angular rate and yaw angle around the z axis. The x- and y-axis rate sensors would measure zero angular rates for this operation. The magnetic sensors are aligned with the same axes definitions and sign as the linear accelerometers.

The Crossbow DMU AHRS400CA-200 technical specification brochure is provided in "Appendix H". This brochure provides information on the measurement range, resolution and total accuracy of the angular rates, pitch and roll angles (Altitude) and yaw angle (Heading) and three-axis acceleration. A summary of these and the calculated maximum errors associated with measurement is presented below in [Figure 4-16].

Sensor Specification	***Angular Rates***	***Acceleration***
Range	*±200 (°/sec)*	*±10 (g)*
Resolution	*< 0.05 (°/sec)*	*< 1.25 (mg)*
Bias Error	*<±0.05 (°/sec)*	*<± 12 (mg)*
Non-Linearity (%FS)	*< 0.3*	*< 1*
Scale Factor Accuracy (%)	*< 1*	*< 1*
Total Error (%)	*1.044*	*1.458*
Maximum Error Value (FS)	*±2.089 (°/sec)*	*±0.146 (g)*

Figure 4-16 Error specification of the DMU sensor.

The DMU measures the parameters at a sampling rate of 75 samples per second. The sensor also has an on board temperature sensor which is used to monitor the internal temperature of the DMU for sensor temperature calibration. The DMU-AHRS outputs

the yaw angle with referenced to magnetic north[10]. The declination[11] needs to be known in order to translate the DMU-AHRS magnetic heading into a heading referenced to true north.

4.1.3 Wheel Travel: Gefran PZ12A Linear Potentiometer – 100mm

A Gefran PZ12A analog linear potentiometer with a 100 mm stroke has been selected to measure the individual displacement of the four wheels of the test rig during dynamic trials. The sensor consists of an anodised aluminium cylinder case with an internal moveable control rod made from stainless steel, with an extension capacity of 100 mm. At the end of the moveable rod and the bottom of the sensor there are 5 mm diameter self aligning ball joints used for mounting purposes. The sensor can be seen mounted to the test rig in [Figure 4-17]

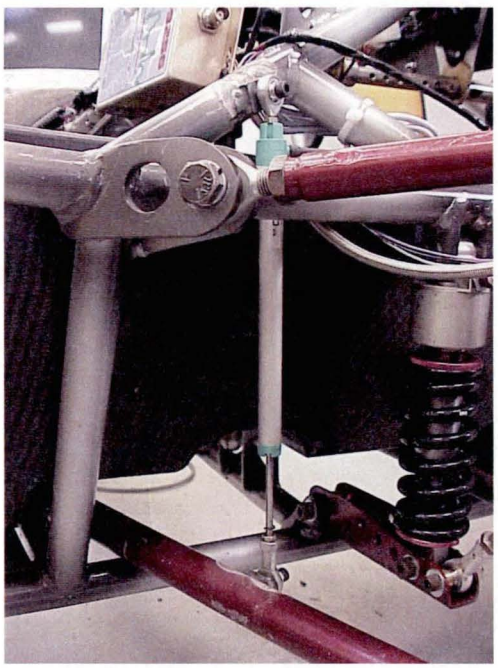

Figure 4-17 Wheel travel linear potentiometer mounted to the test rig.

[10] Magnetic north is the direction toward the magnetic north pole; true north is the direction towards the true North Pole.

[11] The direction of true north varies from magnetic north depending on your location on the globe. The difference between true and magnetic north is called declination or magnetic variance.

The electrical configuration of the sensor is depicted in [Figure 4-18]. It consists of three wires, one wire is the power source or voltage, the second wire supplies the sensor ground and the third wire is the signal wire that provides the output or measurement.

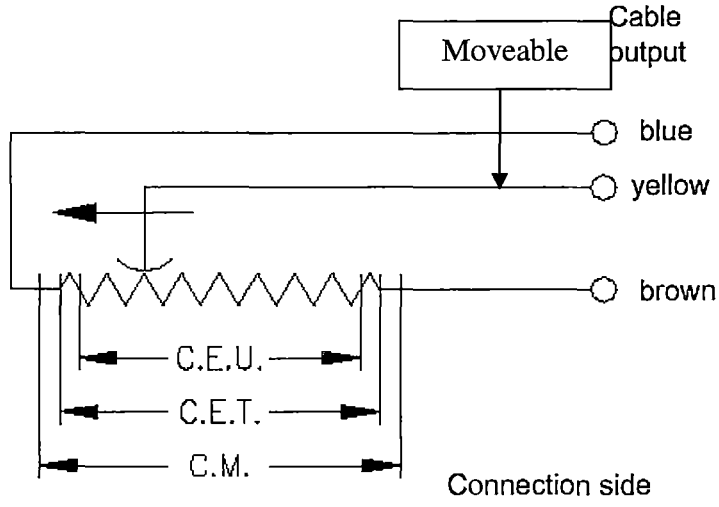

Figure 4-18 Electrical configuration of the linear potentiometer sensor

A linear potentiometer is an analog sensor that operates on the basis that electrical resistance is proportional to resistance length and that voltage is proportional to resistance. A linear potentiometer consists of a moveable component that makes contact to an internal resistor. The contact motion can be translation or rotation thus allowing for the measurement of linear and rotatory motion. The resistance element is applied with an excitation voltage (V_{ex}) as shown on the following page in [Figure 4-19]. Motion of the testing apparatus, in this case the movement of the wheels of the Racecar, forces the moveable contact (the moveable control rod) of the sensor upwards or downwards resulting in an output voltage being induced across the sensor's moveable contact. This induced voltage or output voltage is proportional to the input displacement and forms the sensor's signal. It can be shown that the output voltage is a linear function of input displacement with reference to [Figure 4-19] as follows.

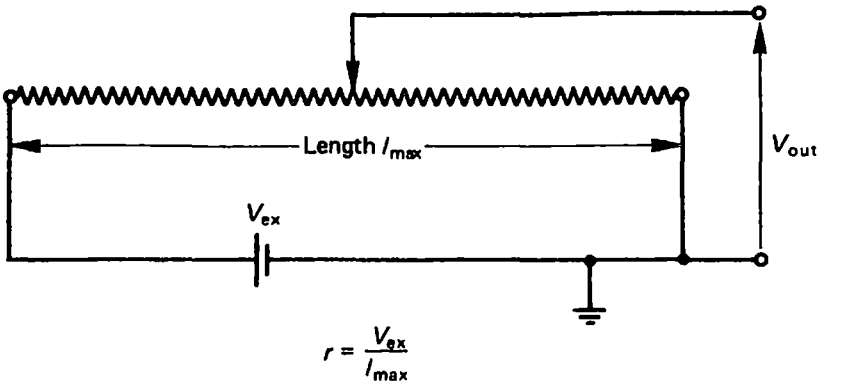

Figure 4-19 A representation of a Linear Potentiometer

$$\frac{\delta V}{V_{ex}} = \frac{\delta l}{l_{\max}}$$

Rearranging

$$\delta V = \frac{V_{ex}}{l_{\max}} \delta l \qquad \text{as} \qquad \frac{V_{ex}}{l_{\max}} = cons\tan t = c$$

$$\delta V = c\delta l$$

The Gefran PZ12A Linear Potentiometer technical specification brochure and the MoTeC Linear Potentiometer CAD drawing are both provided in "Appendix H". The resolution of the sensor is infinite according to the Gefran technical specification brochure. The resolution of the sensor was investigated by connecting the sensor to a multimeter and manually adjusting the moveable rod to determine the minimum voltage output from the signal wire of the sensor. The smallest voltage reading the sensor detected whilst manually adjusting the length of the extension rod was 0.00025 V. This translates to a resolution of $\pm 5 \times 10^{-3}$ mm as a 8 V corresponds to maximum extension of 100 mm. The sensor has a linearity accuracy of 0.1%.

4.1.4 Linear Potentiometer Installation and Calibration

A fixed mount was deemed necessary on the test rig to prevent the sensor mount from moving during operation. Eight mounts were required for the installation of the four sensors. The mounts were fabricated from six-millimetre thick steel plate cut into rectangles, fifteen millimetres in width and twenty millimetres in length. A M5 threaded hole was machined into the middle of the mount. The mounts were then welded to the frame and the wishbones of the test rig. The sensor installation points on the frame and wishbones were accurately measured on both sides of the automobile, to ensure symmetrical installation. M5 bolts were cut to size to pass through the sensor rose joints so as to screw into the mounting bracket and thus hold the sensor into position. Such an installation allowed for the quick and easy removal of the sensors when required. Washers were used to ensure that the ball joints of the rose joint had the potential to self align during vehicle operation. [Figure 4-20] depicts the M5 bolt holding the sensor to the mount.

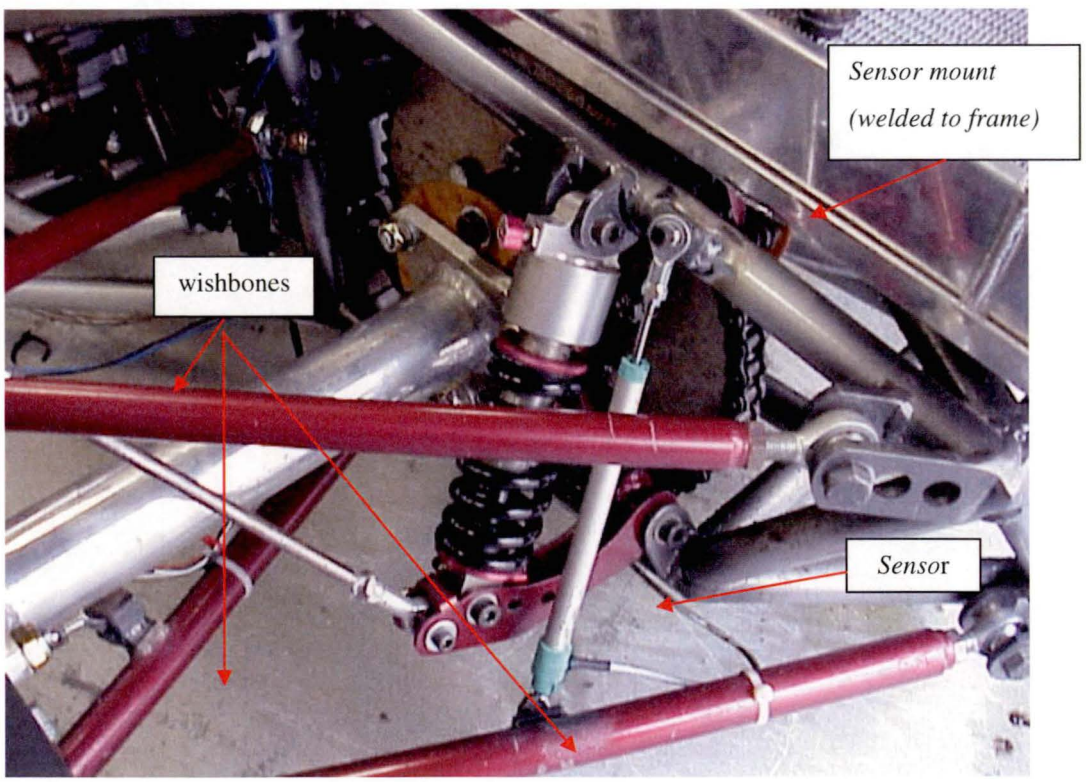

Figure 4-20 Installation of rear linear potentiometer.

Calibration of the linear potentiometers involved applying a known deflection at the wheels of the test rig and assigning this known input deflection to the subsequent sensor voltage reading output. This process was accomplished using the calibration function of the ADL Dash Manager software. This lead to the development of a linear calibration curve that allowed for the conversion of the analog voltage output signal from the sensor into the identifiable physical deflection of the wheels. The four potentiometers were selected and calibrated on an individual basis in the calibration software.

The first stage in the calibration process involved the zeroing of the linear potentiometers. The zero output voltage position of the sensors was established by a driver, of average weight, sitting very still in the drivers seat of the Racecar. The individual voltage output readings of the four sensors was recorded with the driver in the car. During this process the car was moved up and down a number of times to find the resting zero voltage position of each of the four potentiometers. A number of zero voltage readings were recorded for each potentiometer and the recorded values averaged to obtain a single zero voltage reading.

The next stage in the calibration procedure involved elevating the four wheels of the test rig above ground level by using two wooden blocks placed beneath the frame of the car. The potentiometers were calibrated individually by selecting their designated channel in the Dash Manager software. The wheels of the car were then removed and a vernier height gauge was positioned underneath the stub axel castle nut of the wheels. The wheel assembly was then raised and lowered by using the vernier height gauge and the sensor voltage signal was read via the calibration software. The height adjustment process of the wheel assembly continued until the sensor voltage reading output in the software became equal to the sensor zero position reading for that wheel, as determined in the first stage of calibration. This process established the hubs equivalent zero height position without wheels attached. The height gauge was then zeroed at this position and used as the reference zero position for that particular wheel.

The next stage in the calibration procedure involved moving the height gauge, in increments of five millimetres (5 mm) over a range of twenty millimetres (20 mm) in either direction i.e. up and down. The calibration software was used to read the voltage

signal output from the sensor at each incremental position of the wheel assembly. The applied wheel assembly deflection value was then manually typed into the software and assigned to the recorded analog sensor voltage output. The software assigned positive deflection for sensor compression, when the height gauge moved the hub upwards and negative for sensor deflection, for height gauge movement downwards. The zero reading of each potentiometer was checked when using the gauge in the cross over region of upward to downward movement or vice versa. With this calibration information the software has the capacity to graph the relationship between input deflection and output signal voltage. This calibration procedure was then repeated at each of the wheels of the Racecar to develop individual calibration curves for each of the linear potentiometers. [Figure 4-21] is a screen shot of the developed linear relationship between voltage signal output and input deflection for the front right linear potentiometer only, similar curves were produced for the other wheels. [Figure 4-14] shows the test rig during calibration setup used of the linear potentiometers using the dial height gauge.

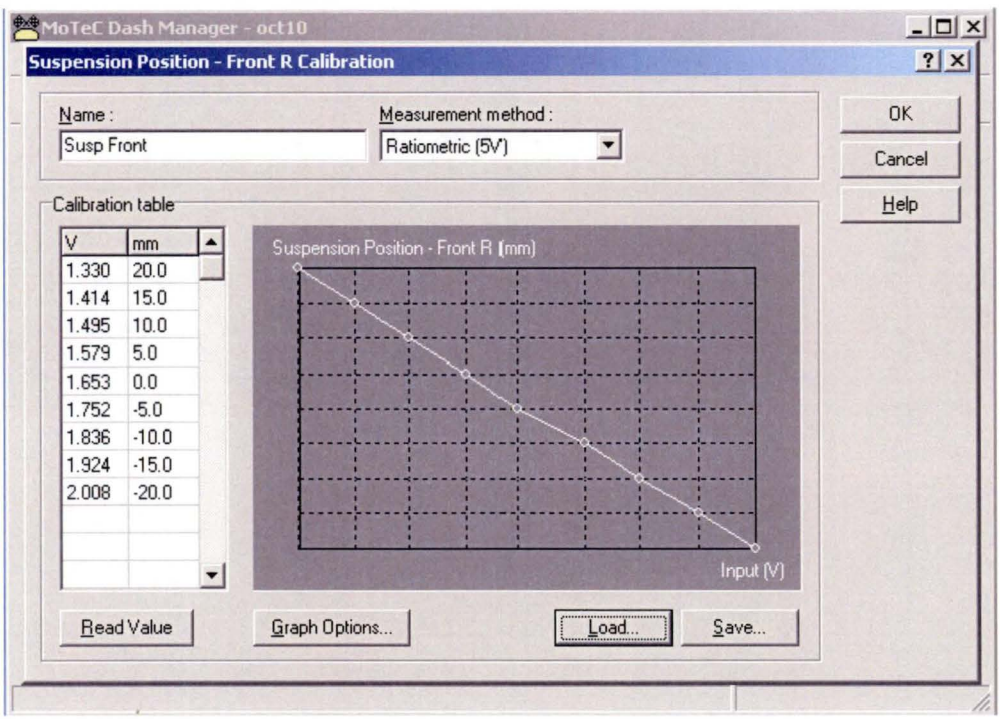

Figure 4-21 calibration curve for front right linear potentiometer.

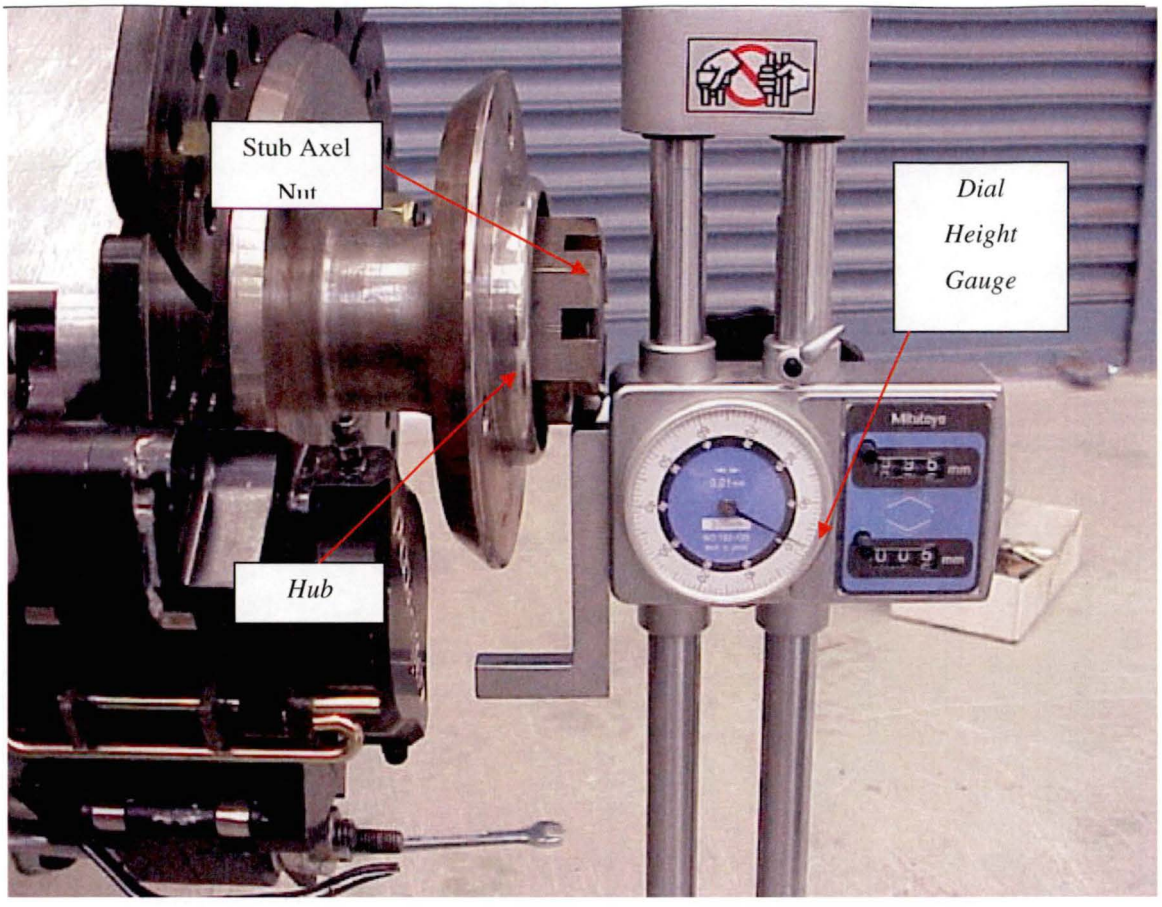

Figure 4-22 The dial height gauge placed underneath the stub axel nut.

4.1.5 Steering Angle: MoTeC 10 Turn, Gear Driven Rotary Potentiometer

The MoTeC steering angle sensor is composed of a Specrol 3 Watt, 10 Turn – 534 Series rotary potentiometer, and two different size gears. The smaller of the two gears is mounted on the rotating shaft of the potentiometer while the larger of the two gears is attached to the steering shaft of the automobile. A gear belt connects the gear located on the steering angle sensor to the gear attached to the steering shaft. As the steering shaft turns due to rotation of the steering wheel, the shaft on the sensor rotates and this is detected as a change in steering wheel angle by the synchronised gear movement arrangement. The steering angle sensor with the two gears is shown in [Figure 4-23] and [Figure 4-24].

Figure 4-23 Steering Angle Sensor.

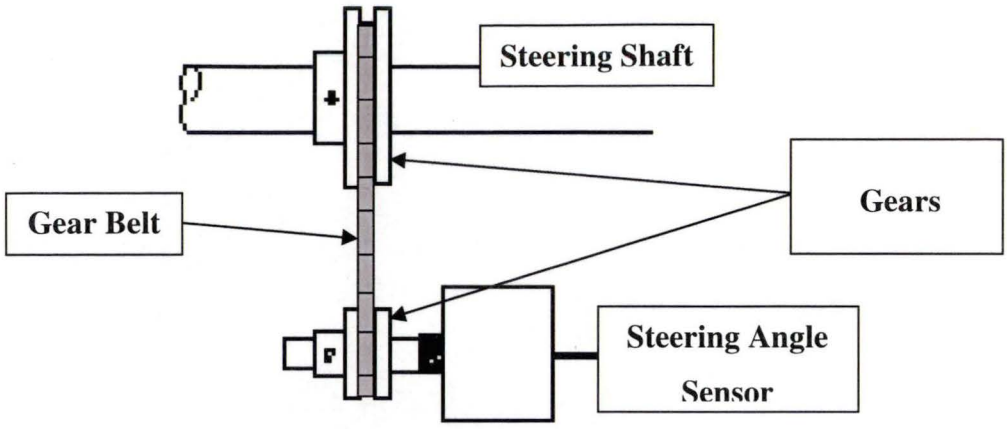

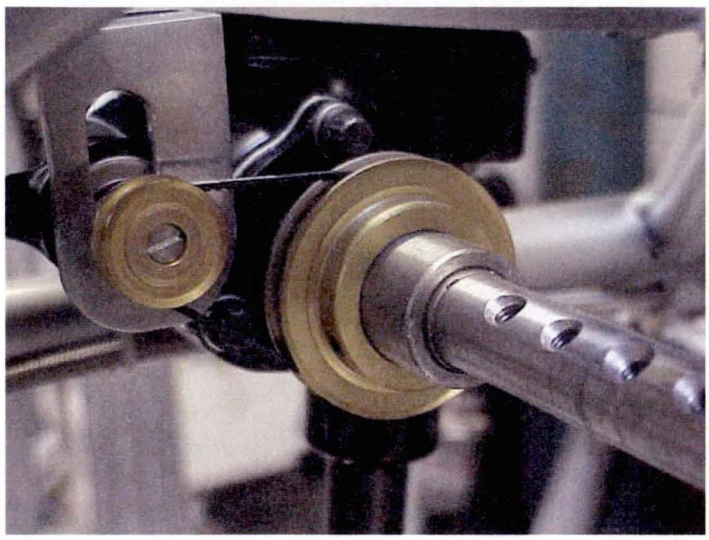

Figure 4-24 Steering Angle Sensor installed on the test rig.

This sensor uses the same operational principals as those described previously for the linear potentiometer. The major difference in operation is that a rotary motion causes the movement of the resistor contact component instead of linear motion. The resistor element in a rotary potentiometer is coiled in a circular formation around the inside case of the sensor. Inside the housing of the sensor there is a slip ring resistor contact slider that is attached to the shaft of the sensor. As the shaft rotates due to rotation of the steering column the slip ring slider rotates making contact to the resisting element and thus changing the voltage output of the sensor. The voltage output is proportion to the rotation angle of the steering wheel.

The Spectrol 3 Watt, 10 Turn – 534 Series Potentiometer technical specification brochure and the MoTeC Steering Angle Sensor CAD drawing are both provided in "Appendix H". This sensor has a linearity error of ±0.25%.

The steering wheel sensor was calibrated to measure the actual change in the steering wheel angle. This was achieved by turning the wheel through a known angle of rotation and then reading the voltage output from the sensor to develop a calibration curve, by using the calibration function in the Dash manager software.

The calibration process consisted of mounting a protractor to the test rig's steering wheel by three clamps. The centre of the steering wheel was found by positioning the wheel into the rotating spindle on a lathe. The lathe was then turned on and a dead centre was used to mark the centre of the steering wheel. The protractor was then mounted to the wheel by ensuring the protractor's origin aligned with the mark at the centre of the wheel. The zero position of the wheel was then established for when there was no steering wheel rotation present i.e. the wheels of the Racecar were directed in a straight line ahead. A clamp attached the reference pointer to the frame of the Racecar to display the change in angle of the steering wheel, as it was rotated. The reference pointer was adjusted until it displayed a reading of zero degrees on the protractor, when the wheel was at its zero position. [Figure 4-25] shows different shots of the apparatus used in the calibration of the steering wheel angle.

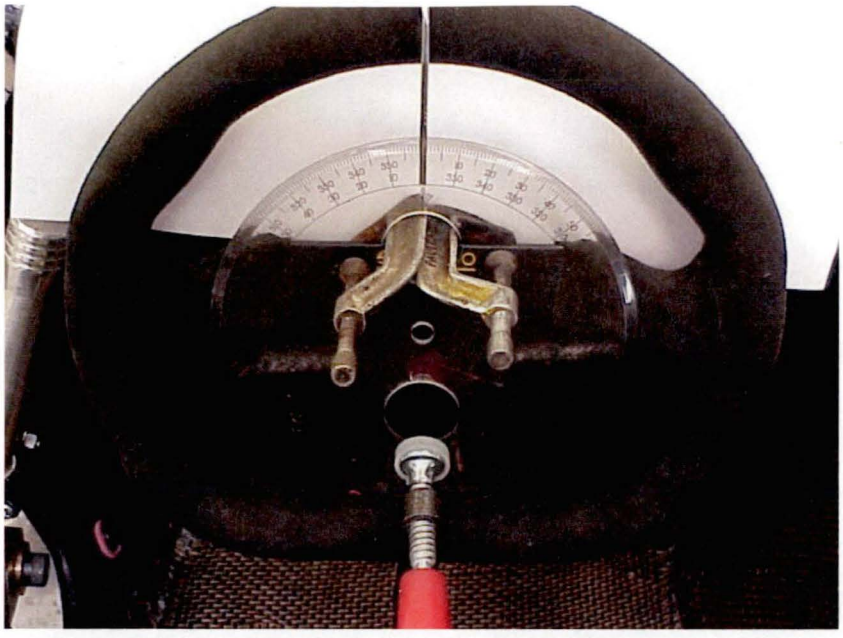

a

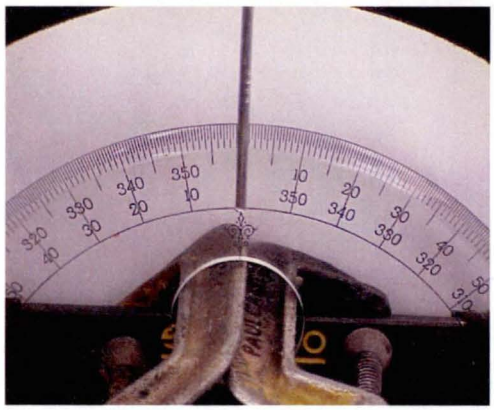

b

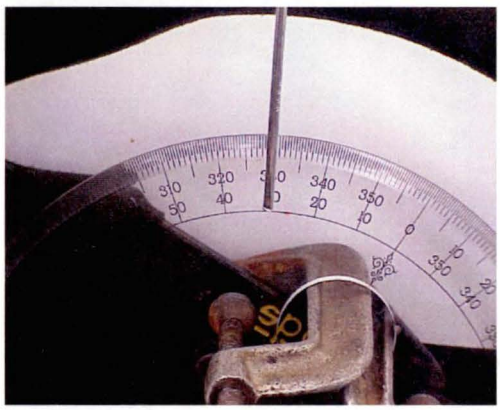

c

Figure 4-25 a) The protractor clamped to the steering wheel at its zero position, b) the reference pointer at zero degrees and, c) thirty degrees clockwise.

The steering wheel connection to the steering shaft was found to have some movement and it was determined, from the calibration apparatus configuration, that the steering wheel had one degree of play. The steering wheel was then turned through increments of thirty degrees up to one hundred and fifty degrees, in both a clockwise and anti clockwise direction. Using the calibration function in Dash Manager software the sensor voltage output was read at each thirty-degree increment rotation of the wheel. The corresponding actual steering angle position, determined from the pointer position

with respect to the protractor, was assigned to the sensor voltage signal for the development of a calibration curve. [Figure 4-26] below shows the calibration curve for the steering angle sensor developed in the calibration function in the Dash Manager software of the ADL.

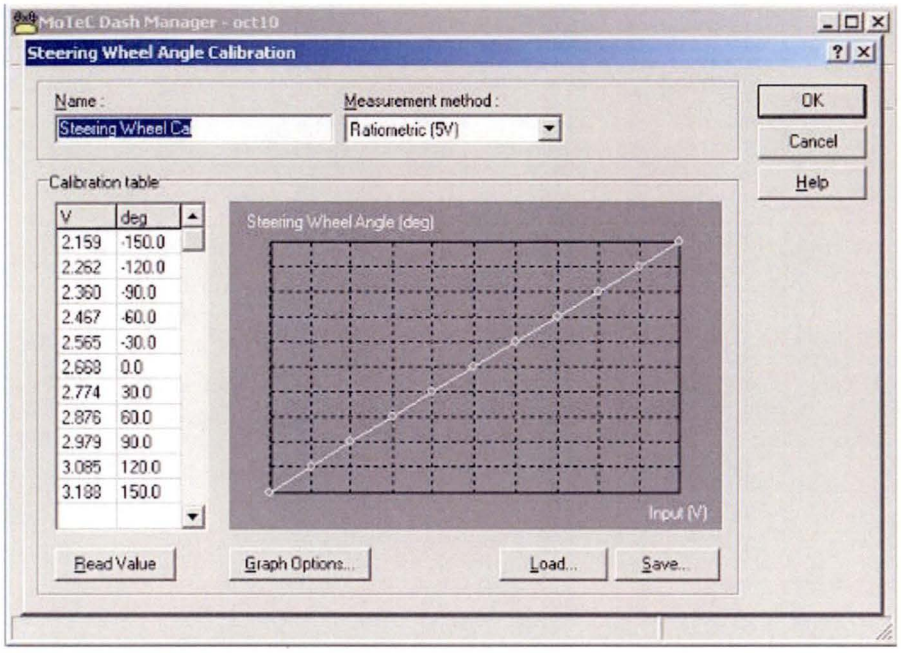

Figure 4-26 The calibration curve for the steering angle sensor.

4.1.6 Brake Force: Honeywell Eclipse Hydraulic Pressure Sensor – 2000psi

An analog 2000 psi Eclipse OEM pressure transducer was selected to measure the pressure in both the front and back brake lines of the test rig. The pressure transducer screws into the brake lines of the automobile and measures the dynamic pressure fluctuations of the brake fluid pressure when brake pressure is applied. The pressure transducer can be seen in [Figure 4-27].

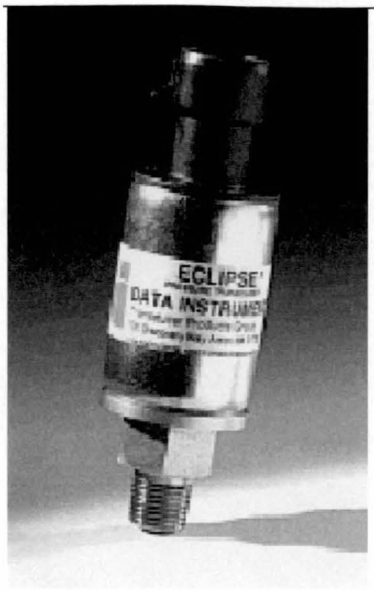

Figure 4-27 The Eclipse Pressure Transducer.

The pressure transducer measures dynamic pressure by using the piezoelectric[12] effect. The piezoelectric effect occurs when a crystalline substance, such as quartz or a salt group is strained by an external force and deforms resulting in a charge accumulation on the surface of the crystal. When the crystal is compressed, the individual ions that compose the structure are displaced, causing a small electric polarisation. Because of the large quantity of ions present in even a small crystal, the small charge accumulates and throughout the structure, causing a measurable electric potential difference across of the crystal. The piezoelectric effect is also reversible in that if a charge is applied to the material it will mechanically deform in response. The electric voltage that develops across the crystal due to mechanical displacement is proportional to the input pressure that causes the deformation of the crystal.

Quartz crystals are used in most pressure traducers as they provide stable, repeatable operation. The quartz crystals are usually preloaded in the sensor configuration to ensure good linearity. [Figure 4-28] illustrates the cross-section of a typical quartz pressure sensor similar to the one that is being used in the measuring system. When the crystal is stressed a high impedance output voltage is detected. This voltage signal

[12] "Piezo" is a Greek term which means "to squeeze."

undergoes signal conditioning and amplifying. The primary function of the amplifier is to convert the high-impedance output to a useable low-impedance voltage signal for recording purposes.

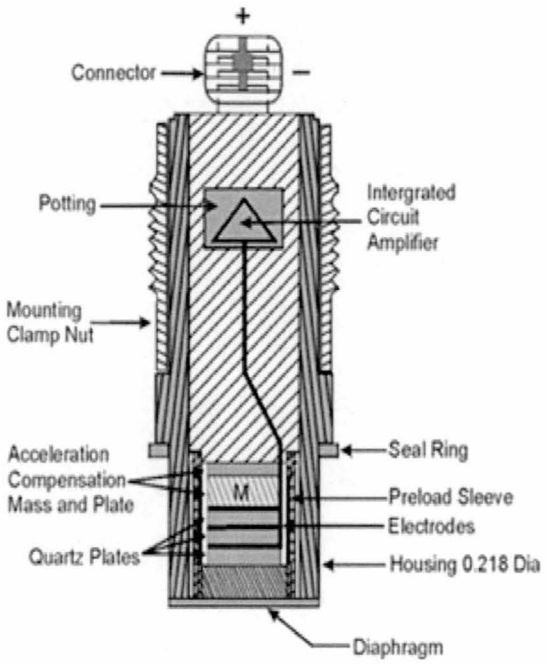

Figure 4-28 Cross-section of a typical quartz pressure sensor.

The sensor can measure a range of pressure up to 2000 psi or 13790 KPa. The pressure transducer has a total error of ±4% of the full scale reading, including the combined effects of zero output error, temperature, calibration, repeatability, hysteresis and nonlinearity errors. This corresponds to maximum uncertainty in the sensor reading of ±80 psi at full scale. The Honeywell Eclipse Pressure Transducer technical specification brochure and the MoTeC Pressure Transducer CAD drawing are both provided in "Appendix H". The technical specification brochure provides the dimensions of the sensor.

The calibration curve for the pressure transducers did not have to be manually entered into the Dash Manager software in a similar fashion to that used in the calibration of the linear potentiometers. Calibration involved selecting the Honeywell Eclipse 2000 psi calibration table file from a index of existing calibration files for different types of

pressure sensors listed in the Dash Manager software. This calibration file was loaded and saved into both pressure transducer channel inputs of the ADL, resulting in both pressure transducers being calibrated. [Figure 4-29] depicts the calibration curve for the Honeywell Eclipse 2000 psi pressure transducer.

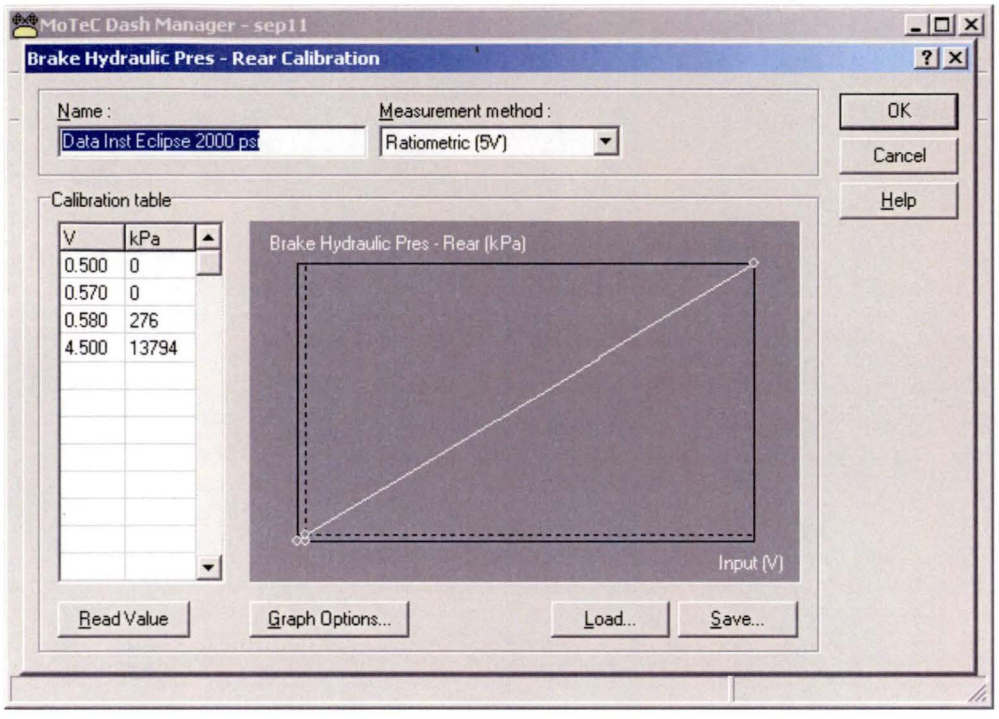

Figure 4-29 The calibration curve loaded from the existing index available in the Dash Manager software.

4.2 DATA ACQUISITION TYPE INSTRUMENTATION

In this section the various components of the ADL and other items needed for successful acquisition of all the required data is outlined. Data acquisition type Instrumentation refers to the actual selected Data Acquisition System and all associated auxiliary items necessary to connect the automobile sensors and other electrical devices to the DAS for logging purposes. This instrumentation also facilitates the telemetry requirement of the measuring system discussed in the next section.

MoTeC was identified as the company that could provide the most suitable data acquisition instrumentation for automobile testing. The following data acquisition instrumentation was obtained from MoTeC:

- An Advance Dash Logger
- A basic wiring loom
- A CAN communications cable and telemetry support with remote logging capabilities.

The components that constitute the data acquisition system will be briefly described in the following.

4.2.1 MoTeC Advance Dash Logger (ADL-4)

The MoTeC Advanced Dash Logger (ADL-4) is a compact complete data acquisition system suitable to control the on-board acquisition of data from the automobile sensors and the Engine Control Unit (ECU) in the Intelligent Car Project. A picture of the ADL-4 is provided in [Figure 4-30].

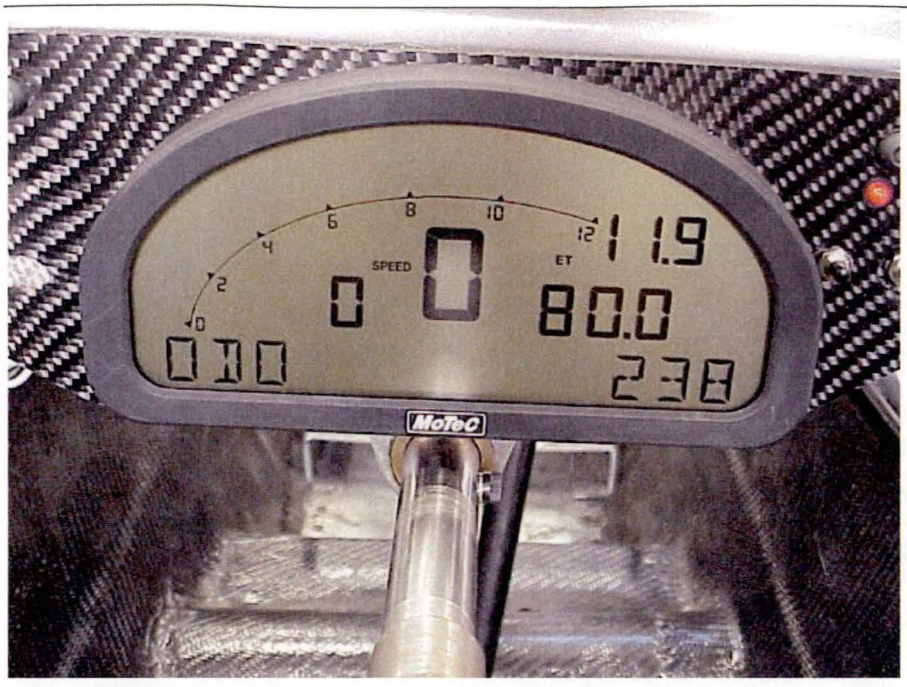

Figure 4-30 The MoTeC Advance Dash Logger.

The ADL also serves as the dash display unit for the test rig and has the potential to be upgraded to 4 Mb of data storage memory capacity. The ADL used in this measuring system is the basic input output model supporting 10 analog inputs, 8 digital inputs, one RS232 serial input and 4 auxiliary outputs. The ADL has 1 Mb of memory, which enables 16 minutes of automobile testing before the ADL data memory bank becomes full. The advantages of the ADL, compared to other investigated DAS is that it is a purpose designed automobile testing DAS, with a proven record of operating in similar automobile dynamic testing conditions[13]. The ADL uses a high speed 32 bit microprocessor to process information.

The ADL consists of two main components. The actual DAS in the form of the dash display unit and a removable wiring loom that enables data input and output to and from the ADL. The wiring loom allows sensors and other electrical devices to be connected to the ADL and also allows for data output from the ADL.

---

[13] The MoTeC ADL is used by a number of Australian V8 Touring Car Teams and many Rally Car Teams around the globe as a DAS in automobile testing.

The ADL display as shown in [Figure 4-30] uses high contrast LCD technology to show information to the driver of the automobile. The actual display is composed of a 70 segment bar graph, three numeric displays, a centre numeric display and a bottom alpha/numeric display. The display positions on the ADL face can be set up to show any information that is sent to the ADL. This includes rpm, gear, engine temperature, battery voltage etc. The numerical displays all have a different number of display digits therefore are suited to display different automobile parameters. The configuration of the display will be discussed in detail in Chapter 6.

4.2.2 Wiring Loom

The ADL uses a 79 pin Auto Sport connector as the wiring loom adaptor. The adaptor can be twisted to remove it from the back of the ADL, providing easy access to the wires of the wiring loom. A basic vehicle style-wiring loom was purchased from MoTeC. The basic wiring loom serves as the interface between the ADL and all sensors and associated equipment such as the ECU. The sensors purchased from MoTeC are fully adaptable with this wiring loom.

The ADL comes with Microsoft Windows based software called Dash Manager and Interpreter. The Dash Manager program is used in the configuration of the sensor and other instrumentation with the ADL. It is also the means by which logged automobile data is downloaded from Racecar during testing. The Interpreter software is used to analyse the logged data from the Racecar. The ADL can collate data on over 200 channels composed of both measured data, in the form of sensor input data to the ADL and calculated information. The calculated information refers to indirect measurement of variables that can be quantified mathematically from the direct measurement of other parameters. This function is being used to calculate the ground speed velocity of the vehicle and the distance travelled.

There is an inbuilt function in the Dash Manager software that incorporates the use of two wheel speed sensors in the calculation of ground speed velocity of the Racecar. In

a similar way the software is able to calculate the distance travelled using the ground speed velocity of the test vehicle.

The sampling rate of the sensor channels can be individually set up to a maximum sampling rate of 1000 times per second. The display has the ability to be set up in three different and independent modes, which can be cycled through with the push of a button.

4.2.2.1 Real-time Clock

A Real-time clock is included in the wiring harness and provides time and date channels to the ADL, facilitating time and date stamped logging of measured data. This unit also provides an additional RS232 communications port. A picture of the real time clock is provided below in [Figure 4-31]

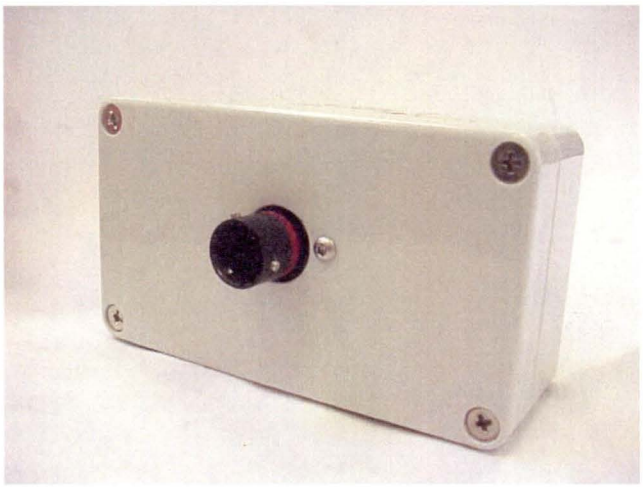

Figure 4-31 Real Time Clock

4.2.2.2 Telemetry Upgrade

The telemetry upgrade enables remote real time access to the data collected by the ADL via a telemetry link. The telemetry link is achieved via a radio modem, and transfers measured data to a computer. Logged data fluctuations can be viewed in real time through the Interpreter software.

4.2.2.3 Remote Logging

Remote logging software is needed as this allows the data received via telemetry to be stored on the PC for later analysis. The data that is logged by the telemetry equipment can be independent to the data that is being logged to the ADL. This allows different parameters to be logged by the ADL and telemetry data storage processes.

ADL Input & Output Requirements and Wiring Diagram

The input output requirements of the ADL unit, the sampling rate of the parameters and other associated ADL configuration information is provided in "Appendix H". The wiring diagram of the ADL depicting which sensors are connected to which ADL inputs and the MoTeC ADL specification brochure are also provided in "Appendix H".

4.2.3 CAN Communication Cable

The CAN communication cable is a high-speed communication cable that enables the ADL to be connected to the parallel port of a PC. This cable allows the transfer of the logged data from the ADL to a computer for processing and analysis. The download speed of logged data from the ADL, using this cable can reach a maximum transfer rate of 19 seconds per megabyte of data transferred. This cable is addition option to the basic wiring loom.

4.3 OUTPUT TYPE INSTRUMENTATION

This section will briefly discuss the telemetry equipment required for the real time transmission of logged data from the DAS to a remote computer located trackside. The output instrumentation is primarily composed of the research computer to which ADL logged data is transmitted, stored and displayed in real time, the radio modem system that facilitates the transmission of data and auxiliary related telemetry equipment.

4.3.1 Research Computer

A research computer, located track-side is used to store and display the modem transmitted logged ADL data in real time during testing. The computer is a PC mini tower, powered by twin 1000 MHz Pentium III Processors with 524 megabytes of RAM and an internal 20-Gigabyte hard drive operating Microsoft Windows 2000. The computer displays transmitted data to observers on a 17" monitor. The computer is shown in [Figure 4-32].

Figure 4-32 Research Computer

4.3.2 Radio Modems: RFI-9256 Data Strike Series 3 Spread Spectrum Radio Modem and Auxiliary Equipment

The RFI-9256 Data Strike Series 3 Spread Spectrum Radio Modem is shown in [Figure 4-33]

Figure 4-33 RFI-9256 Data Strike Series 3 Spread Spectrum Radio Modem

The radio modem system consists of two modems, a transceiver modem and a receiver modem. The transceiver modem is the modem located on the test vehicle that transmits the ADL logged data. This data is then received by the receiver modem that is connected to the data storage and display on the track-side research computer [Figure 4-28]. Both modems operate in the 900 MHz frequency band and transmit data in a psudo-random code. The pseudo-random code enables the transceiver modem to hop throughout this frequency band sending information at different frequencies to the receiver modem. The receiver modem uses the same hopping code to receive the data. The pseudo-random code minimises interference from other radios and associated radio waves.

The receiver modem also known as the local modem has been setup as the Master modem and the transceiver or the remote/distant modem has been set up as the Slave

modem. The Master modem is used to synchronise communication, however either modem and can initiate communication.

The telemetry modems have been linked together in a point to point or direct connection format. Point-to-point communication is similar to a wire that directly connects the modem devices together for data transfer. Currently data is transferred in one direction only, from the Racecar to the remote computer. Such data transferral is known as Simplex communication.

In operation the master modem is connected to the remote computer via Comm Port 2 and also requires an external power supply. The transceiver modem is connected to the ADL using switch input 4 and an additional Telemetry RS232 output wire that was acquired through the Telemetry Upgrade from MoTeC. Antennas are connected to both modems to facilitate data transfer.

4.4 THE DEVELOPED MEASURING SYSTEM

The integration of the three different types of instrumentation as described allows for the development of the test rig's dynamic measurement system. The integration of the equipment involves the fusing together of the individual components forming an instrumentation cluster that allows electrical interaction and communication between the different components for the successful transmission of measured data to a remote computer. Combining the instrumentation in order to obtain a reliable measurement interface involves the physical installation and connection of the components.

The dynamic measurement system can be defined using a block diagram that describes the function of components in the measuring system. [Figure 4-34] depicts the measuring system showing the measurand inputs to the DAS and the different forms of data presentation in block diagram form. [Figure 4-35] shows the measuring system in a pictorial form, clearly identifying the inputs and outputs of the measuring system.

This chapter has provided a brief description of the operational principals of the instrumentation that constitutes the measuring system. The next chapter deals with the results form the physical testing of the vehicle and the use of neural networks as a tool for predicting dynamic braking pressures in a real world environment.

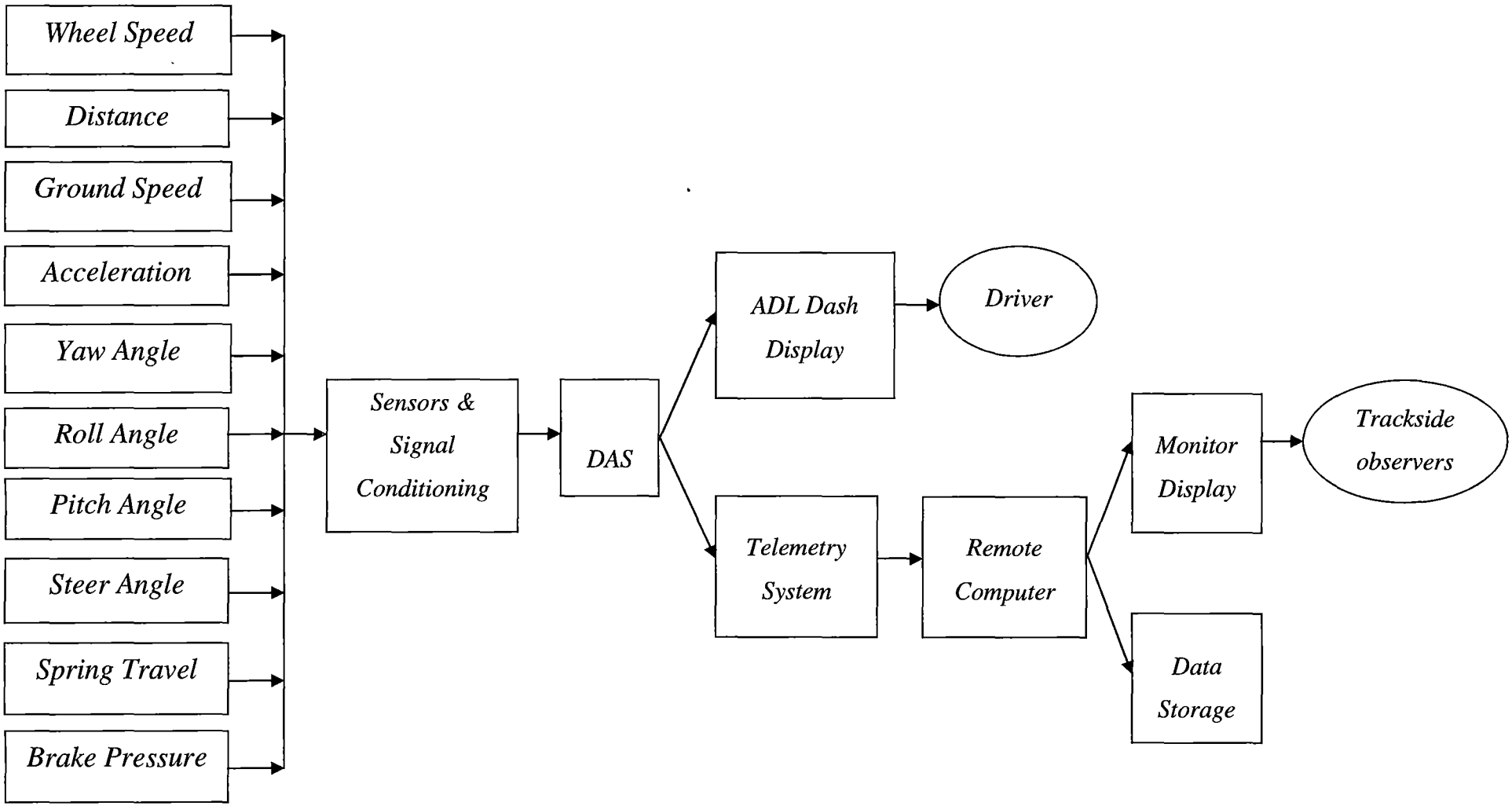

Figure 4-34 Block diagram of the complete measuring system

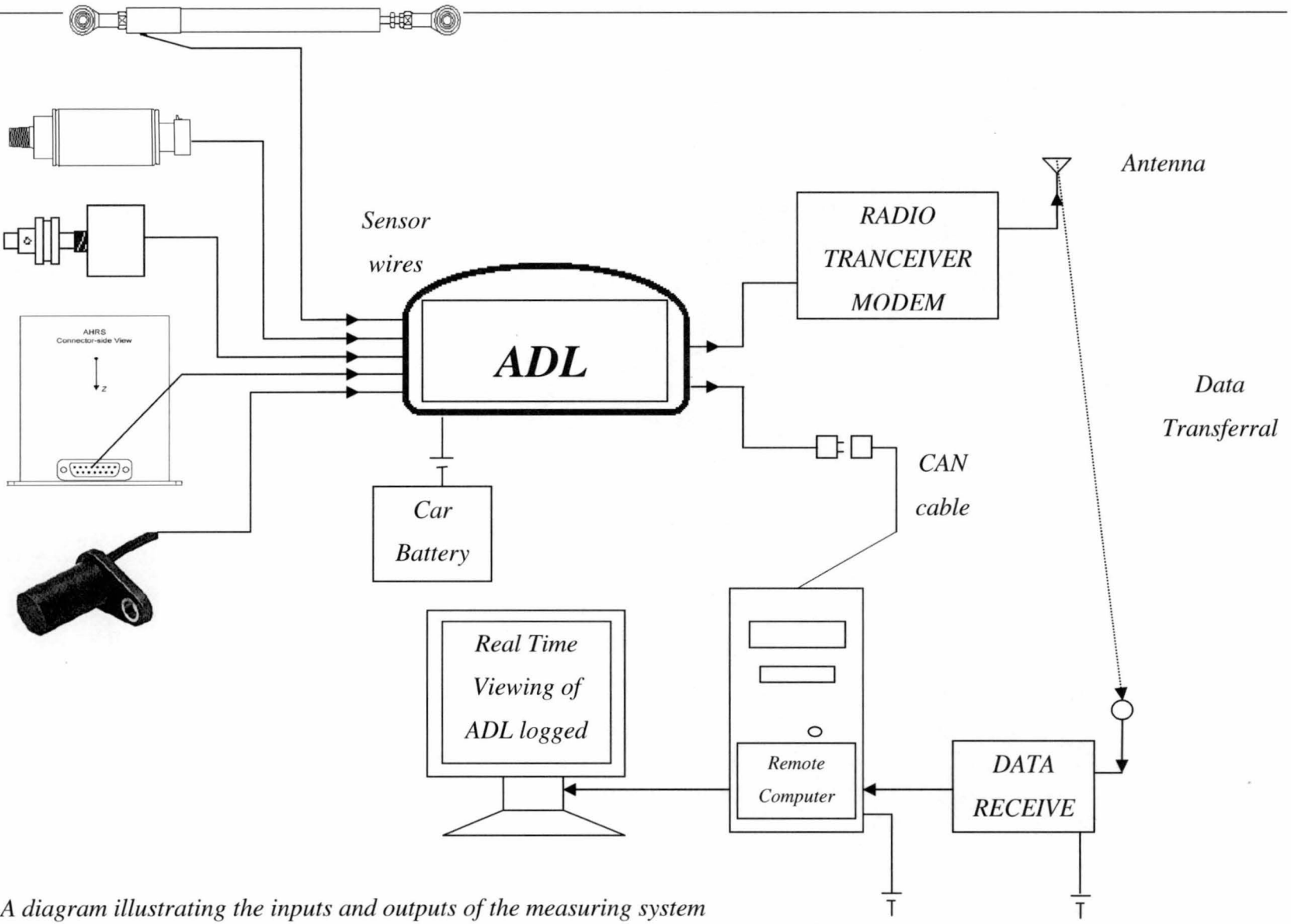

Figure 4-35 A diagram illustrating the inputs and outputs of the measuring system

Chapter Five

TRAINING AND TESTING OFF-LINE NEURAL NETWORK MODELS

The development of the training set for any neural network will dictate its performance. The size of the training set required to provide the network with adequate training is one of the most important considerations of neural network training. Limiting the size of the training set in this case are the constraints of computing power and processing time. More training sets can be used at the expense of computing time. In the interests of keeping training to manageable levels and time scales, training sets of up to 18000 input vectors have been used.

Figure 5-1 Test Vehicle gathering data during dynamic vehicle trials

Data measured during dynamic vehicle trials [Figure 5-1] requires sorting into specific manoeuvres and assembled into training sets capable of providing adequate representation of all manoeuvre sub groups where there exists a tendency toward particular trends and patterns. For example, it was found that the brake force pattern that existed for braking into a tight radius turn was different from braking into a sweeping corner. In the development of a useful training set it is of great importance to achieve sufficient representation of all variables in **all** manoeuvre subgroups.

To accurately estimate and predict the brake forces for a comprehensive range of braking manoeuvres, the neural network itself must be trained using a statistically balanced set of input vectors which represent the extent of the predictive capacity required.

Early testing and recording of data revealed that this statistical variation, especially in the acceleration data from the test vehicle, is predominantly caused by vibration (mechanical noise) from the motorcycle power plant. This noise was very prominent in the data since, as outlined in chapter 3, the motorcycle engine is rigidly connected to the vehicle frame.

In an attempt to gather data sets with balanced statistical variation and accurate readings a sampling rate was chosen at 100 Hz for the sensors on the test vehicle. Careful attention was taken while deciding this rate to avoid resonant and common frequencies set up in the frame. With several different sampling rates, tests were conducted throughout the rev range of the motorcycle power plant to locate unacceptable resonances.

Early tests found that sampling rates significantly higher than the selected 100Hz results in data sets that are either too large in terms of computational time or too small in terms of the number of incorporated manoeuvres when used as training inputs to the proposed neural network models.

Sampling rates significantly lower than 100 Hz on the other hand, were found to be too low to accurately follow and represent some of the more rapidly changing parameters such as the suspension movement.

5.1 STRATEGY FOR PREDICTION

This study is focused around understanding the degree of influence of various process parameters on predicting brake force and eliminating those that are non-contributing to develop a reliable neural network based brake force prediction model. The goal of this study is to have a workable neural network capable of predicting brake force values for use in the intervention decision making process of driving assistance systems to be later developed on-line.

As discussed in chapter two, many neural network architecture models are available for predictive purposes. Out of these, two models were selected for predicting brake forces. These two models were chosen as the most successful after initial trials with many different models.

1. Back propagation Neural Network (BP)
2. General Regression Neural Network (GRNN)

Before these networks can be applied, clearly defined training courses must be identified for generating good training and testing sets. For the purposes of this research, training sets must be developed that contain sufficient examples of straight line braking and simultaneous braking and cornering. This lead to the development of two specific training courses as identified in the following section.

5.2 TYPES OF TRAINING COURSES

In an effort to achieve reasonable range of braking conditions the following test courses were laid out [Figure 5-2]:

a) Straight-line acceleration and braking [Figure 5-2, a)]

b) Figure eight with hairpin and sweeper [Figure 5-2, b)]

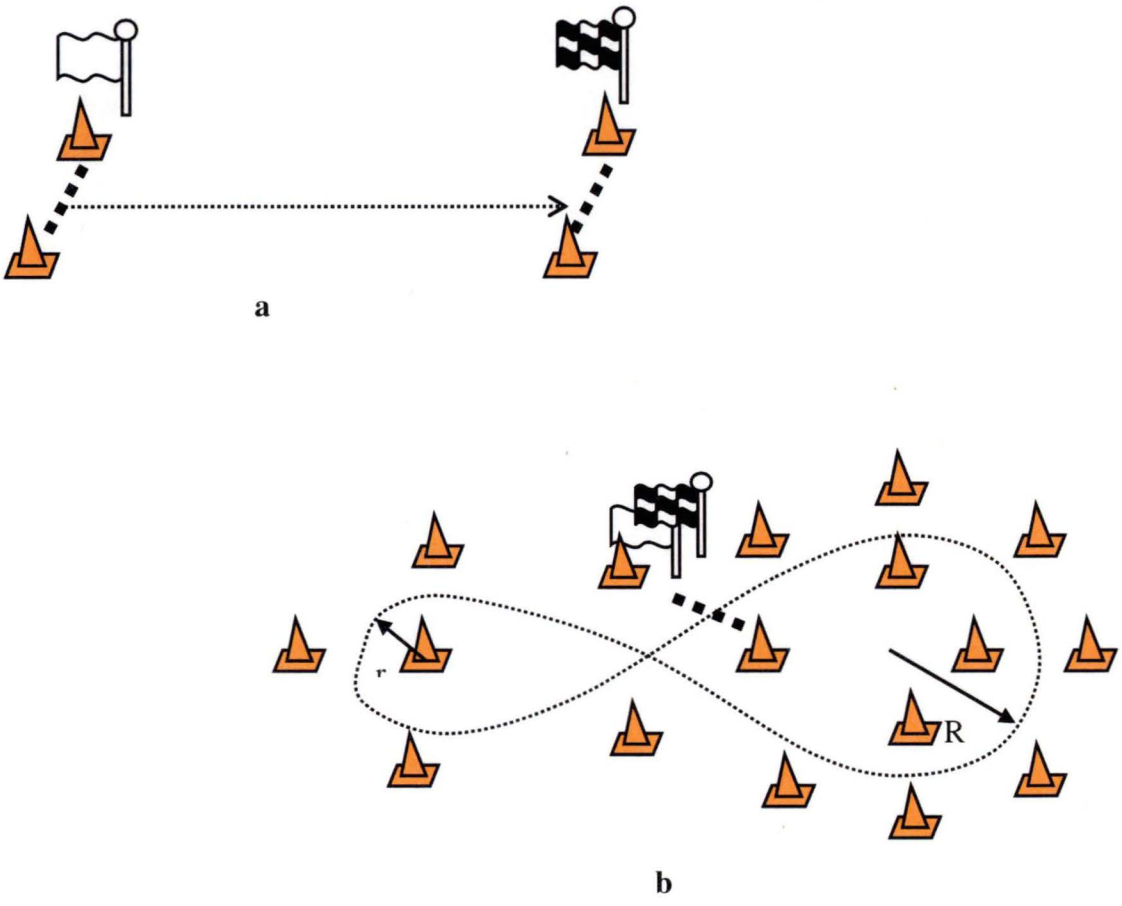

Figure 5-2 Test courses for neural network training: a) Straight-line acceleration and braking: course 1. b) Figure eight with hairpin and sweeper: course 2.

These two test courses [Figure 5-3] and [Figure 5-4] were driven at various speeds close to the limits of adhesion corresponding to different levels of slip during acceleration, braking and cornering. This was done in an attempt to gather data sets covering a reasonable range of tyre slip situations. Training sets were composed of a montage of these tyre slip levels to include as many varied examples as possible.

Figure 5-3 Course 1: Straight-line acceleration and braking test photographed during early stages of testing.

Note that the Figure eight [Figure5-2 (b)] and [Figure 5-4] as layed out has a large radius, R, corner (sweeper) and a tight radius, r, corner (hairpin). The driving approach and braking for these two types of corner are very different.

In some examples, on the approach to the hairpin, the driver tries to unsettle the test rig in order to improve turn in and flick the vehicle around the corner. This can be seen in the data set as a pre-corner steering input or turning of the steering wheel in the opposite direction to the corner before the corner. This *Scandinavian Flick* is a manoeuvre commonly used in racing. In complete contrast, on approach to the sweeper the driver is smoothly on and off the brakes to avoid upsetting the vehicle's balance.

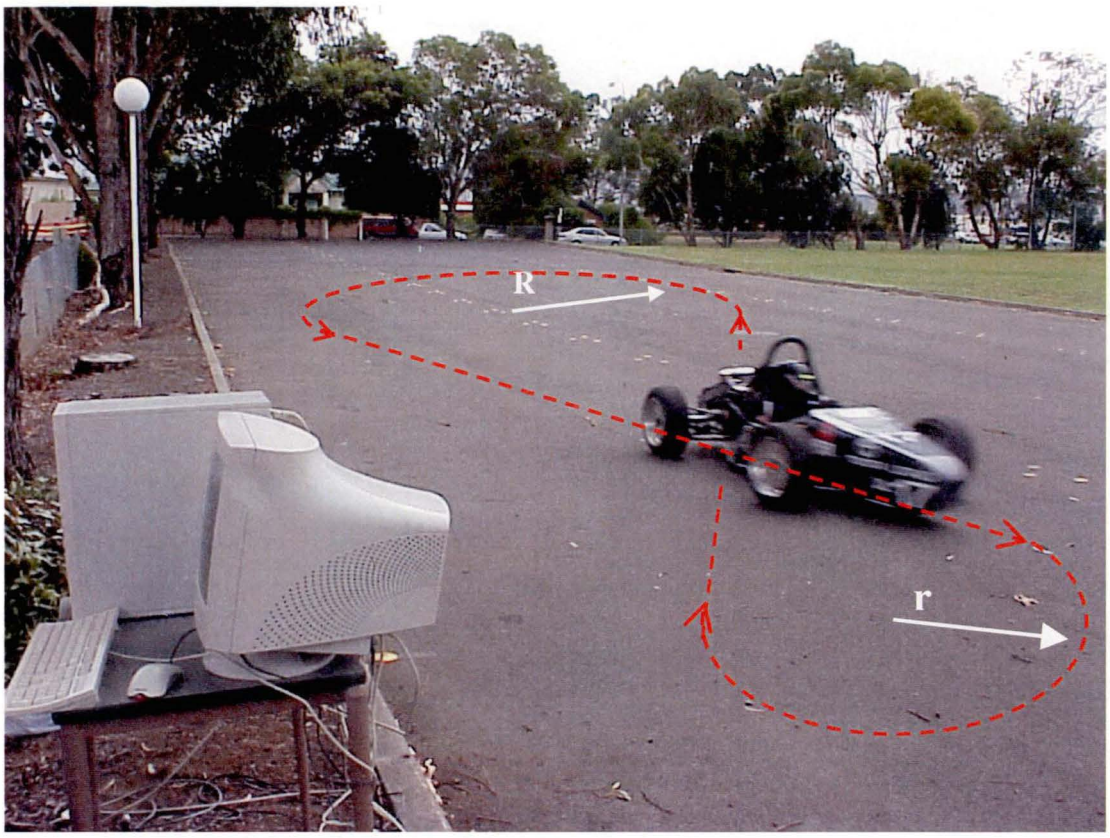

Figure 5-4 Course 2: Figure eight test course data generation.

These are two cornering extremes however, since the driver was varying their level of attack [Figure 5-5] on the test course. The resultant training sets were found to contain various braking and cornering examples covering the spectrum from below threshold to complete four wheel locking and sliding.

Figure 5-5 Braking and cornering at different levels of attack producing data sets at different levels of tyre slip.

5.3 BACK PROPAGATION NEURAL NETWORK RESULTS

Backpropagation networks are multi layered feed-forward neural networks that have been trained using an error backpropagation procedure. This is a supervised mode of learning where a systematic method is used to adjust the weighted connections within the network.

Various network architectures were trialed in an attempt to find a specific architecture which best predicted the brake force for the two test courses. To this end, brake pressures recorded for the Figure eight course (test course 2) data proved more difficult to predict than the brake pressures for straight line acceleration and braking (test course 1). Inputs to the neural network were chosen as:

1. Yaw Angle
2. Lateral Acceleration
3. Longitudinal Acceleration
4. Distance
5. Steering Wheel Angle
6. Throttle Position
7. Engine RPM
8. Suspension Position:
    - Front Left
    - Front Right
    - Rear Left
    - Rear Right
9. Wheel Speed:
    - Front Left
    - Front Right
    - Rear Left
    - Rear Right

Neural networks were then trained with outputs of front Brake Hydraulic Pressure (BHP F) and rear Brake Hydraulic Pressure (BHP R).

Combinations of single and double layer backpropagation networks were trialed for both courses. Many of the single layer backpropagation networks trialed were found to give good predictions for straight line braking, however the Figure eight test course

braking force was not predicted by any of the single layer networks trialed to any useful level of accuracy.

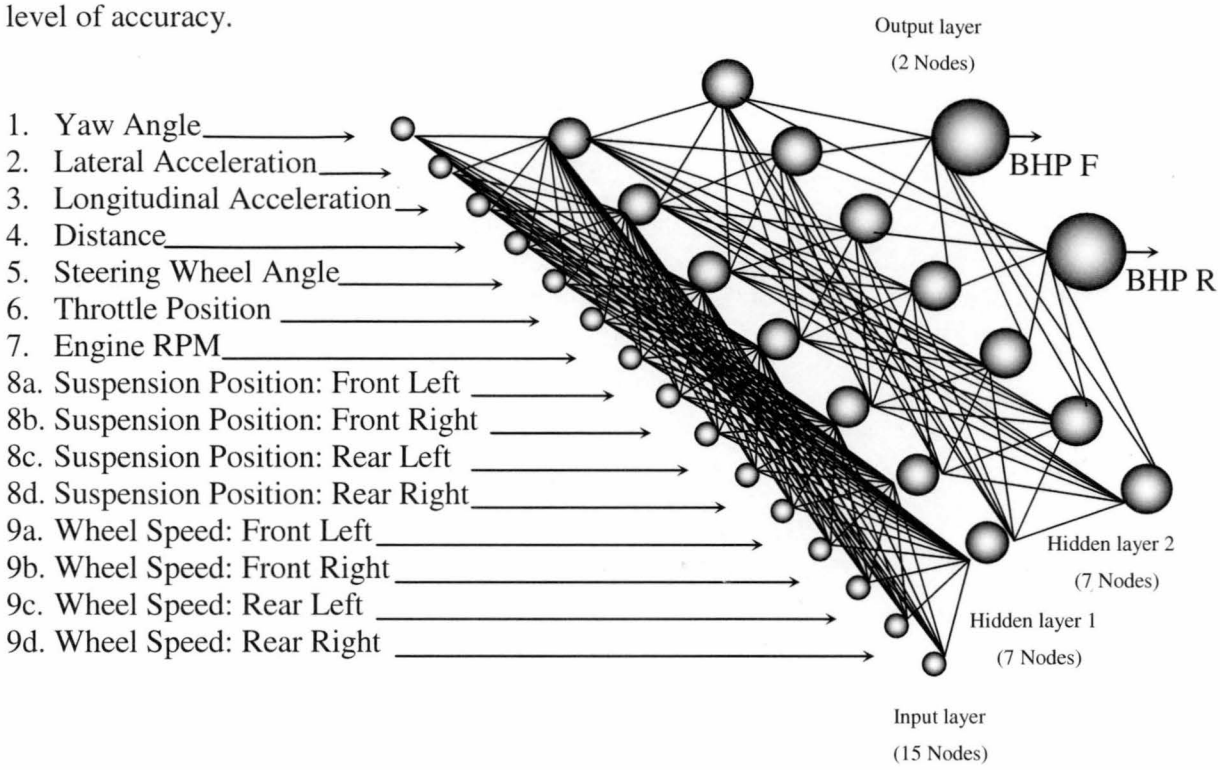

Figure 5-6 Selected backpropagation neural network featuring double layer architecture with seven hidden layer nodes in each.

The final chosen network architecture was a two-layer backpropagation with seven layer nodes in each layer. This network was found to corresponded to the lowest combined average absolute error for the two test courses.

The sigmoidal or logistic activation function was selected for the network and 100 iterations were performed in each case to achieve the following results.

For all neural network model testing results to follow, the absolute error between brake pressures, predicted and recorded, has been plotted. This error is calculated as the difference between the measured and the predicted brake hydraulic pressures (kPa) and is expressed as a percentage of full scale.

5.3.1 Course 1: Straight Line Acceleration and Braking – Front Brake Force Prediction

[Figure 5-7] shows the double layer backpropagation neural network prediction result from network testing. The network was found to consistently under predict brake line pressures once a discreet pressure value has been reached. This particular condition was found to correlate with vehicle dynamics where full wheel lock-up occurred. Full wheel lockups were found to correspond to peaks 1,2 and 4 of the estimation graph in [Figure 5-6]. This is not a problem with the neural network prediction but is purely related to the brake hydraulic pressure effect on vehicle dynamics.

Once full wheel lock has occurred the actual value of the hydraulic brake pressure is arbitrary since increases in brake pressure will not at all effect the vehicle's dynamics. When the wheels on the test vehicle wheels are fully locked, they have reached a state where further pressure increase in the brake lines has no effect. Thus the neural network sees no dynamic change in the behaviour of the vehicle and predicts the pressures at the constant value where full wheel lockup initially occurs. For this reason any brake hydraulic pressure information over this full lockup threshold is not useful in describing any part of the vehicle's dynamics and the neural network should not be scrutinised for the failure to predict these values.

Therefore, in [Figure 5-7] it is not surprising that the maxim predictive error occurs at the peak where the brake hydraulic pressure reaches the highest level over and above the level corresponding to wheel lockup (peak four of the test data). The peak errors must be ignored. Far more important features of the straight line prediction are how closely the neural network estimation follows the measured brake force pressure on the ramps up to the threshold lockup values and back down to zero pressure. The Absolute error graph clearly shows that these errors are typically (average) less than 2% and less than 10% (average) in regions where a typical rate of change of pressure is 4000 kPa/second.

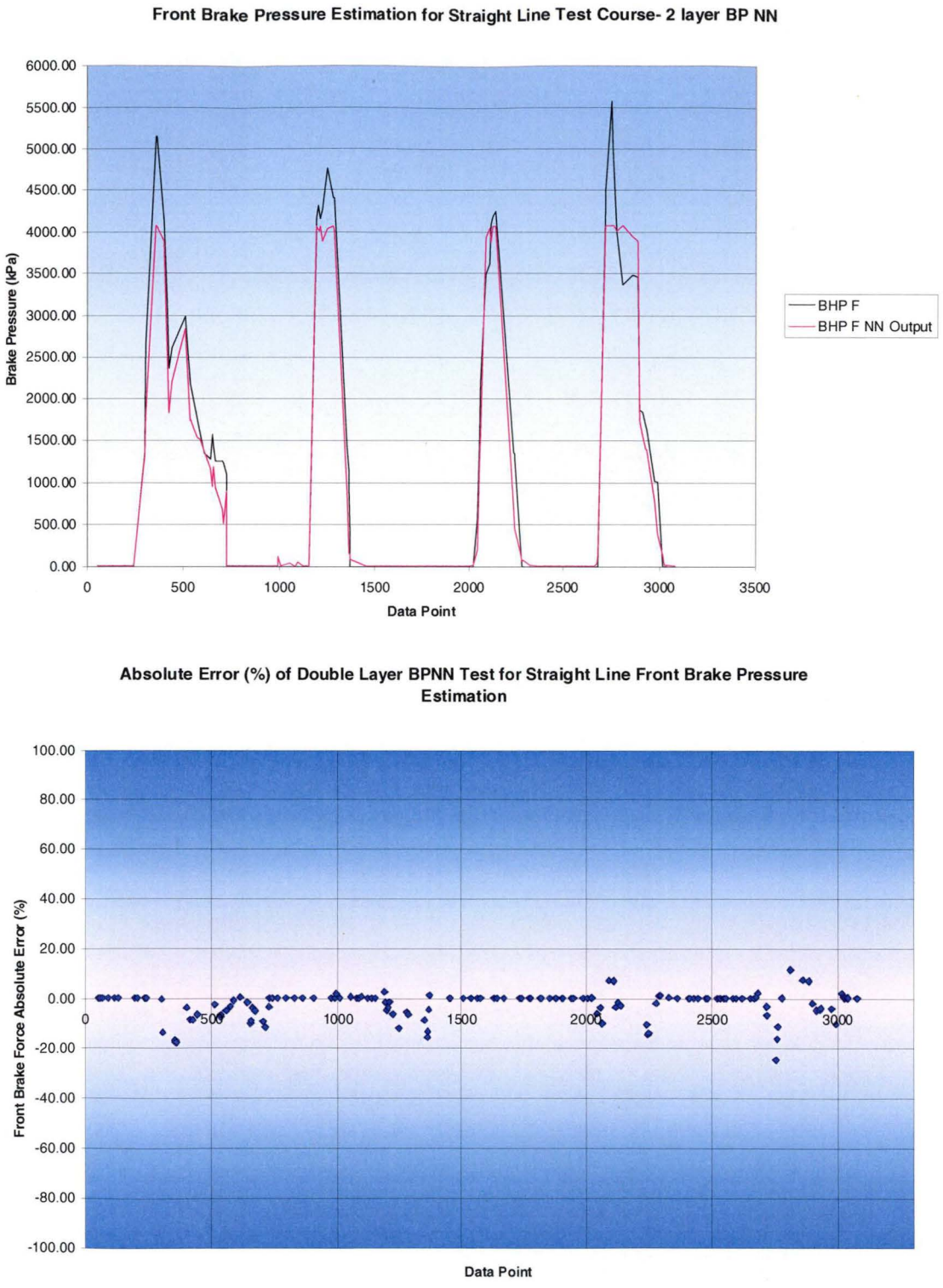

Figure 5-7 Front Brake Hydraulic Pressure estimation for test course 1 and calculated absolute error. Errors for peaks 1, 2 and 4 are not due to the neural network (see text for explanation).

The network here is seen to predict numerically zero brake pressure values to a highly consistent level and to a greater level of accuracy than the numerical values attained under braking. Note that the neural network is not directly given any information to show when the brakes are actually being applied. The network is only given data related to the dynamic movement of the test rig itself. In this manor the neural network is seen to be able to differentiate between engine braking, drag forces etc. and braking force applied through the pressure in the brake lines to an extremely high level of accuracy. In predicting numerically zero brake pressure values, the network usually has no (0%) error with only small errors of less than five percent found during transitions between zero pressure and application of the brake pedal. An example of these errors can be observed around data point 1000 in [Figure 5-7].

5.3.2 Course 1: Straight Line Acceleration and Braking – Rear Brake Force Prediction

[Figure 5-8] shows the double layer backpropagation neural network prediction result for the rear wheel braking under the same test. Similarly to the front brake result, the network was found to consistently under predict brake line pressures once the complete wheel lock up threshold was exceeded. However, the 100% lock up threshold is much more visually apparent in this result with the broader peaks clearly highlighting the threshold value determined by the neural network. As before, the predictions are a lot closer than the quantitative analysis would indicate since beyond 3250 kPa the brake hydraulic pressure is arbitrary

Again, numerically zero brake pressure information is predicted to a higher level of accuracy than brake pressures measured under application of the brake pedal. Errors related to zero pressure in this test are found to be more localised toward the base of each brake application.

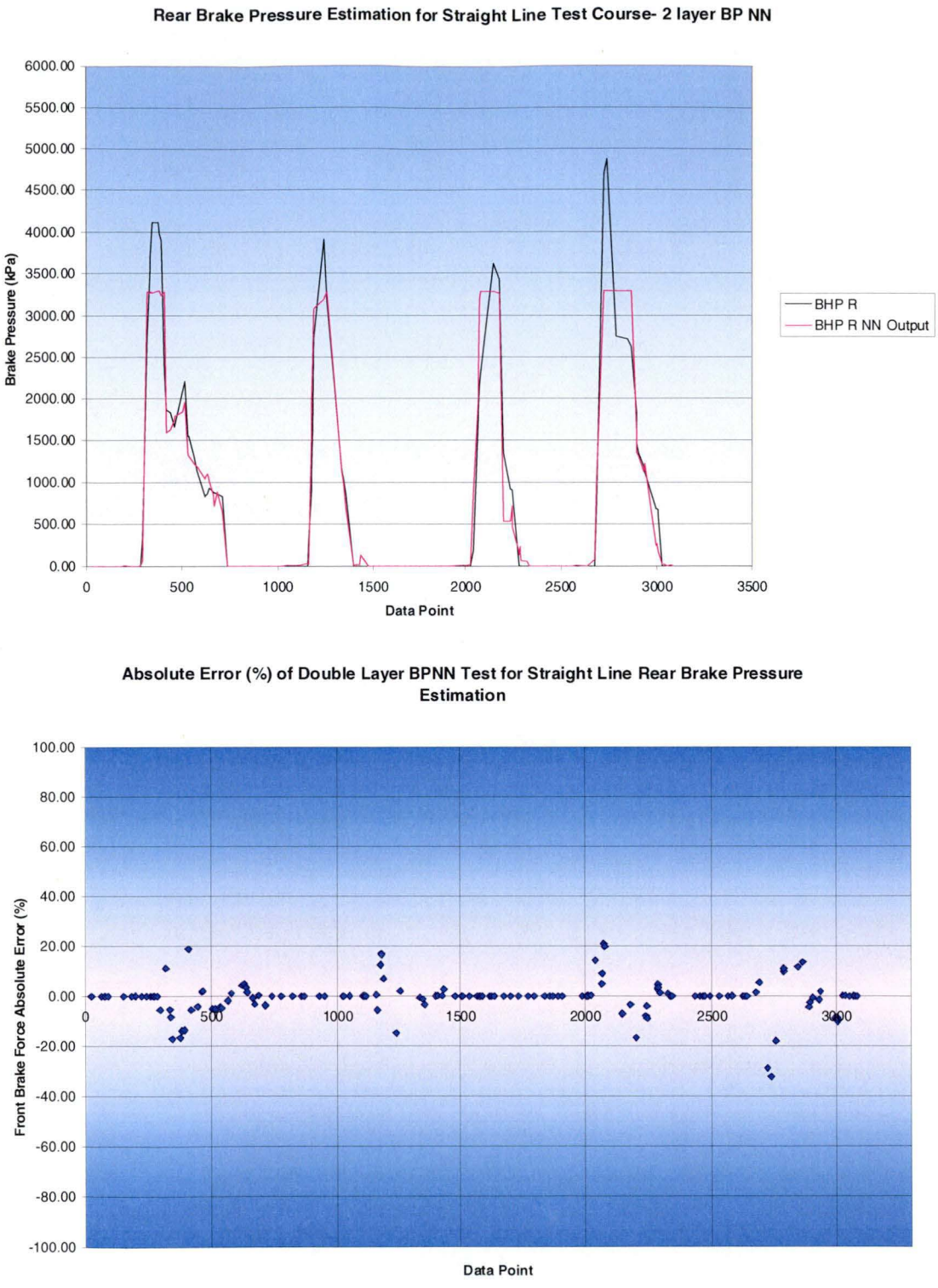

Figure 5-8 Rear Brake Hydraulic Pressure estimation for test course 1.

Similar to the front brake hydraulic pressure estimation, the rear brake hydraulic estimation [Figure 5-8] finds maximum predictive error occurs at the peak where the

rear brake hydraulic pressure is at the maximum level over this wheel lockup threshold. For reasons discussed, this type of error is to be ignored. The remainder of the absolute error is on average less than 4%.

The result from rear hydraulic brake pressure estimation is noted to be slightly less accurate than the front hydraulic brake pressure estimation. This was found consistently throughout the different courses and models with the rear brake pressure estimation typically giving higher errors than the corresponding front values.

One possible explanation for this is related to the level of loading of the rear wheels during braking manoeuvres. As the rear tyres are unloaded, the level of instability related to tyre flexing increases. Tyre flex rate is progressive with very little force required to initially cause distortion of the tyre and progressively more force required as the tyre is loaded. Thus a lightly loaded tyre will move around and change shape due to surface irregularities, driver inputs and other disruptive external variables more readily than a heavily loaded tyre. This effectively produces less consistent braking on the rear wheels of the test rig and is evident when comparing the front [Figure 5-7] and rear [Figure 5-8] measured brake hydraulic pressure plots.

5.3.3 Course 2: Figure Eight – Front Brake Force Prediction

Wheel locking is not as prevalent in the Figure eight data sets and predictions, [Figure 5-9] and [Figure 5-10]. This is due to the nature of the course, where excessive wheel locking would result in a lack of directional control and failure of the test rig to follow the course layout. This is reflected in the results from the neural network testing [Figure 5-9] where the 100% lock up threshold is only realised in the third peak of the Figure. At this peak the driver's level of attack is at its maximum and the brakes are held into the hairpin turn at peak values for the longest amount of time causing locking of the front wheels which can be seen clearly in [Figure 5-9].

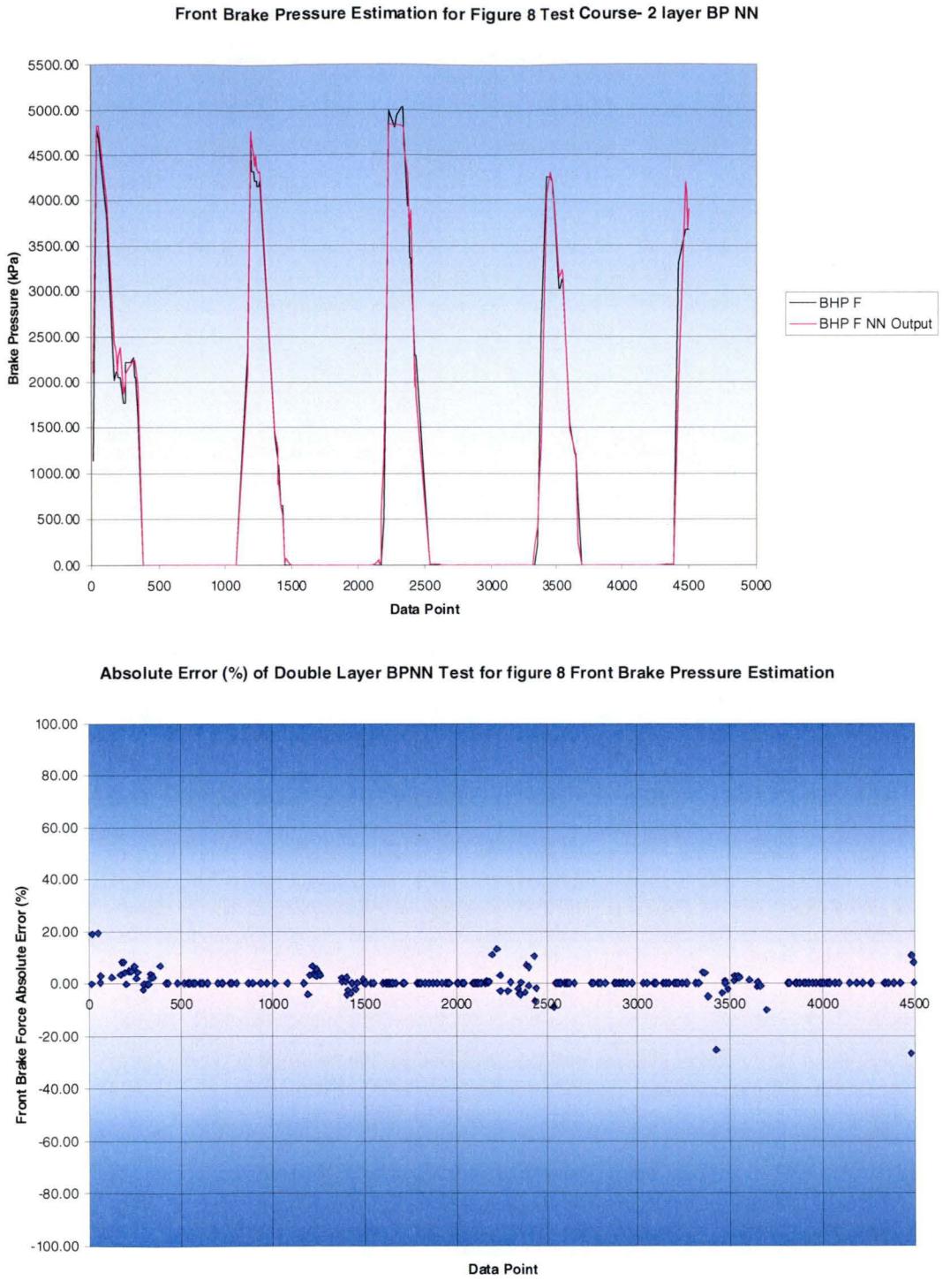

Figure 5-9 Figure eight front brake hydraulic pressure estimation by double layer backpropagation neural network.

Results from testing the front brake pressure prediction by the two layer BP NN model [Figure 5-9] show that from a purely predictive point of view these brake force predictions are the closest to the measured values of all models and test courses, with an average error of less than 2%. This prediction has the least absolute error for testing, which can be observed in the accompanying error plot.

The Figure eight test course (test course 2) brake hydraulic pressures are consistently more readily predicted since the information such as lateral acceleration and steering wheel angle are likely to have a greater influence on the brake pressure.

5.3.4 Course 2: Figure Eight – Rear Brake Force Prediction

[Figure 5-10] shows the double layer backpropagation neural network prediction result for the rear wheel braking under the same Figure eight test course. Here it can be seen that the result, rear hydraulic brake pressure estimation, for this test course is significantly less accurate than the front hydraulic brake pressure estimation [Figure 5-9].

Here the neural network is seen to slightly under-predict the brake pressure where the pressures are increasing on peaks 1 and 5, while over predicting brake pressure values on peaks 2, 3 and 4. However there is still very little bias on the prediction.

It is shown in [Figure 5-10] that predictions for rear brake pressure during cornering manoeuvres are the most challenging for the neural network, owing to the complex wheel weight transference and tyre distortion occurring during such a test. However the neural network is still very accurate in predicting brake values and is seen to be particularly accurate in predicting occurrences when the brake pressure is numerically zero.

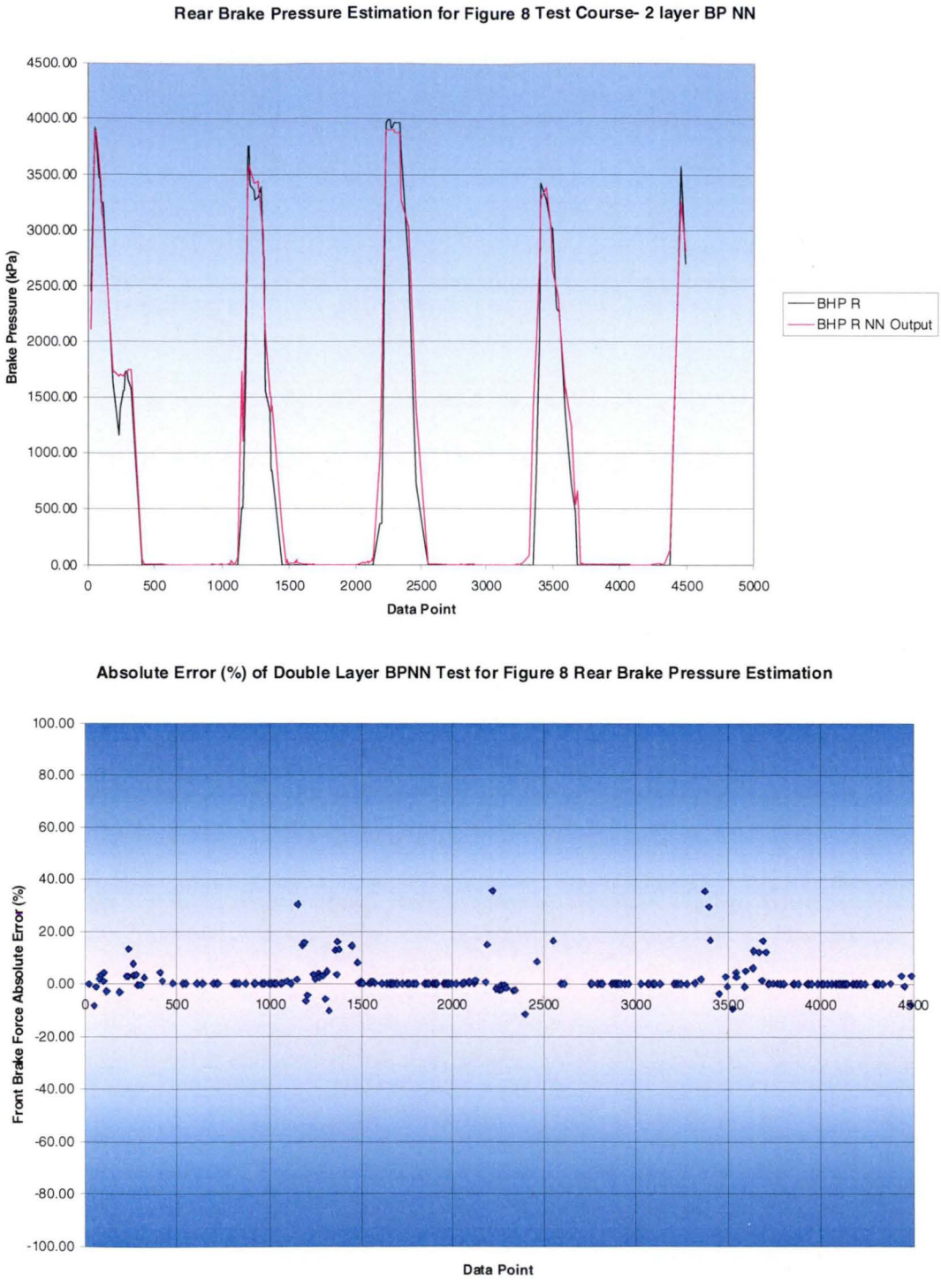

Figure 5-10 Figure eight rear brake hydraulic pressure estimation by double layer backpropagation neural network

5.4 General Regression Neural Network Results

The results for brake hydraulic pressure predictions by the General Regression Neural Network (GRNN) architecture can be seen in "Appendix A". At first glance it is apparent that the estimations by the GRNN are not nearly as accurate as those by the Back Propagation Neural Network (BP NN).

The GRNN architecture was trialed in brake force prediction due to the vast reductions in computational time required by the architecture over the much more accurate BP NN to predict brake pressure values. Unfortunately the results show that the difference in performance between the networks far outweighs the computational advantages of GRNN architecture.

The straight line (test course 1) predictions of the GRNN have greater associated error than the Figure eight (test course 2) predictions, particularly when the numerical value of the brake hydraulic pressure is zero. This gives the impression that this network architecture has difficulty in differentiating between engine braking, drag forces etc. and the braking force applied though the brake lines.

5.5 Concluding Remarks

The predictive capabilities of the Back Propagation Neural Network (BP NN) trialed here far exceeded all expectations relating to accuracy and performance given that the selection was based on trials of only a small number of architectures. The selection of the optimum two layer BP NN has not been carried out and the model chosen here has not been fine tuned. With this in mind, the results from the predictions demonstrate the massive potential of neural networks as predictive tools for dynamic automobile performance.

The predictions shown in this chapter have no notable bias. That is that the network is found to over-predict and under-predict the measured brake force values to the same

level. This demonstrates the adaptability of neural network processing and indicates that the networks have received statistically balanced input vectors. However to create a neural network capable of predicting brake forces under all conditions and for all manoeuvres the training data would need to be very large and would require excessive computing power.

Once training has been carried out and network weights have been established the predictive calculations can be made in feasible timeframes by commercially available computers. The incorporation of such a computer into the on board electrical system in the test rig represents the next step in using neural networks to predict brake forces.

CHAPTER SIX

FINAL CONCLUDING REMARKS AND PROPOSED FUTURE WORK

The extensive literature review highlighted the need for accurate dynamic brake pressure in any sophisticated electronic driving assistance system. However, the extent to which modern automobiles use brake force measurements for electronic brake force distribution to avoid accidents and overturning is limited form both sensory and adaptability points of view. In this way current state of the art automotive systems are reactive to emergency braking situations and systems use robust controllers to alter brake pressures only once the vehicle is deemed to be 'out of control'. As the future of brake force control, this work highlights the requirement for accurate quantitative brake force predictions to determine, in advance, when and how the vehicle will become out of control given the current course of actions.

Thus development in future electronic brake force controllers will focus around the ability to predict dynamic performance and make pre-emptive changes to the car dynamics to avoid instability all together while capable of maintaining threshold-braking much closer to optimum than current, conventional, robust, approaches allow. While many manufacturers are constantly addressing their conventional control systems, emerging technologies such as neural networks and fuzzy logic are replacing conventional systems in increasingly complex non-linear dynamic applications.

Neural network modelling has already proved itself as an accurate and useful performance estimation tool in manufacturing applications. This report shows, from the artificial neural network results in this preliminary investigation, the possible applications of ANN's in dynamic vehicle parameter prediction with the aim of

providing an effective electronic brake force controller. The results from this preliminary investigation far exceeded expectations with typical (average) accuracy of less than 3% full scale absolute error when using the back propagation model, which could be further improved upon in future development. That said, the results from this preliminary investigation stand by themselves as predictive tool that could be integrated almost immediately with current brake force controllers to further improve and develop current accuracy and performance.

In this work an extensive research is carried out in the design and development of an open wheel prototype test vehicle. The use of Finite Element Modelling (FEM) and full 3-D CAD modelling in the design are some of the techniques that made possible the transition from project conception to full size fully operational prototype in the space of six months. Extensive testing of the vehicle has proved the design with the prototype having covered over 1600 racing kilometres without the need to alter or redesign any major components.

Technical aspects covered were the intricate positioning of sensors and allowance in the overall prototype design to cater for such a position. Some of the more innovative components of the chassis which have been used to save weight such as the composite drivetrain and aluminium brake rotors have proven to be very effective from a testing point of view, pushing the engineering envelope in this innovative prototype. This is a reflection of the way the dimensional details of each part together with their function and relation to other components were meticulously documented. The design must of other systems such as the electrical circuitry, telemetry for data acquisition, and MoTeC engine management system were coordinated with other research members of the Intelligent car team.

As part of experimental investigation two testing courses, straight line and Figure eight, were identified for testing purposes. During this testing many parameters were measured along with the independent front and rear brake hydraulic pressures. The level of care directed toward the measuring system featuring telemetry and data acquisition has resulted in reliable, accurate, quantitative measurements. It is the

reliability of this data that resulted in the low error neural network modelling and testing that followed. While the results from the neural networks are encouraging, there is room for improvement to optimise the networks for input selection accuracy, minimum training times and converging rates.

Suggested improvements are in the selection and refinements of sampling rates and input parameters to enable the compression of the most relevant data into the smallest useful data sets. This would enable the networks to train themselves more efficiently, and over a wider range of driving conditions than was possible within the scope of this work. Refinement in the selection of network architecture is another area were networks could be further optimised.

It has been shown in these results that the choice of network type and structure can have a large effect. Therefore future work will involve conducting the testing for a number of additional ANN models, as well as optimising each by experimentation with different network configurations and characteristics. This would include trials in properties such as the number of nodes and their arrangement, trying different training and converging parameters, altering the number of iterations to convergence and investigating the effects of different transfer functions. Investigations of this nature have shown to produce significant improvements in the ANN accuracy far beyond what has been covered in this work.

In addition to improving the accuracy of the network, further work will need to be conducted in development of ANN brake force prediction hardware and the interface to existing electronic brake force control systems. The aim here is to provide a pro-active brake force controller that reliably and consistently allows for optimum braking performance under all conditions and surfaces encountered by an automobile.

REFERENCES

[1] H. Bauer, "ESP – Electronic Stability Program", Robert Bosch GmbH, 1999

[2] BMW World Technology, http://www/bmwworld.com/technology/dsc.htm

[3] A Van Zanten, R Erhardt, K landesfeind and G Pfaff, "VDC Systems Development and Perspective", Robert Bosch GmbH, Society of Automotive Engineers, 1998.

[4] R. P. Lippman, "An Introduction to Computing with Neural Nets", IEEE ASSP Mag., April 24, 1987.

[5] H. Bauer, "Driving Safety Systems", Robert Bosch GmbH, 1999

[6] B. Heremans "Car Handling" http://www.gallery.uunet.be.heremanss.htm

[7] W. Henke, "Vehicle Dynamics Control – Form ABS to ESP", http://www.whnet.com/4x4/abs.html

[8] Zhejun Fan, Yoram Koren and David Wehe, "Practical Rule-Based Vehicle Traction Control", Society of Automotive Engineers ref no. 942402.

[9] D. R. McLellan, J. P. Ryan, E. S. Browalski, J. W. Heinricy, "Increasing the Safe Driving Envelope – ABS, Traction Control and Beyond", General Motors Corp., Society of Automotive Engineers, 1992.

[10] C. Campbell, "Design of Racing Sports Cars", 1st edition, Chapman & Hall, 1973

[11] Alfred Sigl, Herbert Demel, "ABS-Traction Control, State of the Art and Some Prospects", Society of Automotive Engineers ref no. 900204.

[12] R. K. Jurgen, "Electronic Braking , Traction and Stability Control", Society of Automotive Engineers, 1999

[13] J. Mack, "ABS - TCS – VDC: Where Will Technology Lead Us", Society of Automotive Engineers, 1996

[14] R.K. Jurgen, "Automotive Electronics Handbook", 2nd edition, Society of Automotive Engineers, 1999

[15] Reinhard Auffhammer, Reent Heyken, Harald Roth, "New Driving Stability Control System with Reduced Technical Effort for Compact and Medium Class Passenger Cars", BMW AG, Society of Automotive Engineers, 1998.

[16] Ross Bannatyre, "Future Developments in Electronically Controlled Braking Systems", Transportation Systems Group, Motorola Inc, Society of Automotive Engineers, 1999.

[17] Chris M Atkinson "Neural Network Engine Control", Society of Automotive Engineers, 1996.

[18] R. Hecht-Nielsen, "Neurocomputing", Addison-Wesley Publishing Company, 1990.

[19] J.A. Freeman and D.M.Skapura "Neural Networks: Algorithms, Applications and Programming Techniques", Addison-Wesley Publishing Company Inc., 1992.

[20] M. Chow, R.N. Sharpe, J.C. Hung, "On the Application and Design of Artificial Neural Networks For Motor Fault Detection – Part 1, IEEE Transactions of Industrial Electronics Vol. 40, No.2 1993. pp181-188.

[21] L.P. Veelenturf, "Analysis and Applications of Artificial Neural Networks", Prentice Hall International (UK) Ltd., 1995.

[22] R. Rojas "Neural Networks: A Systematic Introduction", Springer-Verlag, New York, 1996.

[23] J. E. Dayhoff, "Neural Network Architectures – An Introduction", Van Nostrand Reinhold, 1990.

[24] M. P. Taylor, W. D. Zhang, V. Willis, S. Schmid, "A Dynamic Model for the Energy Balance of an Electrolysis Cell" Trans. Institute of Chemical Engineers, Vol 74, pt.A, Nov. 1996 pp 913-933.

[25] F. Frost "Neural Network Applications to Aluminium Manufacturing", School of Science and Engineering, University of Tasmania, 2000.

[26] N. Urata, "Magnetics and Metal Pad Instability", Proc. 114th TMS Annual Meeting, Atlanta Georgia, Mar 1985, pp. 581-591.

[27] J. M. Zuranda, "Introduction to Artificial Neural Networks", West Publishing Co., St Paul, 1999.

[28] F. Frost, V. Karri, "Identifying Significant Parameters for Hall-Heroult Process Modelling using General Regression Neural Network" Proc. 13th International Conference on Industrial and Engineering Applications of Artificial Intelligence, New Orleans, USA, Jun. 2000 pp. 73-78.

[29] F. Frost, V. Karri, "Combined Kohnen and RBF Networks to Predict Electrolyte Additives in Hall-Heroult Cell" Proc. International Conference on Advances in Intelligent Systems: Theory and Applications, Canberra, Australia, Feb. 2000 pp. 19-24.

[30] F. Frost, V. Karri, "Intelligent Control of Aluminium Reduction Cells Using Backpropagation Neural Networks" Proc. International Conference on Advances in Intelligent Systems: Theory and Applications, Canberra, Australia, Feb. 2000 pp. 350-356.

[31] Formula SAE Rules 2001, SAE International, 2000

[32] K. Singh, "Automobile engineering Vol. 1", 8th edition, A. K. Jain, 2000.

[33] K. Singh, "Automobile engineering Vol. 2", 8th edition, A. K. Jain, 2000

[34] Strand 7 Finite Element Analysis System, G+D Computing, 1999.

[35] CADKEY 98 Release 1 Baystate Technologies, Inc., USA, 1998.

[36] D. Butler, V Karri, "Design Analysis Between On and Off-Centre Bearing for Racecar Wheel Using Finite Element Method", University of Tasmania, 2001.

[37] Design of Rolling Bearing Mountings Catalogue WL 00 200/5 EA, FAG OEM und Handel AG, 1998.

[38] Technical Information Catalogue WL 43 1190 EA, FAG OEM und Handel AG, 1997.

[39] J. Brandlein, P. Eschmann, L. Hasbargen and K. Weigand, "Ball and Roller Bearings: Theory, Design and Application", 3rd edition, Wiley.

[40] K. Jayakumar, K.V.Rajaram and M.A. Faruqi "Machine Intelligence for Crisis Handling in Navigation Vehicles Using Neuro Controllers", 6th International Conference on Neural Information Processing, Institute of Electrical and Electronics Engineers

[41] E. Gohring, "Electronic Traction Control System ASR and its Integration in the Anti-Lock Braking Systems ABS to Form a Safety System 'ABS/ASR' for Commercial Vehicles", ", Society of Automotive Engineers ref no. 881137.

[42] James Walker "Chassis controls and their considerations", www.teamscR.com, SCR Motorsports, 2001

[43] H. Heisler, "Advanced Vehicle Technology", 1st edition, Edward Arnold, 1989

[44] M. Platt, "Elements of Automobile Engineering", 2nd edition, Sir Isaac Pitman and Sons, 1959

[45] T. P. Newcomb, R. T. Spurr, "A Technical History of the Motor Car" 1st edition, IOP Publishing, 1989

[46] J. E. Duffy, M. T. Stockel, M. W. Stockel, "Automotive Mechanics Fundamentals", 1st edition, Gregory's Scientific Publications, 1985

[47] L. Terry, A. Baker, "Racing Car Design and Development", 1st edition, Robert Bentley, 1973

[48] David Hodges, "A-Z of Formula Racing Cars 1945-1990", 1st edition, Bay View Books, 1990

[49] R. L. Norton, "Design of Machinery", 2nd edition mechanical engineering series, McGraw-Hill, 1999

[50] Fag Rolling Bearings Catalogue WL 41 520/2 EA, FAG OEM und Handel AG, 1998.

[51] M. Costin, D. Phipps "Racing and Sports Car Chassis Design", 2nd edition, B. T. Batsford, 1966.

[52] C. P. Nakra, "Basic Automobile Engineering", 8th edition, Dhanpat Rai Publishing, 1999.

[53] V. V. Vantsevich, M. S. Vysotski, S. V. Kharitont, "Control of wheel dynamics", International Congress and Exposition, Society of Automotive Engineers, 1998.

[54] K. C. Cheok, F. B. Hoogterp, W. K. Fales"Fuzzy Logic Approach to Traction Control Design" , Society of Automotive Engineers ref no.942402, 1998.

[55] K. Lyon, M. Phlipp and E. Grommes, "Traction Control for a Formula 1 Racecar: Conceptual Design, Algorithm Development and Calibration Methology", Robert Bosch GmbH, Society of Automotive Engineers, 1994.

[56] S. K. Mohan, R. C. Williams, "A Survey of 4WD Traction Control Systems and Strategies" New Venture Gear, Society of Automotive Engineers, 1995.

[57] A. T. Van Zanten, R. Erhardt, G. Pfaff, "VDC, The Vehicle Dynamics Control System of Bosch" Robert Bosch GmbH, Society of Automotive Engineers, 1995.

[58] A. T. Van Zanten, R. Erhardt, A. Lutz, W. Neuwald, H. Bartels "Simulation for the development of the Bosch-VDC" Robert Bosch GmbH, Society of Automotive Engineers, 1996.

[59] A. Strickland, K. Dagg, "ABS Braking Performance and Steering Input", Royal Canadian Mounted Police, Society of Automotive Engineers, 1998.

[60] H. Saito, N. Sasaki, T. Nakamura, M. Kume, H. Takinata, M. Nishikawa, "Acceleration Sensor for ABS", Sumitomo Electric Industries, Society of Automotive Engineers, 1992.

[61] D. E. Schenk, R. L. Wells, J. E. Miller, "Intelligent Braking for Current and Future Vehicles" Delco Chassis, Society of Automotive Engineers, 1995.

[62] G. Mauer, G. Gissinger and Y. Chamaillard, "Fuzzy Logic Continuous and Quantising control of an ABS Braking System", University of Nevada , Society of Automotive Engineers, 1994.

[63] L. Evans, "ABS and Relative Crash Risk Under Different Roadway Weather, and Other Conditions", General Motors Corp, Society of Automotive Engineers, 1995.

[64] T. Bach, H. Schmitt, W. Schwanke, H. J. Tumbrink, "'Roadrunner'- Real Time Simulation in Anti-Lock Brake System Development" Lucas Braking Systems, Society of Automotive Engineers, 1995.

[65] M. J. Scheider, "Use of a Hazard and Operability Study for Evaluation of ABS Control Logic", Ford Motor Company, Society of Automotive Engineers, 1997.

[66] W. Maisch, W. Jonner, R. Mergenthaler, A. Sigl, "ABS5 and ASR5: The New ABS/ASR Family to Optimise Direction Stability and Traction" Robert Bosch GmbH, Society of Automotive Engineers, 1993.

[67] Thomas G. Beckwith, Roy D. Marangoni, John H. Lienhard V, Mechanical Measurements, Fifth Edition, Addison-Wesley Publishing Company Inc, 1995, p 4

[68] Ryoji Ohba, F.R.D. Apps, Intelligent Sensor Technology, John Wiley & Sons Ltd, 1992 pp.1, 2, 13

[69] H.H. Braess, "Electronics-The Co-Evolution of Intelligence in Automobiles and Road Traffic", in Proceedings of the 1987 International Conference on Automotive Electronics 1987, pp. 1-6.

[70] Ross Bannatyne, The Sensor Explosion and Automotive Control Systems http://sensormag.com/articles/0500/92/main.shtml

[71] Nd Mathews, P E An, M Roberts, C J Hariss, "A neaurofuzzy approach to future driver support systems", in Proceedings of the Institute of Mechanicla Enginneers, London 1998

[72] M. Murayama, "The Situation of Automobile Electronics in Japan", in Proceedings of the 1987 International Conference on Automotive Electronics 1987, pp. 7-9.

[73] Introduction to Sensor Fusion http://lca.kaist.ac.kr/Researches/2000/sensorfusion.html

[74] Delphi Homepage/Products/Intellek Smart Sensors http://164.109.59.132/products/nextech/products/intellek

[75] Dale J. Long, Sensors, An Integral Part of Today's Automobile, Department of engineering Technology New Mexico State University, 1999

[76] Peelamedu, S., Naganathan, G., and Buckley, S., 1999, "Impact Analysis of Automotive Structures with Distributed Smart Material Systems", SPIE Proceedings, Vol. 3667, pp 813-824.

[77] Peelamedu, S., Naganathan, G, 1999, "Smart automobiles through Smart Sensors"

[78] Stability Control: Get your Yaws Out http://www.edmunds.com/onership/safety/articles/45992/article.html.

[79] Traction Control http://www.edmunds.com/onership/safety/articles/46352/article.html

[80] Ralf Klein, "Antilock-Braking System and Vehicle Speed Estimation using Fuzzy Logic Fuzzy", in Proceedings of the 1996 Embedding Computer Conference, 1987 (Http://www.fuzzytech.com/e/e_a_sie.html)

8 APPENDIX A –GENERAL REGRESSION NEURAL NETWORK RESULTS

A-1: GRNN front brake pressure prediction for Course 1 (straight line) 217

A-2: GRNN rear brake pressure prediction for Course 1 (straight line) 218

A-3: GRNN front brake pressure prediction for Course 2 (Figure eight) 219

A-4: GRNN rear brake pressure prediction for Course 2 (Figure eight) 220

A-1

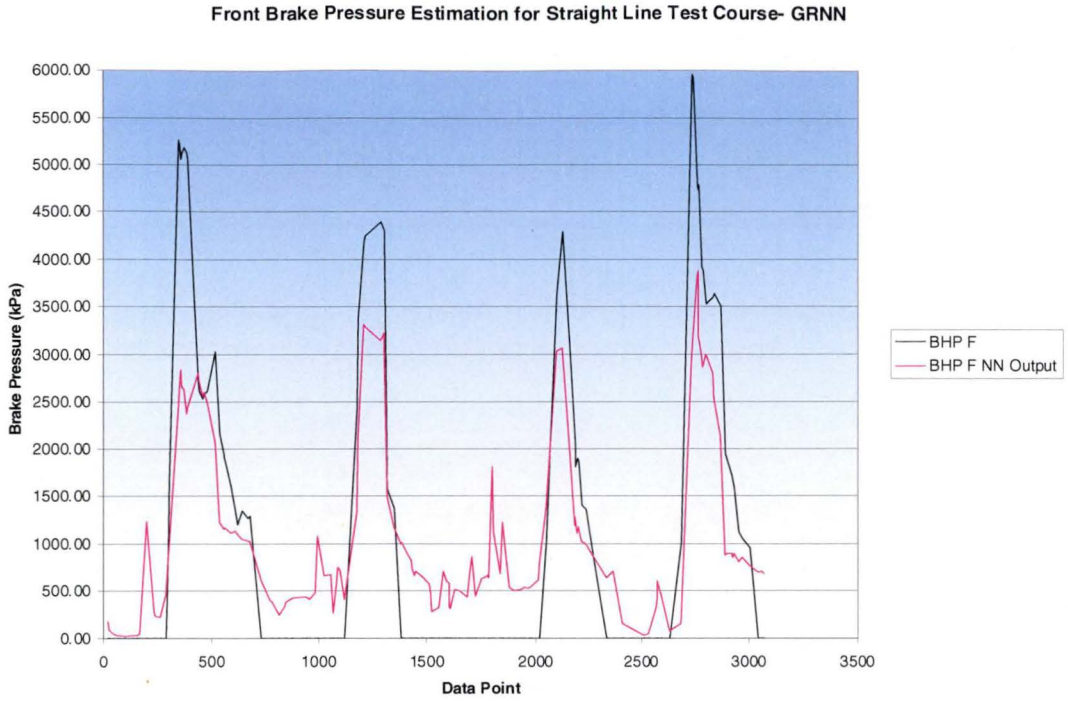
Front Brake Pressure Estimation for Straight Line Test Course- GRNN
Brake Pressure (kPa)
6000.00
5500.00
5000.00
4500.00
4000.00
3500.00
3000.00
2500.00
2000.00
1500.00
1000.00
500.00
0.00
0
500
1000
1500
2000
2500
3000
3500
Data Point
BHP F
BHP F NN Output

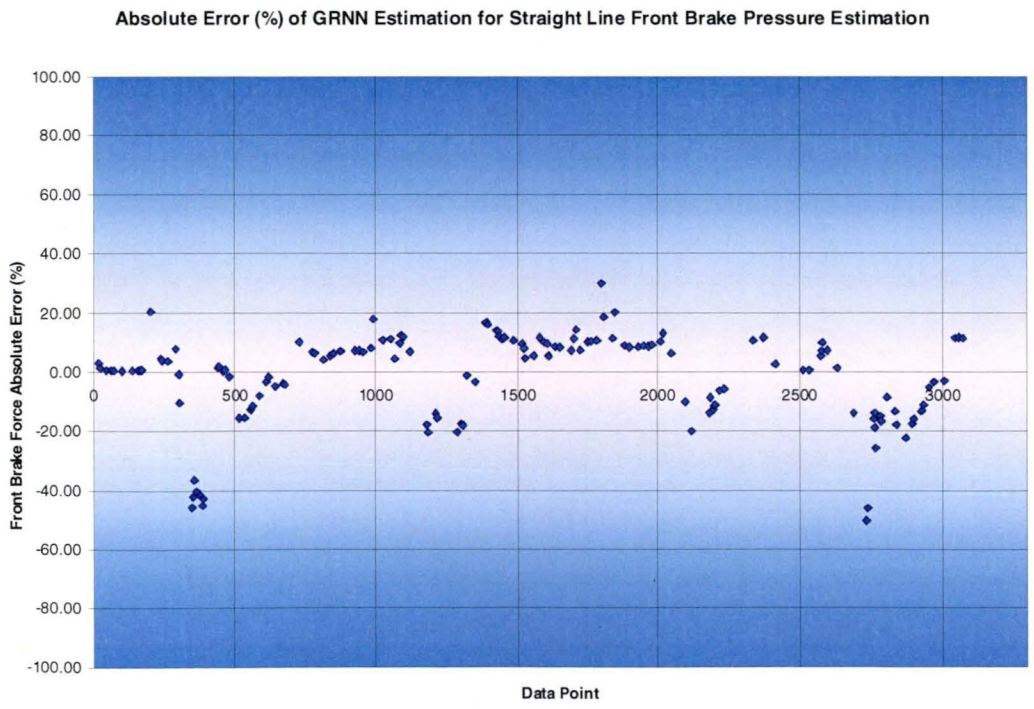
Absolute Error (%) of GRNN Estimation for Straight Line Front Brake Pressure Estimation
Front Brake Force Absolute Error (%)
100.00
80.00
60.00
40.00
20.00
0.00
-20.00
-40.00
-60.00
-80.00
-100.00
0
500
1000
1500
2000
2500
3000
Data Point

A-2

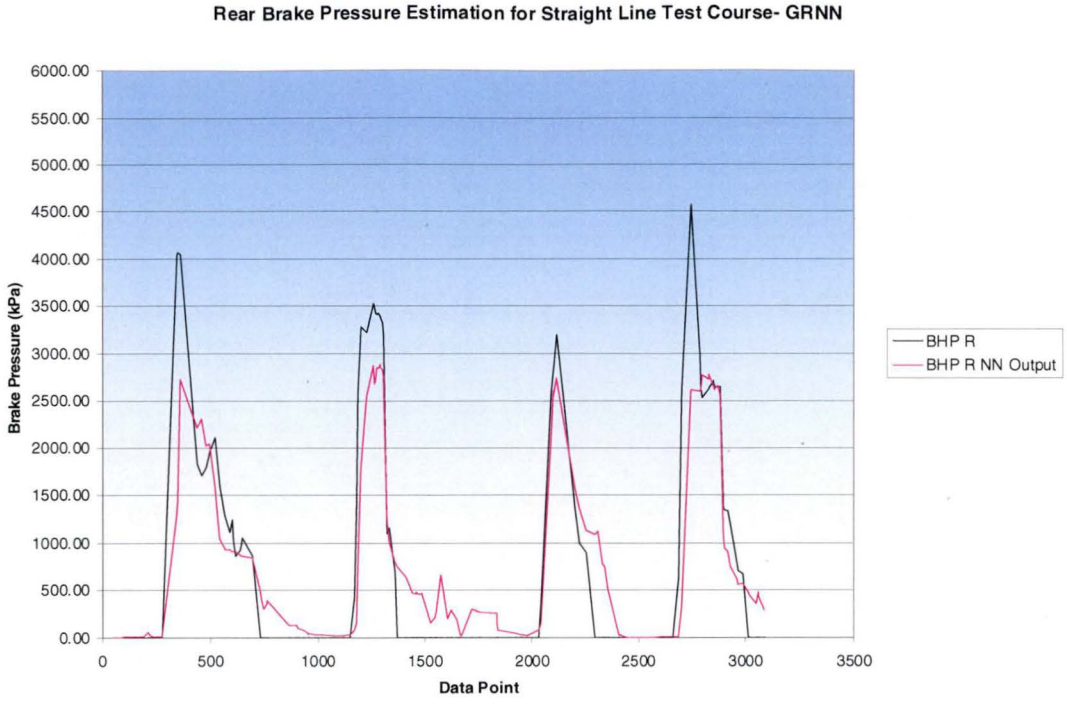
Rear Brake Pressure Estimation for Straight Line Test Course- GRNN
Brake Pressure (kPa)
6000.00
5500.00
5000.00
4500.00
4000.00
3500.00
3000.00
2500.00
2000.00
1500.00
1000.00
500.00
0.00
0
500
1000
1500
2000
2500
3000
3500
Data Point
BHP R
BHP R NN Output

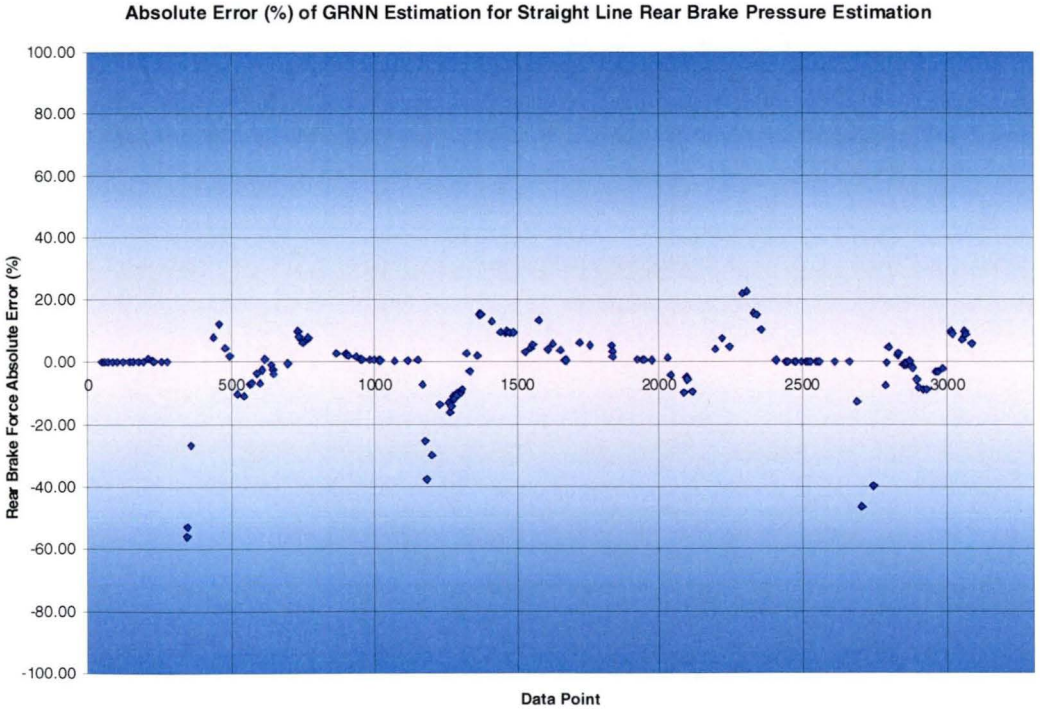
Absolute Error (%) of GRNN Estimation for Straight Line Rear Brake Pressure Estimation
Rear Brake Force Absolute Error (%)
100.00
80.00
60.00
40.00
20.00
0.00
-20.00
-40.00
-60.00
-80.00
-100.00
0
500
1000
1500
2000
2500
3000
Data Point

A-3

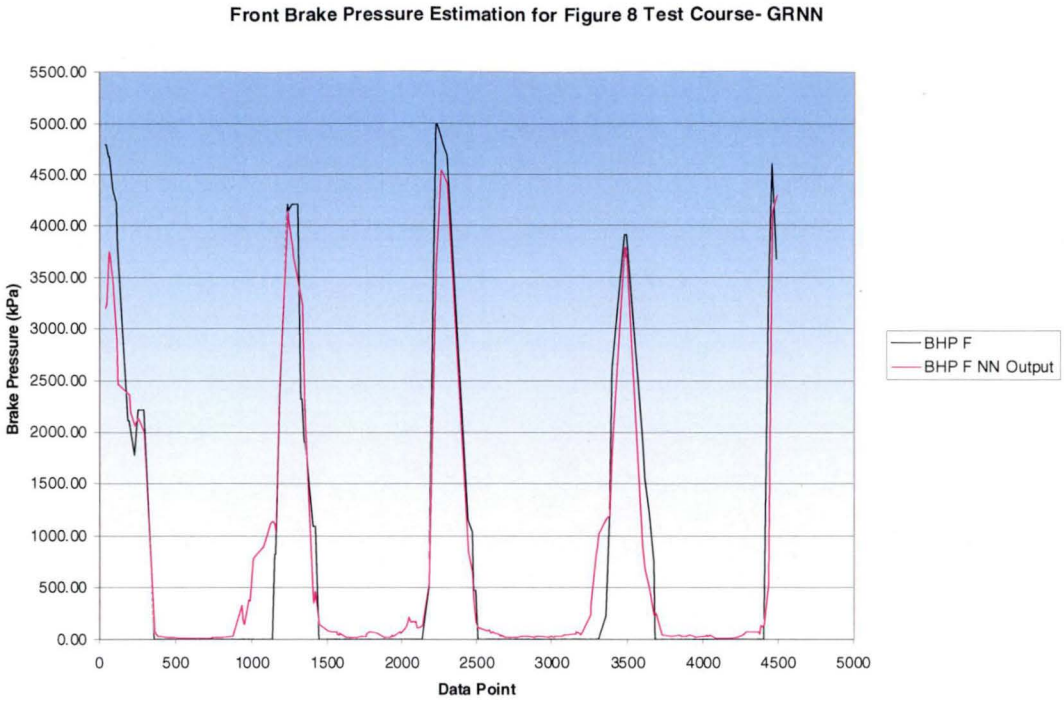
Front Brake Pressure Estimation for Figure 8 Test Course- GRNN
Brake Pressure (kPa)
5500.00
5000.00
4500.00
4000.00
3500.00
3000.00
2500.00
2000.00
1500.00
1000.00
500.00
0.00
0
500
1000
1500
2000
2500
3000
3500
4000
4500
5000
Data Point
BHP F
BHP F NN Output

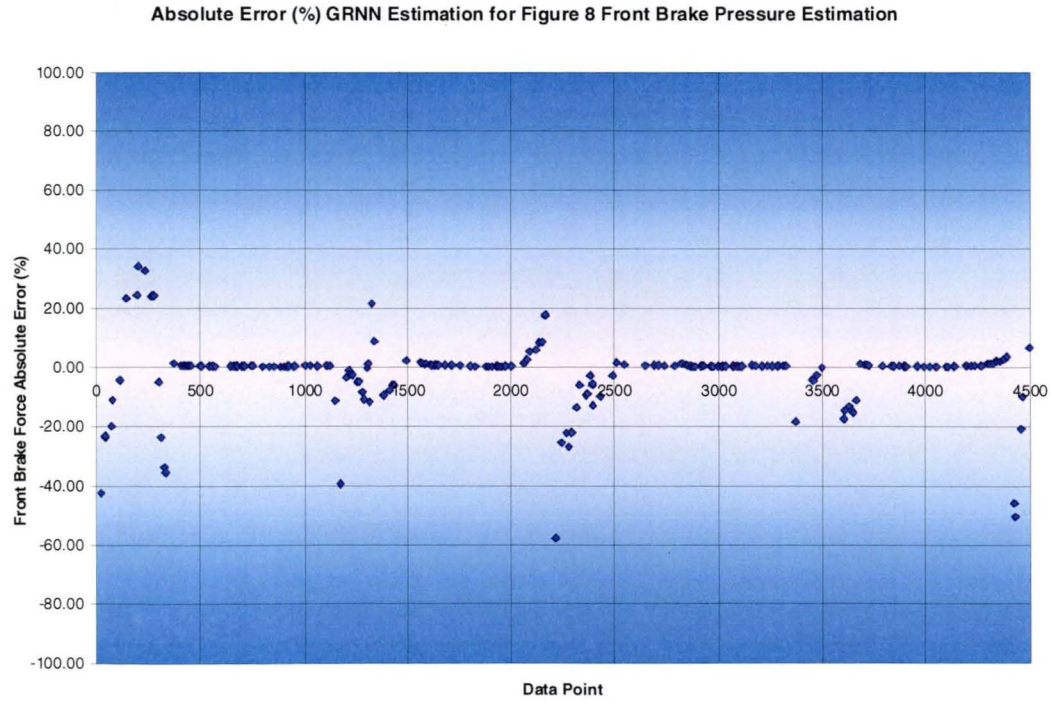
Absolute Error (%) GRNN Estimation for Figure 8 Front Brake Pressure Estimation
Front Brake Force Absolute Error (%)
100.00
80.00
60.00
40.00
20.00
0.00
-20.00
-40.00
-60.00
-80.00
-100.00
0
500
1000
1500
2000
2500
3000
3500
4000
4500
Data Point

A-4

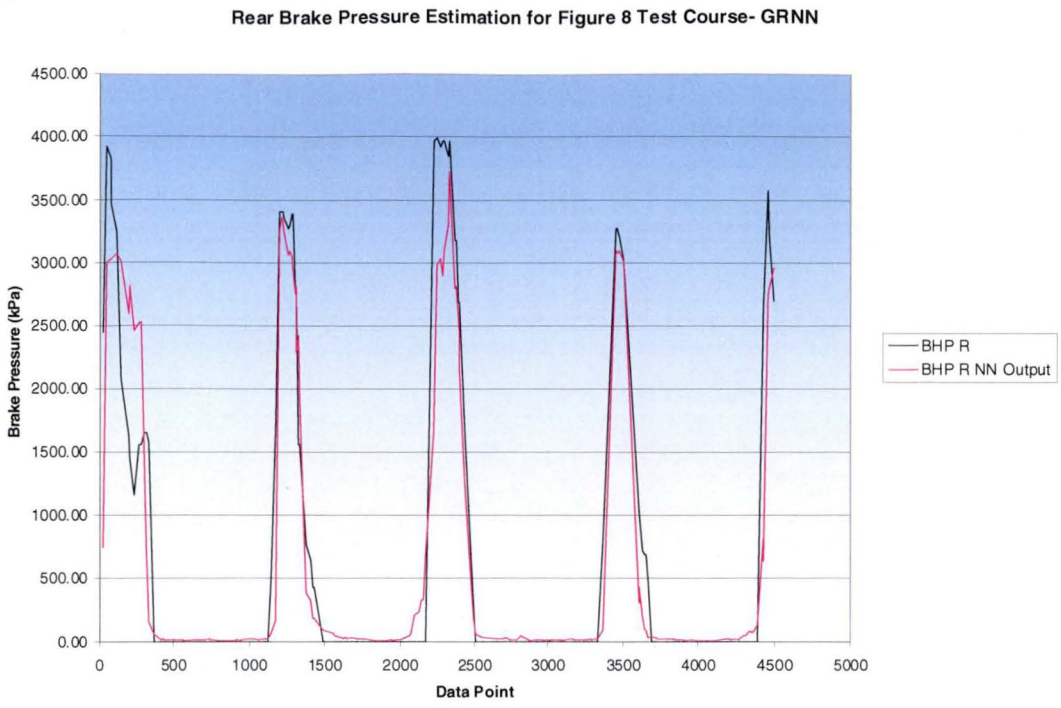
Rear Brake Pressure Estimation for Figure 8 Test Course- GRNN
Brake Pressure (kPa)
4500.00
4000.00
3500.00
3000.00
2500.00
2000.00
1500.00
1000.00
500.00
0.00
0
500
1000
1500
2000
2500
3000
3500
4000
4500
5000
Data Point
BHP R
BHP R NN Output

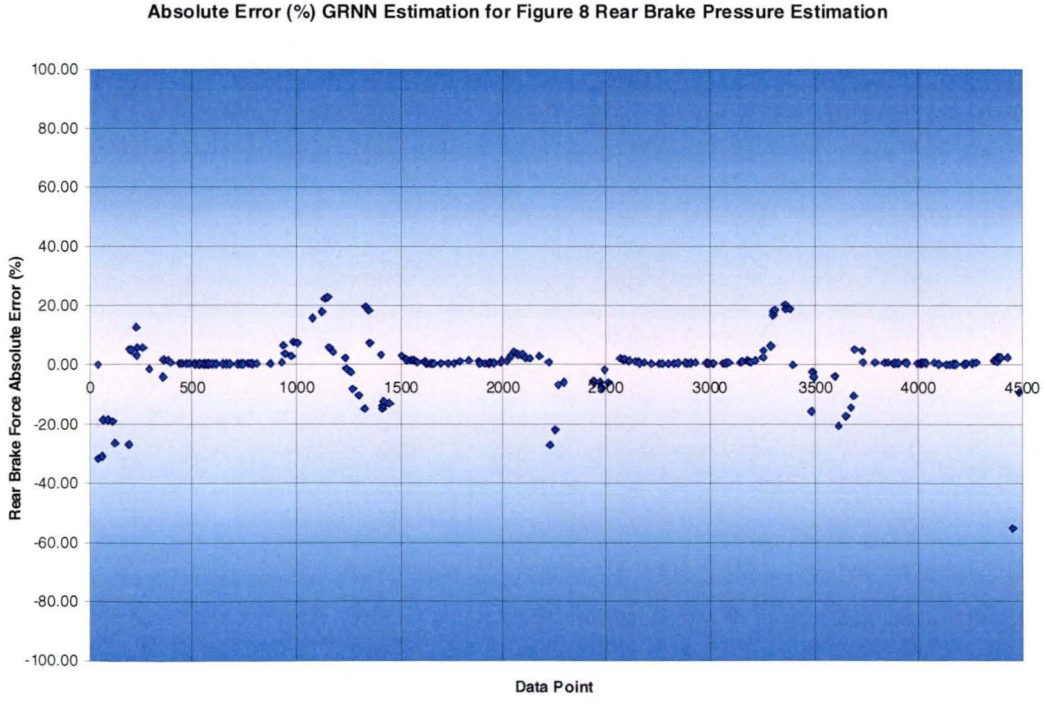
Absolute Error (%) GRNN Estimation for Figure 8 Rear Brake Pressure Estimation
Rear Brake Force Absolute Error (%)
100.00
80.00
60.00
40.00
20.00
0.00
-20.00
-40.00
-60.00
-80.00
-100.00
0
500
1000
1500
2000
2500
3000
3500
4000
4500
Data Point

9 APPENDIX B –FRAME DESIGN AND FEA

B-1: FEA of frame under normal driving 222

B-2: FEA of frame under acceleration 222

B-3: FEA of frame under braking 223

B-4: FEA of frame during cornering 223

B-5: FEA of frame during cornering under acceleration 224

B-6: FEA of frame during cornering under acceleration 224

B-7: FEA torsional results under 1 Nm 225

B-8: Left view of frame (Three Dimensional member lengths) 226

B-9: Top view of frame (first set of dimensions) 227

B-10: Top view of frame (second set of dimensions) 228

B-11: Top view of frame (member angles) 229

B-12: Top view of frame (member angles of mid-section) 230

B-13: Front view of frame 231

B-14: Roll hoop dimensions 232

B-1: FEA of frame under normal driving

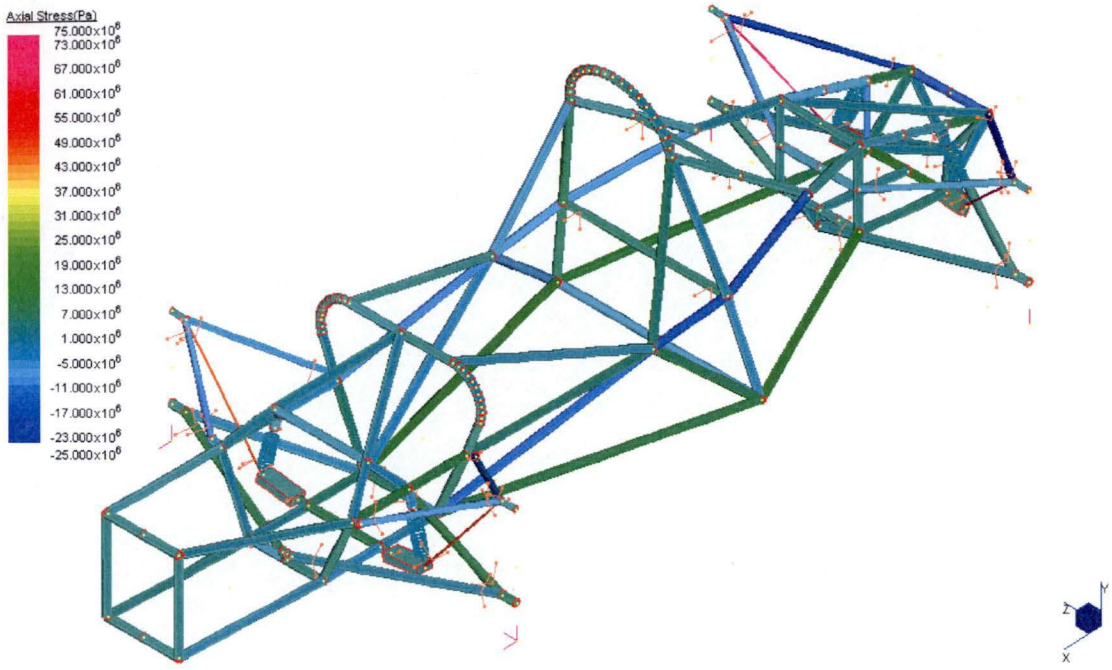

B-2: FEA of frame under acceleration

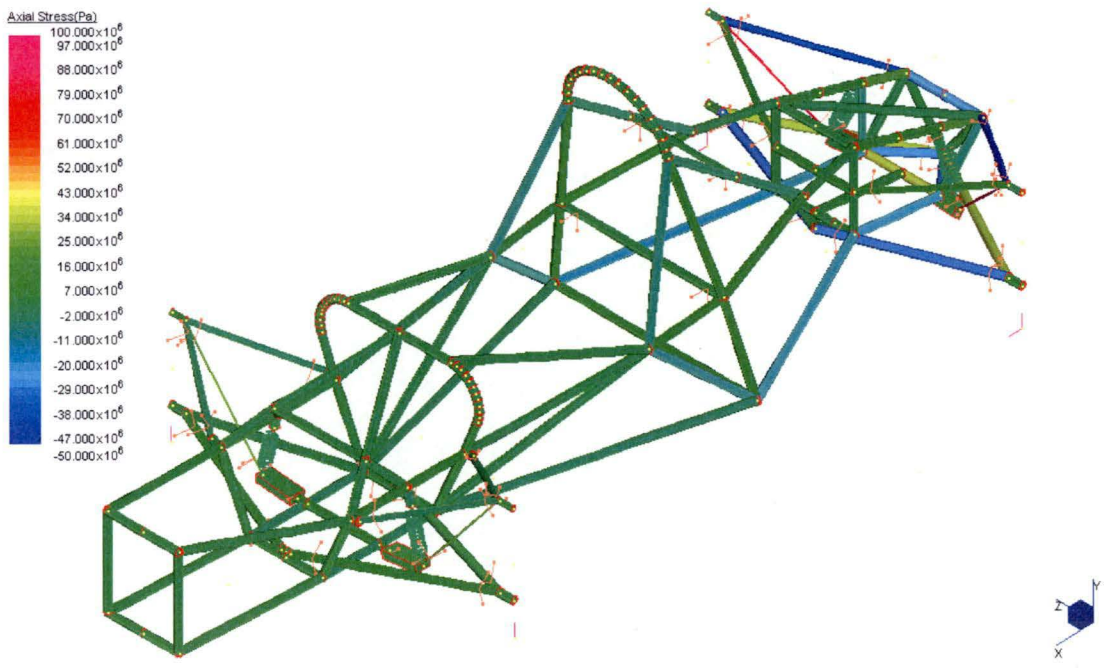

B-3: FEA of frame under braking

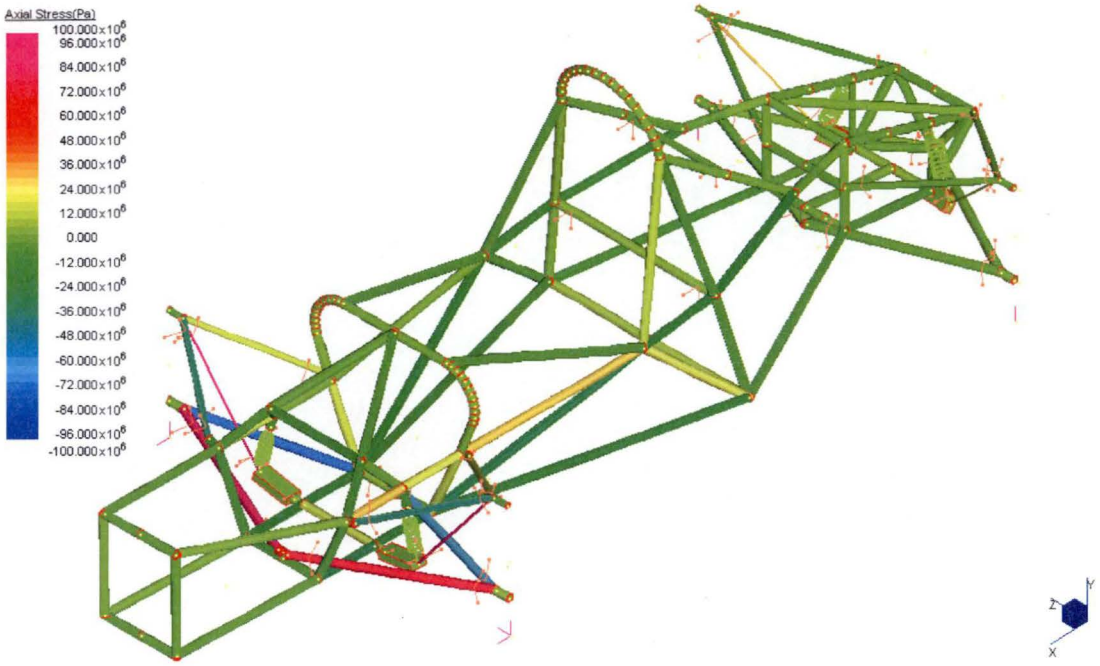

B-4: FEA of frame during cornering

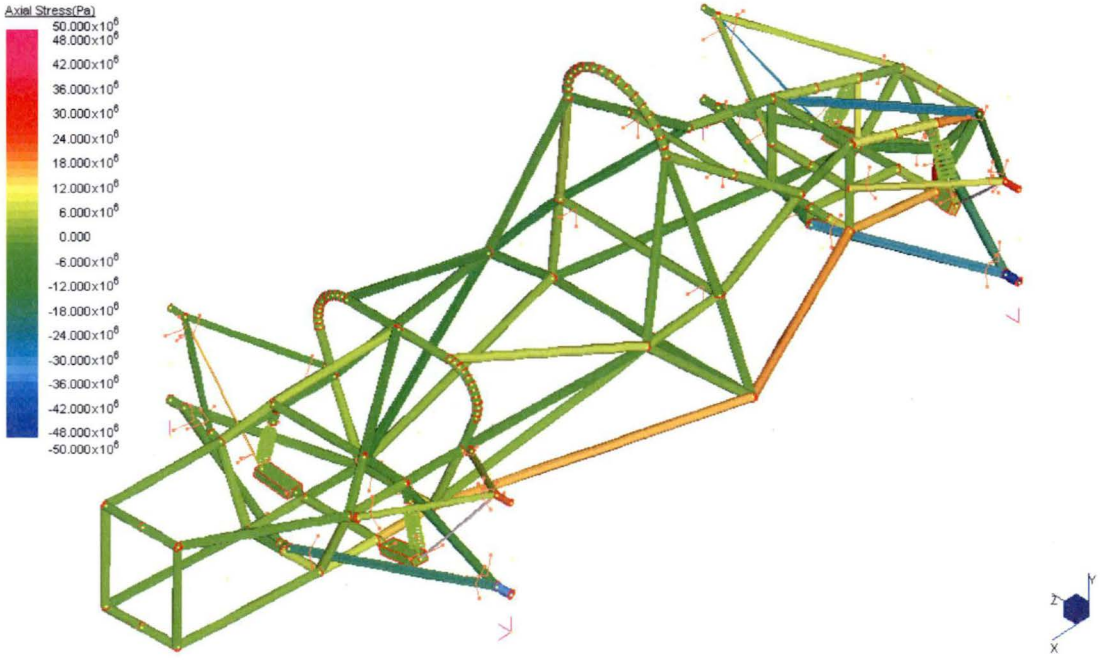

B-5: FEA of frame during cornering under acceleration

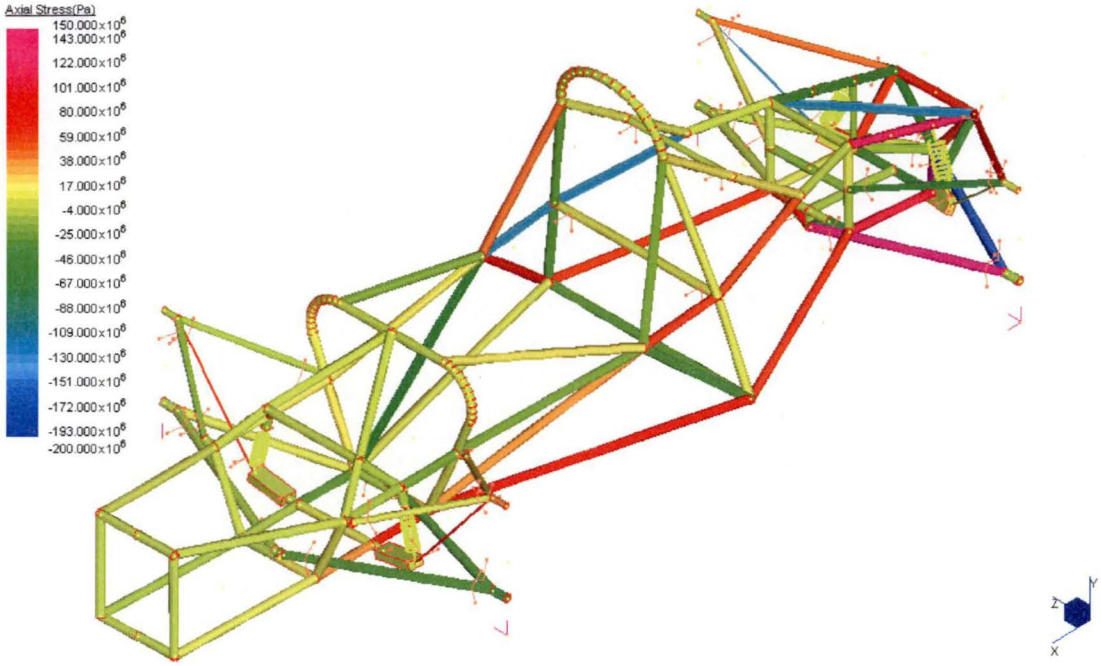

B-6: FEA of frame during cornering under acceleration

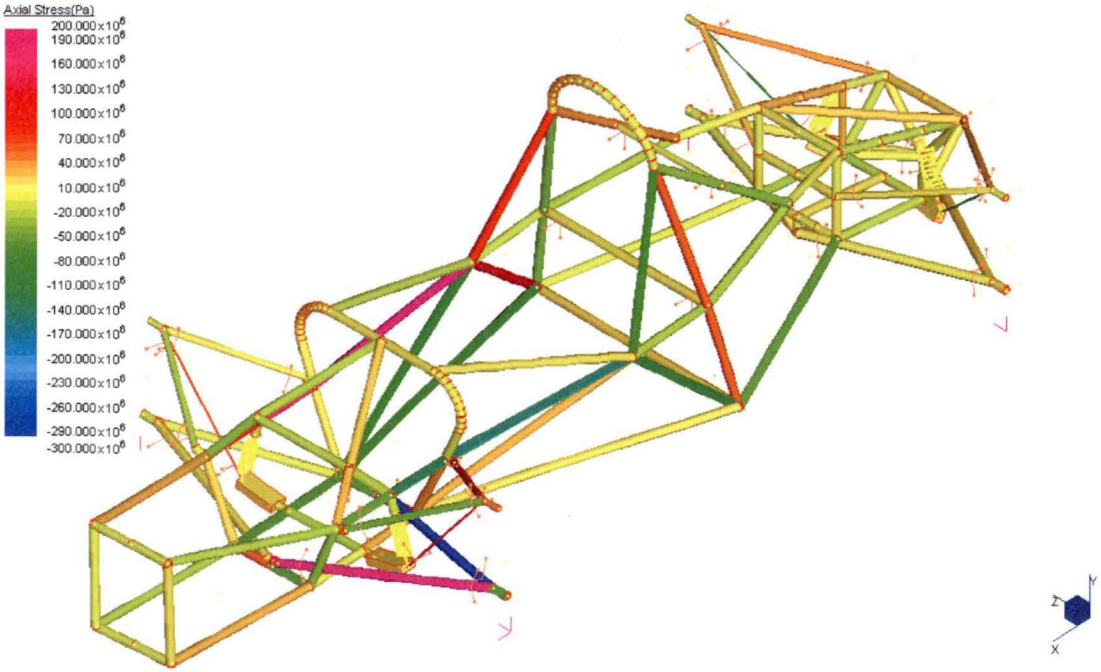

B-7: FEA torsional results under 1 Nm

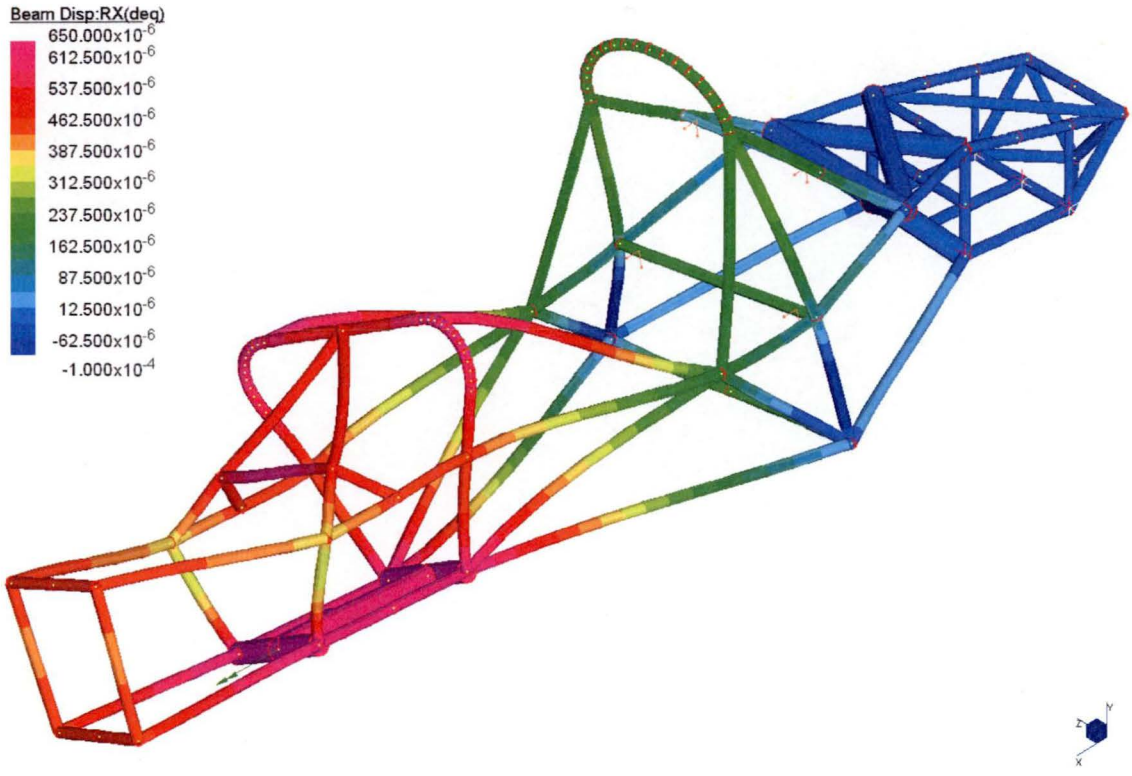

B-8: Left view of frame (three dimensional member lengths)

TITLE	Left View - 3D Member Dim.		
DRAWN BY	DAVID BUTLER		
DATE	4/4/01	DWG NO. 4	SCALE: 1:10 (A3)

All member lengths are 3D

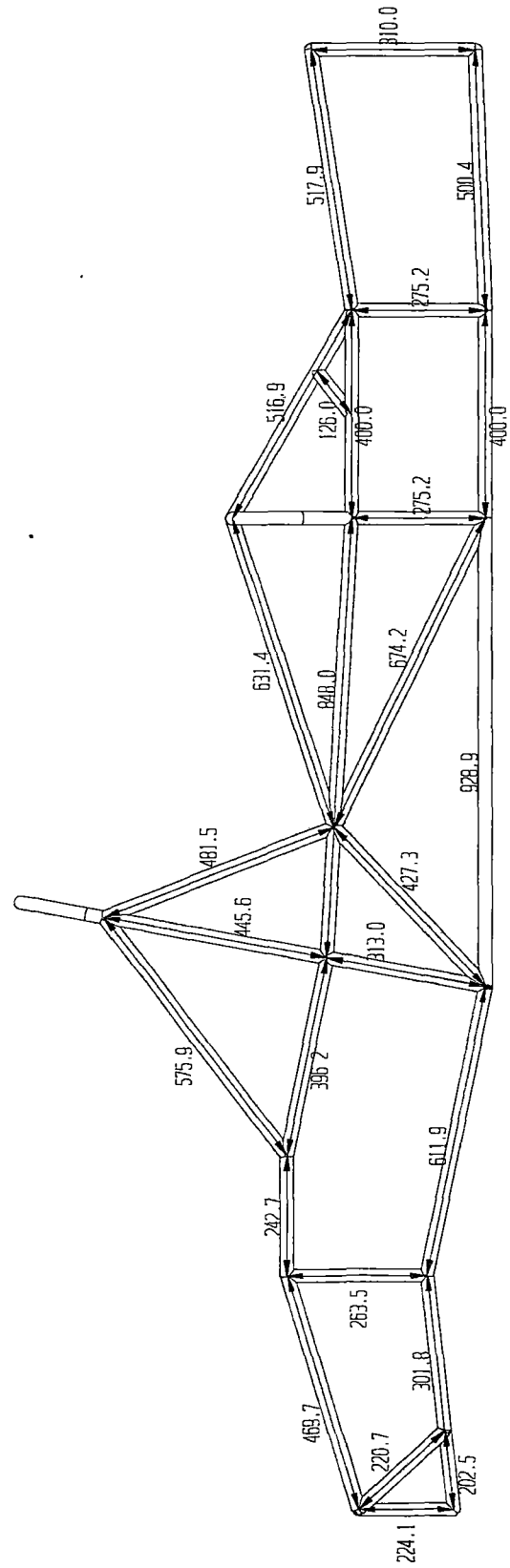

B-9: Top view of frame (first set of dimensions)

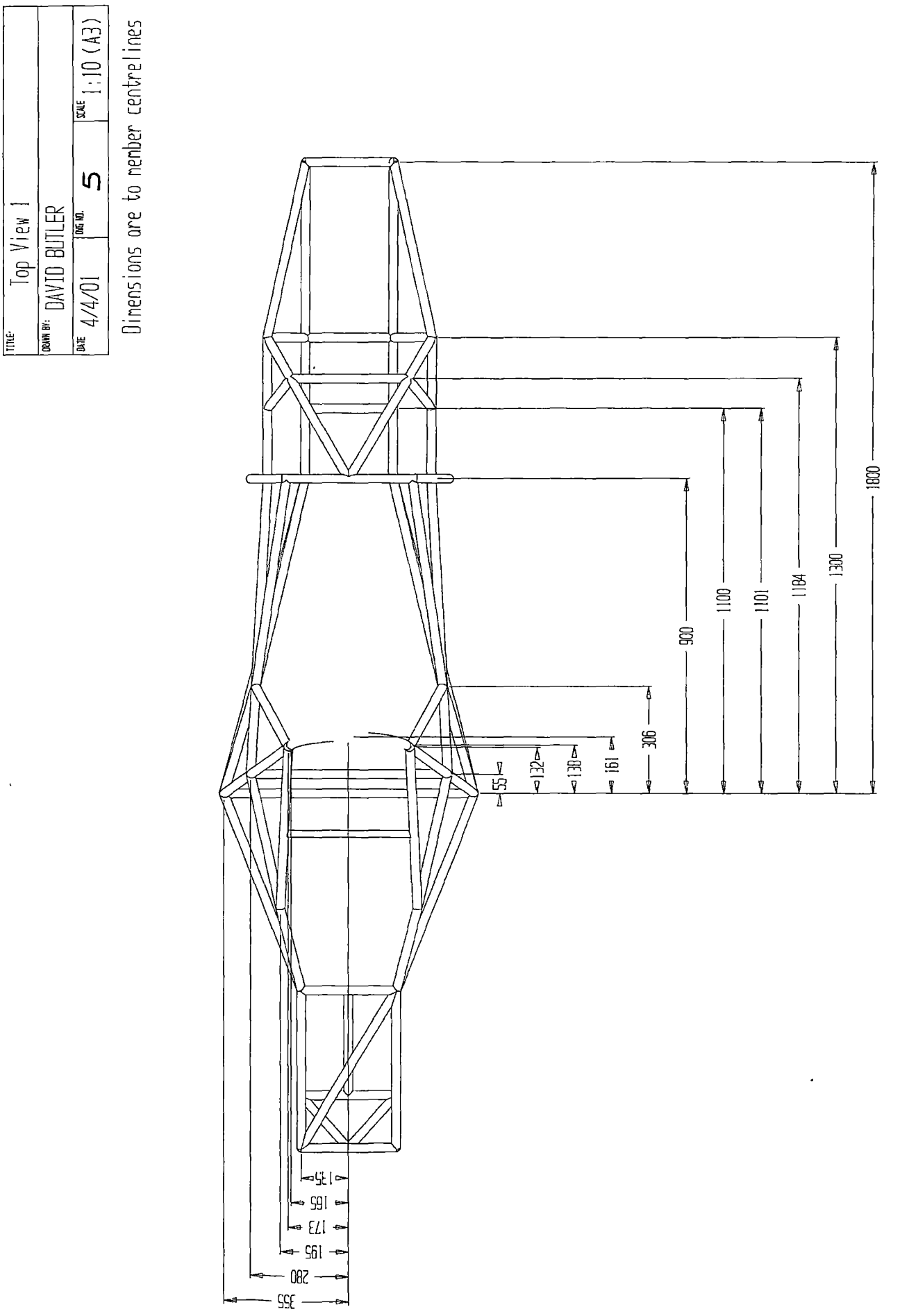

B-10: Top view of frame (second set of dimensions)

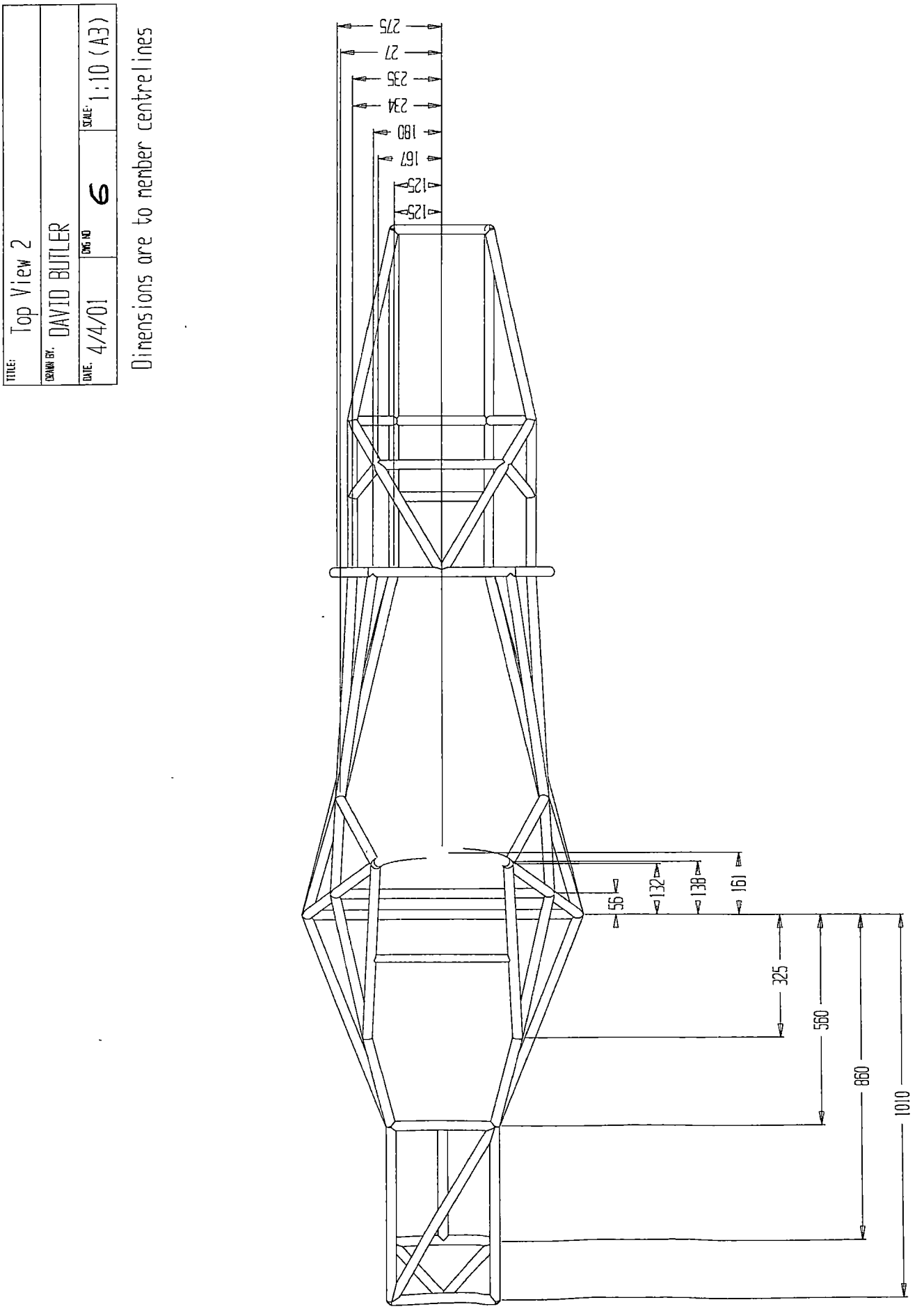

B-11: Top view of frame (member angles)

TITLE:	Top View Angles
DRAWN BY	DAVID BUTLER
DATE	4/4/01
DWG NO	7
SCALE	1:10 (A3)

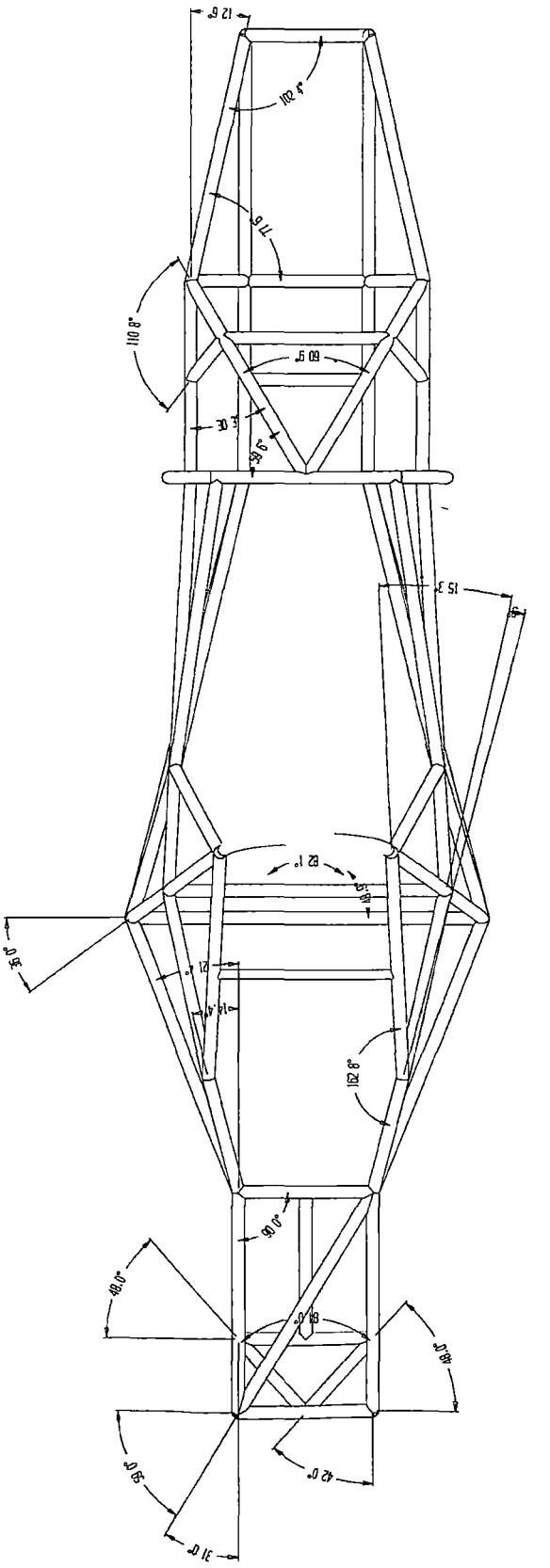

B-12: Top view of frame (member angles of mid-section)

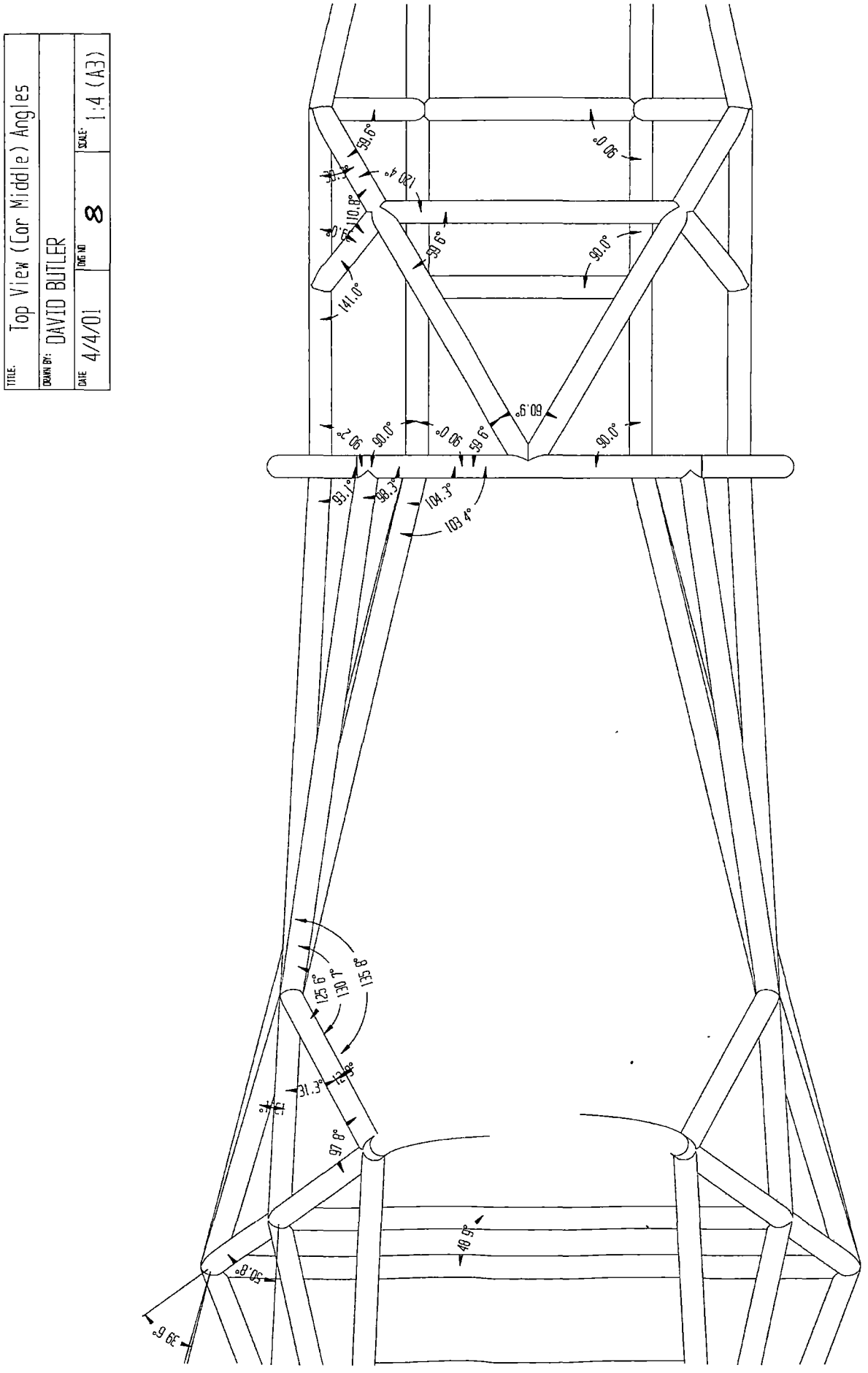

B-13: Front view of frame

TITLE:	Front View
DRAWN BY:	DAVID BUTLER
DATE:	4/4/01
DWG NO.	9
SCALE:	1:5 (A3)

Dimensions are to member edges

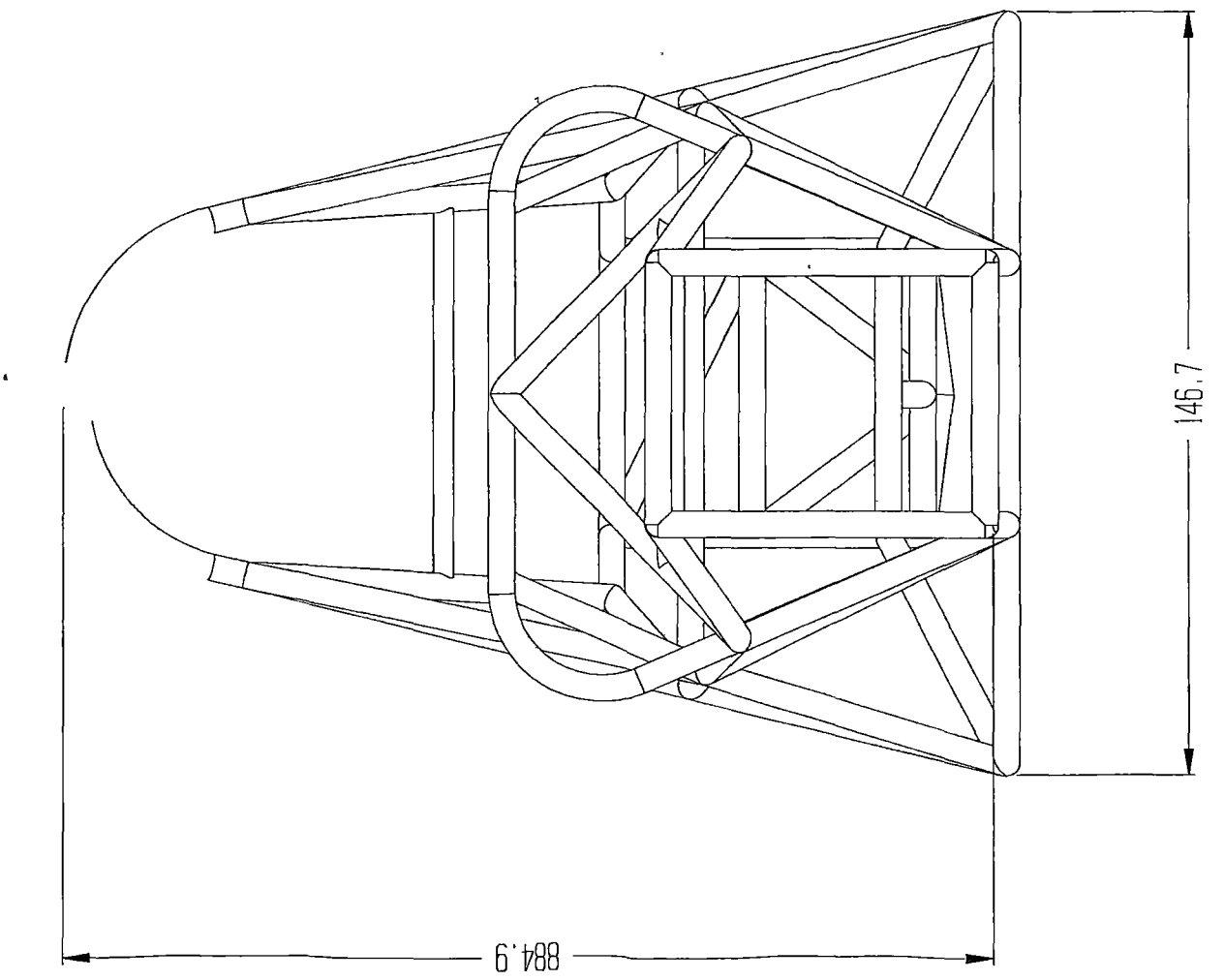

B-14: Roll hoop dimensions

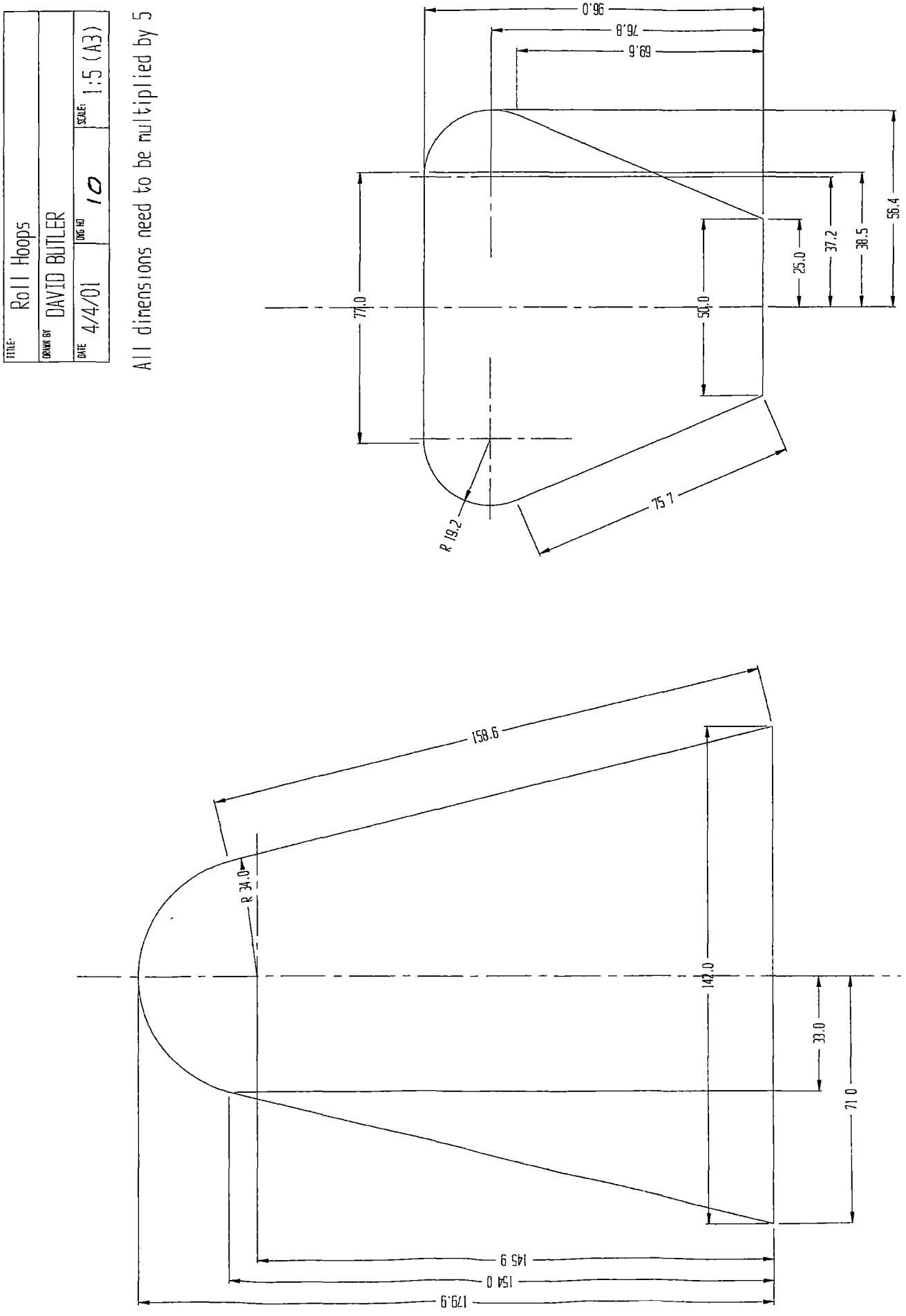

10 APPENDIX C – SUSPENSION DESIGN

C-1: Preliminary front suspension geometry 234

C-2: Front suspension geometry 235

C-3: Preliminary rear suspension geometry 236

C-4: Rear suspension geometry 237

C-5: 7/16" high capacity rod ends 238

C-6: 1/4" aircraft grade rod ends 239

C-7: Suspension spring specifications 240

C-1: Preliminary front suspension geometry

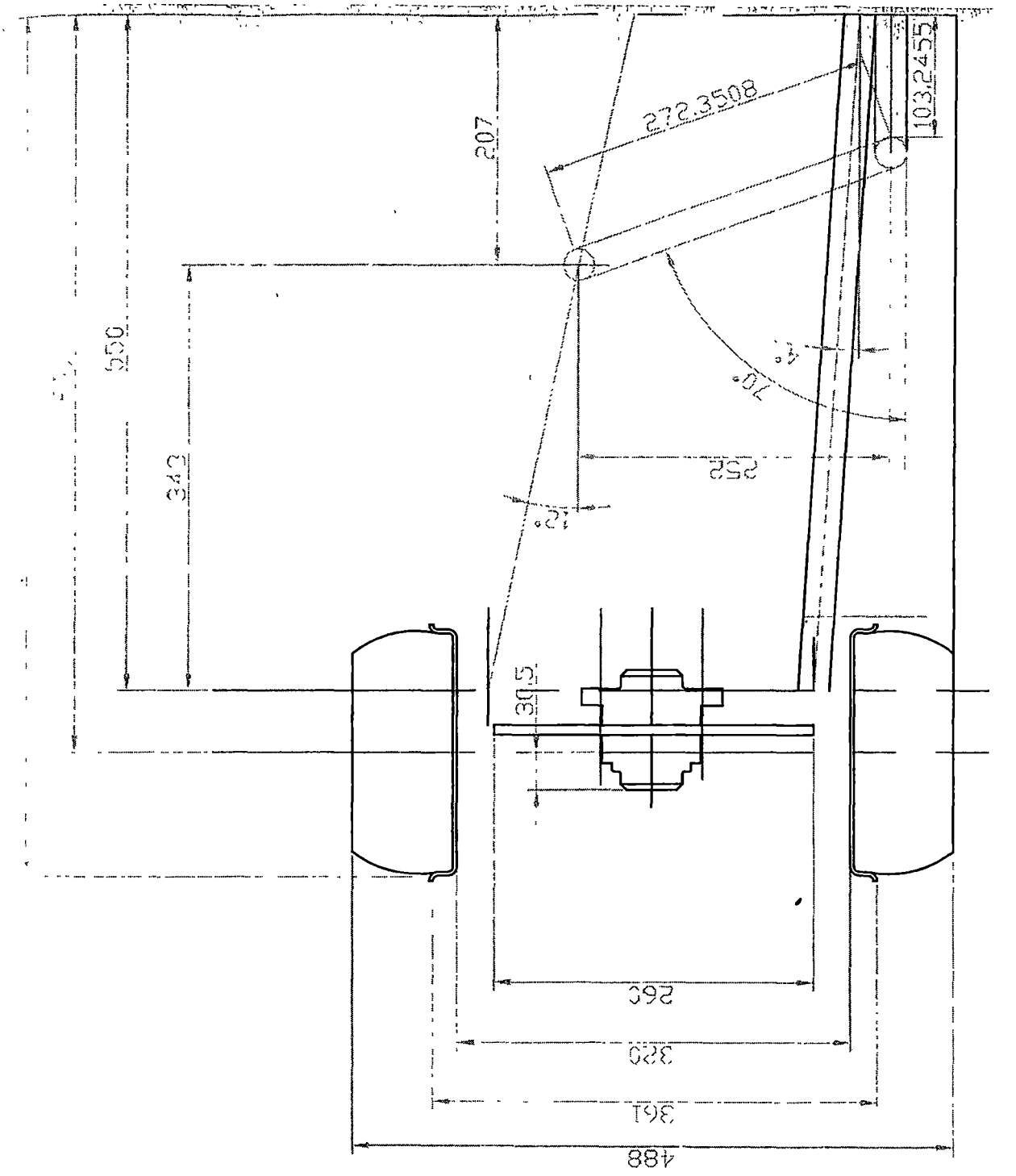

C-2: Front suspension geometry

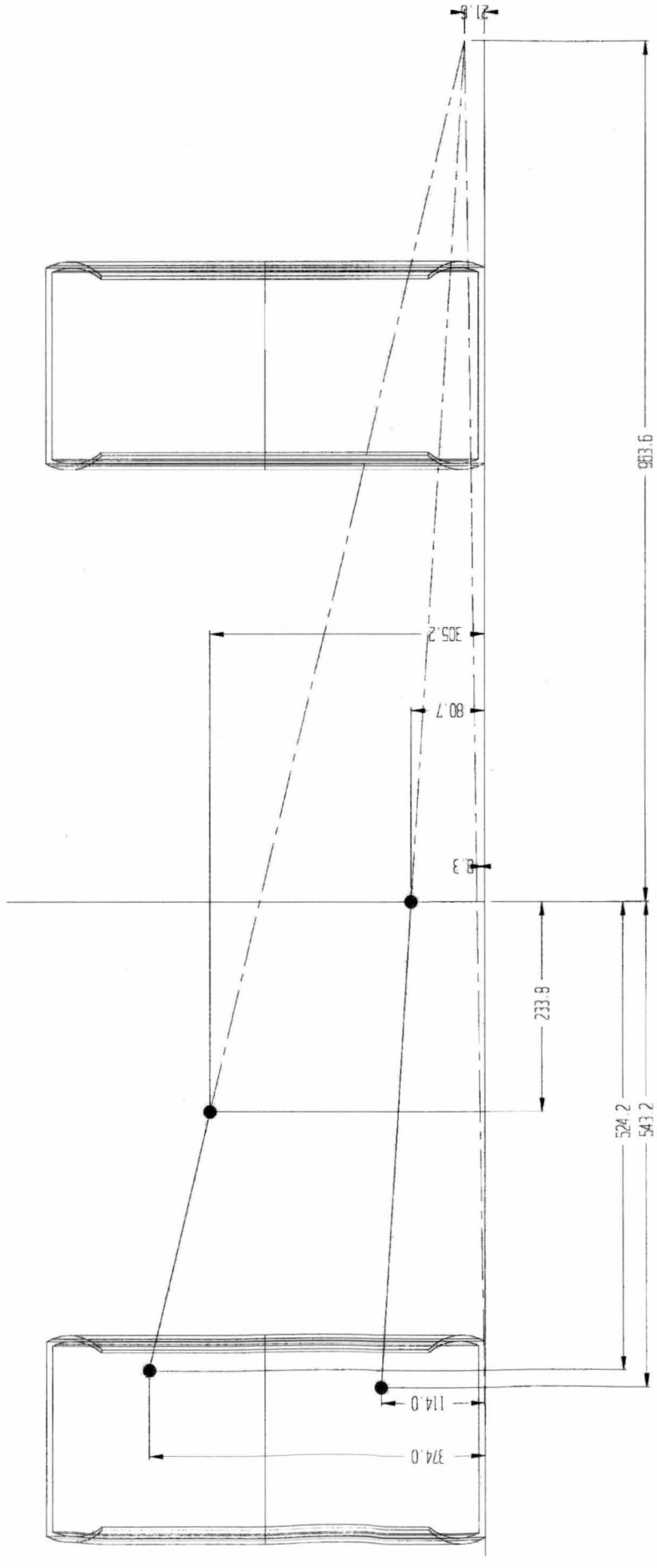

C-3: Preliminary rear suspension geometry

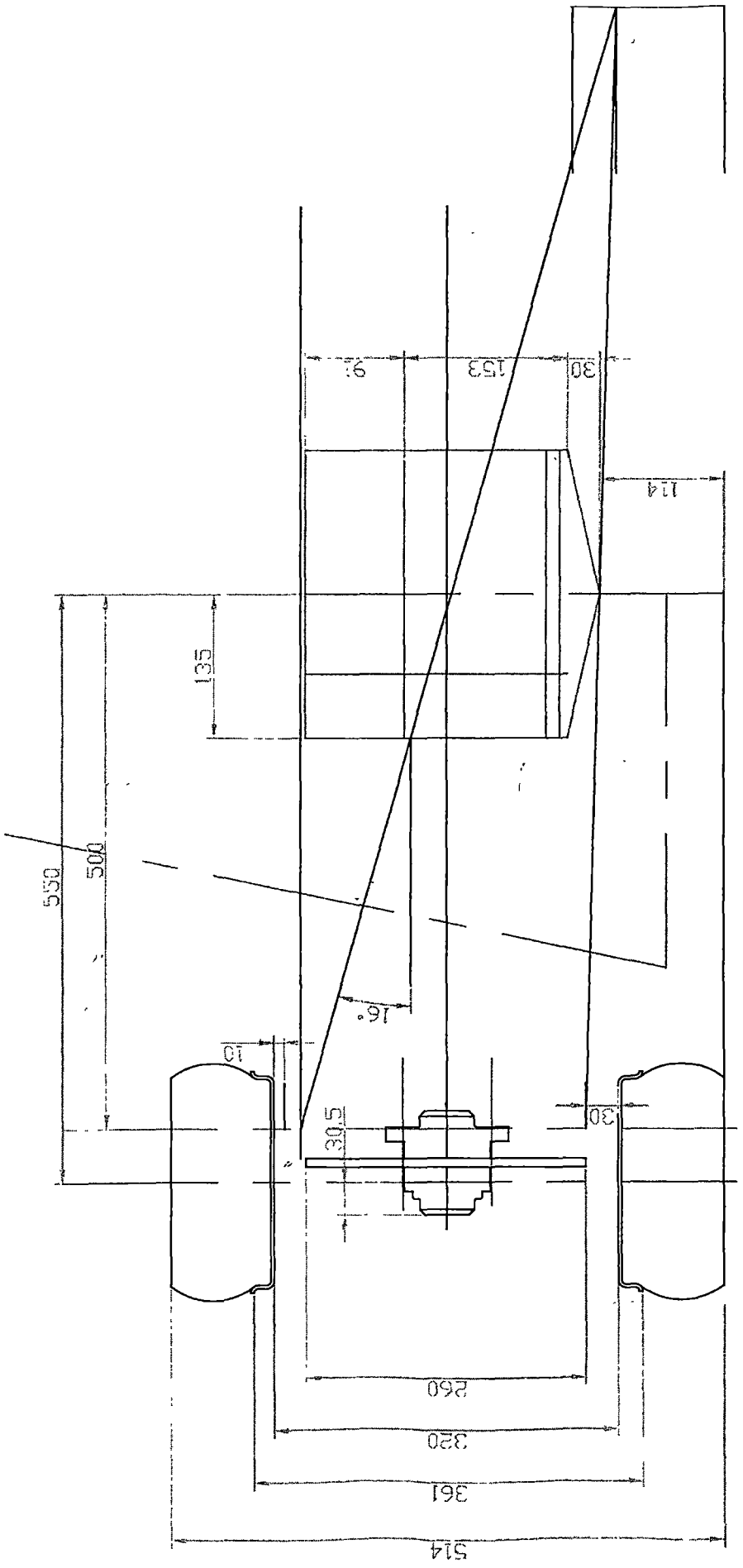

C-4: Rear suspension geometry

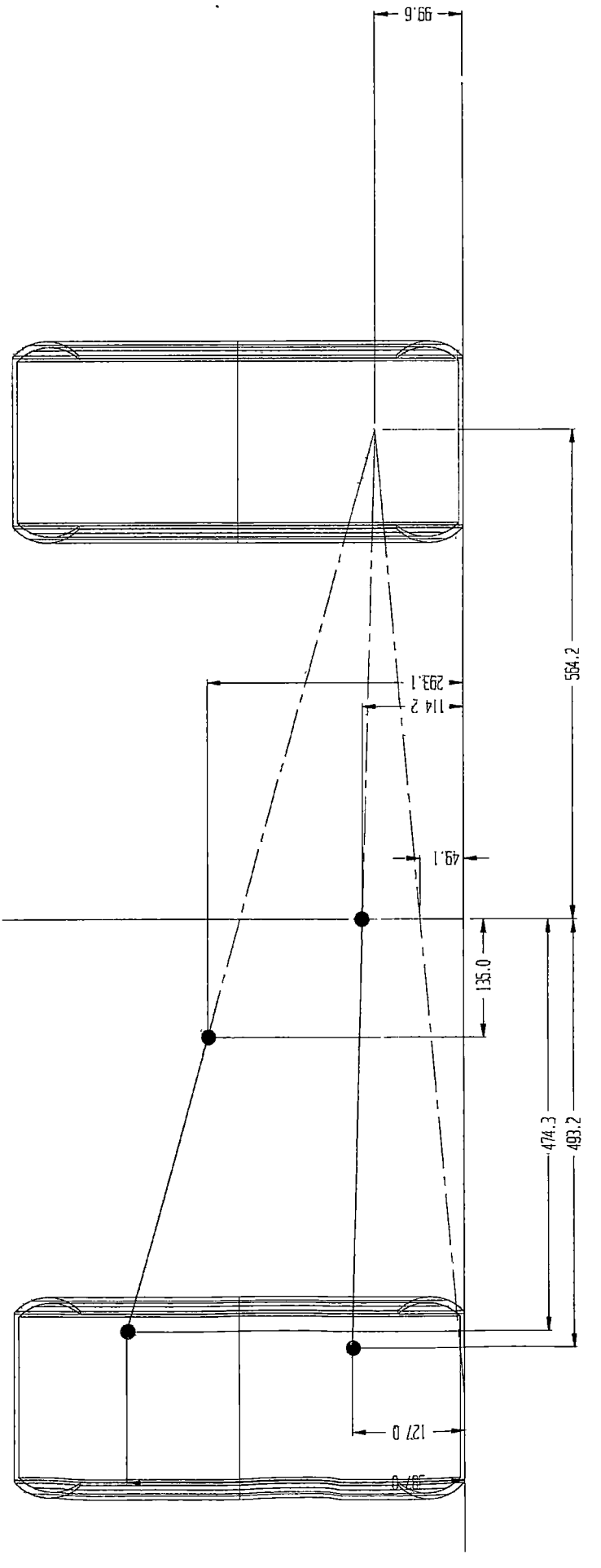

C-5: 7/16" high capacity rod ends

High Capacity Rod Ends

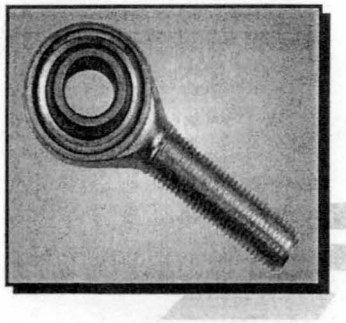

RM SERIES • CHROME MOLY STEEL HOUSING, BALL AND RACE • PLATED FOR CORROSION RESISTANCE

Alinabal's High Capacity Series combines high strength material with three piece construction to produce increased static load ratings.

Materials:

Housing: Chrome moly or low carbon steel - heat treated - plated for corrosion resistance
Ball: Heat treated chrome moly steel - plated for corrosion resistance and wear
Race: Heat treated chrome moly steel - plated for corrosion resistance
Liner: Self lubricating woven Teflon fabric (optional)

Notes:

1. Add letter "L" to prefix to indicate left hand thread (examples: RML-6-X5)
2. Add letter "T" to prefix to indicate permanently bonded Teflon material to the race I.D. (examples: RMLT-6-X5)

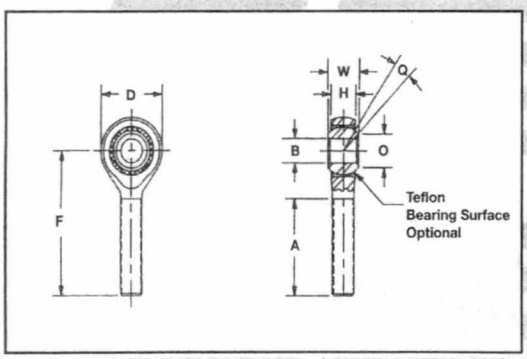

Other variations can be supplied as specials. For additional information and ordering instructions, contact ALINABAL CUSTOMER SERVICE

Rod End Numbers High Capacity (Chrome Moly Steel)	Dimension in Inches										Approx Weight	Ultimate (Radial)Static Load Rating (lbs)
	B	W	H	A	F	D	O	Ball Dia	Thread	Q		
	+.0025 -.0005	±.005	(REF)	±.060	±.030	±.010	(REF)	(REF)	Class UNF-2	(REF)	lbs/ Piece	High Strength
RM-5-X5	.3125	.437	.344	1.250	1.875	.875	.438	.618	5/16-24	±14°	.07	3,940
RM-6-X5	.3750	.500	.406	1.250	1.938	1.000	.508	.713	3/8-24	±15°	.12	6,800
RM-7-X5	.4375	.562	.437	1.375	2.125	1.125	.578	.806	7/16-20	±16°	.16	8,830
RM-8-X5	.5000	.625	.500	1.500	2.438	1.312	.690	.931	1/2-20	±16°	.24	13,990
RM-8/6-X5	.3750	.500	.406	1.500	2.438	1.312	.508	.713	1/2-20	±15°	.24	20,850
RM-10-X5	.6250	.750	.562	1.625	2.625	1.500	.801	1.098	5/8-18	±15°	.38	16,110
RM-10/8-X5	.5000	.625	.500	1.625	2.625	1.500	.690	.931	5/8-18	±16°	.38	26,280
RM-12-X5	.7500	.875	.687	1.750	2.875	1.750	1.010	1.336	3/4-16	±12°	.65	21,950
RM-12/10-X5	.6250	.750	.562	1.750	2.875	1.750	.801	1.098	3/4-16	±12°	.65	35,900

C-6: 1/4" aircraft grade rod ends

LINEAR BEARINGS PTY LTD

IMPERIAL ROD ENDS MALE

Bronze lined	Nylon lined	Steel on steel	Teflon lined heavy duty aircraft quality	Teflon lined light duty stainless steel	Basic size reference	Eye diameter	UNF thread diameter	Thread length	Centre of eye to thread end	Head diameter	O/A ball width	Studded see page 2	
						d	g x pitch	G	H	D	B	P	K
VM-G	PM-G	AM-G	ART-E	AHMT	* 3	3/16	3/16 X 32	.750	1.250	.750	.312	.500	.500
					* 4	1/4	1/4 X 28	1.000	1.562	.750	.375	.500	.562
					5	5/16	5/16 X 24	1.250	1.875	.875	.437	.562	.687
					6	3/8	3/8 X 24	1.250	1.938	1.000	.500	.625	.875
					7	7/16	7/16 X 20	1.375	2.125	1.125	.562	.875	1.125
					8	1/2	1/2 X 20	1.500	2.438	1.312	.625	.875	1.125
					10	5/8	5/8 X 18	1.625	2.625	1.500	.750	1.000	1.500
					12	3/4	3/4 X 16	1.750	2.875	1.750	.875	1.250	1.812
					16	1	1¼ X 12	2.375	4.125	2.750	1.375	-	-

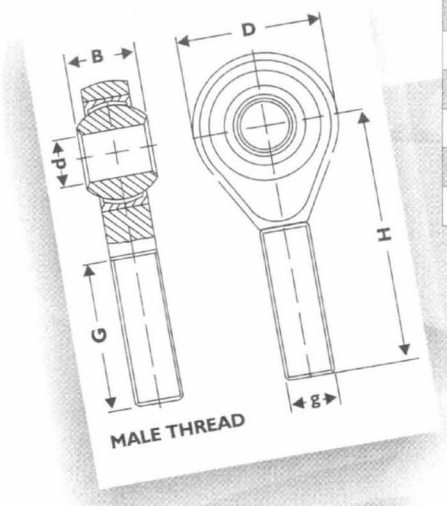

* For ART-E sizes 3 & 4 thread is .312 diameter x 24TPI

Ordering example: **VM10G** (Bronze lined, male, right hand 5/8" basic size)
For left hand versions add **L** to prefix letters **VML10G.**

IMPERIAL ROD ENDS FEMALE

Bronze lined	Nylon lined	Steel on steel	Teflon lined light duty stainless steel	Basic size reference	Eye diameter	UNF thread diameter	Thread length	Centre of eye to thread end	Head diameter	O/A ball width	Studded see page 2	
					d	g x pitch	G1	H1	D	B	P	K
VF-G	PF-G	AF-G	AHFT	3	3/16	3/16 X 32	.562	1.062	.750	.312	.500	.500
				4	1/4	1/4 X 28	.750	1.312	.750	.375	.500	.562
				5	5/16	5/16 X 24	.750	1.375	.875	.437	.562	.687
				6	3/8	3/8 X 24	.937	1.625	1.000	.500	.625	.875
				7	7/16	7/16 X 20	1.062	1.812	1.125	.562	.875	1.125
				8	1/2	1/2 X 20	1.87	2.125	1.312	.625	.875	1.125
				10	5/8	5/8 X 18	1.500	2.500	1.500	.750	1.000	1.500
				12	3/4	3/4 X 16	1.750	2.875	1.750	.875	1.250	1.812
				**16	1	1¼ X 12	2.125	4.125	2.750	1.375	-	-

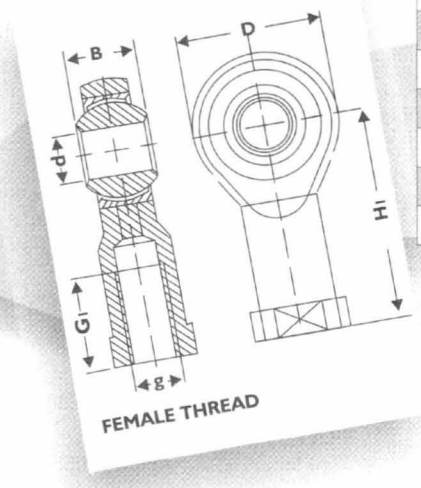

** 1" x 12 UNF thread also available. Please enquire

Ordering example: **PF8G** (Nylon lined, female, 1/2" basic size)
For left hand versions add **L** to prefix letters. **PFL8G.**

C-7: Suspension spring specifications

RST 58

Coil spring with internal hydraulic floating piston

A6061-T6 aluminum body

Spring pre-load adjustment

Spring standard color : black

	58
COMPRESS DAMPING ADJUSTMENT	YES
COMPRESS LOCKOUT	YES
REBOUND DAMPING ADJUSTMENT	YES
EYE TO EYE LENGHT	155mm~190mm
TRAVEL	26mm~37mm

RST 58

★This information is for reference Only. please contact RST local agent or RST web site to get fully product information.

No	Description	Qty
1	Body pivot	1
2	Pivot spacer	4
3	Spring collar	1
4	Shaft pivot	1
5	Adjuster knob	1
6	Adjuster screw	1
7	Spring	1
8	Spring retainer	1

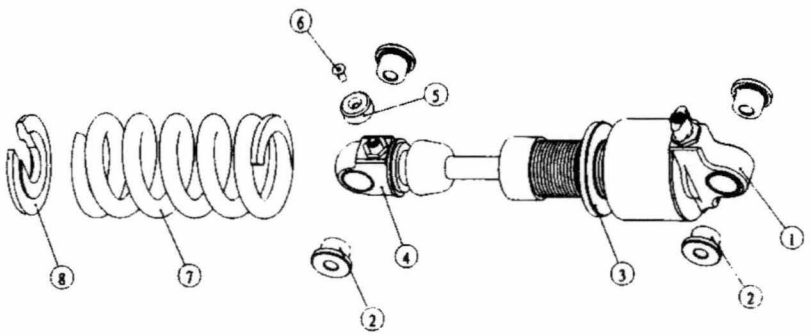

11 APPENDIX D – WHEEL ASSEMBLY

D-1: Brake aluminium rotor dimensions 242

D-2: Brake caliper aluminium rotor pad dimensions 242

D-3: Brake caliper dimensions 243

D-4: Stub axle (30mm dia.) FEA for centred bearing design 244

D-5: Stub axle (35mm dia.) FEA for off centre bearing design 244

D-6: FEA stub axle bearing loads for centred design 245

D-7: FEA stub axle bearing loads for off centre design 245

D-8: Upright dimensions 246

D-9: Oil seal dimensions 247

D-10: Stub axle dimensions 248

D-11: Wheel hub dimensions 249

D-12: King pin and caster reference angles 250

D-1: Brake aluminium rotor dimensions

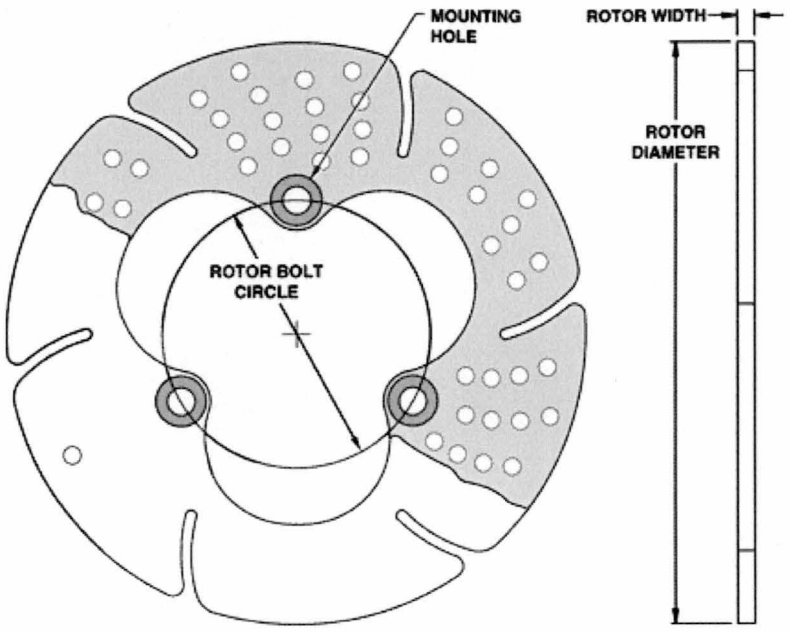

D-2: Brake caliper aluminium rotor pad dimensions

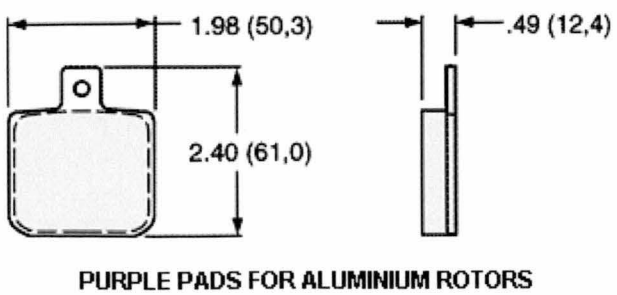

D-3: *Brake caliper dimensions*

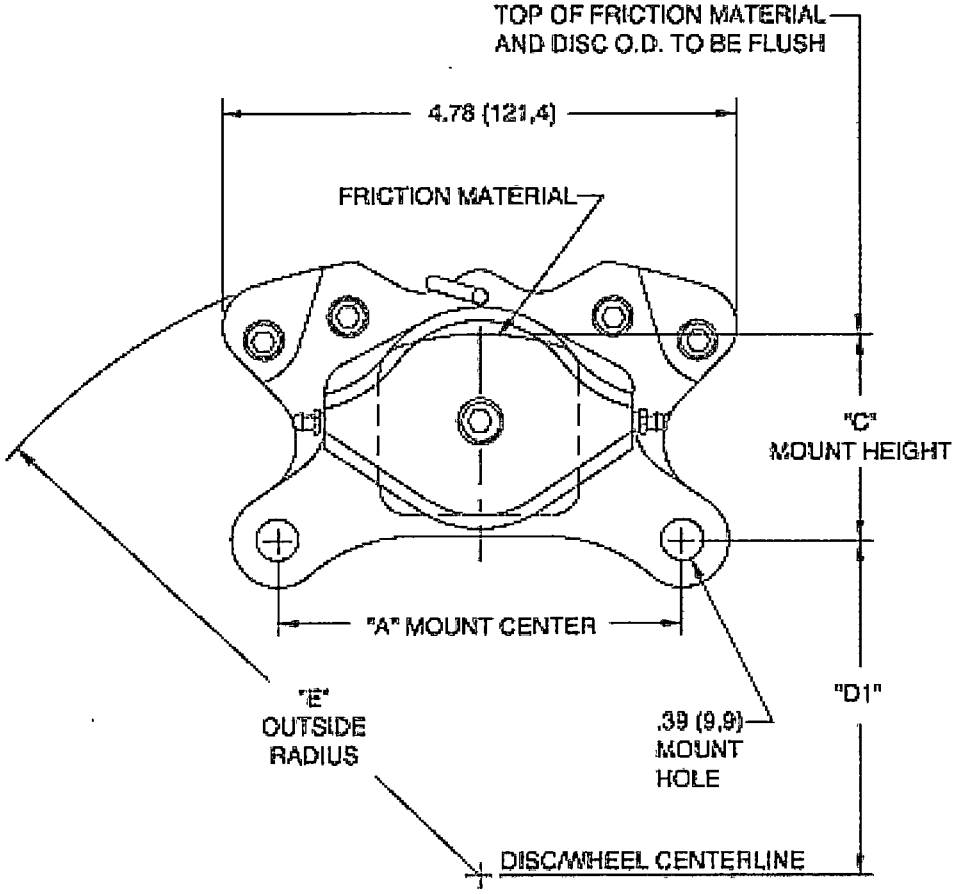

DIMENSION "D1" =
(DISC DIAMETER/2) - "C" MOUNT HEIGHT

BORE SIZE	DISC WIDTH	MOUNTING
44.5mm	9.7mm	95.3mm

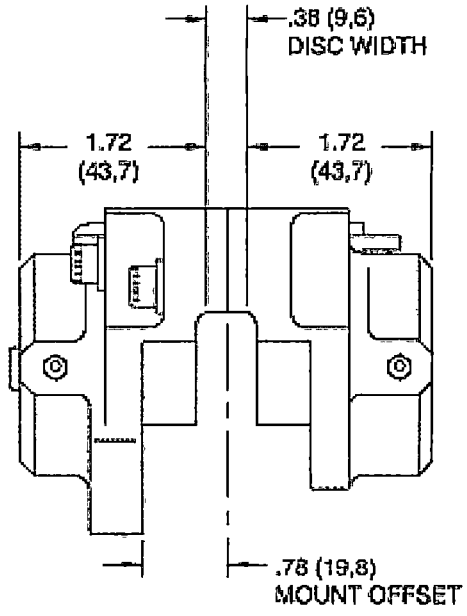

"A" MOUNTING CENTER	"C" MOUNTING HEIGHT
3.25 (82,6)	1.92 (48,8)
3.75 (95,3)	1.92 (48,8)

DISC DIAMETER	"E" OUTSIDE RADIUS
10.00 (254,0)	5.84 (148,3)
10.25 (260,4)	5.96 (151,4)
10.50 (266,7)	6.07 (154,2)
11.00 (279,4)	6.31 (160,3)

D-4: Stub axle (30mm dia.) FEA for centred bearing design

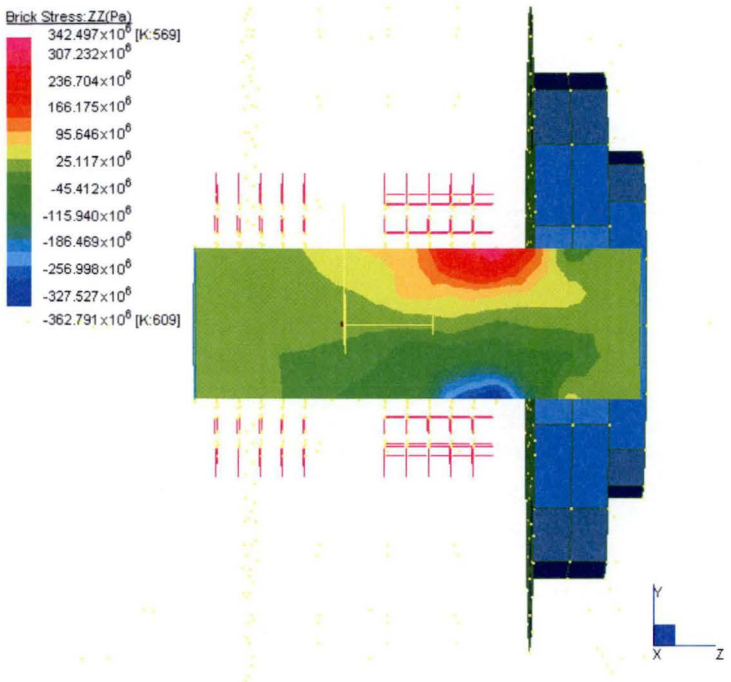

D-5: Stub axle (35mm dia.) FEA for off centre bearing design

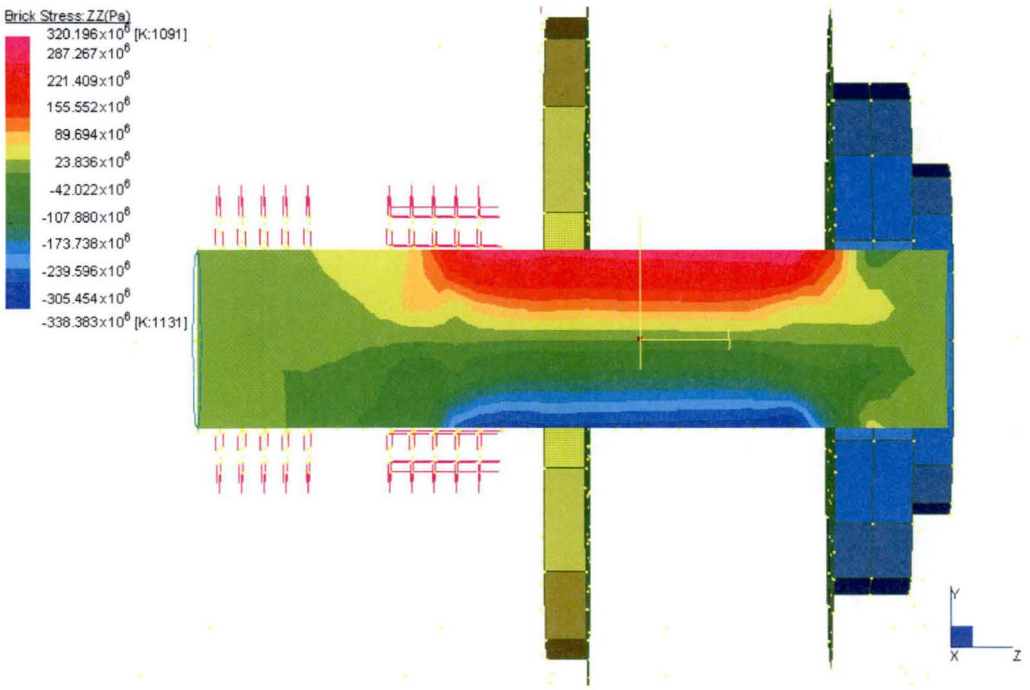

D-6: FEA stub axle bearing loads for centred design

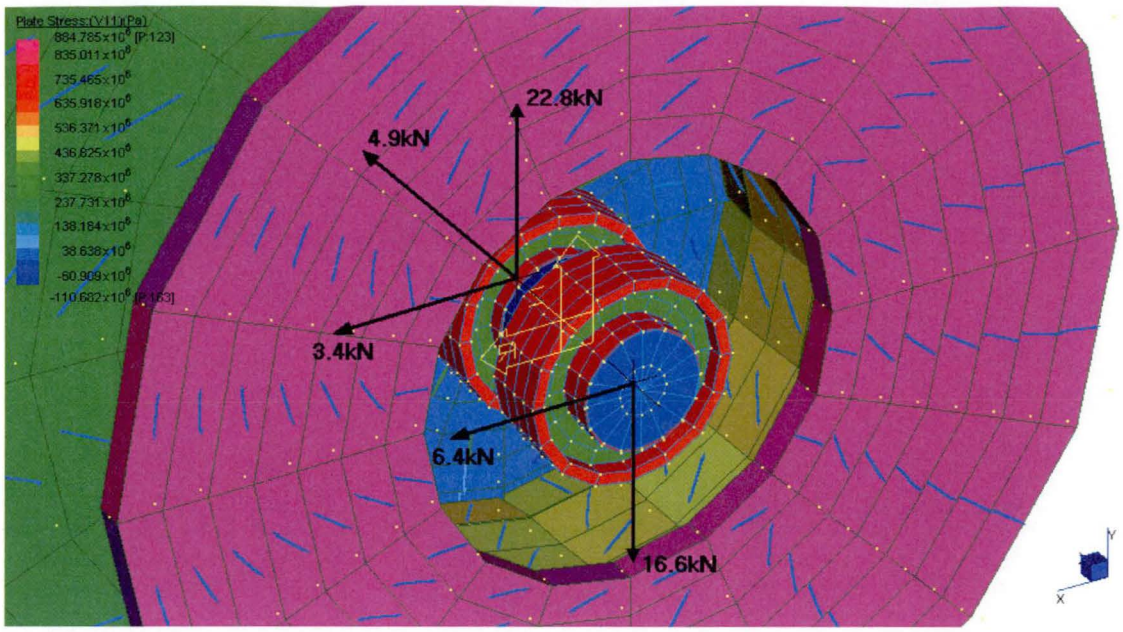

D-7: FEA stub axle bearing loads for off centre design

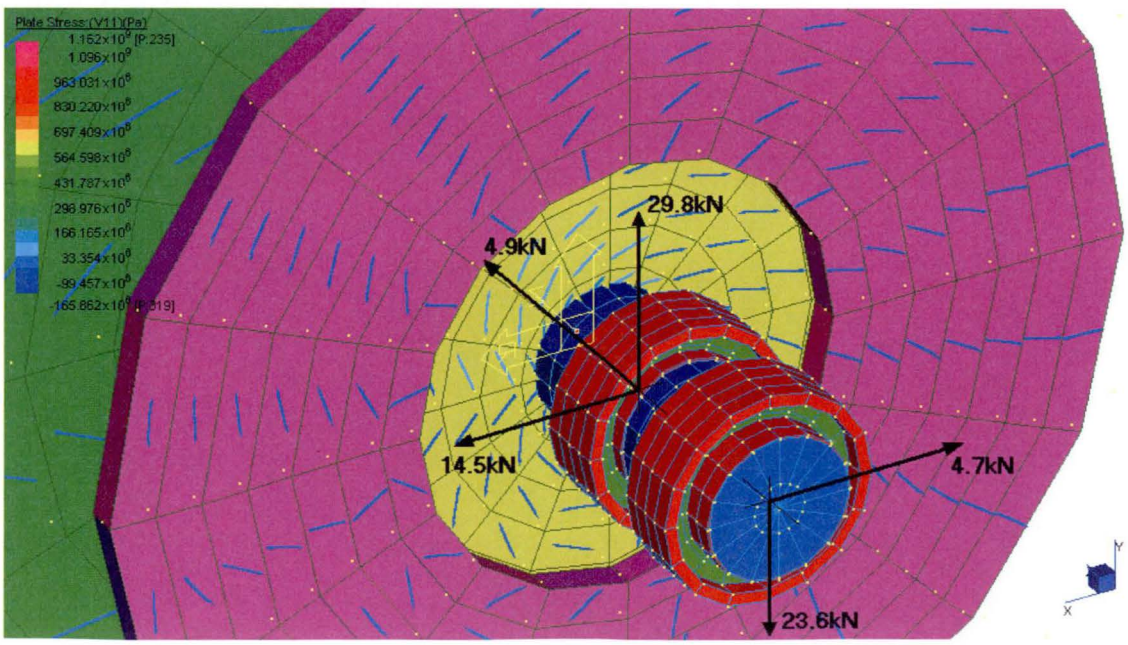

D-8: Upright dimensions

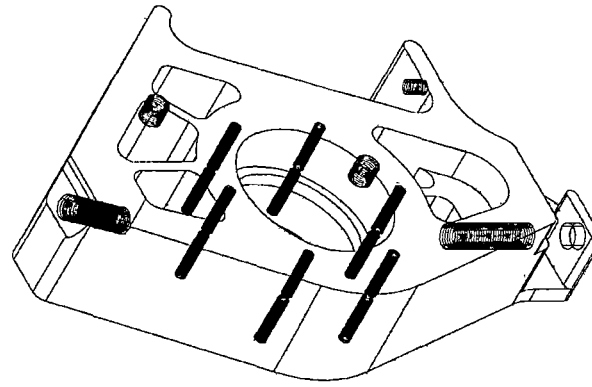

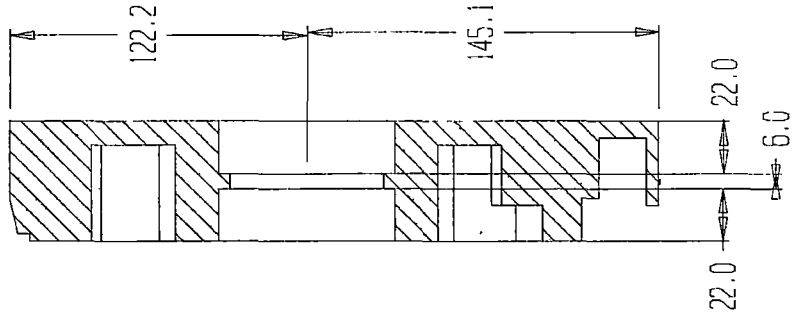

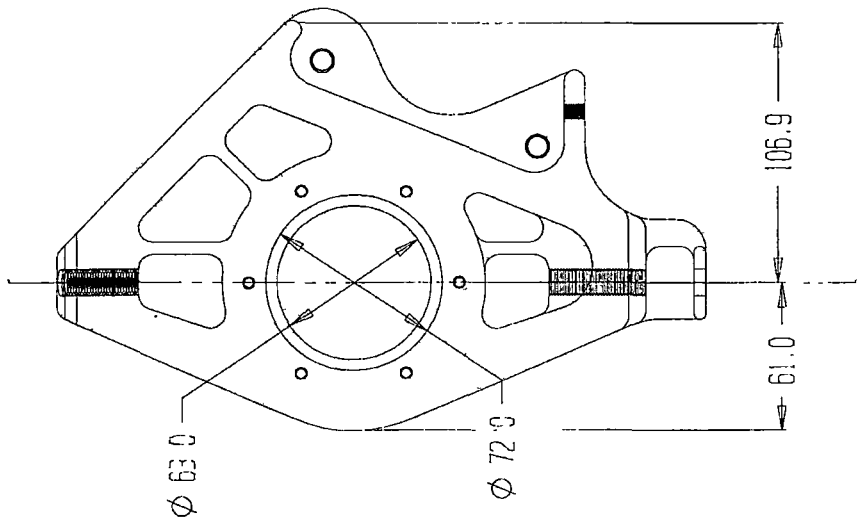

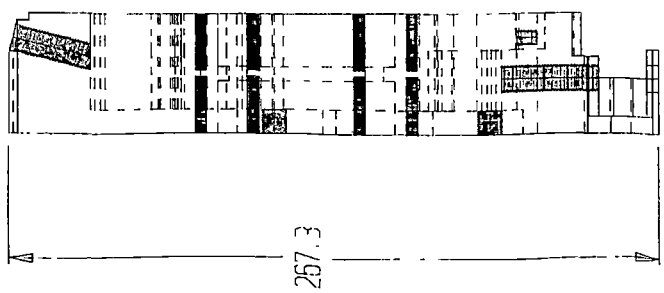

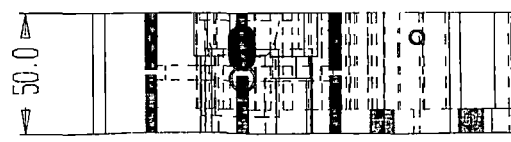

TITLE	Upright		
DRAWN BY	DAVID BUTLER		
DATE	15/5/01	DWG NO.	1
		SCALE	1.2

Bearing [illegible] Tolerence M7
(0 to -0.025 mm on diameter)

D-9: Oil seal dimensions

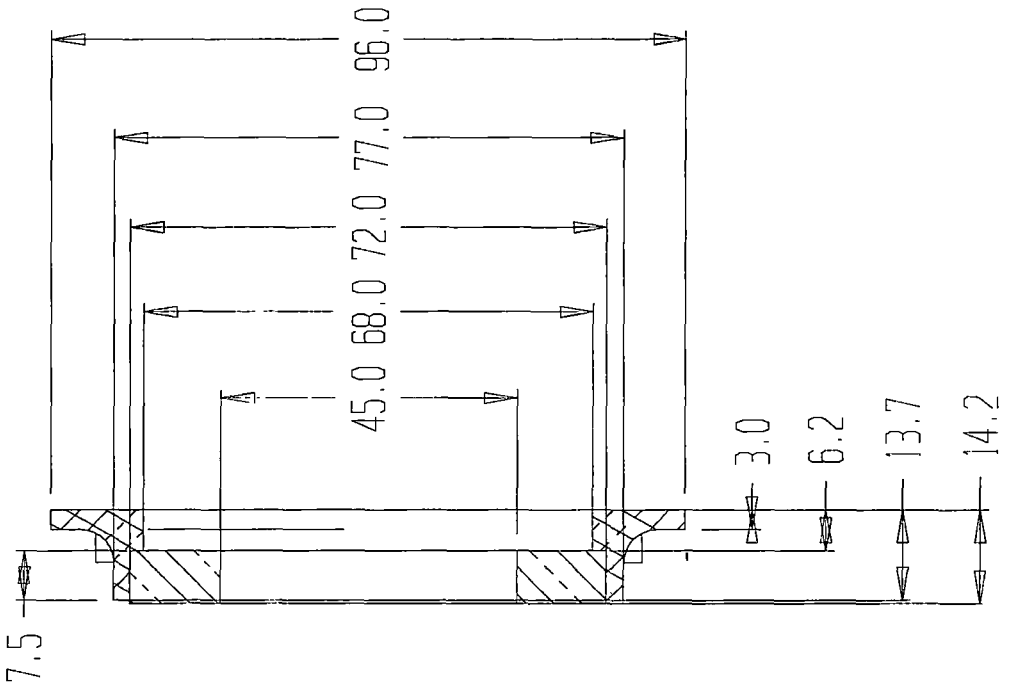

TITLE:	Oil Seal
DRAWN BY	DAVID BUTLER
DATE:	6/6/01
DWG NO.	2
SCALE:	1:1 (A4)

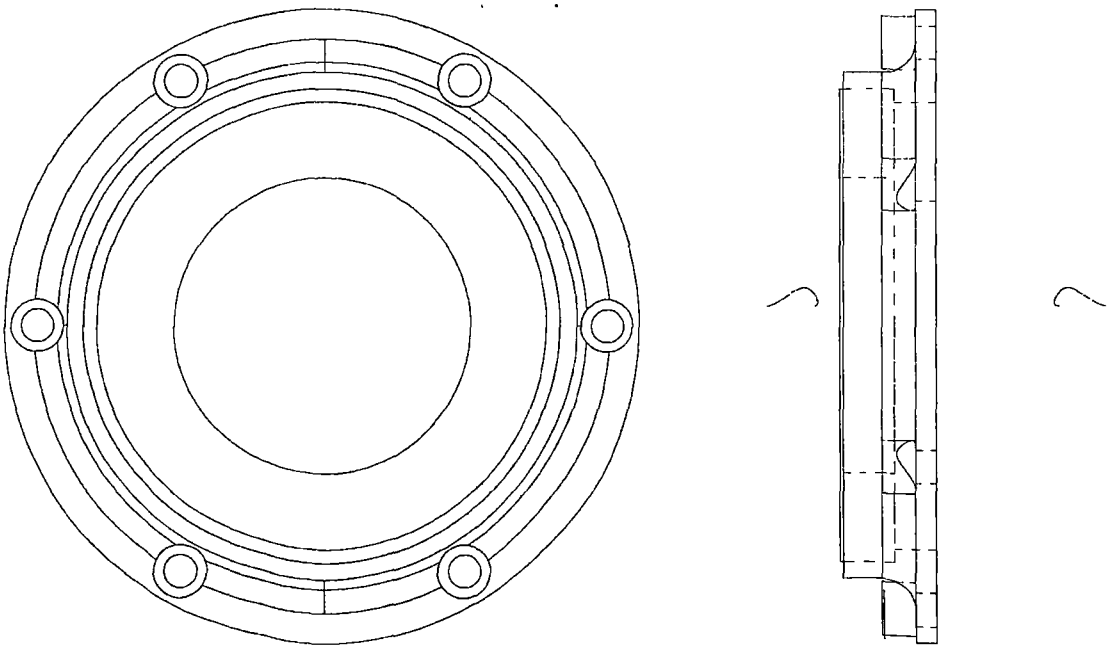

D-10: Stub axle dimensions

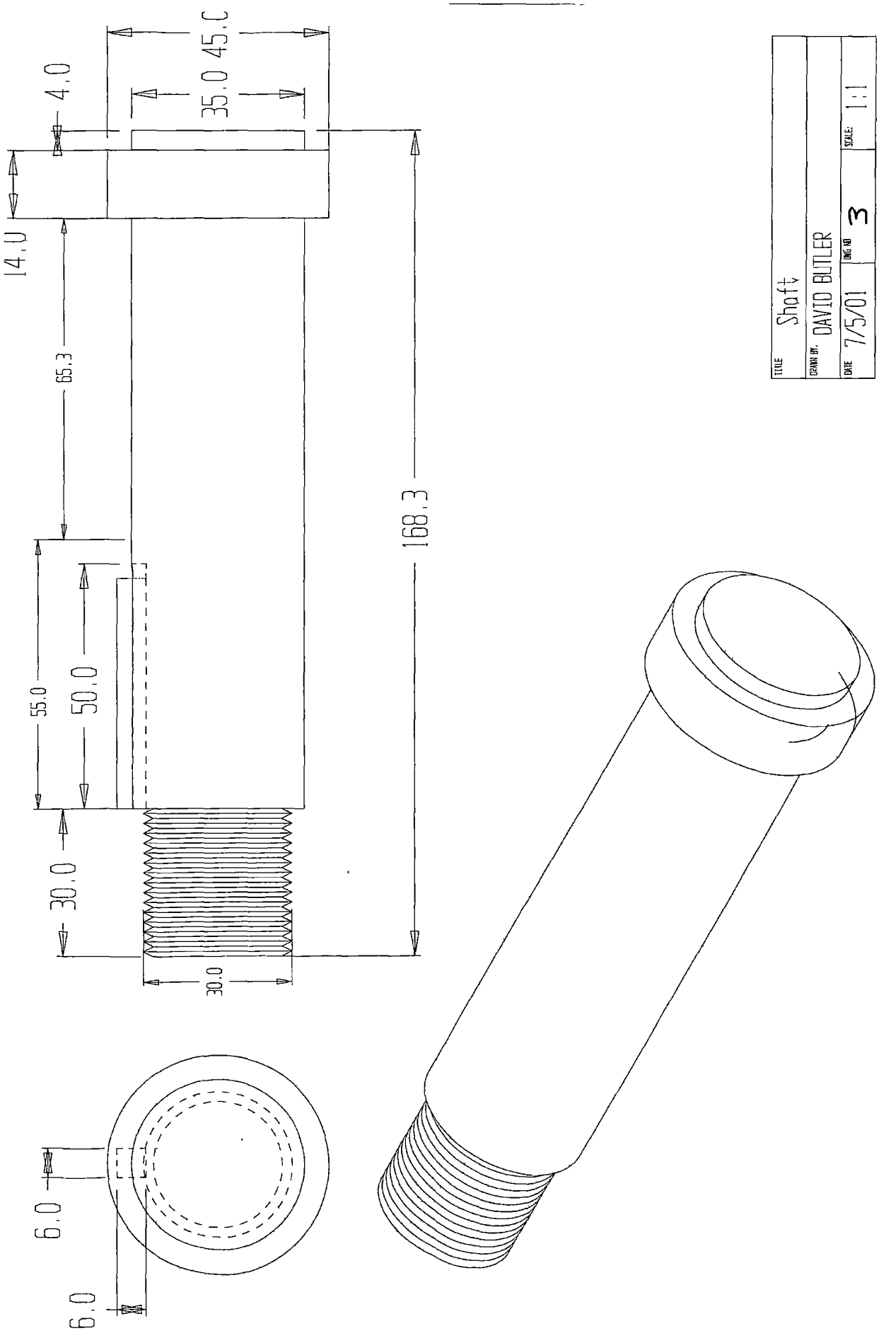

D-11: Wheel hub dimensions

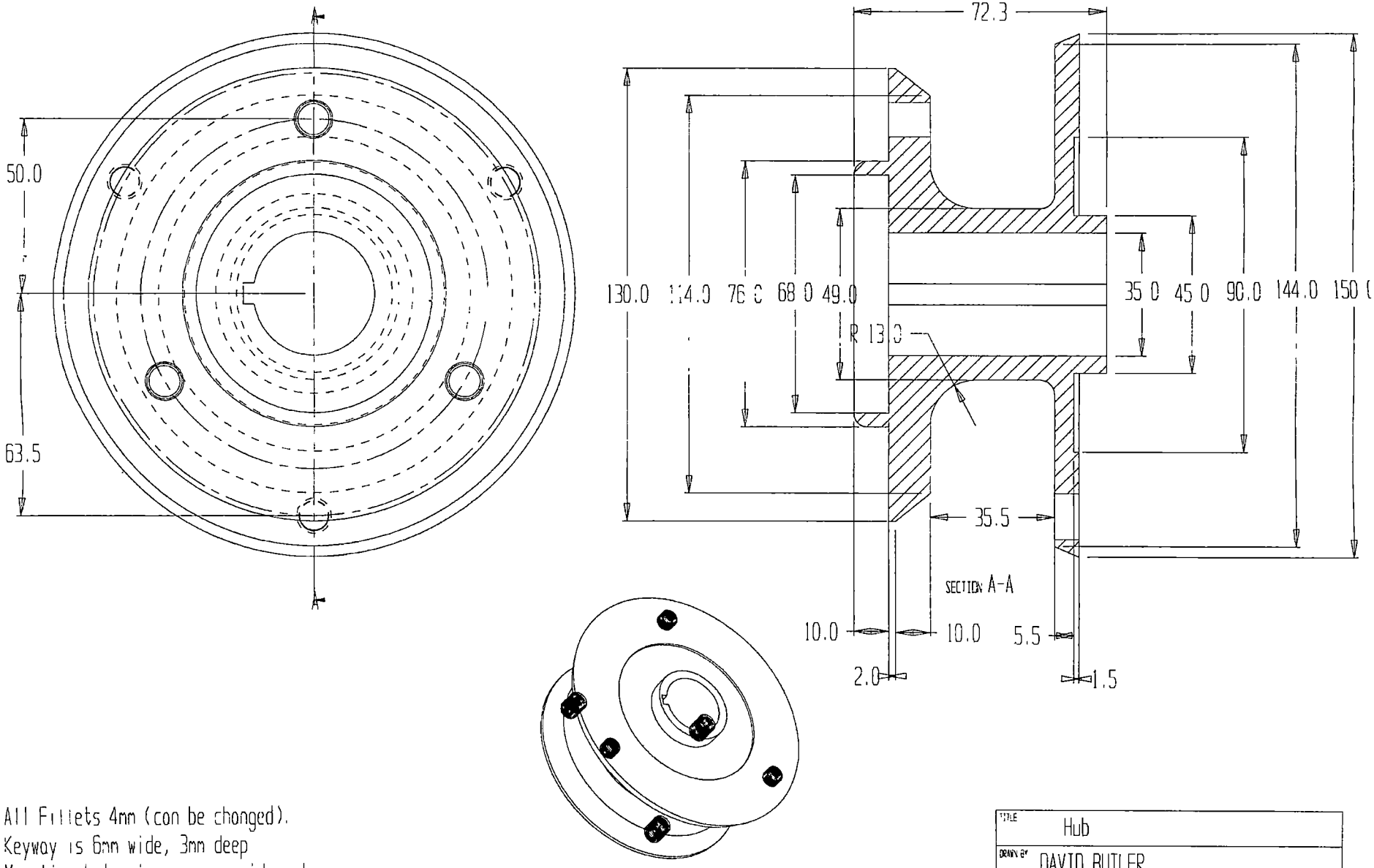

All Fillets 4mm (can be changed).
Keyway is 6mm wide, 3mm deep
Mounting hole sizes are a guide only
Hub inner hole to Clearance G6 (about +0.01mm on diameter).

TITLE: Hub		
DRAWN BY: DAVID BUTLER		
DATE: 6/6/01	DWG NO.: 4	SCALE: 1:1

D-12: King pin and caster reference angles

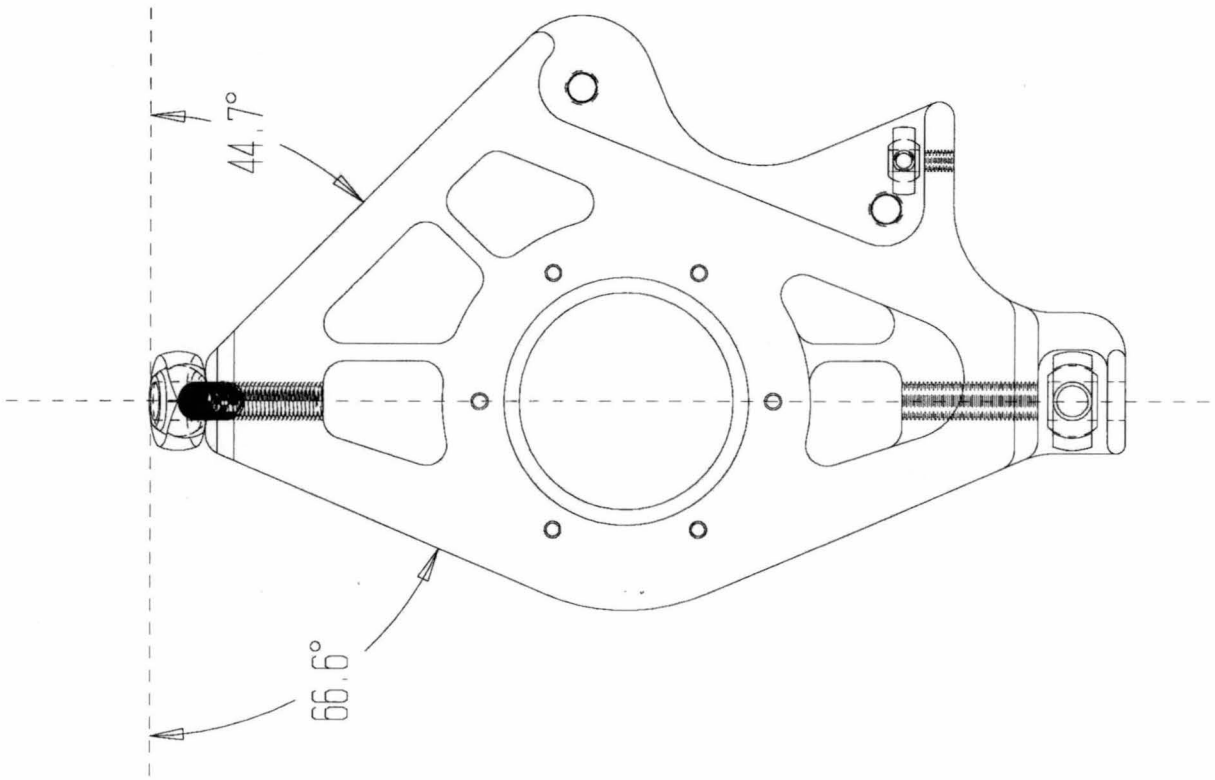

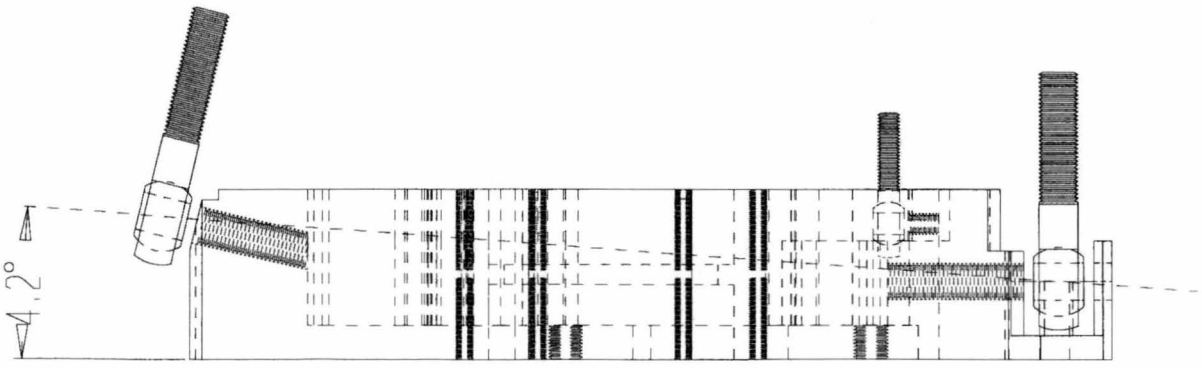

12 APPENDIX E – BRAKE PEDAL ASSEMBLY

E-1: Brake pedal dimensions with balance bar 251

E-2: Brake master cylinder dimensions 252

E-1: Brake pedal dimensions with balance bar

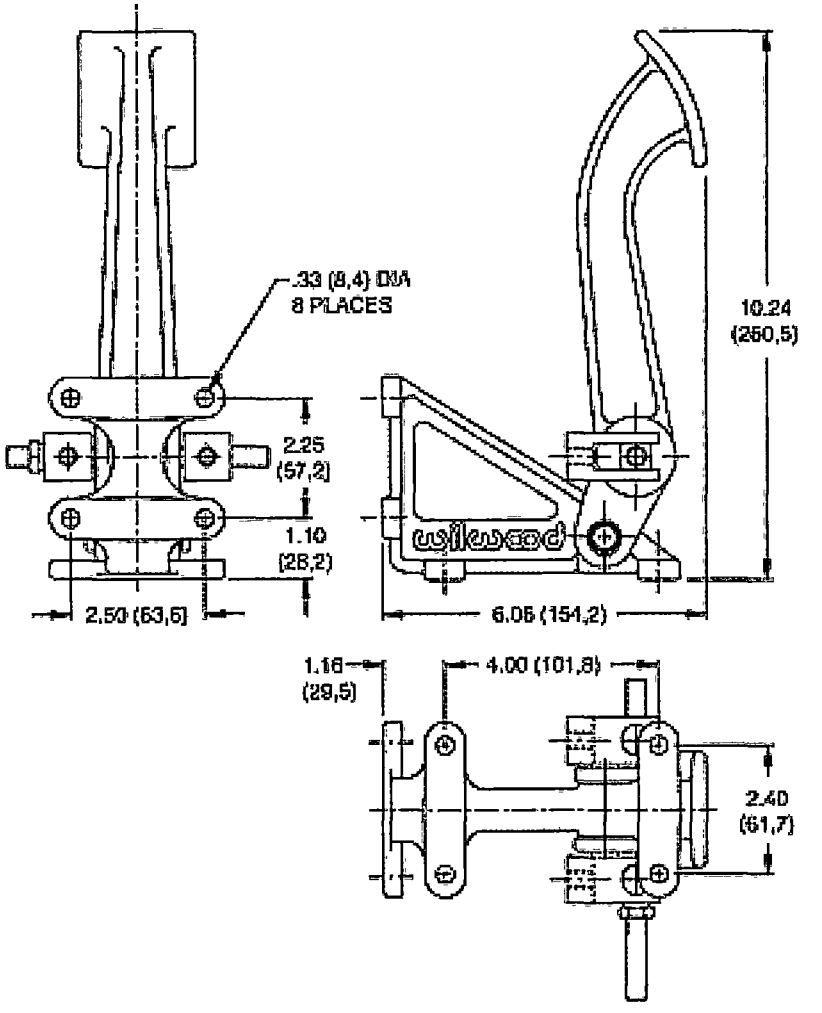

E-2: Brake master cylinder dimensions

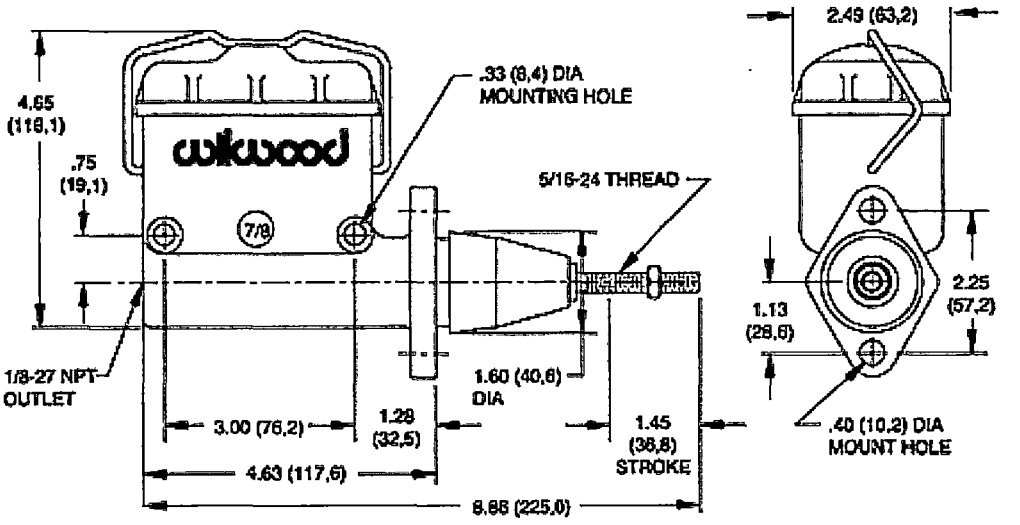

13 APPENDIX F – DRIVETRAIN DESIGN

F-1: Gearbox specifications 253

F-2: Clutch assembly exploded view 254

F-3: Transmission exploded view 255

F-4: Quaife ATB differential description 256

F-5: Quaife ATB differential operation 257

F-6: Quaife ATB differential specifications 258

F-7: Quaife ATB differential dimensions 259

F-8: Composite disc dimensions 260

F-1: Gearbox specifications

Drive Train:		
Primary reduction system:		
Type		Gear
Reduction ratio		2.022 (89/44)
Clutch type		Wet multi disc
Transmission:		
Type		6-speed, constant mesh, return shift
Gear ratios:		
	1st	2.923 (38/13)
	2nd	2.062 (33/16)
	3rd	1.631 (31/19)
	4th	1.380 (29/21)
	5th	1.217 (28/23)
	6th	1.083 (26/24)
Final drive system:		
Type		Chain drive
Reduction ratio		2.666 (40/15)
Overall drive ratio		5.843 @Top gear

F-2: Clutch assembly exploded view

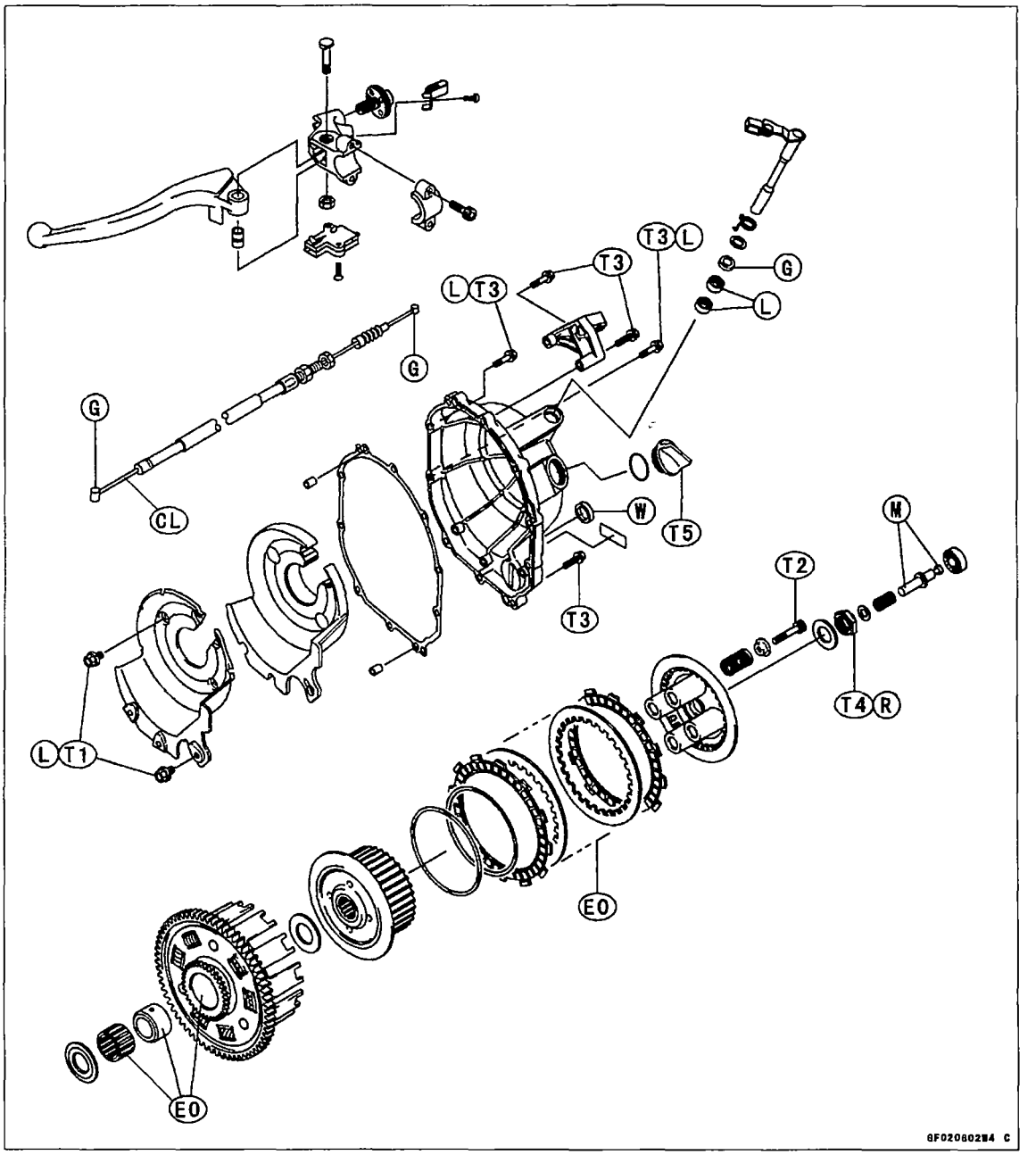

CL: Apply cable lubricant.
G: Apply grease.
EO: Apply engine oil.
L: Apply a non-permanent locking agent
M: Apply molybdenum disulfide grease.
R: Replacement Parts
W: Apply water.

T1: 5.9 N·m (0.60 kg·m, 52 in·lb)
T2: 8.8 N·m (0.90 kg·m, 78 in·lb)
T3: 12 N·m (1.2 kg·m, 104 in·lb)
T4. 130 N·m (13.5 kg·m, 98 in·lb)
T5: 1.5 N·m (0.15 kg·m, 13 in·lb) or Hand-Tight

F-3: Transmission exploded view

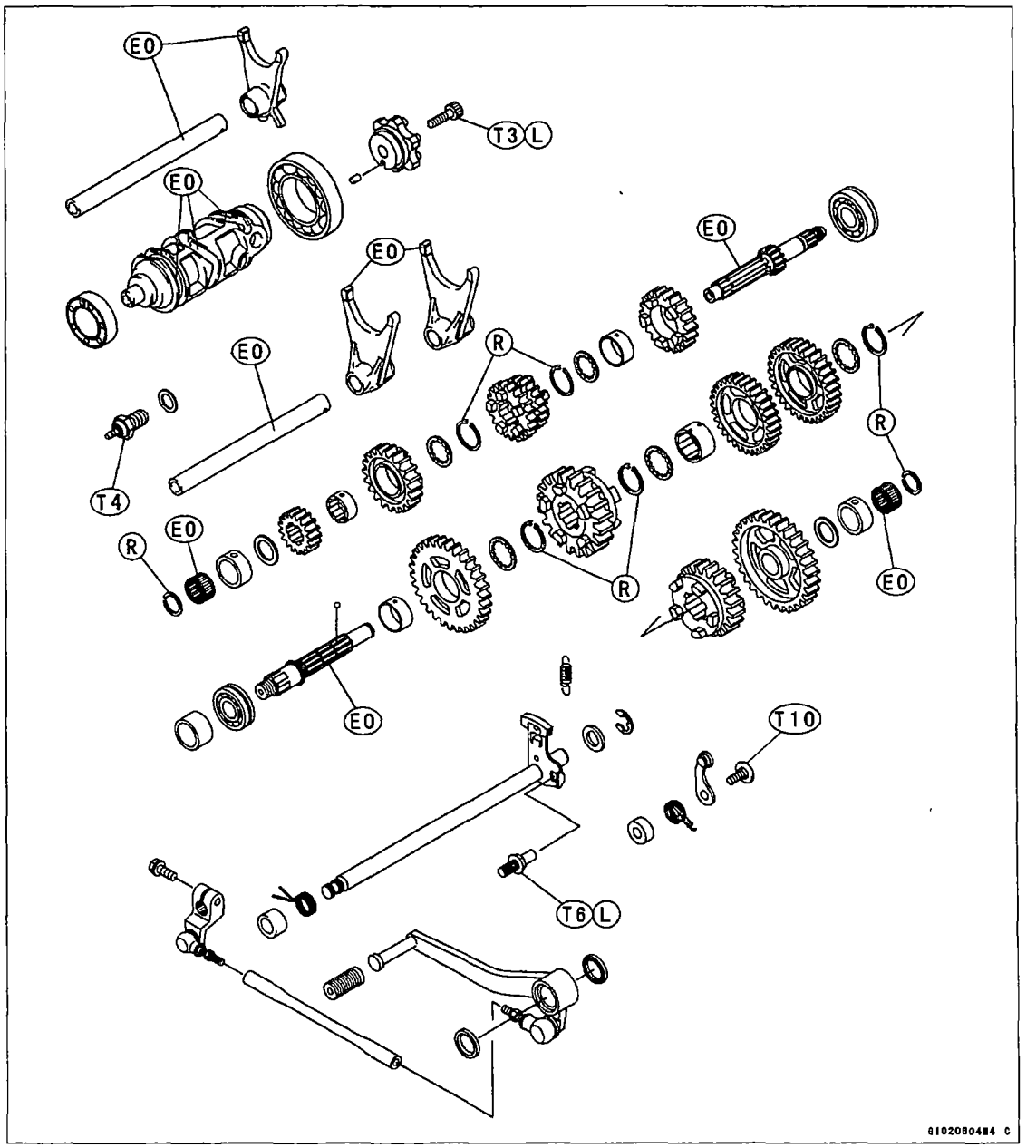

D: Do not apply any grease or oil
G: Apply grease.
L: Apply a non-permanent locking agent.
M: Apply molybdenum disulfide grease.
SS: Apply silicone sealant (56019–120).
LG: Apply silicone sealant (92104–1063).
EO: Apply engine oil.
R: Replacement parts.
S: Tighten the fasteners following the specified sequence.

Quaife Automatic Torque Biasing Differential for Added Traction

Design

The Quaife ATB Differential is designed to prevent the complete loss of drive that occurs with a conventional differential when one wheel slips.

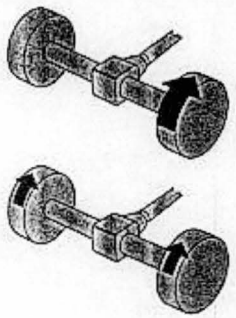

Whilst requiring some torque in the slipping wheel the Quaife unit is progressive in action but never locks - controlled power is transmitted to all the driving wheels. Although ideally suited to high-powered front-wheel drive systems, Quaife ATB differentials are used in rear and four-wheel drive vehicles where optimum traction is required. The four-wheel drive layout includes a centre differential as well as one in each axle.
The torque capacity of the Quaife unit is increased or decreased by varying the helix and pressure angles of the gear teeth. A combination is available to meet user requirements varying from Formula One racing to high mileage Ambulance fleets.
The operation is automatic, normal axle lubrication is retained and the unit is interchangeable with the conventional differential.

Operation

The Quaife Differential is an automatic gear-operated Torque Biasing Differential. Sets of floating helical gear pinions (1) mesh to provide the normal speed differential action. To pre-load the gear packs there is a selection of centre spring discs (2) available. In the event of wheel slip torque bias is generated by the axial and radial thrusts (red) of the pinions in the pockets (3). The resultant friction force enables the driving road wheel and sun-gear (4) to transmit a greater proportion of the torque. This effect is progressive, but at no stage does the differential lock solid. Hence the inherent safety of the Quaife Automatic Torque Biasing Differential.

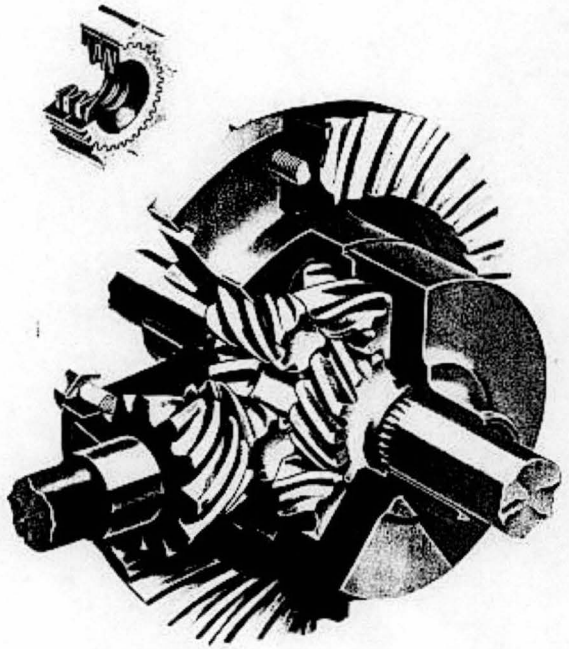

Fitting and Maintenance

Installation is identical to the normal differential with bearing pre-loads and pinion mesh being restored to the original manufacturers' recommendation. Servicing of the unit is simple as all gear pinions are free fitting and normal final drive lubrication oils are retained. Due to the internal design of the Quaife differential, all driving wheels must be elevated when servicing brakes, tyres, etc.

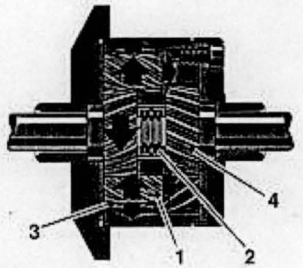

KEY
1 Helical gear pinions
2 Centre spring discs
3 Pocket
4 Sun Gear

Applications

Quaife differentials are used in all forms of motor sport from circuit to rallying in two and four-wheel drive systems. A wide variety of emergency vehicles, where all-weather mobility is essential, also use Quaife differentials. Major users being Ambulance, Police, HM Coastguard, MOD, Forestry Commission and Public Utilities where the addition of a Quaife ATB differential improves vehicle handling and stability without compromising service life or operating costs. The benefits being available all year round whatever the traction conditions.

Company Profile

R.T. Quaife Engineering (established 30 years in UK) manufactures racing gear boxes (car and motor cycle), differentials, steering components and drive line power take-offs. The Differential design is patented and the Quaife name is a registered mark.

R. T. Quaife Engineering Ltd
Vestry Road, Otford, Sevenoaks, Kent.
TN14 5EL. England
Tel: 01732 741144
Fax: 01732 741555

F-5: Quaife ATB differential operation

SPECIFICATION

Design

The Quaife Differential is designed to power both wheels and control loss of drive. The differential provides constant and infinitely variable drive, traction being transferred from the spinning wheel to the static wheel automatically without the use of the normal friction pads in other designs. The operation is fully automatic and requires no manual control.

The unique design offers full maximum traction, improves handling and steering, and puts the power where it is needed most. With all the gears being the helical type, the helix and pressure angle of the gear teeth can be varied to increase or decrease the torque capacity.

Suitability

The differential is ideally suited to four wheel drive applications, as well as competition vehicles. Can also be used in all four wheel drive units, both front and rear. Even when fitted to front wheel drive vehicles, there is no adverse resistance to the steering.

Fitting and Maintenance

Fitting the Quaife Differential is the same as installing the standard differential unit. Any maintenance can be carried out by a competent mechanic and no special tools are required.

Operation

The Quaife Differential is gear operated and therefore requires no plates which may wear or break. The unit is smooth in use and requires no special lubricants.

Designed & Manufactured in England.

F-6: Quaife ATB differential specifications

CROWN WHEEL BOLT PCD	D1	5·2362	133mm
NO. OF BOLTS		6 & 8	
THREAD / HOLE		ø 27/64	
CROWN WHEEL SPIGOT DIA	D2	4·4882/4·4870	
BEARING DIA	D3	1·5000/1·5016	
BEARING DISTANCE	L1	3·767	
SPIGOT LENGTH	L2	·915/·750	L2/A
OVERALL LENGTH	L3	5·502	
BEARING/CROWN WHEEL	L4	·400	
BORE	D4	1·1632/1·1629	

DRIVE SHAFT SPLINE:-	
NO. OF TEETH	23T OR 25T
PITCH	24/48 DP
TYPE	FLAT INVOLUTE
PRESSURE ANGLE	45° FILLET

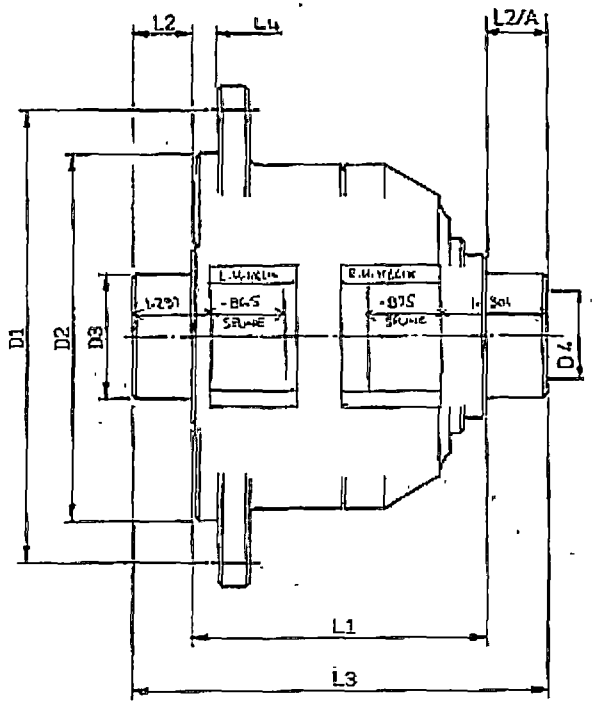

QUAIFE FRONT WHEEL DRIVE DIFFERENTIAL

DESIGN DATA

FIESTA – ESCORT

F-7ZS BODY.

F-7: Quaife ATB differential dimensions

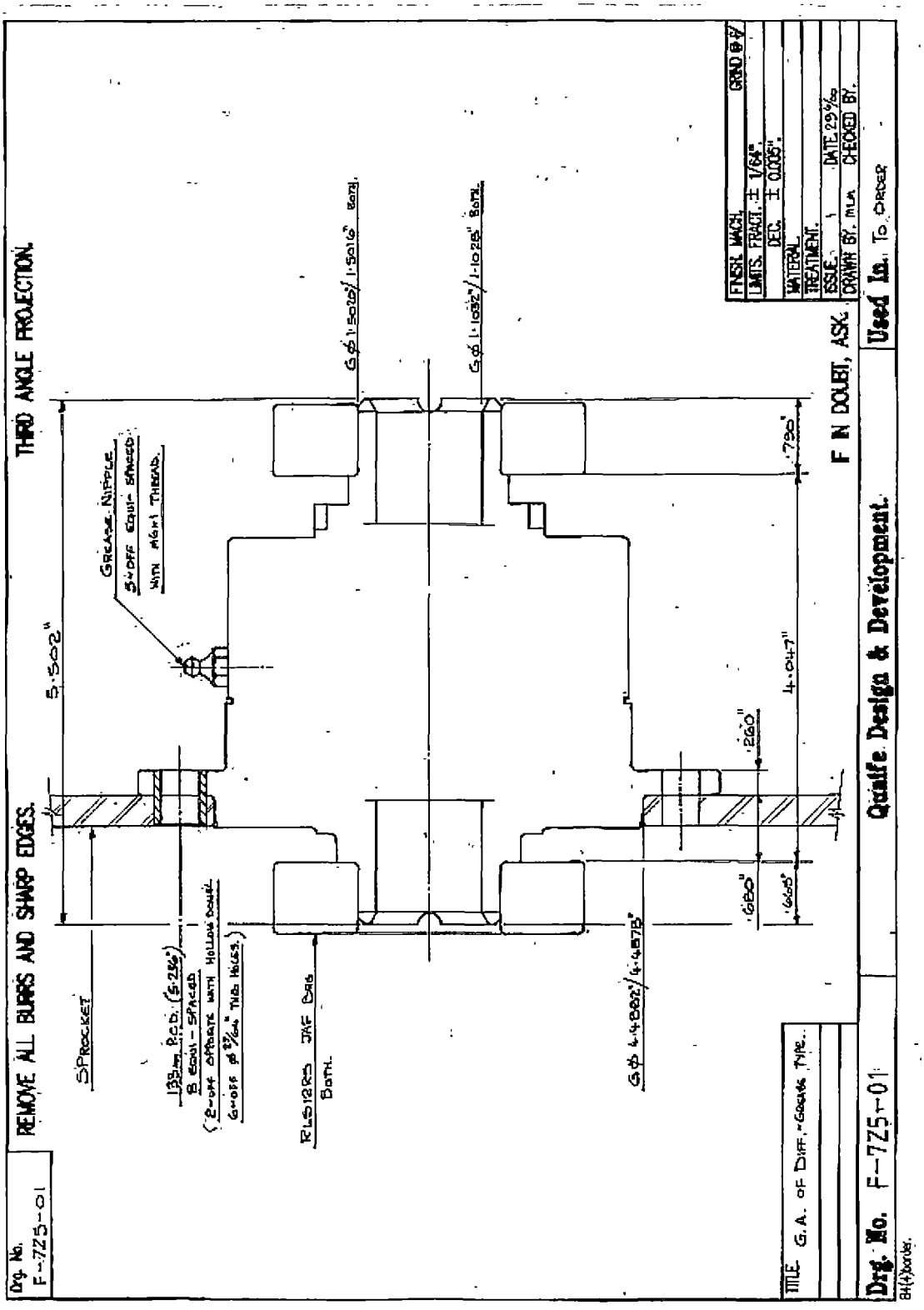

F-8: Composite disc dimensions

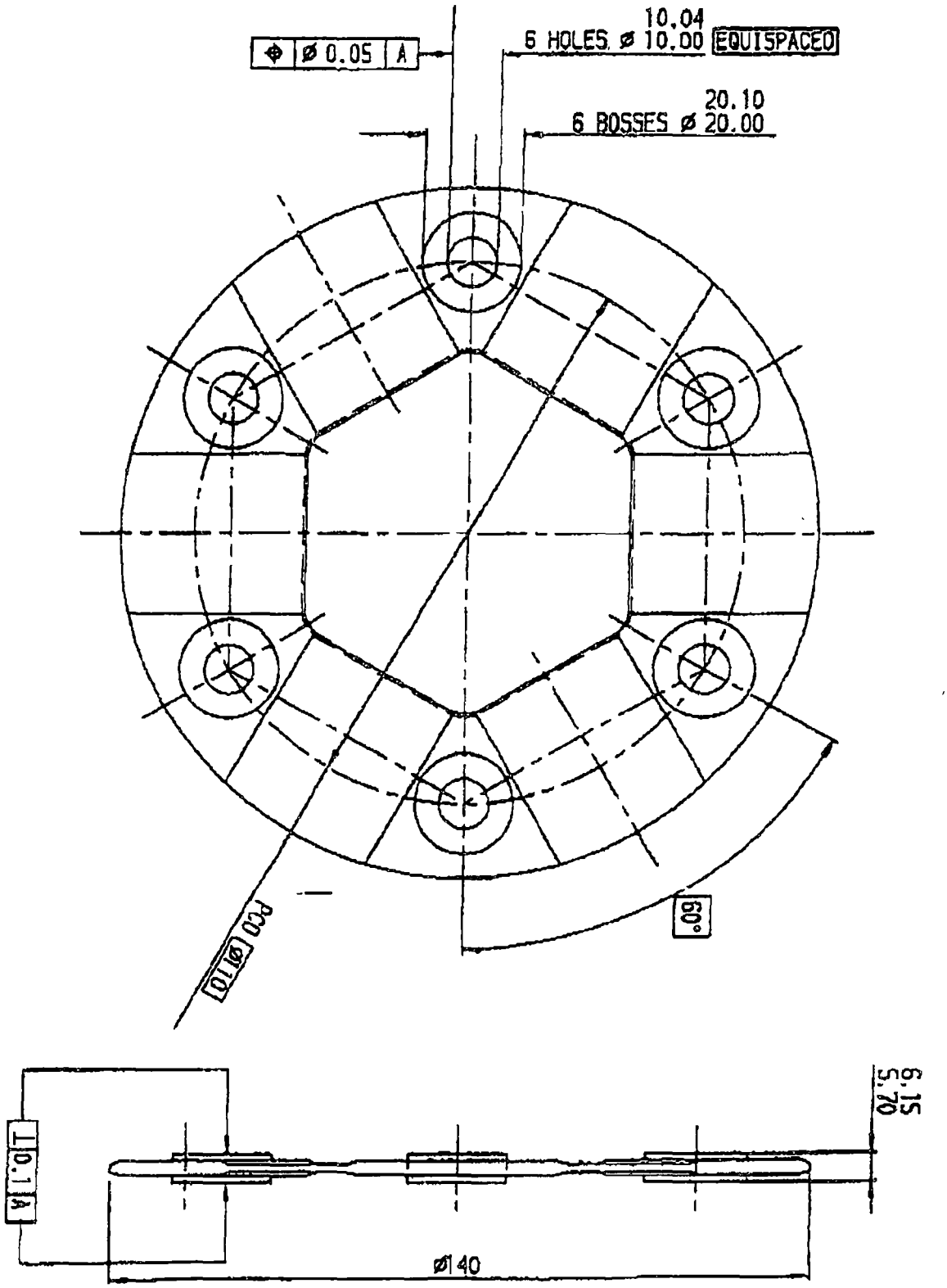

14 APPENDIX G – ELECTRICAL SYSTEMS DESIGN

G-1: Electrical system specifications 261

G-2: Alternator exploded view 262

G-3: Fuse box wiring diagram 263

G-4: Fuse box circuit layout 264

G-1: Electrical system specifications

Battery	
Type	Gel cell
Capacity	15 Ah
Voltage	12.6 V
Charging System	
Type	Three Phase AC
Alternator output voltage	45 V
Stator coil resistance	0.2-0.6 Ohm
Charging Voltage	14 – 15 V
Electric Starter System	
Starter motor	12 V
Brush length	12mm

G-2: Alternator exploded view

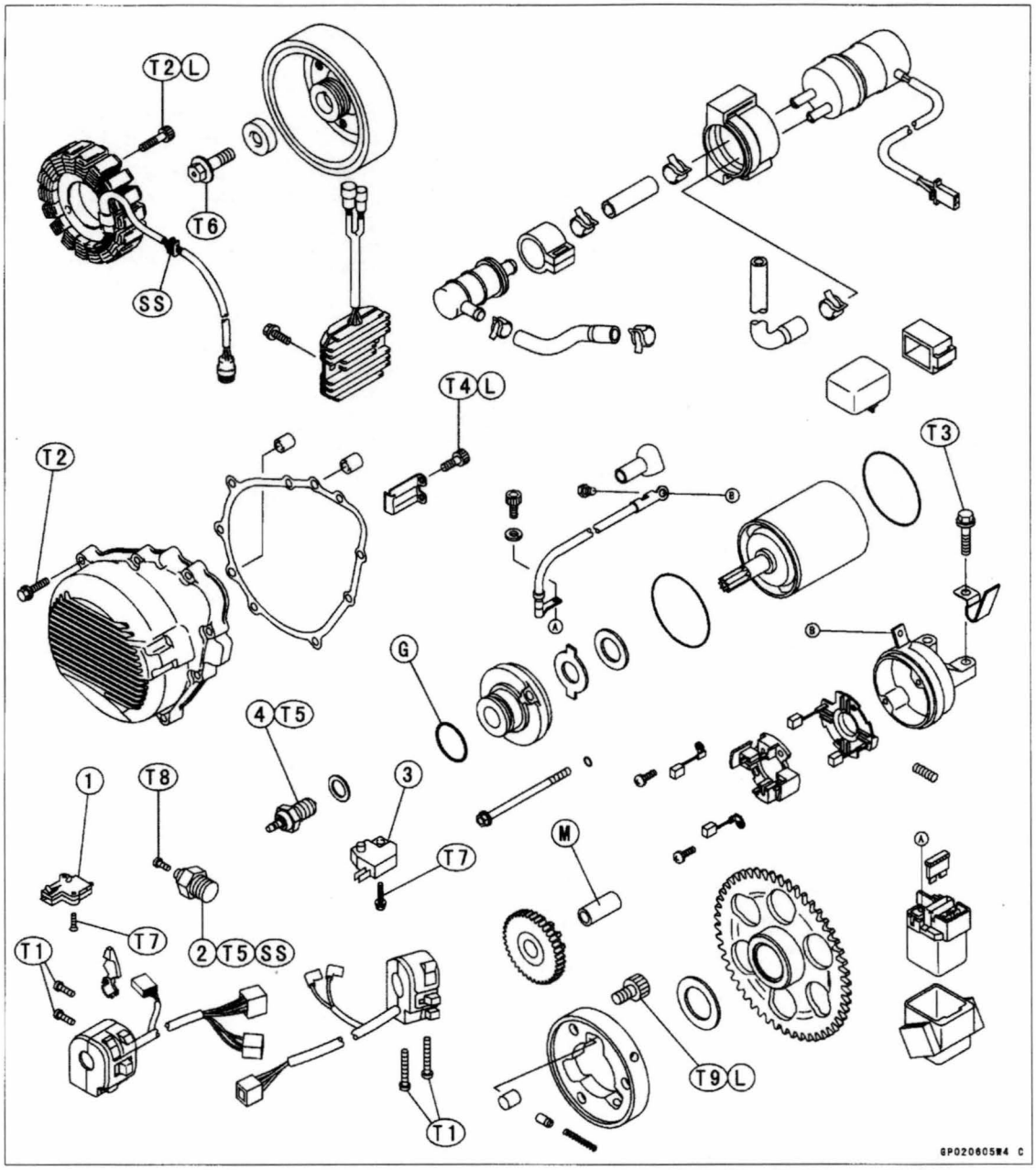

1. Starter Lockout Switch
2. Oil Pressure Switch
3. Front Brake Light Switch
4. Neutral Switch

L: Apply a non–permanent locking agent.
SS: Apply silicone sealant
M: Apply molybdenum disulfide grease.
G: Apply grease or engine oil.

T1: 3.5 N·m (0.35 kg·m, 30 in·lb)
T2: 12 N·m (1.2 kg·m, 104 in·lb)
T3: 11 N·m (1.1 kg·m, 95 in·lb)
T4: 7 N·m (0.7 kg·m, 62 in·lb)
T5: 15 N·m (1.5 kg·m, 11.0 ft·lb)
T6: 120 N·m (12 kg·m, 87 ft·lb)
T7: 1.0 N·m (0.1 kg·m, 9 in·lb)
T8: 1.5 N·m (0.15 kg·m, 13 in·lb)
T9: 33 N·m (3.4 kg·m, 24 ft·lb)

G-3: Fuse box wiring diagram

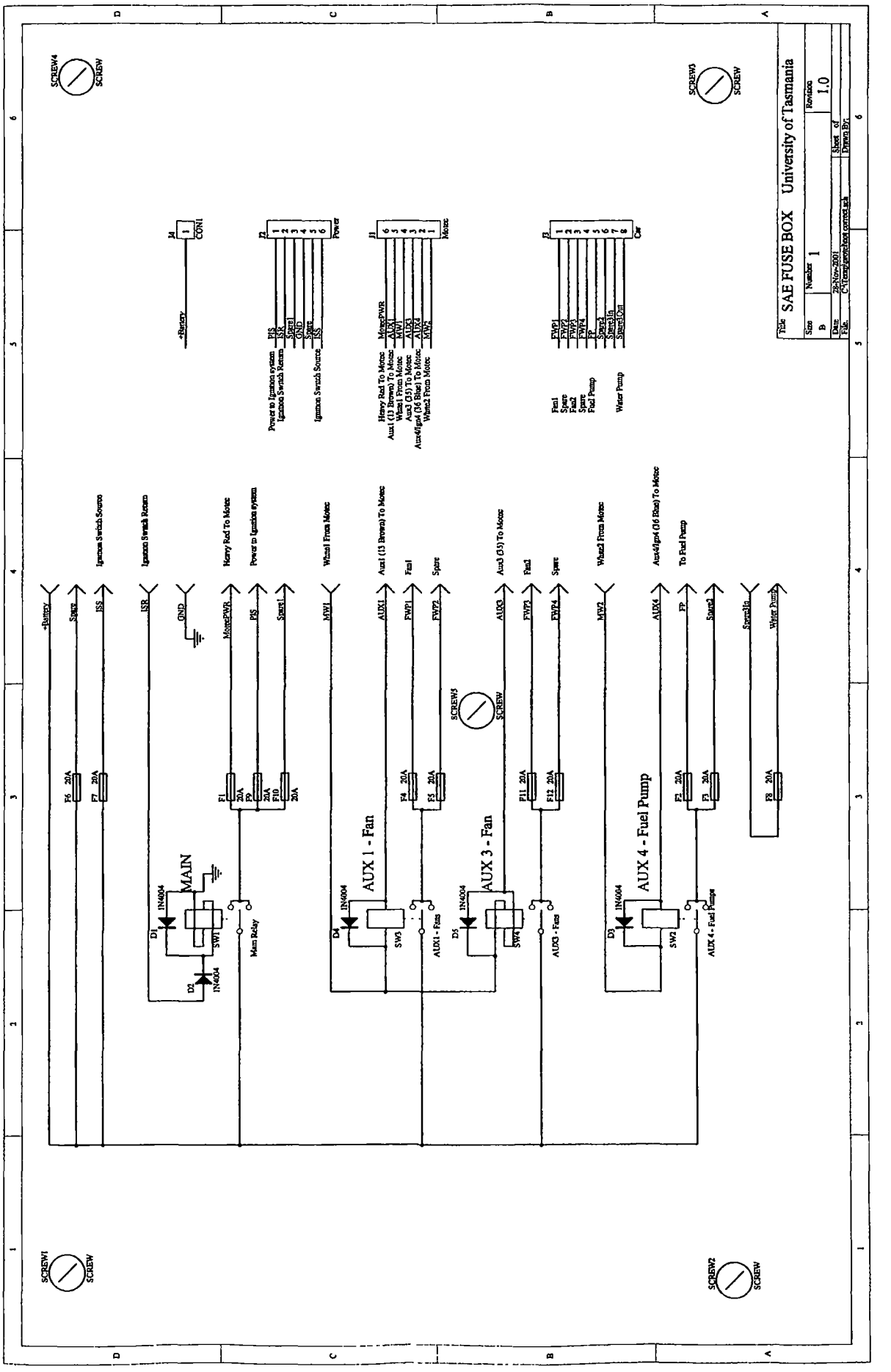

G-4: Fuse box circuit layout

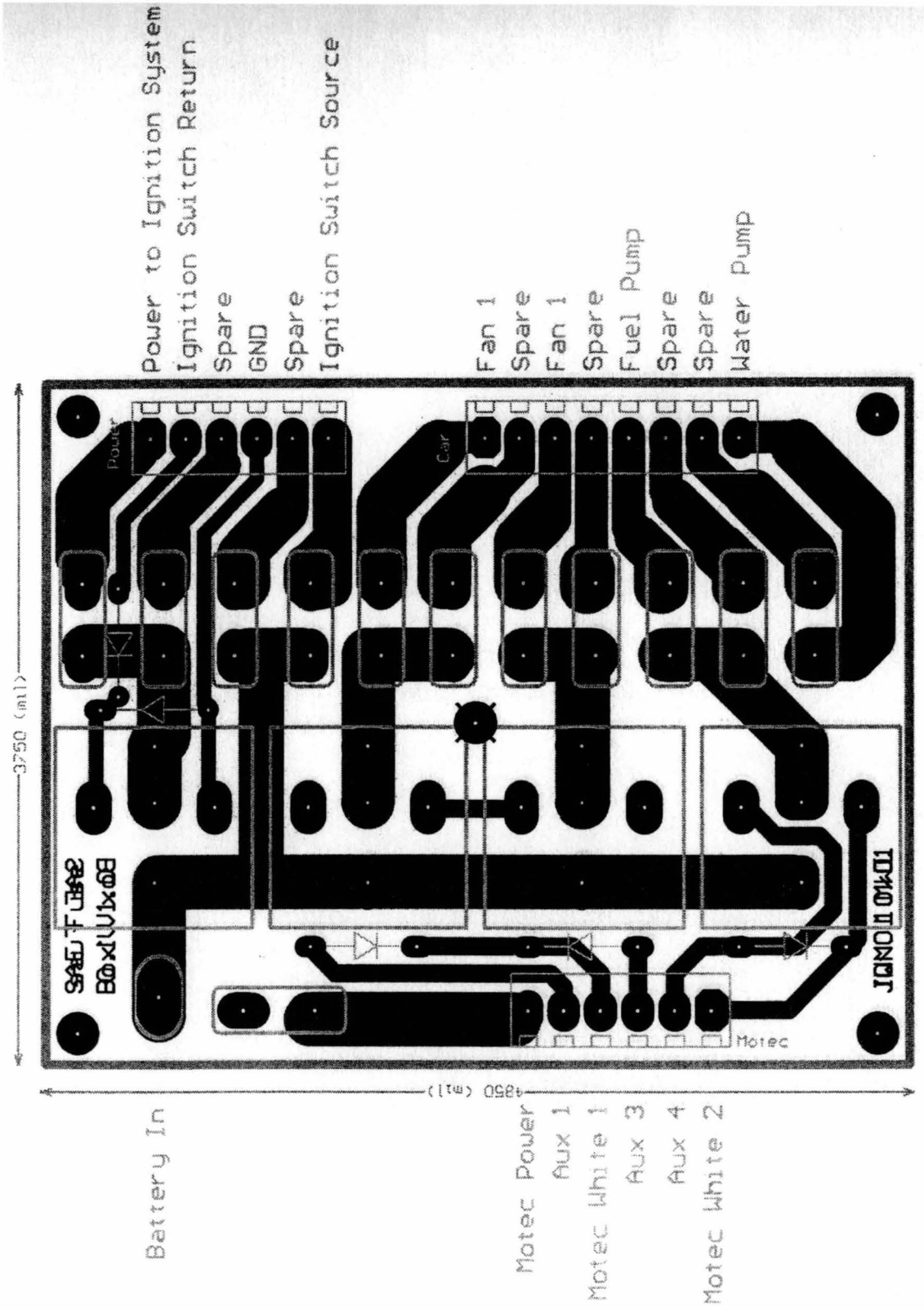

15 APPENDIX H – TEST RIG SENSOR AND TELEMETRY DESIGN

H-1: Advanced dash logger - description 266

H-2: Advanced dash logger - specifications 270

H-3: ADL wiring loom 274

H-4: Radio modem – specifications 275

H-5: Radio modem – installation 277

H-6: Wheel speed hall effect sensor – specifications 278

H-7: Wheel speed hall effect sensor – installation 280

H-8: Suspension position linear potentiometer – specifications 281

H-9: Suspension position linear potentiometer – installation 284

H-10: Steering angle radial potentiometer – installation 285

H-11: Brake pressure transducer - specifications 286

H-12: Brake pressure transducer – installation 288

H-13: Attitude & heading reference sensor – specifications and installation 289

H-1: Advanced dash logger - description

MoTeC Advanced Dash Logger (ADL)

The MoTeC Advanced Dash Logger (ADL) is a fully featured and self contained, programmable logger. The key difference between the MoTeC ADL and other products is its flexibility to be adapted to any application.

Many vehicle, marine and industrial applications require separate products to perform the logging, controlling and displaying. However, the MoTeC ADL offers seamless integration of all three functions.

All aspects of the ADL are fully conFigureurable, including which sensor is connected to which input, what to log, how fast to log it, which channels to display, warning alarms and control outputs.

The MoTeC ADL uses a high speed 32 bit microprocessor and incorporates a 79 pin autosport connector. The ADL is built to internationally recognised quality and manufacturing standards and is back by a full 2 year worldwide warranty.

15.1.1.1.1 Data Logging

Data logging allows for readings taken from Analog, Digital, Serial, CAN or Calculated channels, to be stored in the ADL for later analysis on a computer. The ADL uses permanent non-volatile Flash memory. Data memory may be unloaded at very high speeds (approx. 19 seconds per Mbyte). Different logging options allow 384k, 1MB or the full 8MB to be accessed.

The ADL can store channels at up to 1000 times per second per channel, this can be individually set for each channel. Four logging modes may run concurrently (Normal, Fastest Lap and two Burst Modes) each with selectable start and stop logging parameters. Memory can operate in stack or circular buffer mode.

15.1.1.1.2

15.1.1.1.3 Analog and Digital Channels

In total the ADL can accommodate over 200 channels derived from any mixture of Analog, Digital, RS232 Serial and CAN bus data channels.

The ADL directly supports up to 28 analog inputs, 12 digital/speed inputs, 8 auxiliary outputs and 2 high accuracy Wideband Lambda (Air/Fuel ratio) inputs.

The analog channels sample at up to 1000 samples per second per channel, with a measurement range of 0 to 15 VDC.

Digital inputs are used for state monitoring, counting and pulse width measurement. They accept switch, logic, open collector (Hall Effect), or magnetic signals.

The auxiliary outputs can be conFigured to operate as simple off/on outputs, duty cycle control or frequency based outputs.

15.1.1.1.4 Serial Communications

The RS232 serial port is programmable up to 115k baud and can be used as either a telemetry data output port or serial data input port.

As a telemetry port; devices such as Modems, GSM & Satellite Phones, Radio Modems etc. can be connected to facilitate remote communication.

As a serial data input port; serial communication devices can be connected for displaying and logging purposes. These include Engine Management Systems (MoTeC and other), bar code devices, keypads, GPS Systems or other serial communications devices.

15.1.1.1.5 Display

The MoTeC ADL display is a high contrast, high temperature, custom designed reflective LCD. Its unique design makes it viewable in direct sunlight or artificial light.

The display has 3 modes of operation, where each mode is fully programmable and independent of the other. Each mode may be selected by pressing a button or activated by a condition.

The 70 segment bar graph display is programmable to display any channel, with an optional peak hold marker and setpoint marker. Each numerical display item can be programmed to display any channel value as required. The 13 digit alphanumeric display area has 20 lines available to scroll through and may be used to display any channel value or to display warning messages.

Lap times may be displayed when connected to a MoTeC Lap Beacon (or a driver activated switch). Other performance information may be displayed, including minimum corner and maximum straight speed, fuel used or fuel remaining, and many more.

15.1.1.1.6 Alarms

Warning alarms may be defined for any analog, digital, serial or calculated channel. Alarm limits are fully programmable and may include up to 6 conditions to ensure that the alarms are only activated at the correct time.

When an alarm condition has been detected, a message can be shown on the display and an auxiliary output activated. These outputs can be used for warning lights or the control of other devices.

The alarms remain active until they are acknowledged, either by activating a switch or automatically after a definable period of time.

15.1.1.1.7

Controller Area Network (CAN)

The CAN bus is a high speed communication standard operating at speeds up to 1Mbit.

CAN allows many devices to be connected by a common bus, allowing all devices to share information as part of a larger system.

CAN devices include: automatic transmission controllers, sensors, multi-channel input/output modules, engine management systems etc.

15.1.1.1.8 Host Software

The ADL is supplied with software packages for managing the ADL, analysing the logged data and monitoring a telemetry link.

Ease of use is one of the most attractive aspects of the MoTeC ADL software. There is no complex language to learn, just simple menu driven windows.

A full online help system is easily accessible and is integrated throughout the software.

15.1.1.1.9 Dash Manager Software

The Dash Manager Software is used to conFigure the ADL and download logged data. It is logically laid out, giving the user access to the power of the ADL without requiring high levels of computer knowledge or intense training.

15.1.1.1.10Interpreter Software

The Interpreter software contains predefined configurations for easy data analysis. Screen display formats may be varied to suit all preferences, including user defined graphs, histograms and statistical summaries. By utilising these different display methods, users can view data in many formats to obtain accurate, meaningful analysis.

Data can also be exported into ASCII CSV file format for analysis in other software packages.

The Pro Logging option includes graph overlays, virtual instruments, mathematical functions, XY graphs (scatter plots), track maps (shows minimum and maximum speeds, gear change point and breaking points) and other advanced features.

15.1.1.1.11Telemetry Monitor (Optional)

The Telemetry Monitor software allows for realtime viewing of the telemetry data either via direct serial communications, modems or radio modems. Data can be viewed in various formats such as charts, bar graphs, dial gauges, numerics, lights, XY graphs and scroll charts. All objects are definable by the user.

15.1.1.1.12Upgrades and Accessories

The MoTeC ADL is completely field updateable by the user. The control software and logged data is stored in FLASH memory. No programming interface is required, simply send to the ADL the new program and the latest features are immediately available.

15.1.1.1.13 Upgrade Options

The ADL has field upgradeable options using a password enabling system. Upgrade options include:

Extended inputs & Outputs, Pro Logging (advanced data analysis), Medium Logging (1Mbyte), Large Logging (4Mbyte), Telemetry Support, Remote Logging and Wideband Lambda measurement.

Three wiring options are available for the ADL:

Separate I/O Terminal Module with plug-in screw terminals. Includes a Realtime Clock, additional RS232 port and wide ranging power supply.

Standard (vehicle style) wiring loom for specific permanent installations.

Custom wiring looms for complex installations.

15.1.1.1.14 Accessories

A wide range of sensors are available for use with the ADL including: linear position, accelerometers, pressure, resistive and thermocouple temperature sensors, hall and magnetic speed sensors and many others.

The MoTeC Lap Beacon transmitter and receiver has been designed in conjunction with the ADL. It features high channel count (990), improved optics, low power consumption and multi beacon capability.

And for peace of mind the MoTeC ADL offers a full 2 year worldwide warranty.

H-2: Advanced dash logger - specifications

ADL Specifications

15.1.1.1.15General

- Microprocessor: 32 Bit High Performance
- Manufacturing Quality standard to ISO9001
- Field updateable Operating System
- Non-volatile FLASH memory for data & operating system
- High RFI Immunity
- Rugged Aluminium Housing (IP-55, NEMA 4)
- 79 pin Autosport connector
- Operating Temperature: -10 to 70 DegC
- Operating Voltage: 7 to 22 VDC
- Operating Current: 0.3 A max.
- Weight: 385 gms (0.85 lbs)
- Size: 180mm x 91mm x 18mm (excluding connector)
- Reverse Battery and Transient Protection
- Warranty: 2 years Parts and Labour

15.1.1.1.16Measurement Inputs

- 28 Analog Inputs (10 Standard):
  - 20 Analog Voltage (6 Standard)
  - 8 Analog Temperature (4 Standard)
  - 12 bit resolution, 0 to 15 VDC range
  - Update rate (Max. 8 channels): up to 1000 times/sec
  - Other inputs: up to 500 times/sec

- 4 Digital Inputs (2 Standard)
- 4 Speed Inputs (2 Standard)

  Digital & Speed
  - Switch to OV, logic signal, open collector (Hall Effect), or Magnetic
  - State & Counting (1MHz)
  - Period (1 micro sec)
  - Pulse width (1 micro sec)

- 4 Switch Inputs (4 Standard
- User definable sensor calibrations

15.1.1.1.17Auxiliary Outputs

- 8 Digital Outputs (4 standard)
  - Open Collector (drives to ground) with pullup (10k ohms) to battery positive
  - On/Off or Pulse Width Modulation with variable Frequency and Duty Cycle

15.1.1.1.18Air Fuel Ratio Measurement (Optional)

- 2 high accuracy Wideband Lambda (Air/Fuel ratio) inputs

- Resolution: 0.01 Lambda
- Temperature compensated
- Range: 0.75 to 1.2 Lambda

15.1.1.1.19 Data Logging

- Memory: 384k, 1MB, 2MB, 4MB, 8MB
- Non-volatile FLASH, field upgradeable
- Logging of any Analog, Digital, Serial, CAN bus or Calculated channel
- Maximum Logging throughput: 20k/sec
- 2 Burst Logging buffers with pre triggering (Large logging option only)
- Typical Unload Speed: 19 sec/MB, using parallel port of PC to CAN bus RS232 unload rates dependent on baud rate

15.1.1.1.20 Calculations

- Timers (0.01s, 0.1s, & 1s resolution)
- 2D and 3D Tables
- User conditions
- Math Functions: Differentiate, Integrate, Absolute, Min/Max
- Lap Time and Number
- Lap Gain/Loss
- Speed and Distance
- Gear Detection
- Fuel Prediction
- Tell-tales
- Running Min/Max

15.1.1.1.21 Display

- Custom LCD, High Contrast, High Temperature, Reflective
- Display any Analog, Digital, Serial, CAN bus channel or Calculated channel
- 3 Display Modes
- 70 Segment Bar graph
    - Definable Range
    - Programmable Setpoint and Peak Hold point
- 4 Numeric Display Items
- 13 Digit Alpha Numeric Display area, 1,2 or 3 channels per line (20 scrollable lines per display mode)
    - Alarm messages
    - Channel display
    - Descriptive text

15.1.1.1.22 Communication

- Serial RS232 Coms. (1200 to 115k baud)
- CAN data link (250Kbit to 1Mbit)
- Telemetry Link output (RS232)

15.1.1.1.23 Host Software

1. Dash Manager Software
2. Interpreter Analysis Software
3. Telemetry Software (Optional)

Computer Requirements

- IBM PC compatible running Windows 95/98 or NT4.0
- Pentium (Min.) 90MHz, 16MB RAM

15.1.1.1.24 Upgrades

The MoTeC ADL in its base configuration includes:

- 10 Analog Inputs
- 8 Digital Inputs
- 4 Digital Auxiliary Outputs
- RS232 and CAN bus support
- Software: Dash Manager and Interpreter
- User's Manual

Upgrades Available *(field updateable by the user)*:

- **Extended Inputs & Outputs**
  - 28 Analog Inputs (10 standard)
  - 12 Digital Inputs (8 standard)
  - 8 Digital Auxiliary Outputs (4 standard)
- **Pro Logging** - Advanced Analysis Software
  - Graph Overlays
  - XY Plots
  - Maths functions
  - Virtual Instruments display
  - Track Mapping
- **Medium Logging**
  - 384k to 1MB Memory
- **Large Logging** *(requires Medium Logging Upgrade)*
  - 1MB to 8MB with Burst mode logging
- **Lambda Measurement**
  - 2 Wideband Lambda inputs
- **Telemetry**
  - Enables realtime viewing of data via a telemetry link
- **Remote Logging** *(requires Telemetry Upgrade)*
  - Allows Remote Logging via a telemetry link or hand held computer

15.1.1.1.25 Accessories

- PC Communications Cable (High Speed CAN)
- Wiring Looms
- Input/Output Terminal Module
- Lambda (Air/Fuel ratio) Sensors and Kits
- Telemetry Products
  - GSM mobile phones, radio modems etc
- Sensors and transducers

    - a full range of sensors, amplifiers, transducers, lights and buttons are available
- Lap Beacon: Transmitter and Receiver (990 channel)

H-3: ADL wiring loom

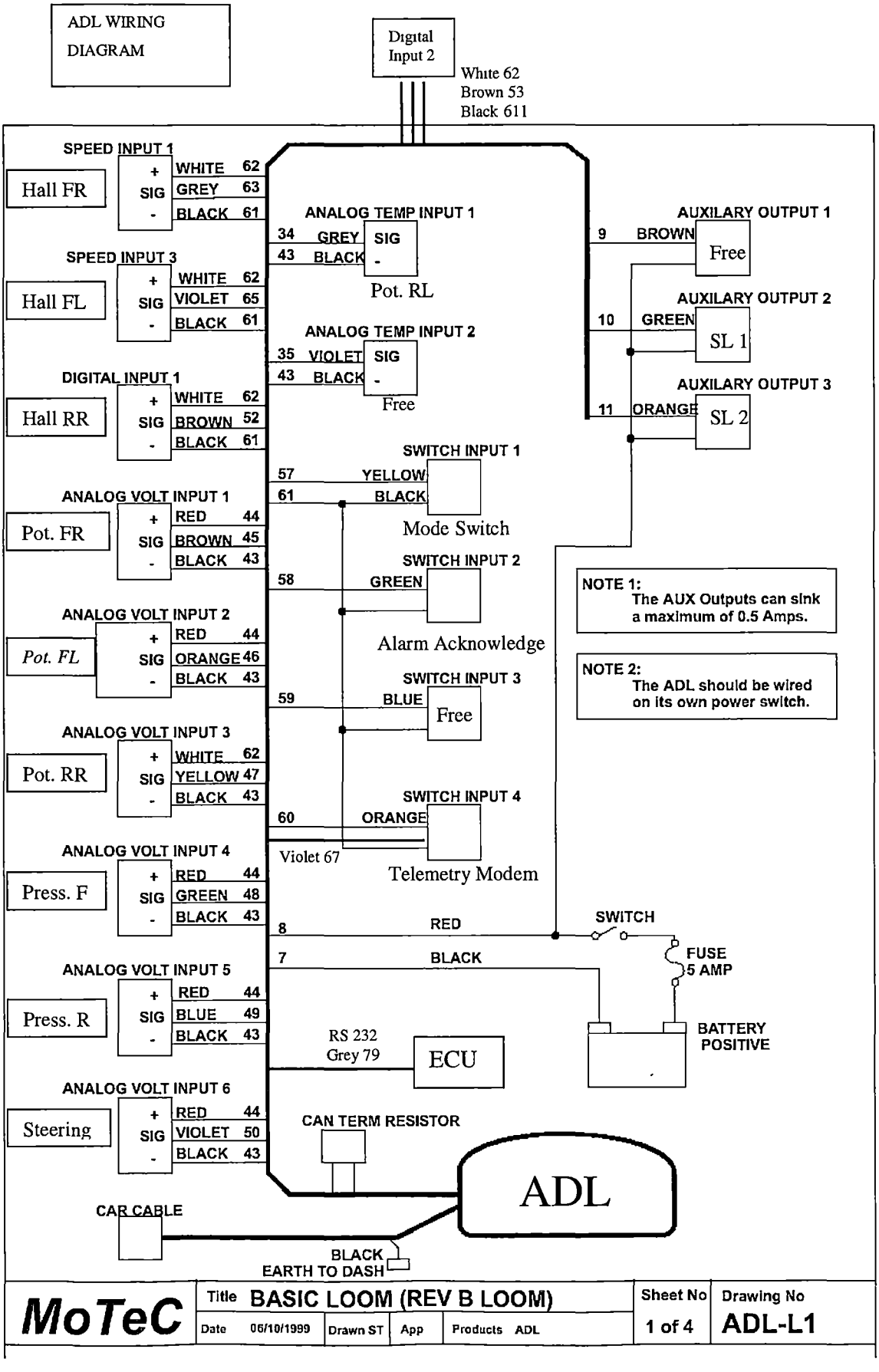

H-4: Radio modem – specifications

RF INNOVATIONS

HIGH SPEED RADIO MODEM

RFI 9256 *Series 3*

SPREAD SPECTRUM 900MHz RADIO MODEM

The RFI 9256 is a license free high performance data radio capable of functioning in hostile RF environments with data throughput of 115 Kbps. Receiver design provides superior rejection of unwanted signals in hostile crowded spectrum environments.

Features

- Economical
- Dual RS-232 ports
- Suitable for voice and data
- Forward error correction
- ARQ is software selectable
- Air data speeds 115 Kbps
- In built diagnostic channel
- Up to 30 Kms point to point
- User friendly intuitive software
- Interface speeds 110 to 115000 bps
- RF power up to 1 Watt software selectable
- Programmable I/O for SCADA applications
- Front panel indicators for RSSI, TX power and status
- Can be installed and commissioned without test equipment

Applications

Point to Multipoint Data Acquisition and Control

Intelligent built in Modem can interface with virtually any standard Data logger, PLC, computer; i.e. any RS232 device. In built buffers handshake with Input/output devices at data speeds up to 115,000 bps and transparently move data to the other end.

Linking of local and remote RS232 serial ports

Depending upon the geography and terrain, the Radio modems can communicate reliably over considerable distances. Good line of site paths from mountain top to hill can extend useful range up to 30 km. The RFI 9256 can be used as a repeater to extend range indefinitely.

Parallel digital I/O and expansion

8 parallel digital I/O in addition to the standard RS232 serial port, are provided in the RFI 9256 model Radio modems. Expansion radio interface modules (RIM) permit very large SCADA capability. For more details regarding interface parameters, contact the manufacturer.

Diagnostics functions

The second RS 232 port can be used as a diagnostics channel for monitoring network performance, and for additional data routing if required.

RF INNOVATIONS PTY LTD ABN 97 065 523 579
22 Boulder Road, Malaga WA 6090
Telephone +61 8 9209 0900 • Facsimile +61 8 9248 2833
Email: sales@rfinnovations.com.au • Web: www.rfinnovations.com.au

Specifications
MODEL RFI 9256 Series 3

PHYSICAL

Dimensions	190mm L x 80mm W x 35mm H
Weight	260 grams
Construction	Alodined aluminium chassis and cover, with integrated display

GENERAL

Operating voltage	9 to 16VDC negative ground
Operating current	
Standby mode	150 mA
Transmit mode (1 Watt)	Averages 350mA
Operating temperature range	-10 to +60 deg C
Operating Humidity range	Up to 95% non-condensing RH @ 50 deg C
Parameter and mode settings	In built software

TRANSMITTER

Output Power	1mW to 1 Watt software selectable
Spurious emissions	<-60 dBc
Output protection	Transmitter is fully protected for any load @ full power @ 60 deg C

RECEIVER

Sensitivity	<-108dBm for BER 1 part in 10^-4
End to end performance	Better than 1 in 10^-6 BER for S/N 20 dB or better
Frequency range	915–928 MHz (Australia) 902–928 MHz (FCC) 921-929 MHz (NZ)
RSSI display range	-110 to -60 dBm in 5 dB steps

DATA SYSTEM

RS 232 handshaking	Hardware/ software/ none software selectable
Protocol modes	All common variants / PLCs supported including point / point, point / multipoint and Hayes modes
Interface data speed	110 to 115,000 bps, software selectable all modes

Distributed by

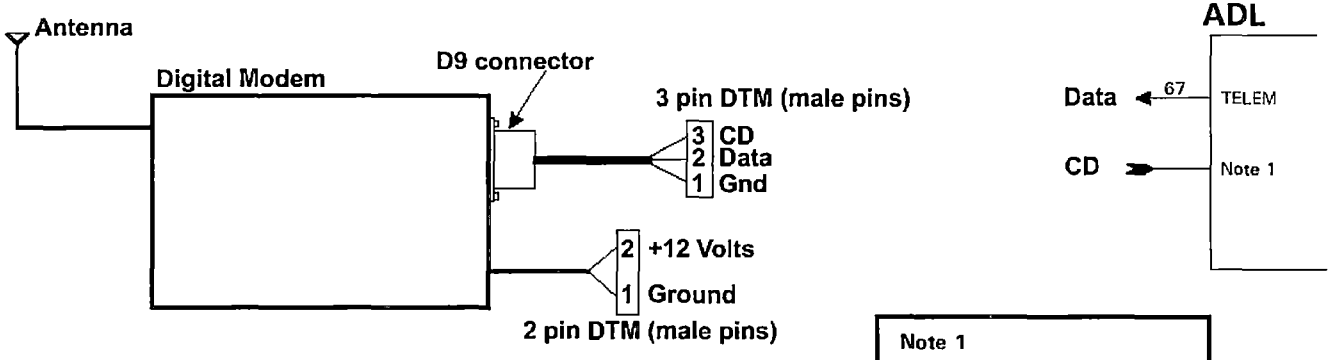

Note 1
The following pins can be used;
Switched Inputs (normally sw4)
Speed Inputs, Digital Inputs

D9 Connector Wiring Details

Male D9 Viewed from loom end

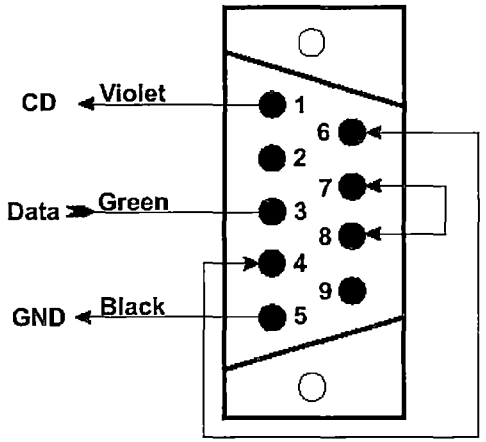

Motec Part No. 61071

ADL Setup

1. Set Input pin's channel to "Carrier Detect"
2. Select one of the templates in the RS232 Communications Setup screen.

NOTE: The modem may need configuration before it will connect.

MoTeC	Title Digital Telemetry Connection				Sheet No	Drawing No
	Date 04/03/1999	Drawn ST	App	Products ADL	1 of 1	TEL01

H-6: Wheel speed hall effect sensor – specifications

Solid State Sensors

GT1 Series

Hall Effect Gear Tooth Sensors

TYPICAL APPLICATIONS

Automotive and Heavy Duty Vehicles:

- Camshaft and crankshaft speed/ position
- Transmission speed
- Tachometers
- Anti-skid/traction control

Industrial:

- Sprocket speed
- Chain link conveyor speed and distance
- Stop motion detector
- High speed low cost proximity
- Tachometers, Counters

FEATURES

- Senses ferrous metal targets
- Digital current sinking output (open collector)
- Better signal-to-noise ratio than variable reluctance sensors, excellent low speed performance, output amplitude not dependent on RPM
- Sensor electronically *self-adjusts* to slight variations in runout and variations in temperature, simplifying installation and maintenance
- Fast operating speed – over 100 kHz
- EMI resistant
- Reverse polarity protection and transient protection (integrated into Hall I.C.)
- Wide continuous operating temperature range (–40° to 150°C), short term to 160°C

GENERAL INFORMATION

1GT1 Series Gear Tooth Sensors use a magnetically biased Hall effect integrated circuit to accurately sense movement of ferrous metal targets. This specially designed I.C., with discrete capacitor and bias magnet, is sealed in a probe type package for physical protection and cost effective installation.

Units will function from a 4.5 to 24 VDC power supply. Output is digital, current sinking (open collector). Reverse polarity protection is standard. If power is inadvertently wired backwards, the sensor will not be damaged. Built-in protection against pulsed transients to +60V, –40V is also included.

Optimum sensor performance is dependent on the following variables which must be considered in combination:

- Target material, geometry, and speed
- Sensor/target gap
- Ambient temperature
- Magnetic material in close proximity

GT1 ORDER GUIDE

Catalog Listing	Description
1GT101DC	Gear Tooth Sensor

MOUNTING DIMENSIONS (For reference only)

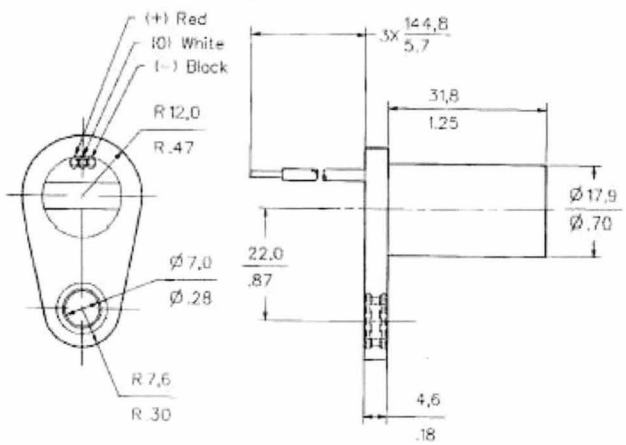

Solid State Sensors

GT1 Series

Hall Effect Gear Tooth Sensors

SENSOR SPECIFICATIONS

All values were measured using 1 K pull-up resistor.

Electrical Characteristics	Supply Voltage	4.5 to 24 VDC
	Supply Current	10 mA typ., 20 mA max.
	Output Voltage (output low)	0.4 V max.
	Output Current (output high)	10 µA max. leakage into sensor
	Switching Time	
	Rise (10 to 90%)	15 µsec. max
	Fall (90 to 10%)	1.0 µsec. max.
Absolute Maximum Ratings*	Supply Voltage (Vs)	±30 VDC continuous
	Voltage Externally Applied to Output (output high)	−0.5 to +30 V
	Output Current	40 mA sinking
	Temperature Range	
	Storage	−40 to 150° (−40 to 302°F)
	Operating	−40 to 150° C (−40 to 302°F)
Switching Characteristics**	Operate Point	3.7±1.25° (3.28±1.13 mm)
	Release Point	4.7±2.50° (4.16±2.21 mm)
	Differential Travel	8.4±3.70° (7.45±3.34 mm)

* As with all solid state components, sensor performance can be expected to deteriorate as rating limits are approached; however, sensors will not be damaged unless the limits are exceeded.
** See Reference Target table.

TARGET GUIDELINES

The Target Guidelines table provides basic parameters when an application is not restricted to a specific target.

Any target wheel that exceeds the following minimum specifications can be sensed over the entire temperature range of −40° to 150°C with any sensing gap up to .080 in. (2.0 mm). This data is based on a 4 in. (102 mm) diameter wheel, rotating 10 to 3600 RPM.

Reference Target Dimensions

Tooth Height:	.200 in. (5.06 mm) min.
Tooth Width:	.100 in. (2.54 mm) min.
Tooth Spacing:	.400 in. (10.16 mm) min.
Target Thickness.	.250 in. (6.35 mm)

Sensor Output (with pull-up resistor added to output circuit)

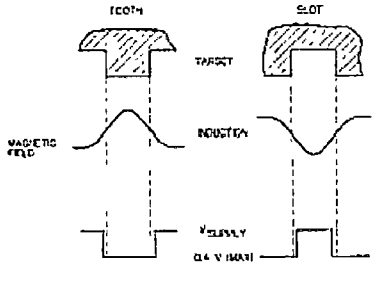

REFERENCE TARGET/CONDITIONS

Characteristics will vary due to target size, geometry, location, and material. Sensor specifications were derived using a cold-rolled steel reference target. See table, right, for reference target configuration and evaluation conditions.

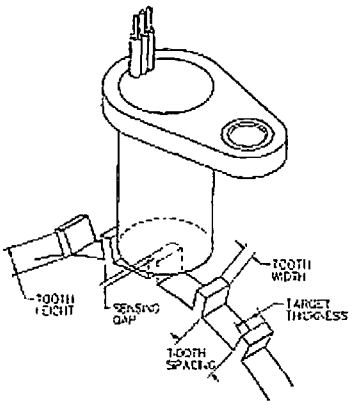

Target	
Diameter:	4 in. (101.6 mm)
Tooth Width:	.350 in. (8.89 mm)
Thickness.	.250 in. (6.35 mm)

Test Conditions	
Air Gap:	.040 to .080 in. (1.02 to 2.03 mm)
V Supply:	4.5 to 24 V
RPM*	10 min., 3600 max.

Operating Temp -40 to +150 deg C
Output States Air : High
Metal : Low (8 sec Hold Typ)

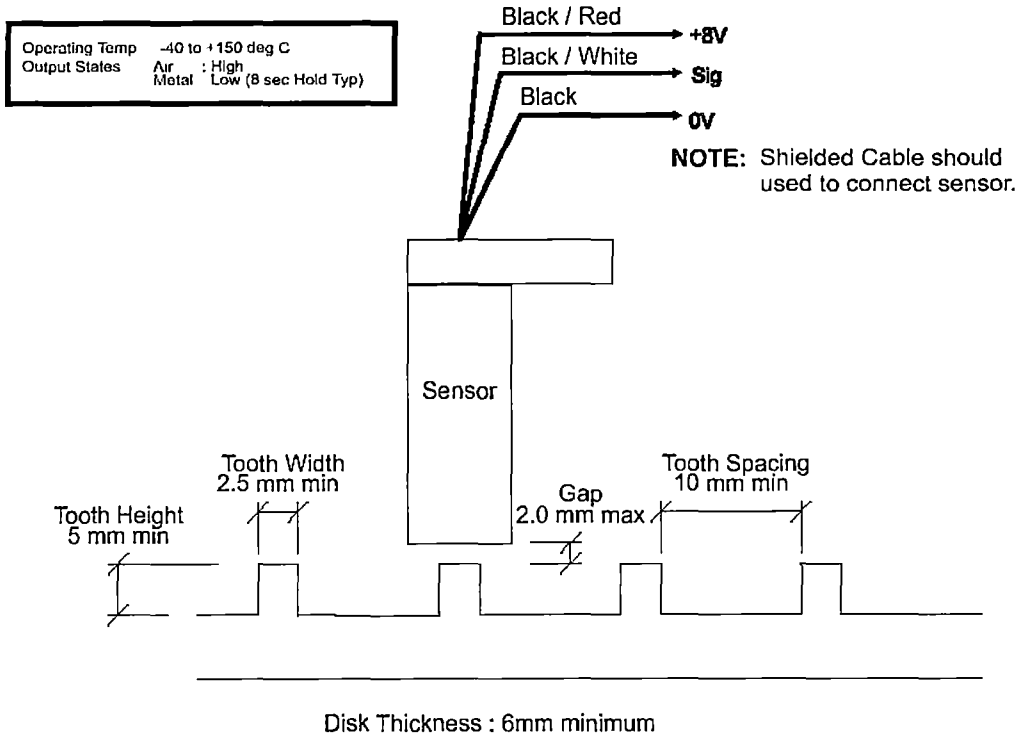

NOTE: Shielded Cable should used to connect sensor.

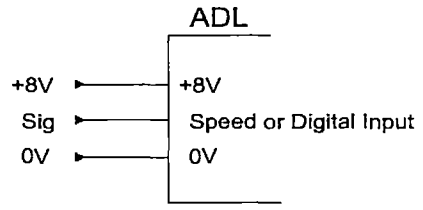

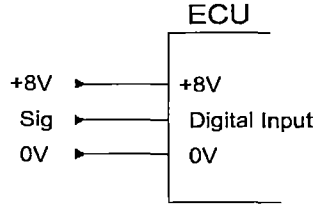

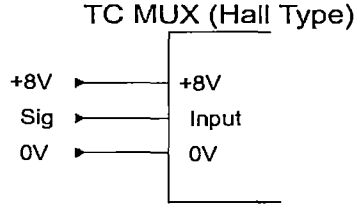

ADL Setup

Speed setup.
Select "HALL" Sensor type

When used for Traction Control the edge variation of the teeth must be less than 0.5% (to give 1KPH in 200KPH accuracy)

eg If the edge spacing is 20mm then the variation must be less than 0.1 mm

MoTeC	Title GT101 Hall Effect Sensor				Sheet No	Drawing No
	Date	Drawn ST	App	Products ADL, ECU, TC MUX	1 of 1	X02

H-8: Suspension position linear potentiometer – specifications

GEFRAN

PZ12

RECTILINEAR DISPLACEMENT TRANSDUCER WITH CYLINDRICAL CASE

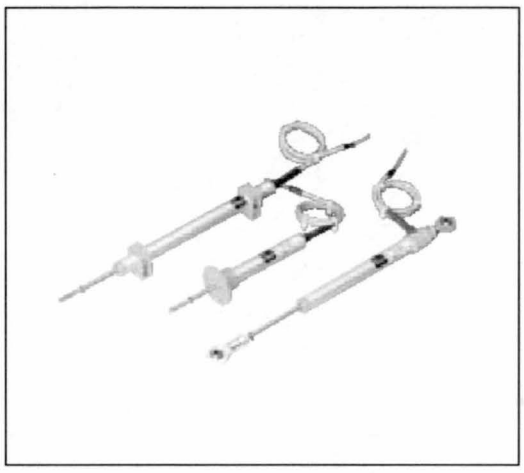

Main features

- *25 to 150 mm. stroke*
- *Mechanical fixing using brackets, selfaligning ball-joints or flange*
- *Independent linearity up to ± 0,05%*
- *Infinite resolution*
- *No variation of electrical signal outside theorical electrical stroke*
- *Displacement speed up to 10 m/s*
- *Working temperature: -30...+100°C*
- *Electrical connection: 3-pole screened cable (1m length)*
- *Life duration: > 25x10⁶ meters or >100x10⁶ operations whichever is the smaller (within C.E.U.)*
- *Grade of protection IP60*

TECHNICAL DATA

Useful electrical stroke (C.E.U.)	25/50/75/100/125/150
Independent linearity (within C.E.U.)	see table
Displacement speed	≤ 10 m/s
Displacement force	≤ 0.5N
Vibrations	5...2000Hz, Amax =0,75 mm amax. = 20 g
Shock	50 g, 11ms.
Tolerance on resistance	± 20%
Recommended cursor current	< 0,1 µA
Maximum cursor current	10mA
Maximum applicable voltage	see table
Electrical isolation	>100MΩ at 500V=, 1bar, 2s
Dielectric strength	< 100 µA at 500V~, 50Hz, 2s, 1bar
Dissipation at 40°C (0W at 120°C)	see table
Temp. Coeff. of the resistance	-200 ± 200ppm/°C
Actual Temperature Coefficient of the output voltage	< 1,5ppm/°C
Working temperature	-30...+100°C
Storage temperature	-50...+120°C
Case material	Anodised aluminium Nylon 66 GV 40
Control rod material	Stainless steel AISI 303
Fixing	Brackets, selfaligning ball-joints or flange

MECHANICAL DIMENSIONS

PZ12-S

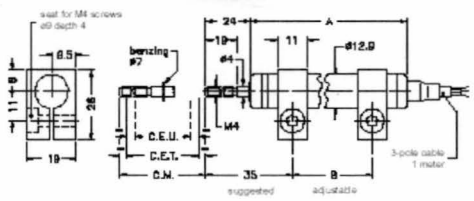

PZ12-A

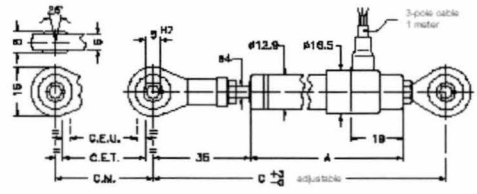

PZ12-F

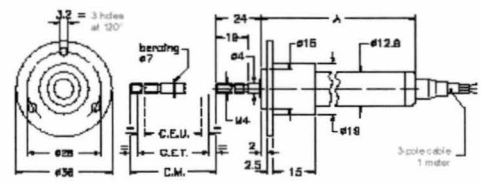

Important: all the data reported in the catalogue linearity, lifetime, temperature coefficient are valid for a sensor utilization as a ratiometric device with a max current across the cursor Ic ≤ 0.1 µA.

MECHANICAL / ELECTRICAL DATA

MODEL			25	50	75	100	125	150
Useful electrical stroke (C.E.U.) + 1 / -0		mm	25	50	75	100	125	150
Theoretical electrical stroke (C.E.T.) ± 1		mm	C.E.U. +1					
Resistance (C.E.T.)		kΩ	1	2	3	4	5	6
Independent linearity (within C.E.U.)		± %	0,2	0,1	0,1	0,1	0,05	0,05
Dissipation at 40°C (0W at 120°C)		W	0,5	1	1,5	2	2,5	3
Maximum applicable voltage		V	20	40	60			
Mechanical stroke (C.M.)		mm	C.E.U. +5					
Case length (A)	mod. PZ12 - S	mm	74,5	99,5	124,5	149,5	174,5	199,5
	mod. PZ12 - A	mm	102	127	152	177	202	227
	mod. PZ12 - F	mm	74,5	99,5	124,5	149,5	174,5	199,5
Recommended distance between brackets (B)		mm	42	67	92	117	142	167
Minimum distance between ball-joints (C)		mm	153	178	203	228	253	278
Weight	mod. PZ12 - S	g	45	55	65	75	85	95
	mod. PZ12 - A	g	70	80	90	100	110	120
	mod. PZ12 - F	g	60	70	80	90	100	110

ELECTRICAL CONNECTIONS

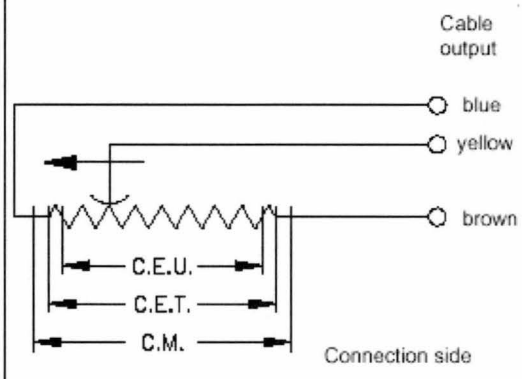

ORDER CODE

Displacement transducer **PZ12** □ □ □

Mounting by brackets	**S**
Mounting by selfaligning ball-joints	**A**
Mounting by flange	**F**

Model

If requested, it is possible to supply models with non-standard mechanical and/or electrical features

Example: **PZ12 - S - 25**
Displacement transducer model PZ12, mounting by brackets, useful electrical stroke (C.E.U.) 25mm

STANDARD ACCESSORIES

	Code
2 mounting brackets for PZ12-S	**STA074**

GEFRAN spa
via Sebina, 74
25050 PROVAGLIO D'ISEO (BS) - ITALIA
ph. 0309888.1 - fax. 0309839063
Internet: http://www.gefran.com

cod. 84875-10/99

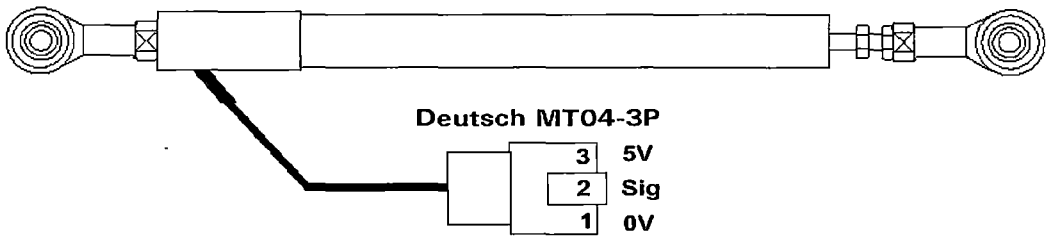

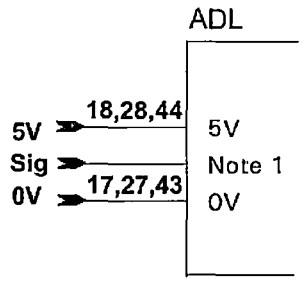

ADL Setup (to measure distance)

Channel Assignments
Assign a distance channel ie: Brake Pedal position

Sensor Calibration

1. In Calibration, select change.
2. Select Ratiometric(5V).
3. In calibration table enter the distance the pedal has moved and press "Read Value". You will end up with a table like the example.

V	mm
1.23	0
1.99	5
2.34	10
2.89	15
3.04	20

Note 1
Analog Voltage (Pins 1,2,3,4,5,19,20,21,22,23,24,25,26 45,46,47,48,49,50) or Analog Temp (Pins 34,35,36,37,38, 39,41,42) input may be used.

MoTeC	Title Linear Position Sensor				Sheet No	Drawing No
	Date 21/09/1999	Drawn ST	App AD	Products ADL	1 of 1	X24

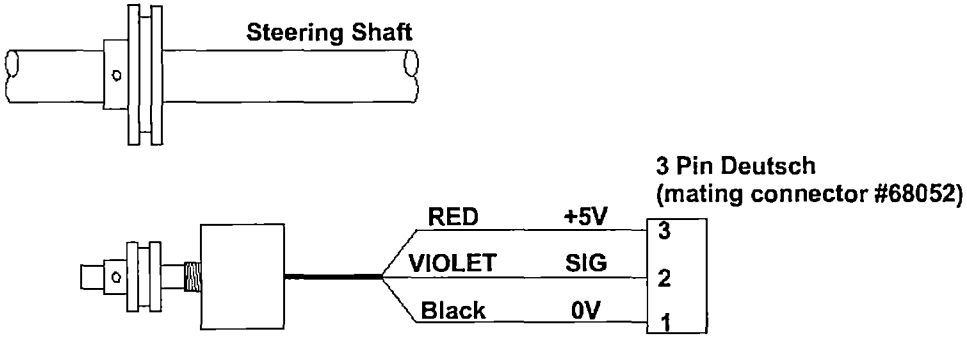

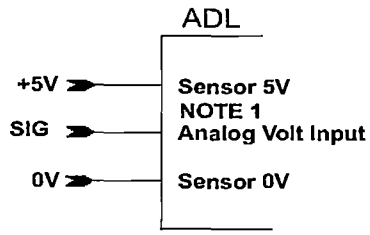

ADL Setup

Channel Assignments
Assign a Steering Channel to the appropriate pin

Sensor Calibration
Measurement method = Ratiometric
Turn wheel to desired angle & enter angle in deg table. Then click on read value to read sensor.,
Right turn = positive angles
Left turn = negative angles
Straight = 0 degree

NOTE 1

ADL PINS

+ 5V Analog Pins are 18, 28, 44
0V Analog Pins are 17, 27, 33, 40, 43
Analog Volt Input Pins are 1, 2, 3, 4, 5, 19, 20, 21, 22, 23, 24, 25, 26, 45, 46, 47 48, 49, 50

MoTeC	Title MoTeC STEERING ANGLE SENSOR				Sheet No	Drawing No
	Date 12/12/2000	Drawn ST	App	Products ADL	1 of 1	X21

H-11: Brake pressure transducer - specifications

ECLIPSE® • *OEM PRESSURE TRANSDUCER*

APPLICATIONS

- HYDRAULIC / PNEUMATIC CONTROLS
- AIR COMPRESSORS
- ENERGY MANAGEMENT: "SMART" COMPRESSORS, REFRIGERATION/ CHILLER CONTROL
- PROCESS CONTROL SYSTEMS
- ENGINE CONTROLS AND MONITORS

The Eclipse® is designed for high volume OEM's needing a low cost pressure transmitter for industrial or other heavy duty applications. The Eclipse's combination of rugged packaging, internal signal amplification and price make it ideal for many applications.

The pressure media is contained by a brazed assembly of stainless steel. There are no hidden O-rings or elastomers containing the media. A plated steel case protects the internal electronics.

It is available with either a 0.5 to 4.5 volt or 4 to 20 mA output. The 4 to 20 mA output is useful for applications where electrical noise may be a concern. Many units are CE compliant.

FEATURES	*BENEFITS*
• Voltage or current output	• Flexibility for the designer
• 15 PSIG through 7100 PSIS ranges	• Suitable for many applications
• High performance at low price	• Reduces OEM system cost
• CE versions available	• Ready for Europe
• Weatherproof type connector	• High reliability and user flexibility
• Reverse polarity protection	• Not damaged by reversed wiring
• Low excitation voltage	• Suitable for ORV or marine use
• IP65 sealed steel case	• Complete environmental protection for electronics

ECLIPSE® • *OEM PRESSURE TRANSDUCER*

TECHNICAL SPECIFICATIONS

RANGE

0-15, 25, 50 PSIG
0-100, 250, 500, 1000, 2000, 3000, 5000, 7100 PSIS

0-1, 2, 4, 7 bar g

(0-10, 15, 20, 35, 50, 100, 200, 350, 700 bar s)

PHYSICAL	
Proof Pressure	1.5 x rated range
Burst Pressure	5 x rated range
Material in Contact With Media	300 series stainless steel, braze compound
Shock	50 g's peak (5 milliseconds)
Vibration	Meets MIL-STD-810-C, Figure 514.2-5, Curve AK, 20.7 g rms minimum

ELECTRICAL	**Voltage output**	**Current output**
Full Scale Output	4.00 Vdc nominal (0.5 - 4.5 Vdc)	16 mA into 0 to 1400 Ω loop resistance (4-20 mA)
Zero Output	0.5 V nominal	4 mA nominal
Excitation	5.0 Vdc ± 0.25 Vdc @ 20mA	10 to 40 Vdc (linear derating to 35 Vdc from 25°C to 100 C°)
Reverse Polarity Protection	Yes	
Insulation Resistance	1000 MΩ @ 50 Vdc	
Electrical Connection	Standard Packard Metri-Pack™ Requires Packard #12065287 mating connector, not included Optional Hirschmann connector, mate included.	

PERFORMANCE	
Accuracy	±1% of FSO from best fit straight line including effects of nonlinearity, hysteresis and nonrepeatability
Operating Temperature Range	-40° to 105°C (-40° to 221°F)
Compensated Temperature Range	-1° to 82°C (30° to 180°F)
Total Error	±4% of full scale. Includes the effects of zero output error, calibration error, temperature, nonlinearity, hysteresis, and repeatability.

DIMENSIONS

xx.xx = inches
(xx.x) = mm

Eclipse with Packard

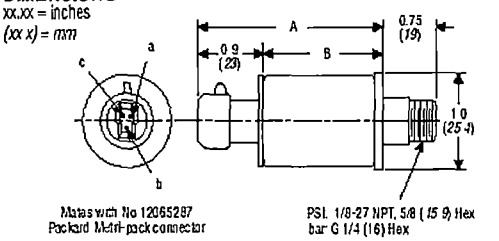

Eclipse with Hirschmann

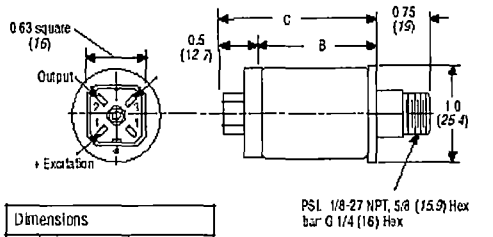

Dimensions		
	Voltage	**Current**
A	2.4 (61)	2.6 (66)
B	1.5 (38)	1.7 (43)
C	2.0 (51)	2.2 (56)

Load resistance in current loop

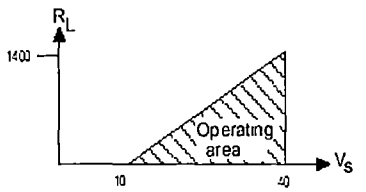

Ratiometric Output

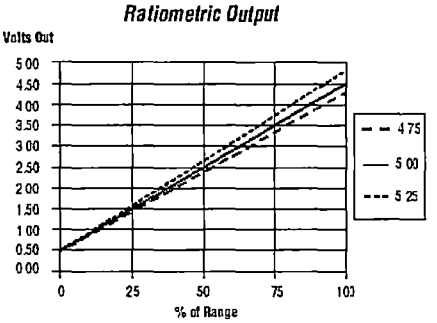

PACKARD CONNECTOR PINS

	Voltage	**Current**
a	+ Excitation	+ Excitation
b	Output	- Excitation (Return)
c	Common	NC

HIRSCHMANN CONNECTOR PINS

	Voltage	**Current**
Pin 1	NC	NC
Pin 2	Signal Output	NC
Pin 3	Common	- Excitation (Return)
Pin 4	+ Excitation	+ Excitation

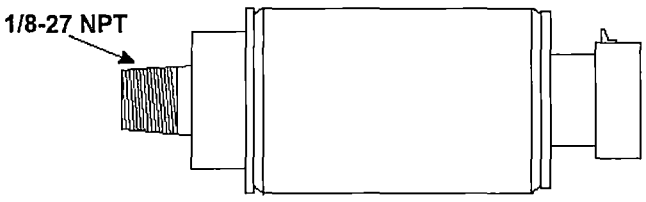

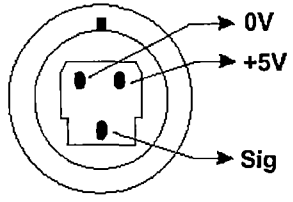

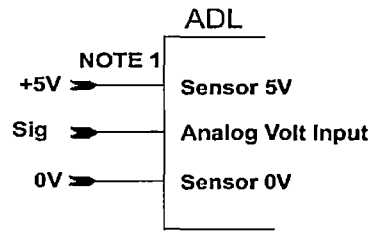

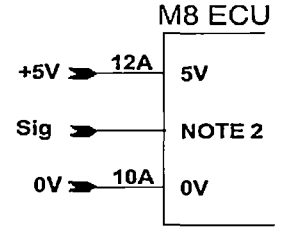

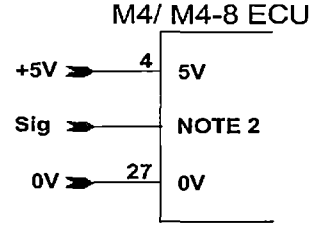

ADL Setup

Channel Assignments
Assign the pressure Channel to the appropriate pin

Sensor Calibration
Press "Select" and choose correct calibration file for the sensor.
For example, Data Inst Eclipse 100 psi MAP.C1P

NOTE 1:
+ 5V Analog Pins are 18, 28, 44
0V Analog Pins are 17, 27, 33, 40, 43
Analog Volt Input Pins are 1, 2, 3, 4, 5, 19, 20, 21, 22, 23, 24, 25, 26, 45, 46, 47 48, 49, 50

ECU Setup M8	
Sensor Calibration	100 PSI sensor
Display in KPA	17
Display in PSI	23
Display in InHg	28

NOTE 2:
M8 input pins are 28A,27A,13B,7B,8B,9B 14B, 15B & 16B
M4 and M4-8 input pins are 17,18 & 30

ECU Setup M4 M4-8	
Sensor Calibration	100 PSI sensor
MAP PIN	-1*
AUX TEMP PIN	-4*
AUX VOLT PIN	-3*

*** = DISPLAY IN KPA**

100 PSI Sensor CalibrationTables for M4-M4-8

Map Pin	0	10	20	30	40	50	60	70	80	90	100	110	120	130	140	150	160	170	180	190	200	210	220	230	240	250
	102	114	125	137	149	161	172	184	196	208	219	231	243	254	266	278	290	301	313	325	337	348	360	372	384	395
	260	270	280	290	300	310	320	330	340	350	360	370	380	390	400	410	420	430	440	450	460	470	480	490	500	
	407	419	430	442	454	466	477	489	501	513	524	536	548	559	571	583	598	606	618	630	642	653	665	677	689	

Aux Temp & Aux VoltPin	0	40	80	120	160	200	240	280	320	360	400	440	480	520	560	600	640	680	720	760	800	840	880	920	960	1000
	102	149	196	243	290	336	383	430	477	524	571	618	665	711	758	805	852	899	940	981	1018	1054	1091	1127	1164	1200

MoTeC	Title DATA INSTRUMENTS (ECLIPSE)				Sheet No	Drawing No
	Date 28/07/1999	Drawn ST	App AD	Products ADL, ECU	1 of 1	X22

H-13: Attitude & heading reference sensor – specifications and installation

New

AHRS

ATTITUDE & HEADING REFERENCE SYSTEM

- Roll, Pitch and Heading Angle in Dynamic Environments
- Enhanced Performance Kalman Filter Algorithm
- High Stability MEMS Sensors
- High Range Gyro and Accel Options

Applications

- UAVRPV Control
- Platform Stabilization
- Avionics

AHRS400CA (DMU-HDX-AHRS)

The Crossbow AHRS400CA is a high performance, solid-state attitude and heading reference system intended for airborne applications such as UAV control, Avionics, and Platform Stabilization. This high reliability, strap-down inertial subsystem provides attitude and heading measurement with static and dynamic accuracy comparable to traditional spinning mass vertical and directional gyros.

This AHRS400 series product builds on the performance of the AHRS300 series. It features higher performance sensors, including silicon MEMS accelerometers and gyroscopes with lower noise and improved bias stability.

The AHRS400CA achieves its excellent performance by employing proprietary Kalman Filter algorithms to determine stabilized roll, pitch, and heading angles in static and dynamics conditions. The Kalman Filter implementation results in a continuous on-line gyro bias calibration, and an adaptive attitude and heading measurement that is stabilized by the long term gravity and magnetic north references. Output data is provided in both analog and digital (RS-232) formats.

Each Inertial System comes with a User's Manual offering helpful hints on programming, installation, and product information. In addition, Crossbow's GYRO-VIEW software is included to assist you in system development and evaluation, and allows you to perform data acquisition.

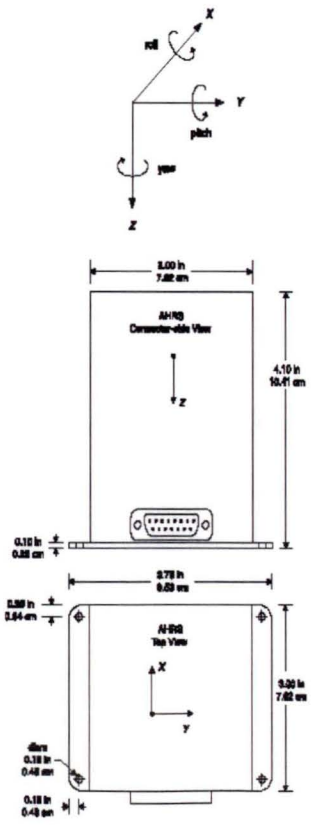

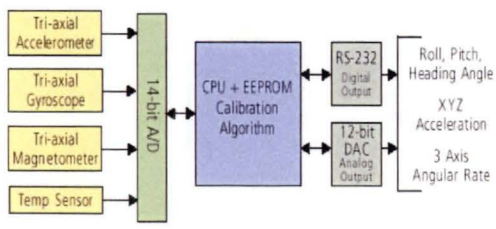

AHRS Block Diagram

inertial systems

Crossbow

Specifications		AHRS400CA-100	AHRS400CA-200	Remarks
Performance				
Update Rate (Hz)		> 60	> 60	Continuous update mode
Start-up Time Valid Data (sec)		< 1	< 1	
Fully Stabilized Data (sec)		< 60	< 60	
Heading				
Range (°)		± 180	± 180	
Static Accuracy (°)		<± 1.5	<± 2	
Dynamic Accuracy (° rms)		± 3	± 4	
Resolution (° rms)		< 0.1	< 0.1	
Attitude				
Range: Roll, Pitch (°)		± 180, ± 90	± 180, ± 90	
Static Accuracy (°)		<± 0.5	<± 1	Measured on level surface
Dynamic Accuracy (° rms)		± 2.0	± 2.5	
Resolution (°)		< 0.1	< 0.1	
Angular Rate[1]				
Range: Roll, Pitch, Yaw (°/sec)		± 100	± 200	
Bias: Roll, Pitch, Yaw (°/sec)		<± 1.0	<± 1.0	Scaled sensor mode
Bias: Roll, Pitch, Yaw (°/sec)		<± 0.05	<± 0.05	Angle mode
Scale Factor Accuracy (%)		< 1	< 1	
Non-Linearity (% FS)		< 0.3	< 0.3	
Resolution (°/sec)		< 0.025	< 0.05	
Bandwidth (Hz)		> 10	> 10	-3 dB point
Random Walk (°/hr$^{1/2}$)		< 0.85	< 1.7	
Acceleration				
Input Range: X/Y/Z (g)		± 2	± 10	
Bias: X/Y/Z (mg)		<± 8.5	<± 12	
Scale Factor Accuracy (%)		< 1	< 1	
Non-Linearity (% FS)		< 1	< 1	
Resolution (mg)		< 0.25	< 1.25	
Bandwidth (Hz)		> 10	> 10	-3 dB point
Random Walk (m/s/hr$^{1/2}$)		< 0.1	< 0.5	
Environment				
Operating Temperature (°C)		-40 to +71	-40 to +71	
Non-Operating Temperature (°C)		-55 to +85	-55 to +85	
Non-Operating Vibration (g rms)		6	6	20 Hz - 2 KHz random
Non-Operating Shock (g)		1000	1000	1 ms half sine wave
Electrical				
Input Voltage (VDC)		9 to 30	9 to 30	
Input Current (mA)		< 300	< 300	
Power Consumption (W)		< 4	< 4	at 12 VDC
Digital Output Format		RS-232	RS-232	"See Digital Data Format"
Analog[1] Range (VDC)		± 4.096	± 4.096	Pins 8, 9, 10, 12, 13, 14
		0 to 5.0	0 to 5.0	Pins 5, 6, 7
Physical				
Size	(in)	3.0 x 3.75 x 4.10	3.0 x 3.75 x 4.10	Includ. mounting flanges
	(cm)	7.62 x 9.53 x 10.41	7.62 x 9.53 x 10.41	Includ. mounting flanges
Weight	(lbs)	< 1.4	< 1.4	
	(kg)	< 0.64	< 0.64	
Connector		15 pin sub-miniature "D" female		

Notes
[1]All analog outputs are fully buffered and are designed to interface directly to data acquisition equipment.
Specifications subject to change without notice

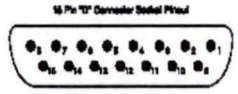

Pin	Signal
1	RS-232 Transmit Data
2	RS-232 Receive Data
3	Input Power
4	Ground
5	X-axis accel voltage[1]
6	Y-axis accel voltage[1]
7	Z-axis accel voltage[1]
8	Roll-axis angular rate[2]
9	Pitch-axis angular rate[2]
10	Yaw-axis angular rate[2]
11	NC – Factory use only
12	Roll angle/X-axis mag voltage[3]
13	Pitch angle/Y-axis mag voltage[3]
14	Not used/Z-axis mag voltage[3]
15	NC – Factory use only

Notes
1. The accelerometer voltage outputs are taken directly from the accelerometers without compensation or scaling.
2. The angular rate analog outputs are scaled to represent degrees/second. Outputs are created by a D/A converter.
3. Actual output depends on AHRS measurement mode. Axis magnetometer scaled analog voltage vs. angle.

Pin Diagram

inertial systems

Ordering Information

Model	Previous Model	Description	Gyro (°/sec)	Accel (g)
AHRS400CA-100	DMU-HDX-AHRS	Attitude & Heading Reference System	± 100	± 2
AHRS400CA-200	DMU-HDX-AHRS	Attitude & Heading Reference System	± 200	± 10

CALL FACTORY FOR OTHER CONFIGURATIONS

phone: 408.965.3300 ▼ fax: 408.324.4840 ▼ e-mail: info@xbow.com ▼ web: www.xbow.com

16 APPENDIX I – ENGINE SPECIFICATIONS

I-1: Engine specifications 291

I-2: Engine top end exploded view 292

I-3: Engine crankshaft exploded view 293

I-4: ECU installation 294

I-1: Engine specifications

Engine:		
Type		4-stroke, DOHC, 4-cylinder
Cooling system		Liquid-cooled
Bore and stroke		66 x 43.8 mm
Displacement		599 mL
Compression ratio		12.8
Maximum horsepower		81.6 kW (111 PS) @12 500 r/min (rpm), (AS) 80.6 kW (109.6 PS) @12 500 r/min (rpm), (PR) 78.2 kW (106.3 PS) @12 500 r/min (rpm), (US) - - -
Maximum torque		65.6 N·m (6.7 kg·m, 48 ft·lb) @10 000 r/min (rpm), (AS) 64.6 N·m (6.6 kg·m, 48 ft·lb) @10 000 r/min (rpm) (FR)(US) - - -
Carburetion system		Carburetors, Mikuni BDSR 36R × 4
Starting system		Electric starter
Ignition system		Battery and coil (transistorized)
Timing advance		Electronically advanced(digital igniter)
Ignition timing		From 12.5° BTDC @1 300 r/min (rpm) to 42.5° BTDC @5 000 r/min (rpm)
Spark plug		NGK CR9E
Cylinder numbering method		Left to right, 1-2-3-4
Firing order		1-2-4-3
Valve timing:		
Inlet	Open	56° BTDC
	Close	80° ABDC
	Duration	316°
Exhaust	Open	61° BBDC
	Close	33° ATDC
	Duration	274°
Lubrication system		Forced lubrication (wet sump with cooler)
Engine oil:		
Grade		SE, SF or SG class
Viscosity		SAE10W-40, 10W-50, 20W-40, or 20W-50
Capacity		3.8 L

I-2: Engine top end exploded view

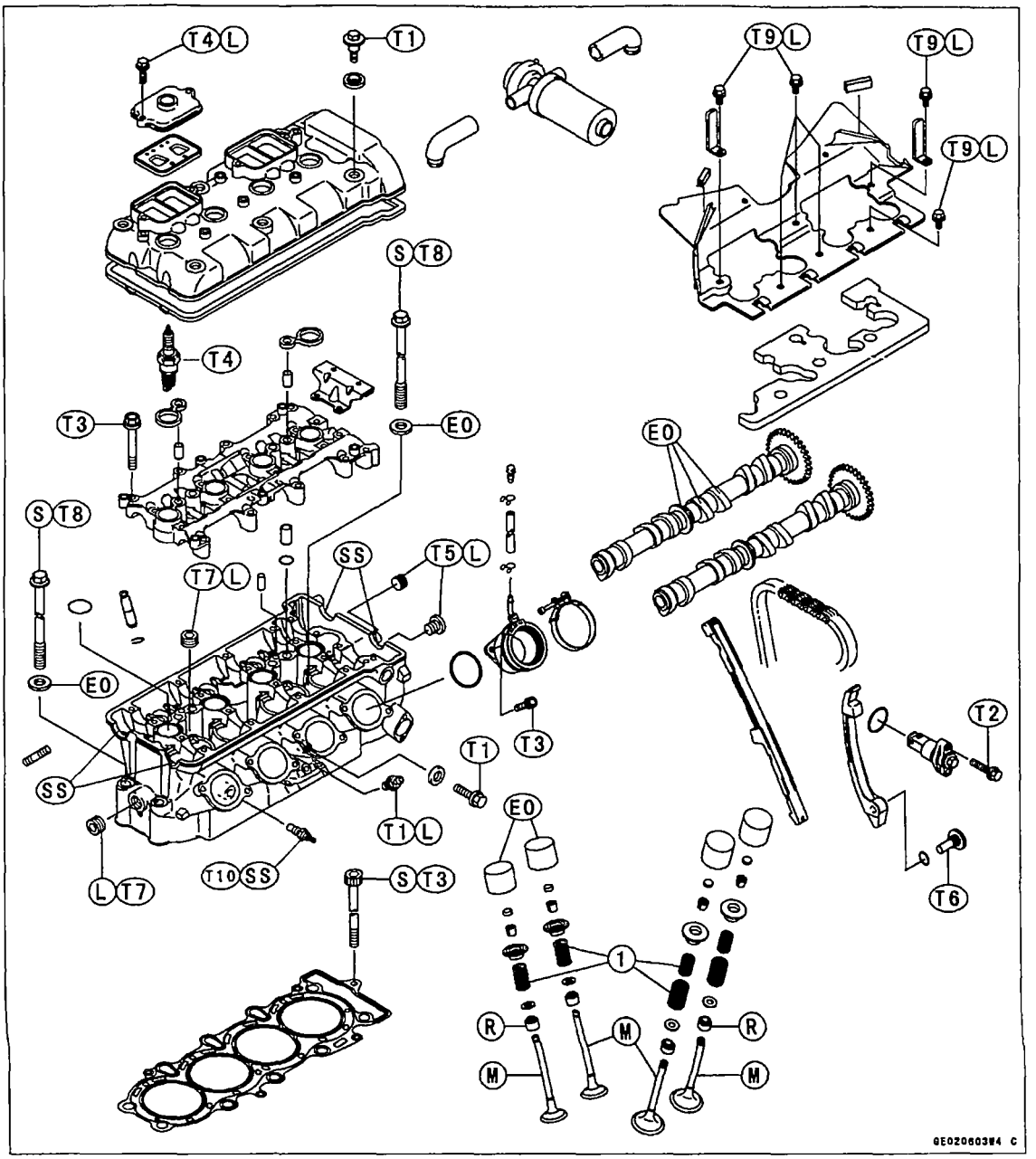

T1: 9.8 N·m (1.0 kg m, 87 in·lb)
T2: 11 N·m (1.1 kg·m, 95 in·lb)
T3: 12 N·m (1.2 kg·m, 104 in·lb)
T4: 13 N·m (1.3 kg·m, 113 in·lb)
T5: 15 N·m (1.5 kg·m, 11.0 ft·lb)
T6: 25 N·m (2.5 kg·m, 18.0 ft·lb)
T7: 20 N·m (2.0 kg·m, 14.5 ft lb)
T8. 49 N·m (5.0 kg·m, 36 ft·lb)
T9: 5.9 N·m (0.60 kg·m, 52 in·lb)
T10: 7 8 N·m (0.8 kg·m, 69 in·lb)

1. Closed coil end faces downward.
L: Apply a non-permanent locking agent.
M: Apply molybdenum disulfide grease.
EO: Apply engine oil.
SS: Apply silicone sealant.
R: Replacement Parts
S: Follow the specific tightening sequence.

I-3: Engine crankshaft exploded view

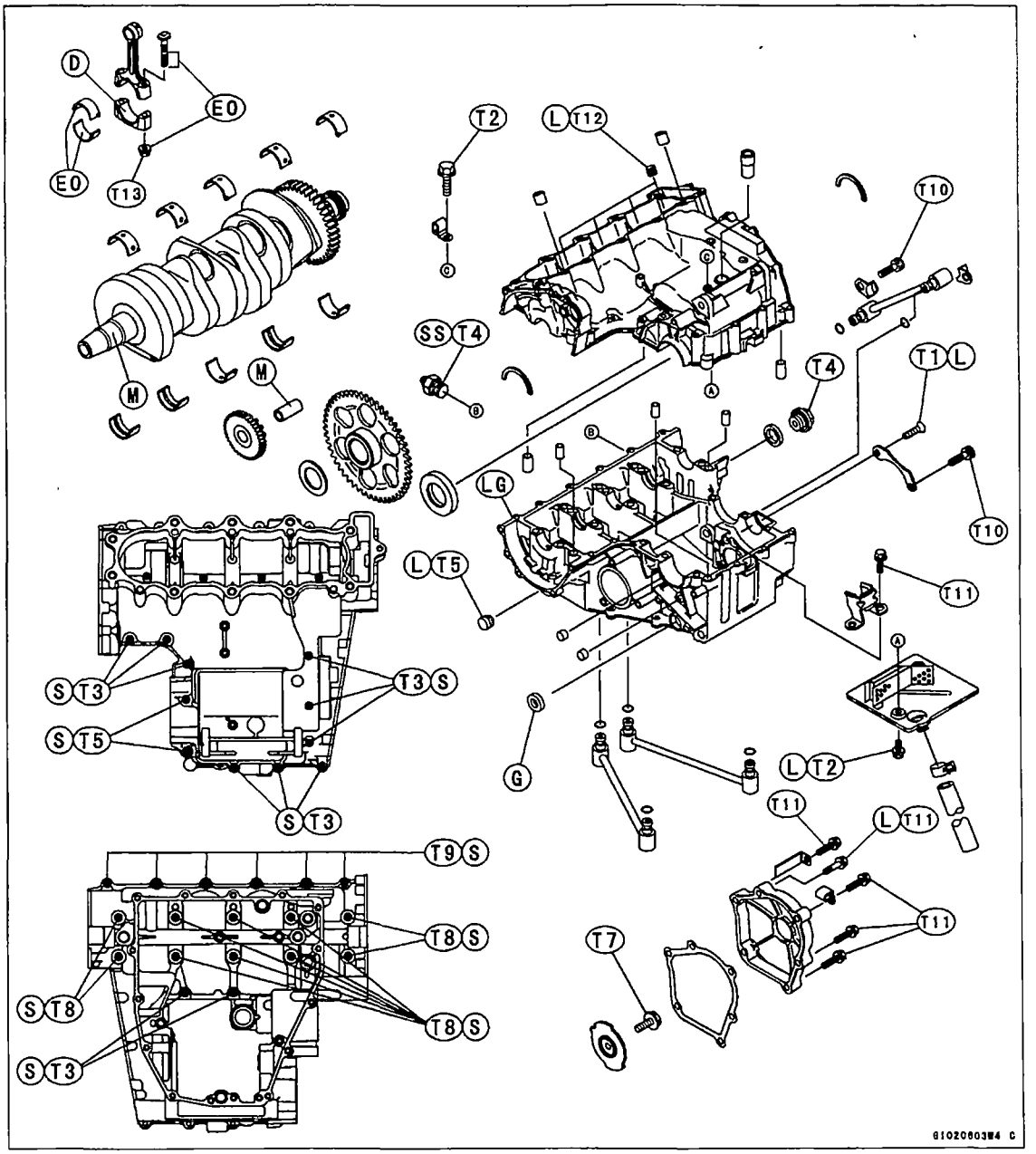

T1: 5.4 N·m (0.55 kg·m, 48 in·lb)
T2: 9.8 N·m (1.0 kg·m, 87 in·lb)
T3: 12 N·m (1.2 kg·m, 104 in·lb)
T4: 15 N·m (1.5 kg·m, 11.0 ft·lb)
T5: 20 N·m (2.0 kg·m, 14.5 ft·lb)
T6: 28 N·m (2.9 kg·m, 21 ft·lb)
T7: 40 N·m (4.0 kg·m, 29 ft·lb)
T8: 30 N·m (3.0 kg·m, 22 ft·lb)
T9: 18 N·m (1.8 kg·m, 13.0 ft·lb)
T10: 13 N·m (1.3 kg·m, 113 in·lb)
T11: 11 N·m (1.1 kg·m, 95 in·lb)
T12: 6.9 N·m (0.70 kg·m, 61 in·lb)
T13: See the text.

I-4: ECU installation

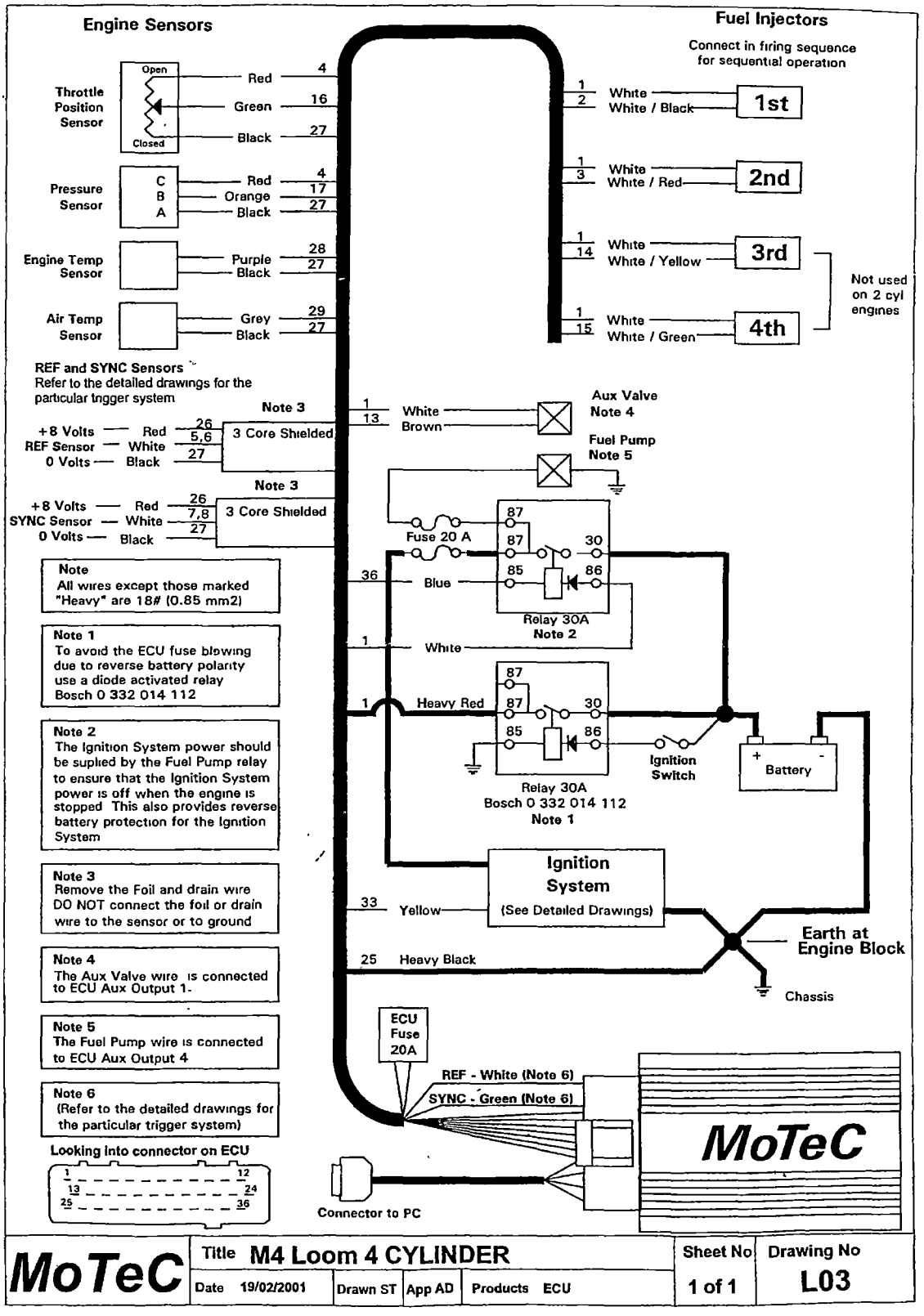

17 APPENDIX J – TESTING DATA

J-1: Testing data, logged at the University carpark straight line course 295

J-2: Testing data, logged at the University carpark Figure 8 course.....300

I-1: Testing data, logged at the University carpark straight line course

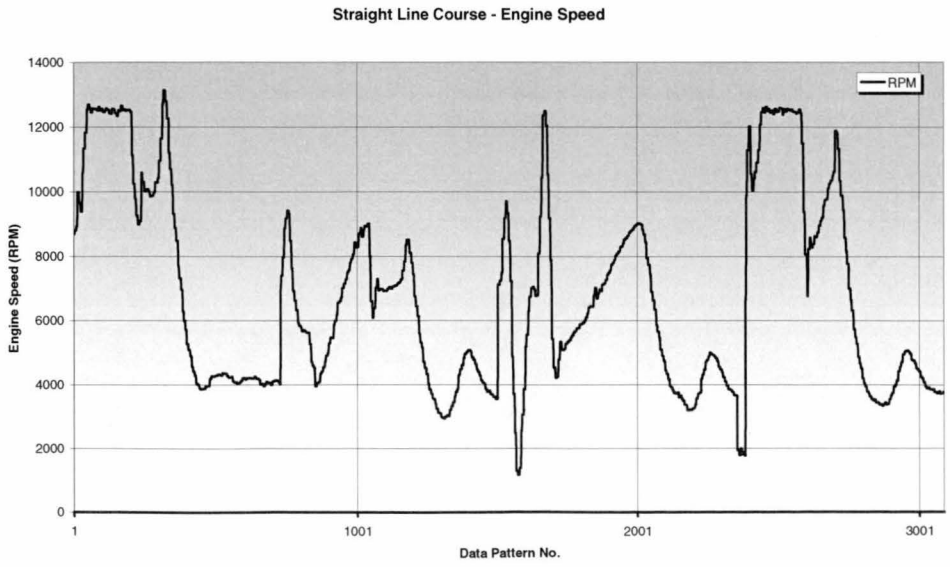

Straight Line Course - Gear

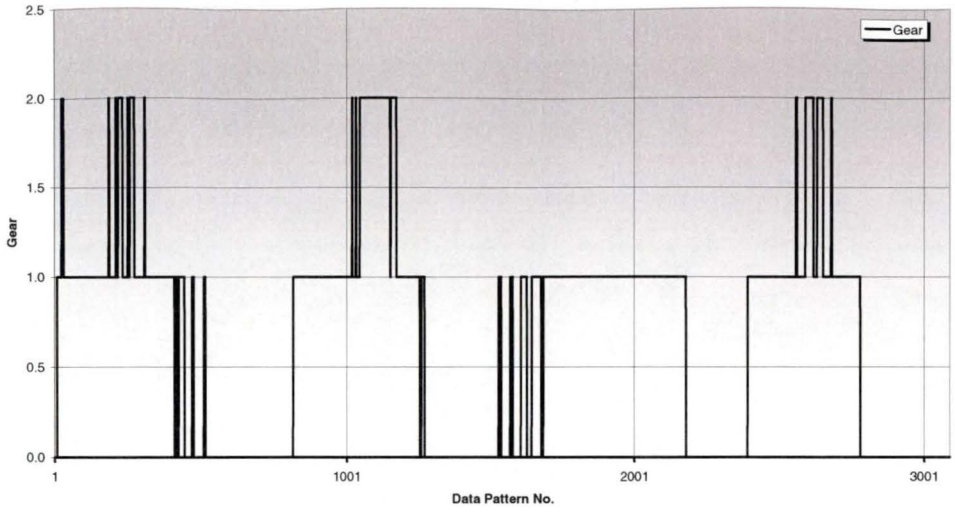

Straight Line Course - Steering Wheel Angle and Throttle Position

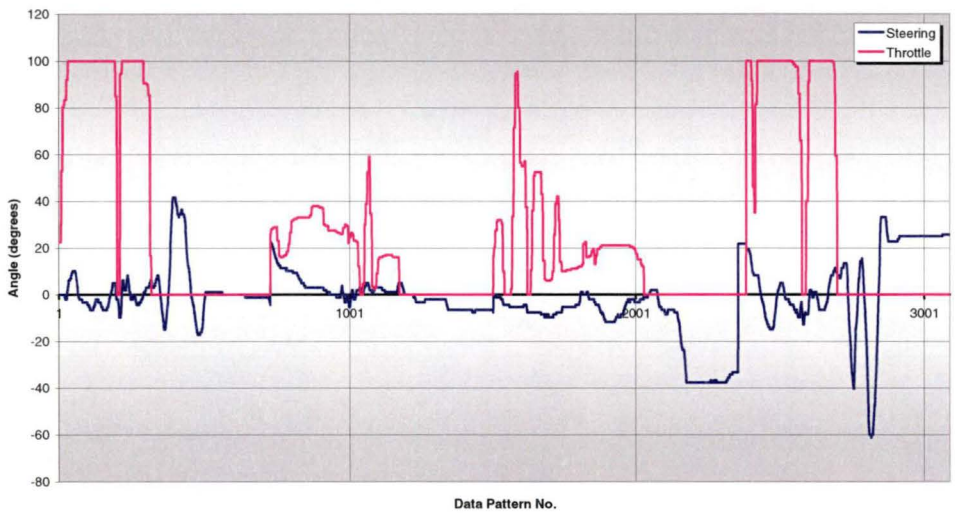

Straight Line Course - Hydraulic Brake Pressure

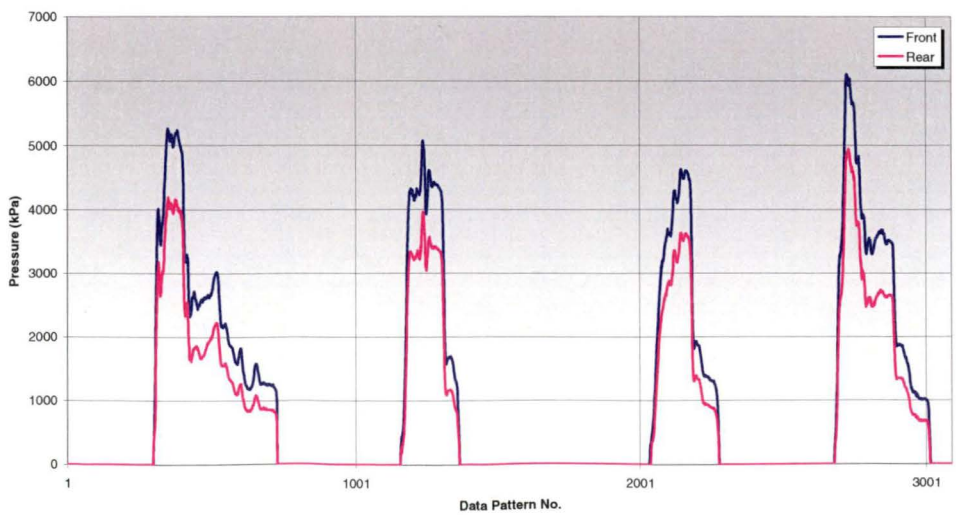

Straight Line Course - Acceleration

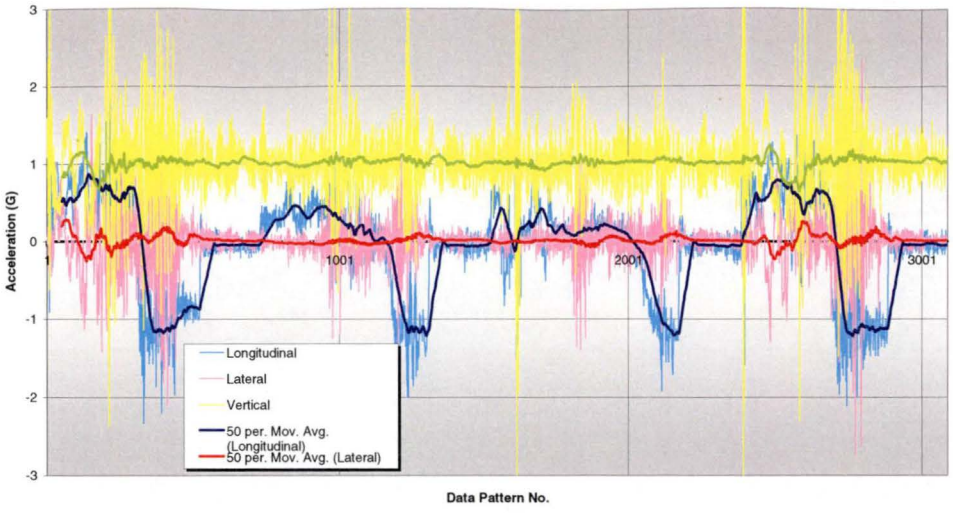

Straight Line Course - Heading Angle

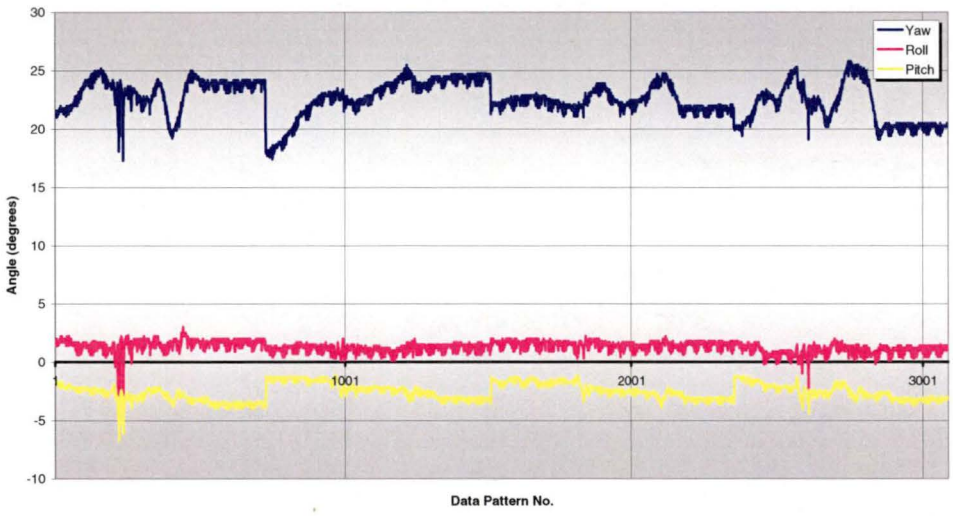

Straight Line Course - Heading Anglular Velocity

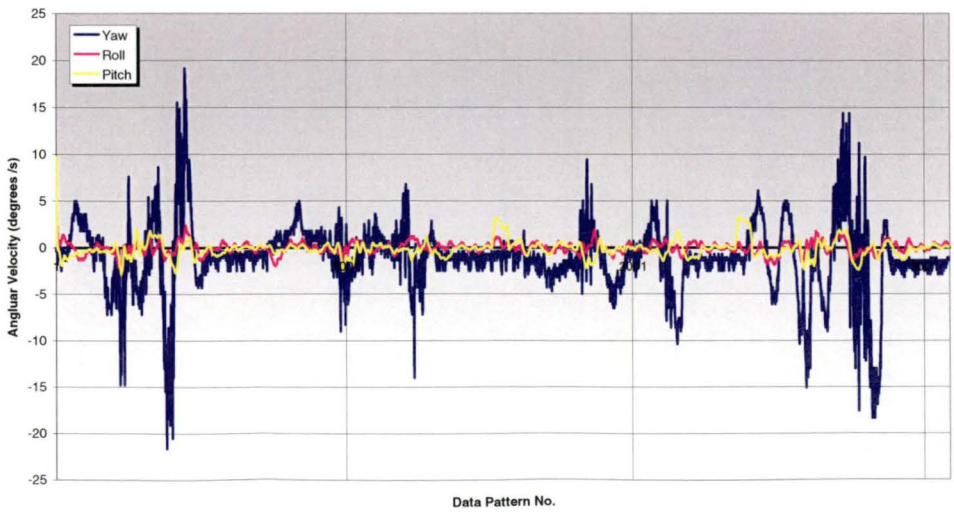

Straight Line Course - Wheel Speeds

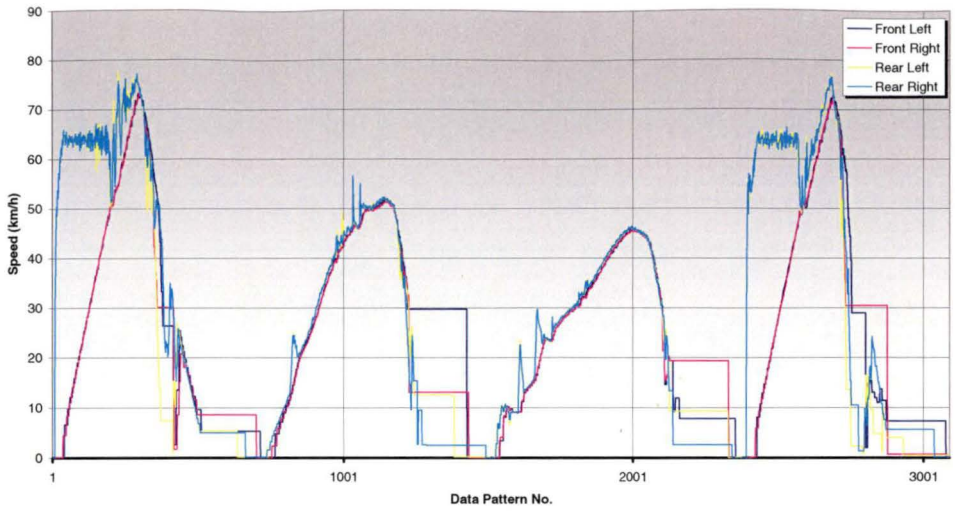

Straight Line Course - Wheel Acceleration

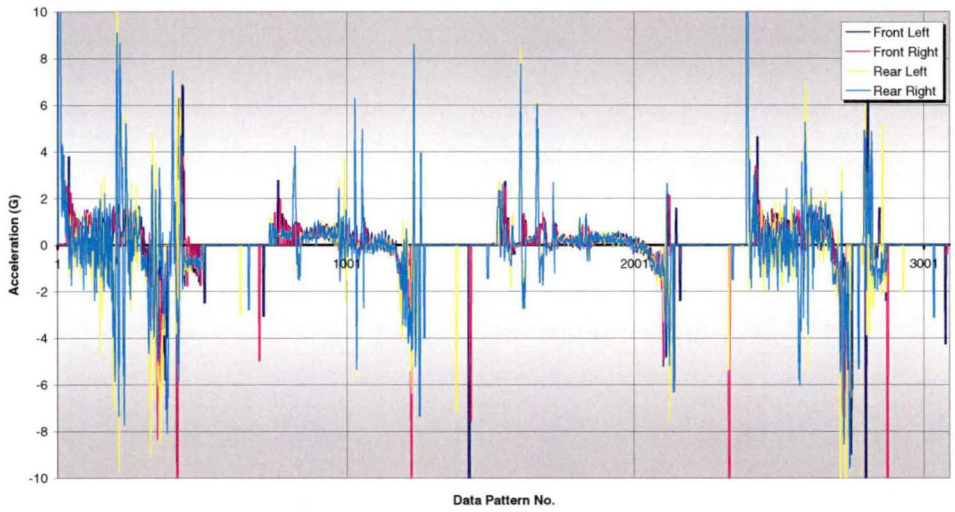

Straight Line Course - Ground and Drive Speed

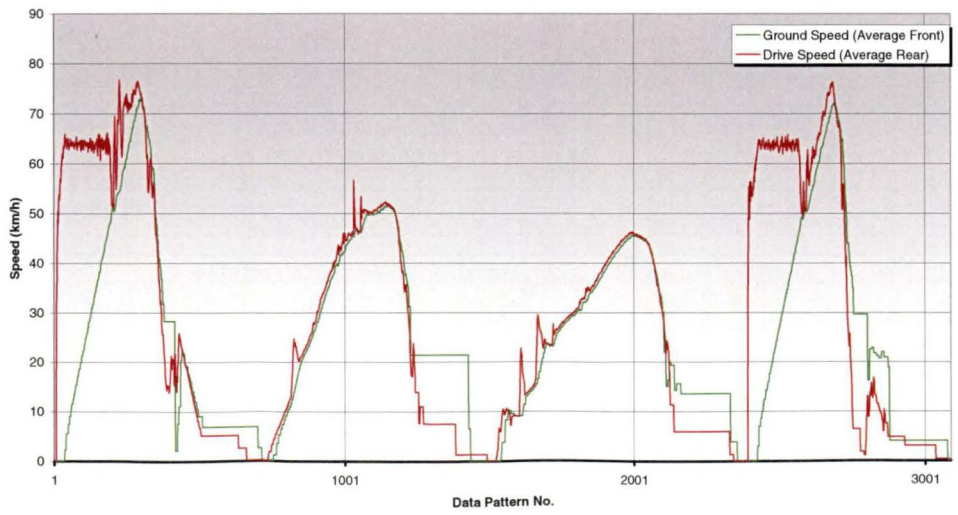

Straight Line Course - Rear Wheel Slip (under Acceleration)

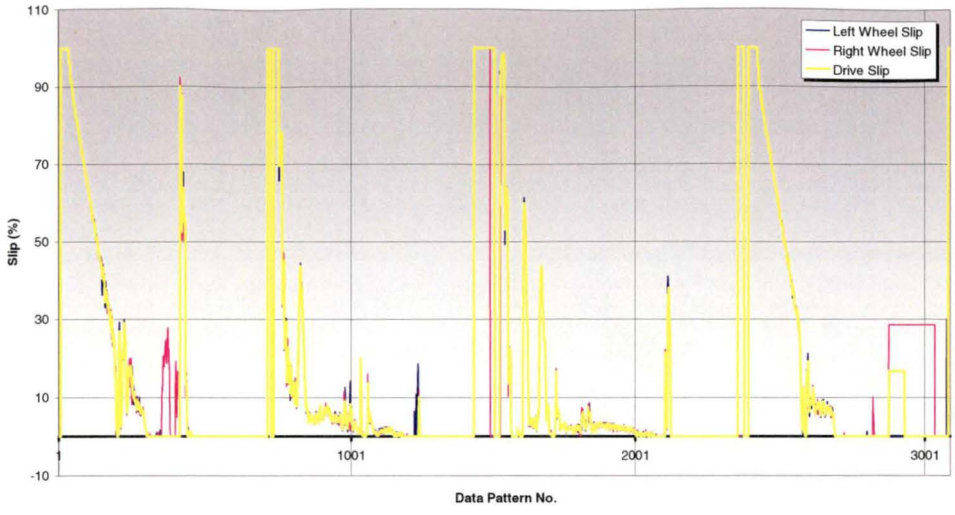

Straight Line Course - Suspension Positions

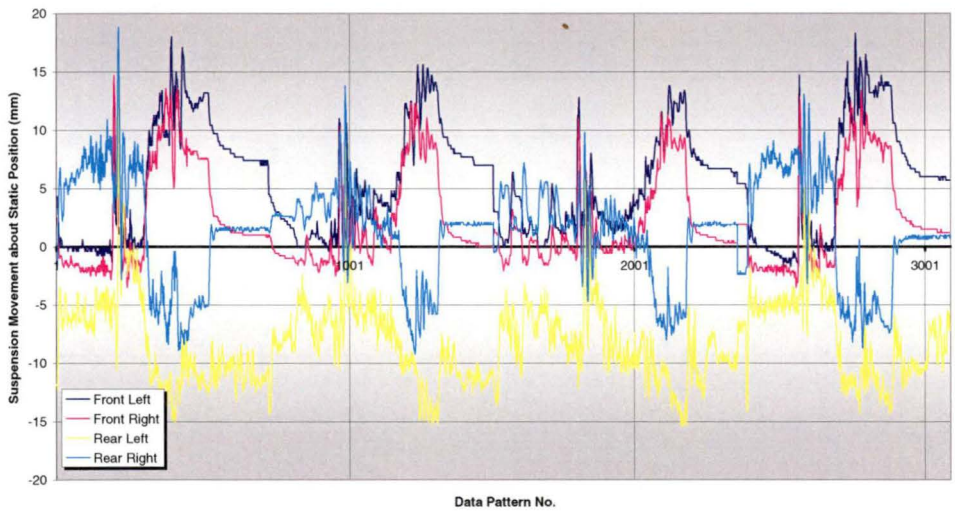

Straight Line Course - Suspension Positions

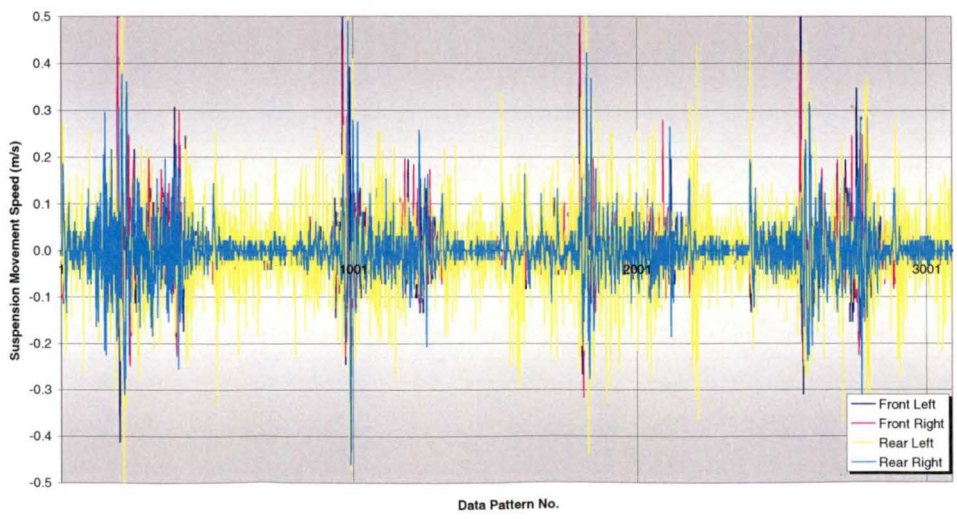

J-2: Testing data, logged at the University carpark Figure 8 course

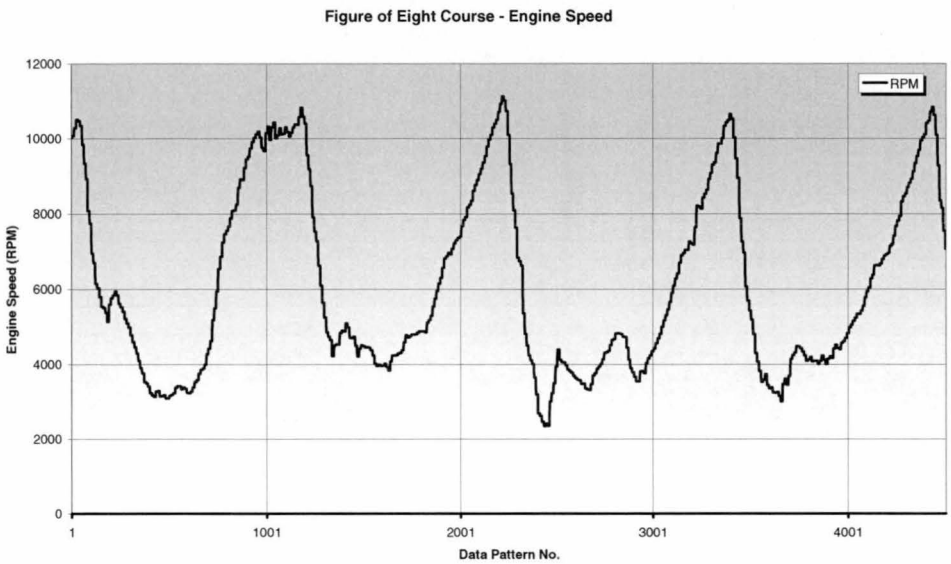

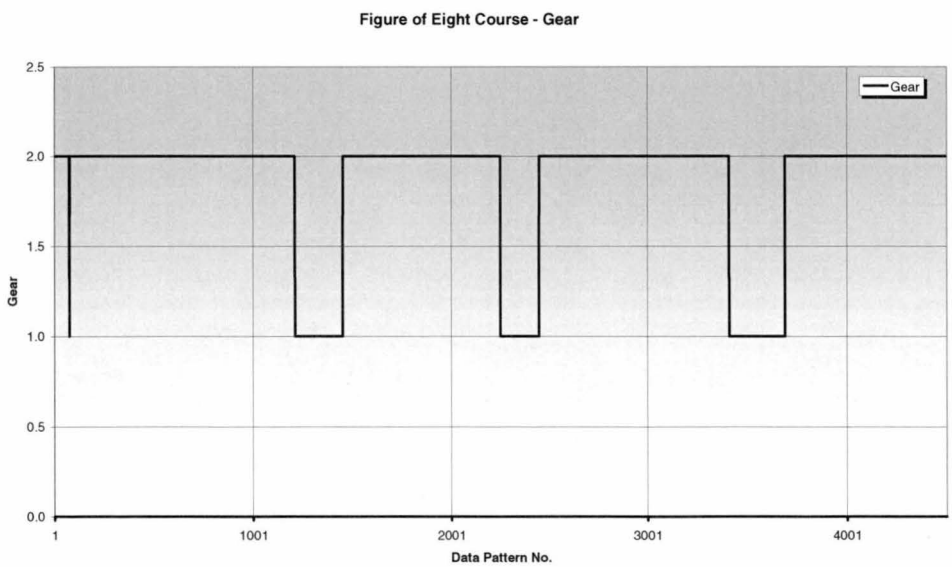

Figure of Eight Course - Steering Wheel Angle and Throttle Position

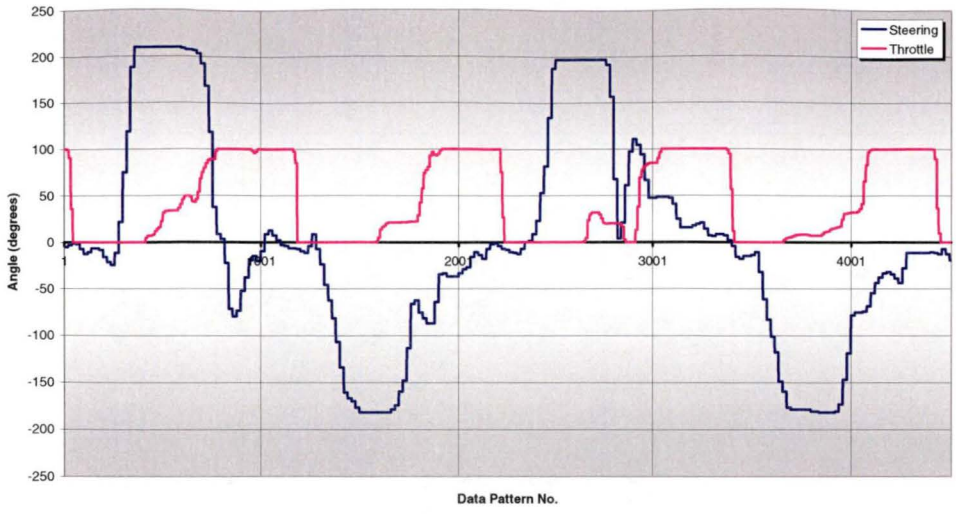

Figure of Eight Course - Hydraulic Brake Pressure

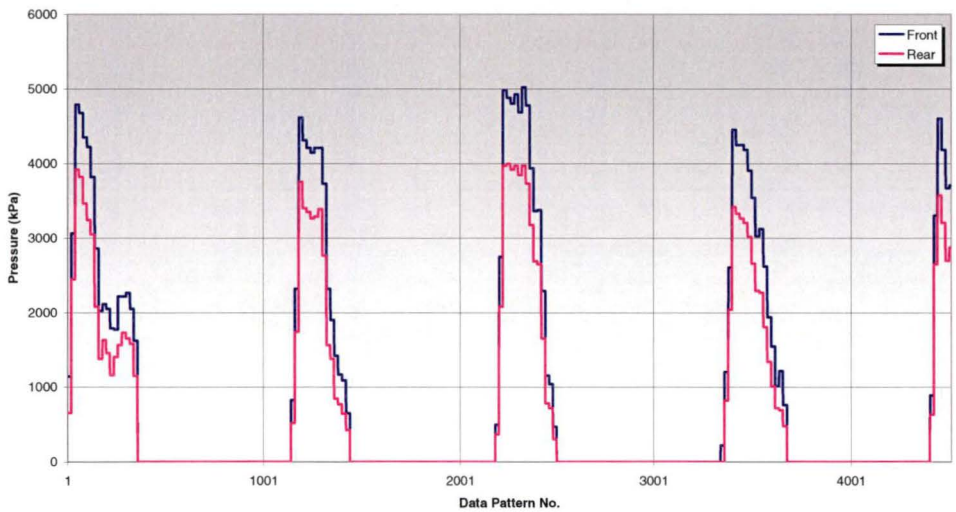

Figure of Eight Course - Acceleration

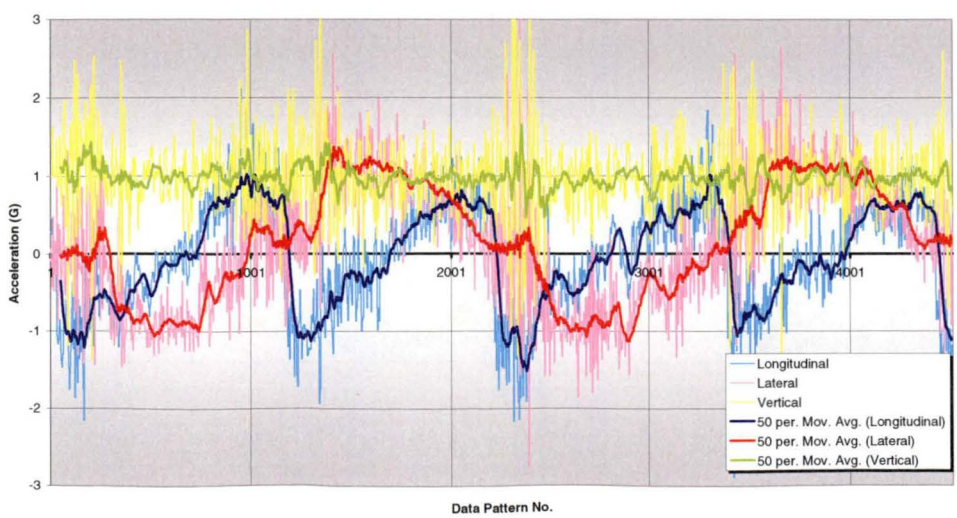

Figure of Eight Course - Heading Angle

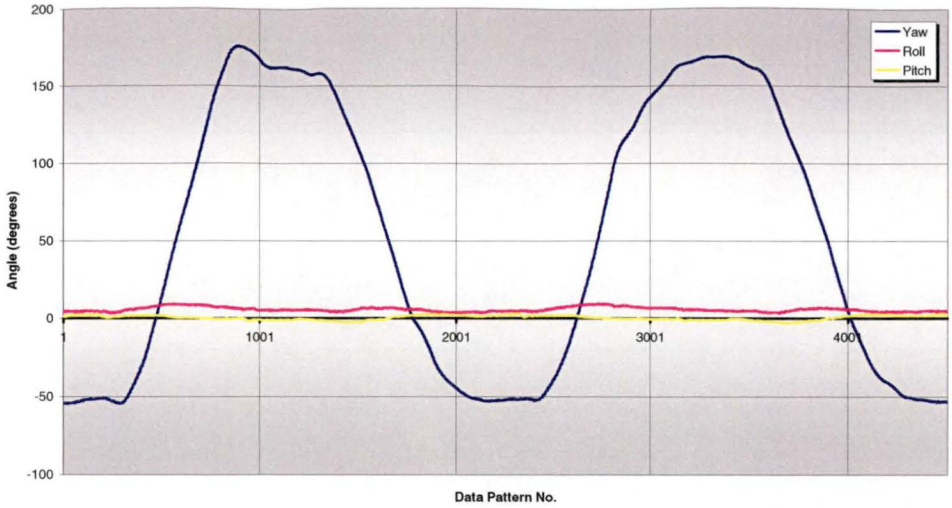

Figure of Eight Course - Heading Anglular Velocity

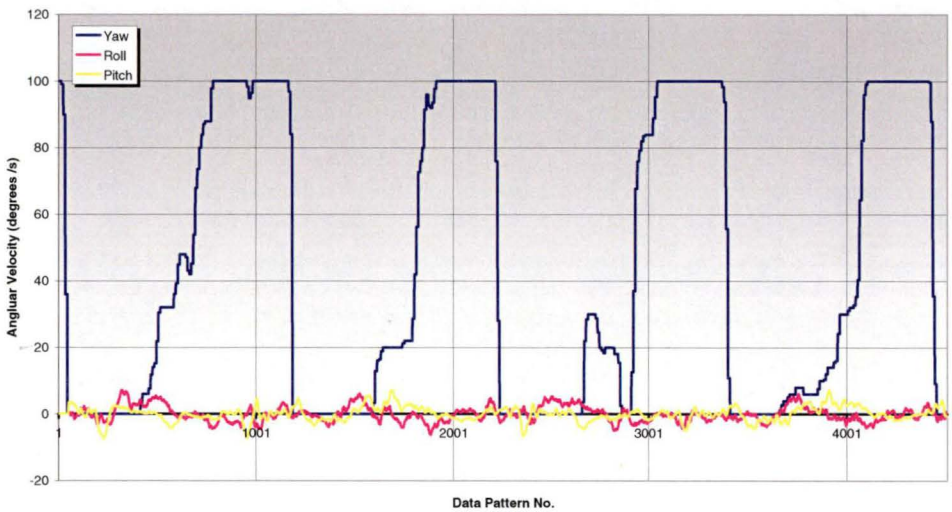

Figure of Eight Course - Wheel Speeds

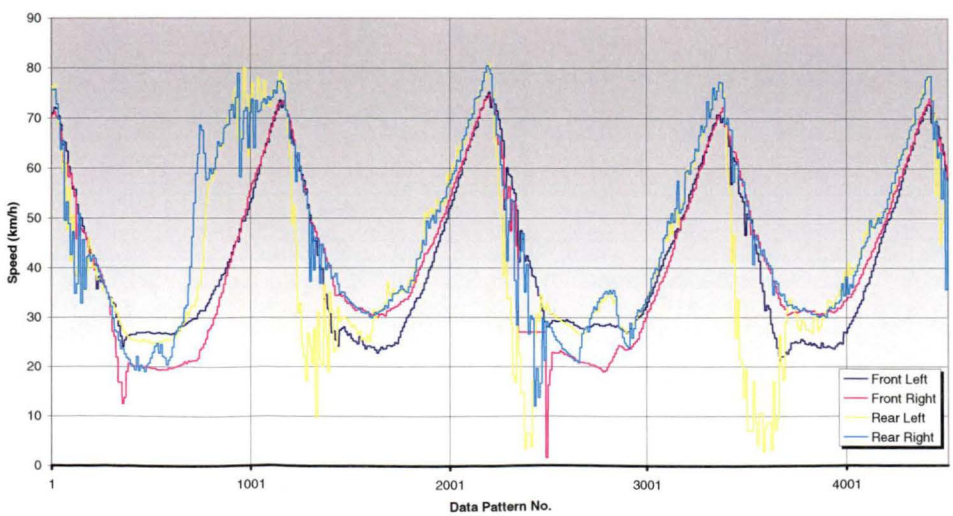

Figure of Eight Course - Wheel Acceleration

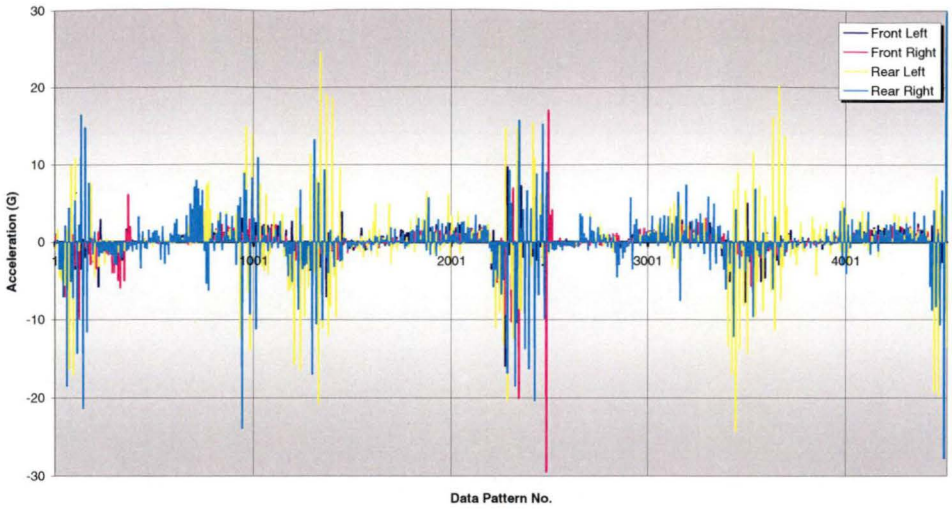

Figure of Eight Course - Ground and Drive Speed

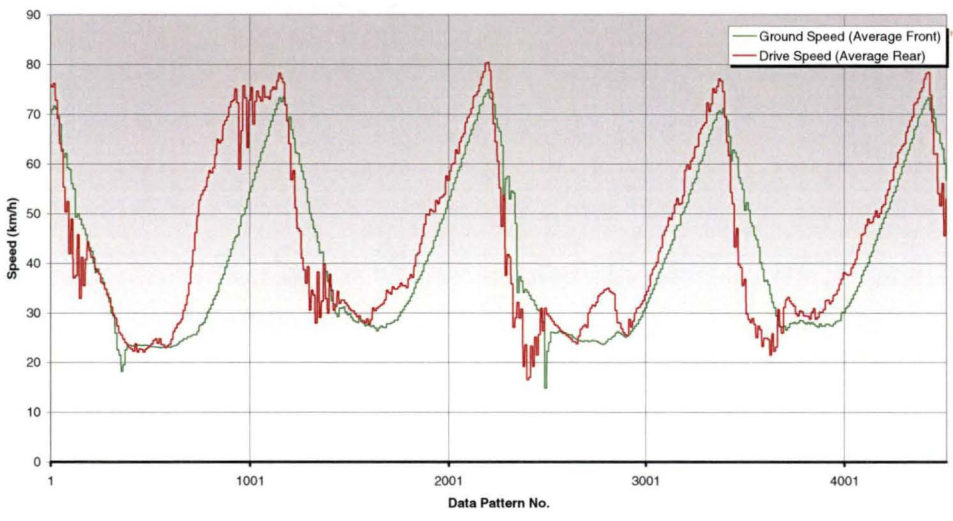

Figure of Eight Course - Rear Wheel Slip (under Acceleration)

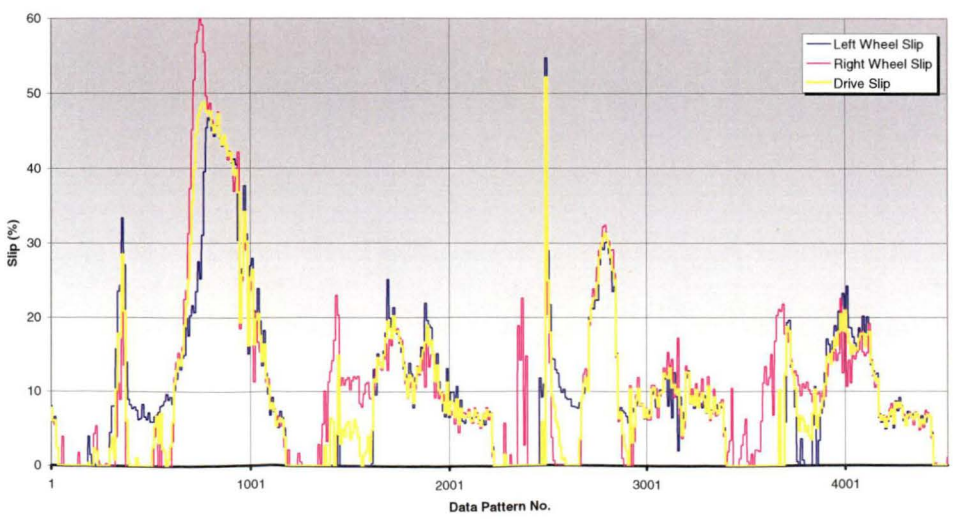

Figure of Eight Course - Suspension Positions

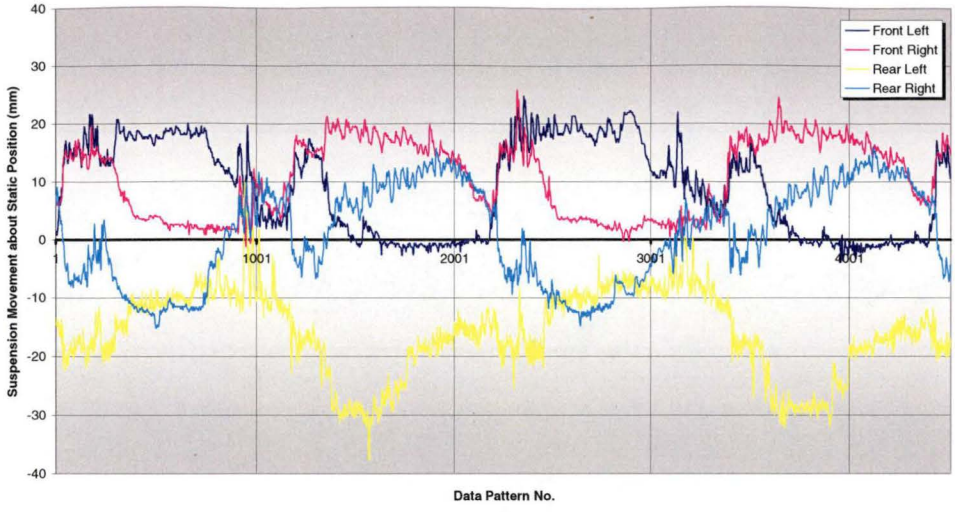

Figure of Eight Course - Suspension Positions